TECHNISCHE UNIVERSITÄT WIEN
Vienna University of Technology

PhD. THESIS

DISSERTATION

Novel Organic Materials for Multi-photon Photopolymerization and Photografting: Powerful Tools for Precise Microfabrication and Functionalization in 3D

ausgeführt zum Zwecke der Erlangung des akademischen Grades eines Doktors der technischen Wissenschaften unter der Leitung von

Ao.Univ.Prof. Dipl.-Ing. Dr.techn. Robert Liska
E163
Institut für Angewandte Synthesechemie

eingereicht an der Technischen Universität Wien
Fakultät für Technische Chemie

von
MSc. Zhiquan Li
0928315
Gießaufgasse 1/14, 1050, Wien

Abstract

Two-photon excitation provides the possibility of the activation of chemical or physical processes with high spatial resolution in 3D. Such strategy has been widely used in microfabrication of photonic crystals, polymer-based optical waveguides on integrated circuit boards, high-density 3D optical data storage and other industries requiring high precision. Since the photo-activated chemical or physical processes are confined only within the small focal volume, excellent spatial control could be obtained. Moreover, the excitation source with long wavelength offers the advantages of deeper tissue penetration and less photodamage, making 2PA especially suitable for various biological applications, such as bioimaging and *in-vivo* biofabrications.

The development of novel two-photon absorption (2PA) active organic materials is essential to realize the desired functions. The first part of the thesis focuses on the novel 2PA photoinitiators (2PIs) used for two-photon induced photopolymerization (2PP), a versatile technique for precise 3D microfabrications. High initiation efficiency is the most important character for an efficient PI. Based on a potent lead structure 1,5-bis(4-(*N,N*-dibutylamino) phenyl)penta-1,4-diyn-3-one, several aromatic ketone-based 2PIs containing triple bonds and dialkylamino groups were synthesized via Sonogashira coupling reactions. 2, 7-substituted fluorenone-based PI **B3FL**, with the largest 2PA cross section of 440 GM at 800 nm, exhibited the broadest processing windows among the investigated PIs. The double bonds conversion of the cross-linking polymeric network and the mechanical properties of the microstructures were also evaluated by FTIR and nanoindentation measurements, respectively.

Beside initiation efficiency of PIs, the ease and cost of preparation are also critical factors from practical aspect. To overcome the problem of the reported 2PIs derived from the complicated syntheses and expensive catalysts, a series of linear and cyclic benzylidene ketone-based 2PIs containing double bonds and dialkylamino groups were synthesized in one step via classical aldol condensation reactions. The results of quantum-chemical calculations and experimental tests indicated that the size of the central ring significantly affected the excited state energetics and emission quantum yields as well as the two-photon initiation efficiency. 4-methylcyclohexanone-based initiator **M2CMK** is far more efficient than its counterparts with a central five-membered ring. The ideal processing windows of **M2CMK** are as broad as those of **B3FL** but with much simpler synthesis.

Straightforward synthesis combined with high 2PA initiation efficiency makes the novel initiator a promising candidate for commercialization.

Based on the efficient core structures of cyclic benzylidene ketone, carboxylic acid sodium salts as water-borne functionalities were incorporated in order to expand the application range of 2PP to biofabrication. Those novel water-soluble 2PIs were applied to microfabrication at a writing speed as high as 100 mm/s within hydrophilic photopolymers with up to 50 wt% of water. Preliminary dark-cytotoxicity tests of the 2PIs were performed and the obtained results were compared to those of Irgacure 2959, the most commonly used photoinitiator in cell encapsulation.

The second part of the thesis concerned on the novel arylazide used for multi-photon induced photografting (MPG), a powerful tool for 3D site-specific functionalization. As a proof-of-concept, commercial aromatic azide **BAC-M** was successfully grafted within the 3D matrix with high resolution under three-photon excitation. In order to enhance the grafting efficiency and reduce the required energies, we designed and synthesized a series of novel 2PA active fluoroaryl azides containing ''push-pull'' structures. Desired functionalities, such as alkene and alkyne groups, were introduced at the terminal amino groups for post-modification after two-photon photografting.

Kurzfassung

Zwei-Photonen-Anregung ermöglicht die Aktivierung chemischer oder physikalischer Prozesse in hoher räumlicher Auflösung in 3D. Diese Strategie ist weit verbreitet in der Mikrofabrikation photonischer Kristalle, polymerbasierter optischer Wellenleiter in integrierten Schaltkreisen, hochkompakte 3D-optische Datenspeicher und andere industrielle Anwendungen, die hohe Präzision erfordern. Da die photoaktivierten chemischen oder physikalischen Prozesse nur auf ein kleines Volumen fokussiert sind, kann eine exzellente räumliche Auflösung erzielt werden. Weiters ermöglicht die langwellige Anregungsquelle eine tiefere Gewebepenetration bei geringeren Lichtschäden, was die Zwei-Photonen-Anregung besonders geeignet für diverse biologische Anwendungen macht, wie beispielsweise Bioimaging und *in-vivo* Biofabrikation.

Die Entwicklung neuer organischer Materialien für Zwei-Photonen-Absorption (2PA) ist essentiell um die gewünschten Funktionen spezifischer Anwendungen zu verwirklichen. Der erste Teil der Arbeit befasst sich mit neuen Zwei-Photonen-Photoinitiatoren (2PIs) die für Zwei-Photonen induzierte Photopolymerisation (2PP), einer vielseitigen Technik für präzise 3D-Mikrofabrikation. Hohe Effizienz der Initiierung ist die wichtigste Eigenschaft eines effizienten PI. Basierend auf der potenten Leitstruktur 1,5-Bis(4-(*N,N*-dibutylamino)phenyl)penta-1,4-diin-3-on wurden mehrere aromatische Keton-basierte 2Pis synthetisiert, die Dreifachbindungen und Dialkylamino-Gruppen beinhalten und durch Sonogashira-Kupplung zugänglich sind. Der 2,7-substituierte Fluorenon-basierte PI **B3FL** besitzt den größten 2PA-Querschnitt von 440 GM bei 800 nm sowie das breiteste Prozessfenster der untersuchten PIs. Der Doppelbindungsumsatz des quervernetzten Polymernetzwerks und die mechanischen Eigenschaften der Mikrostrukturen wurden durch FTIR bzw. Nanoindentation gemessen.

Neben der Initiierungseffizienz der PIs stellen vom praktischen Standpunkt aus auch die Kosten und Einfachheit der Herstellung kritische Faktoren dar. Um das Problem der für die genannten 2PIs erforderlichen komplizierten Synthesen und teuren Katalysatoren zu überwinden, wurde eine Serie linearer und cyclischer Benzylidenketon-basierter 2PIs mit Doppelbindungen und Dialkylamino-Gruppen durch einstufige klassische Aldol-Kondensationsreaktionen synthetisiert. Die Ergebnisse quantenchemischer Berechnungen und experimenteller Tests legten nahe, dass die Größe des zentralen Ringes signifikanten

Einfluss auf die Energetik der angeregten Zustände, Quantenausbeuten der Emission sowie Effizienz der Zwei-Photonen-Initiierung. Der auf 4-Methylcyclohexanon basierende Initiator **M2CMK** ist weitaus effizienter als analoge Verbindungen mit fünfgliedrigem zentralem Ring. Das ideale Prozessfenster von **M2CMK** ist ebenso breit wie das von **B3FL**, die Synthese jedoch ist bedeutend einfacher. Die unkomplizierte Synthese verbunden mit hoher 2PA-Initiierungseffizienz macht diesen neuen Initiator zu einem vielversprechenden Kandidaten für die Kommerzialisierung.

Basierend auf den effizienten Kernstrukturen der cyclischen Benzylidenketone wurden analoge Carbonsäure-Natriumsalze für wasserbasierende Formulierungen hergestellt, um das Anwendungsgebiet der 2PP auf die Biofabrikation auszudehnen. Diese neuen wasserlöslichen 2PIs wurden in der Mikrofabrikation bei Schreibgeschwindigkeiten bis zu 100 mm/s innerhalb hydrophiler Polymere mit bis zu 50 wt% Wasser eingesetzt. Vorläufige Studien zur Zytotoxizität der 2PIs im Dunklen wurden durchgeführt und die erhaltenen Ergebnisse wurden mit denen von Irgacure 2959 verglichen, dem in der Zellverkapselung am häufigsten eingesetzten PI.

Der zweite Teil der Arbeit betrifft ein neues Arylazid das für Multi-Photon induziertes Photografting (MPG) benutzt wird, ein mächtiges Werkzeug in ortsbezogener 3D-Funktionaliserung. Als ''Proof-of-Concept'' wurde das kommerzielle aromatische Azid **BAC-M** erfolgreich innerhalb einer 3D-Matrix mit hoher Auflösung durch Drei-Photonen-Anregung gegraftet. Um die Grafting-Effizienz zu erhöhen und die benötigten Energien zu senken, entwickelten wir eine Serie neuer 2PA-aktiver Fluoraryl-Azide die ''push-pull''-Strukturen beinhalten. Gewünschte Funktionalitäten wie Alken- und Alkin-Gruppen wurden in den terminalen Amino-Gruppen eingeführt um eine Postmodifikation nach dem Zwei-Photonen-Photografting zu ermöglichen.

Acknowledgement

Table of Content

Introduction

The theory of the simultaneous two-photon absorption (2PA) by the same molecule was first predicted by M. Göppert-Mayer (1906-1972) in her doctoral dissertation at Göttingen University in 1931 (**Fig 1**).[1] However, due to the high photon intensities needed, no 2PA had been experimentally confirmed until the advent of the laser in the beginning of 1960s. In 1961, with a continuous-wave (CW) laser which provided sufficient intensity to drive 2PA, the first observation of 2PA induced frequency-upconversion fluorescence in a CaF_2:Eu^{2+} crystal sample was reported by Kaiser and Garrett.[2] Although 2PA was applied in some selective fields since then, its applications had been limited for many years due to the high intensities required and the relatively low 2PA activity of most materials.[3] Such sticky situation has been dramatically changed with the advent of relatively simple, solid-state femtosecond (fs) lasers in the late 1980s and early 1990s. The advantages of high monochromaticity, large peak power, and tunability of coherent radiation from various types of laser devices have led to an explosion of interests in all types of 2PA and multi-photon absorption (MPA) processes.[4]

Fig 1 Göppert-Mayer and part of the front page of her doctoral dissertation[1]

In contrast to one-photon absorption (1PA) process, in which a molecule obtains energy for electron transition through linear absorption, 2PA, the third order optically nonlinear process, basically requires simultaneous absorption of two photons to impart enough energy to drive a transition mediated by a so called "virtual state", a state with no classical analog (**Fig 2**).[5] If the two photons are of the same energy (frequency), the process is called degenerate 2PA. On the other hand, if the two photons are of different energy (frequency), the process is non-degenerate 2PA.[6] Usually, most 2PA applications have been concentrated on the degenerate 2PA process.
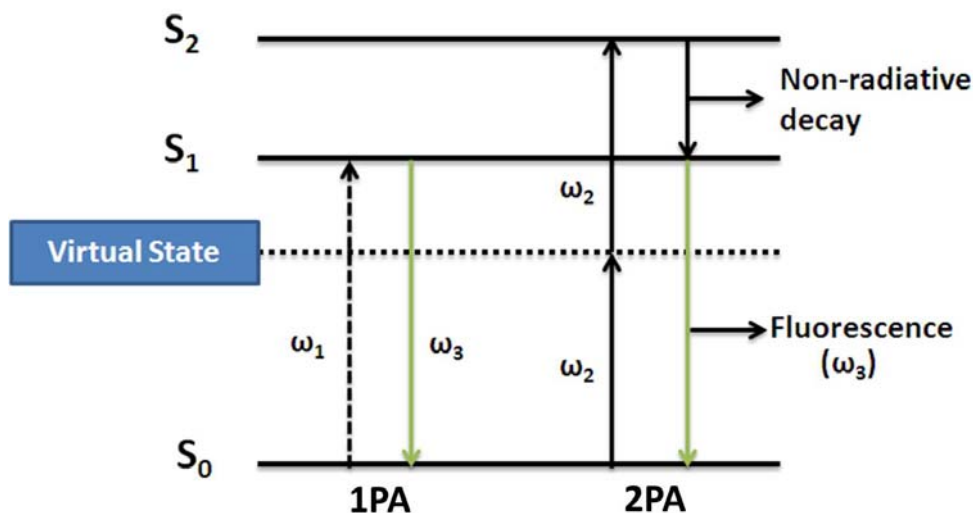
Fig 2 Simplified Jablonski scheme showing 1PA and degenerate 2PA excitation process. S_0, S_1, and S_2 are ground state, one-photon-allowed, and two-photon-allowed excited states, respectively; ω_1 and ω_2 are incident light frequencies and ω_3 is fluorescent emission frequency.[5]

The selection rules of 2PA are different from those of 1PA. For non-centrosymmetric molecules, the excited states reached via 1PA can also be achieved by 2PA (although some states might not be allowable for either or both of the processes). For a centrosymmetric chromophore, the lowest electronic state accessible through 2PA usually lies at higher energy than the 1PA-allowed state. After a rapid non-radiative decay from S2 to S1 (picosecond timescale), various photophysical and photochemical processes would start.[7] The most important pathway for photoinitiators is intersystem crossing (ISC) from excited singlet state to excited triplet state, which is usually the active state of the initiators to produce radicals or ions for initiating the polymerization. Other main photo processes include energy or electron transfer and upconversion fluorescence.[8]

Two-photon absorption is a nonlinear optical process connected with the imaginary part of the nonlinear susceptibility. Under the electric field E, the polarization of a material is described by the following equation:

$$P = \chi^{(1)}E + \chi^{(2)}E^2 + \chi^{(3)}E^3 + \cdots$$

(1)

where $\chi^{(1)}$, $\chi^{(2)}$ and $\chi^{(3)}$ represent linear, second-order and third-order optical susceptibilities, respectively. Since the even-order susceptibilities like $\chi^{(2)}$ and $\chi^{(4)}$ make no contribution in the resonant processes, the nonlinear absorption is described by the

imaginary parts of $\chi^{(3)}$, $\chi^{(5)}$, of which typical effects are two-photon and three-photon absorptions, respectively. Particularly for degenerate 2PA, the energy absorption rate is:

$$\frac{dW}{dt} = \frac{8\pi^2\omega}{c^2n^2}I^2Im[\chi^{(3)}]$$

(2)

Where ω is the incident light optical frequency, c the speed of light in vacuum, n the refractive index, I the intensity of the light and $Im[\chi^{(3)}]$ the imaginary part of the third-order susceptibility. Eq. 2 indicates that 2PA rate is quadratically dependent on the light intensity. 2PA cross-section, σ, currently the most popular parameter used to evaluate the activity of a 2PA chromophore, is defined by

$$\frac{dn_p}{dt} = \sigma NF^2$$

(3)

where N and n_p are the number density of absorbing molecules and number of absorbed photons, respectively, and F=I/hω denotes photon flux. According to Eq.2, the 2PA cross-section is:

$$\sigma = \frac{8\pi^2 h\omega^2}{c^2n^2N}I^2Im\,[\chi^{(3)}]$$

(4)

The relationship of molecular two-photon absorption coefficient, β (cm/GW) and σ can be expressed as follows:

$$\beta = \sigma N_A d_0 \times 10^{-3}$$

(5)

N_A is Avogadro's number, and d_0 the concentration in moles. The SI unit for σ is named Göppert-Mayer (GM), after the Nobel-laureate physicist, and defined as $1\,GM = 10^{-50}\,cm^4\,s\,photon^{-1}$. It should be kept in mind that σ only responds to the absorption behavior of a 2PA active molecule similar to ε of 1PA in Lambert Beer's Law.

Currently the most popular two methods to determine the σ^{2PA} value are two-photon excited fluorescence (TPEF) and z-scan analysis. Due to the high sensitivity of TPEF, only small amount of chromophores in dilute solution is needed for the fluorescence measurement. However, the test solutions must be photoluminescent.[9] Therefore, such measurement is quite suitable for 2PA fluorescent dyes but no for some efficient 2PA photoinitiators, which usually have very low fluorescence quantum yields. Z-scan analysis could effectively solve the fluorescence-less problem but high concentrated

solutions are needed to increase the sensitivity of the measurement.[10] Therefore, the selection of the testing methods depends on the specific applications. Direct comparison of the obtained σ^{2PA} values to ones reported in the literatures is rather complicated, since even with the same method to test the same compound, different measuring conditions and calculations often lead to different results.[11]

Due to the square dependence of light intensity, 2PA induced physical processes or chemical reactions can be localized with high spatial resolution, down to ~60 nanometers (nm), which is inaccessible with classical 1PA techniques because of the diffraction limit of the laser beams. **Fig 3** showed a visualized comparison of one- and two-photon excitation.[12] The dilute fluorescent dye solution was excited either with an ultraviolet lamp of 380 nm (1PA) or with a Ti:S laser of 760 nm (2PA), respectively. 1PA excitation induces a stream of emission with an hour-glass shape along the entire optical path through the solution. The linear absorption behavior in 1PA complies with Lambert Beer's law. However, 2PA excitation produces a very sharp fluorescent dot because only the volume within the focal point could provide enough energy to induce 2PA of the fluorescent dye.
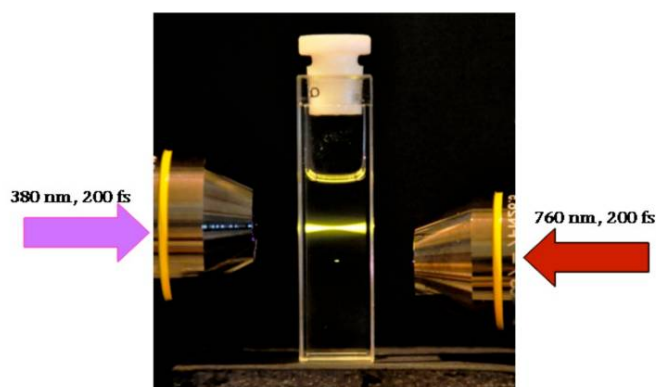
Fig 3 One-photon (left arrow) vs. two-photon (right arrow) excitation, showing the high 3D spatially localized excitation in 2PA in a solution of a fluorescent dye.[12]

Additionally, with a femtosecond laser pulse, the time for transferring energy from photons to a molecule is much shorter than that for energy transfer from electrons to the lattice, or for molecule/atom oscillations via photon emission. Therefore, 2PA is a heat insulation process.[13] Moreover, the wavelength (700-1000 nm) of the excitation source lies into a transparent region for many engineering materials and tissues, meaning that a femtosecond laser beam can penetrate deeply into the transparent materials and realize desired functions in three dimensions (3D).[14]

Above distinct characters of 2PA make it quite versatile in various fields. Some important applications include **two-photon excited fluorescence microscopy** (**2PM**) and **optical power limiting**, which are mainly based on physical change under two-photon excitation. Other applications, such as **2PA therapy**, **two-photon uncaging** and **two-photon polymerization** (**2PP**) are based on two-photon induced chemical reactions.

After the first demonstration from Denk *et al.*,[15] **2PM** has become a powerful fluorescence imaging tool that allows imaging of living tissue with a high depth up to about one millimeter. The basic principle of 2PM involves the simultaneous absorption of two photons of a dye molecule, which subsequently relaxes from the excited state to the ground state via emitting fluorescence. The fluorescence is collected by a detector to form a 3D image. Besides deeper tissue penetration, 2PM provides dramatic improvement on the signal-to-background ratio and therefore a much better resolution compared to standard confocal microscopy with visible light. Selection of suitable dyes enables the visualization with different colors (**Fig 4**).[16] TPM has been successfully commercialized in recent years.
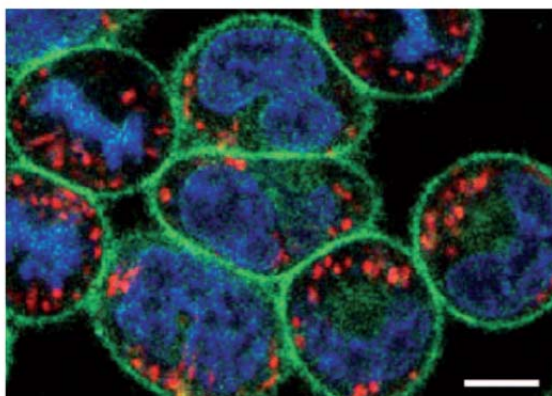
Fig 4 Two-photon confocal microscope images of fibroblast cells using fluorescent stains for DNA.[16]

Optical power limiting refers to an intensity-dependent absorption behavior of a material. Such a material, like a shutter, is transparent to low-intensity light but becomes opaque to light with high intensity (**Fig 5**).[17] The main mechanisms for optical-power limiting involve excited-state absorption (ESA) and nonlinear scattering.[9] The effect could be used for protection of delicate sensors from lasers, for optical telecommunications to remove intensity spikes and for protective goggles.[9]
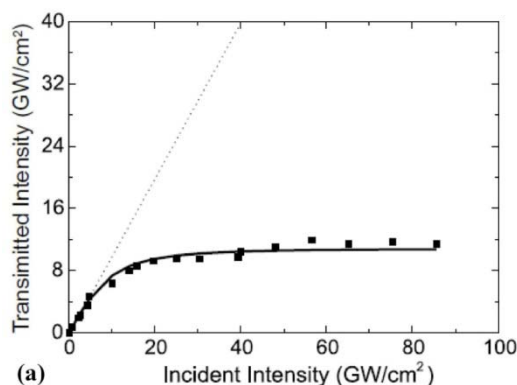
Fig 5 Transmitted intensity versus incident intensity showing an output saturation due to 2PA[17]

Photodynamic therapy (**PDT**) is a promising noninvasive treatment for cancer and nonmalignant tumors. The mechanism involves the photo activation of a non-toxic photosensitizer, preferentially taken up by the target cells/tissue, which subsequently generates high cytotoxic reactive oxygen species to selectively destroy tumor cells/tissue (**Fig 6**). Two-photon PDT was conclusively demonstrated for the first time by Wachter and co-workers in 1997.[18] The highly confined 3D excitation region and deep tissue penetration give two-photon PDT advantage over the traditional PDT.[19] Efficient two-photon PDT requires a photosensitizer with large two-photon cross section combined with high quantum yields for the generation of toxic singlet oxygen. Some promising photosensitizers have been developed with dual capability of two-photon PDT and two-photon imaging, which allows imaging-guided therapy.[20]
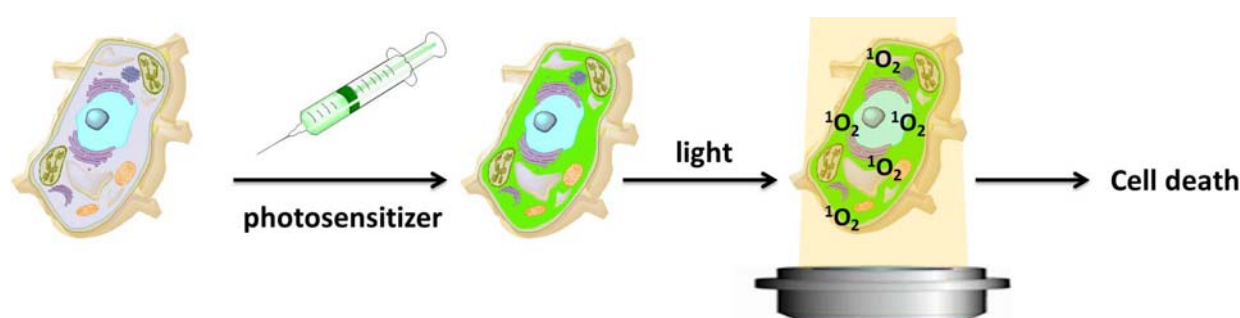
Fig 6 Scheme for Photodynamic therapy (PDT)

Photouncaging, also known as photocleavage, is a light-activated process of releasing a "caged" molecule with desired functions from a caging group to generate an active molecule. Two-photon uncaging provides substantially improved spatial resolution and penetration over conventional methods due to the nonlinear absorption behavior (**Fig 7**). Caged substances include ions, second messengers, amino acids and fluorescent dyes.[21]

Such a general and economical way for spatially confined photolysis of caged compounds has been widely used to control biochemical activity as well as neural activity.[21]
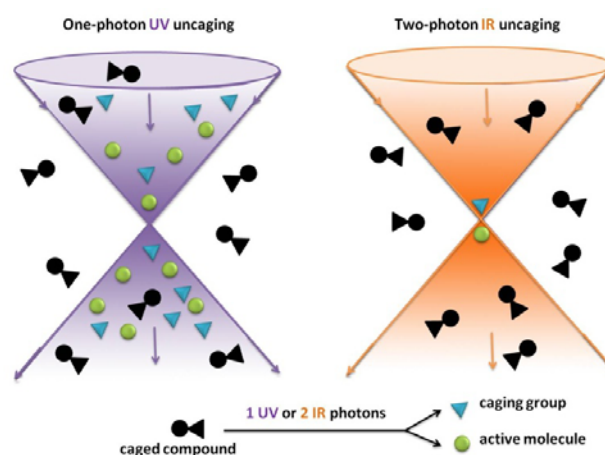
Fig 7 Scheme for photouncaging under one-photon (left) and two-photon (right)[22]

2PP is a solid free-form fabrication technique where a photoactive resin, containing mainly a photoinitiator (PI) and multifunctional monomers, is polymerized within the focal point of a femtosecond pulsed laser. Compared to traditional fabrication methods mainly based on layer-by-layer assembling due to the limited penetration of the UV light, 2PP with near infrared light enables directly fabrications of internal structures point-by-point (**Fig 8**).[23] Therefore, 2PP is a real 3D structuring process. Additionally, 2PP provides excellent spatial control due to the confinement of the photo-activated polymerization within the focus, making such technical especially suitable for various applications requiring 3D structures with resolutions in the (sub)micrometer range, such as electronic and optical micro devices,[24] photonic crystals,[25] microfluidics channels,[26] and polymer based optical waveguides on integrated circuit boards.[27] Moreover, the wavelength of the excitation source falls into the biological tissue transparency window (700-1000 nm), allowing deeper tissue penetration and less photodamage.[20] Therefore, 2PP has been also widely used in many biological applications like biofabrication of hydrogels.[28]
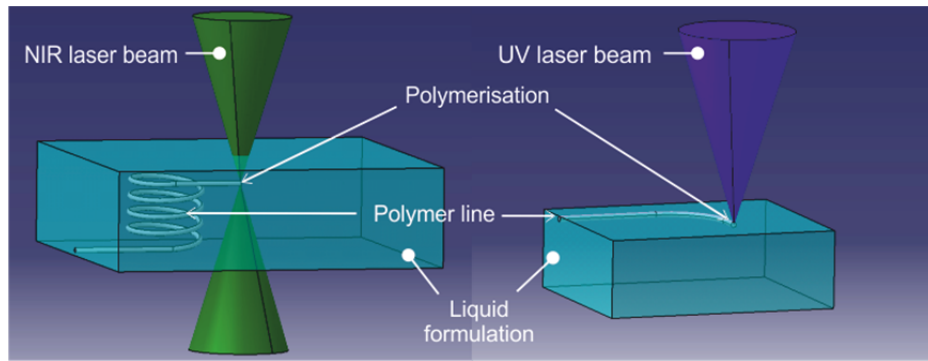
Fig 8 Comparison of 2PP (**left**) and 1PP (**right**) techniques[23]

Fig 9 shows a typical setup for 2PP.[23] A mode-locked Ti:sapphire laser, generally with tens or hundreds of femtoseconds pulse duration and a center wavelength at about 800 nm, serves as an excitation source. When passing through an acusto-optic modulator (AOM), laser beams are diffracted, leading to strong zero- and first-order waves. The zero-order wave is dumped, and the first-order wave, which is turned on and off by switching the AOM, is guided into the optical path of the system. The light intensity can be adjusted via a λ/2 waveplate combined with a polarisation dependent beam-splitter. A microscope, which allows rapid switching of the objectives, focuses the beams into a chamber containing photopolymers. The chamber is placed on a computer-controlled stage which can precisely move in 3D relative to the focal point of the laser beams; an alternative is to use scanning mirrors to realize 3D movement of the focus relative to the chamber. A CCD camera can simplify the positioning of the sample and make it possible for online observation in real time. The whole system is based on an optical table with an air friction damping in order to suppress vibrations.
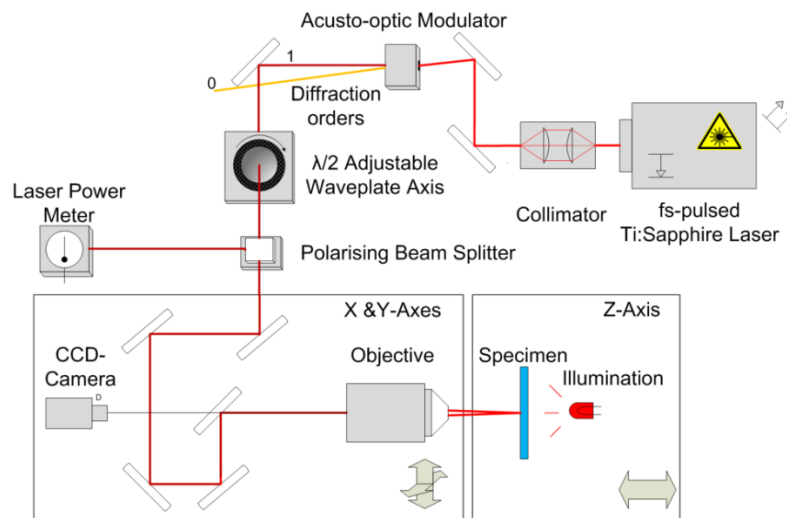
Fig 9 Setup scheme for 2PP[23]

Fig 10 illustrates the whole 2PP fabrication process.[23] It starts with the generation of a computer-aided-design (CAD) model of a 3D object (**Fig 10a**), which is subsequently sliced into a series of 2D layers along the z-axis (**Fig 10b**). A sliced layer is fabricated by photopolymerization along the scanning paths of a laser beam. A further layer is then polymerized over the previous solidified lower layers after translating the position of the focus along the z-axis (**Fig 10c**). Such process repeats continuously until the designed object with desired 3D shape is obtained. After the fabrication, uncured liquid resins are rinsed away by using proper solvent droplets to develop the final 3D microstructures (**Fig 10d**).[29]
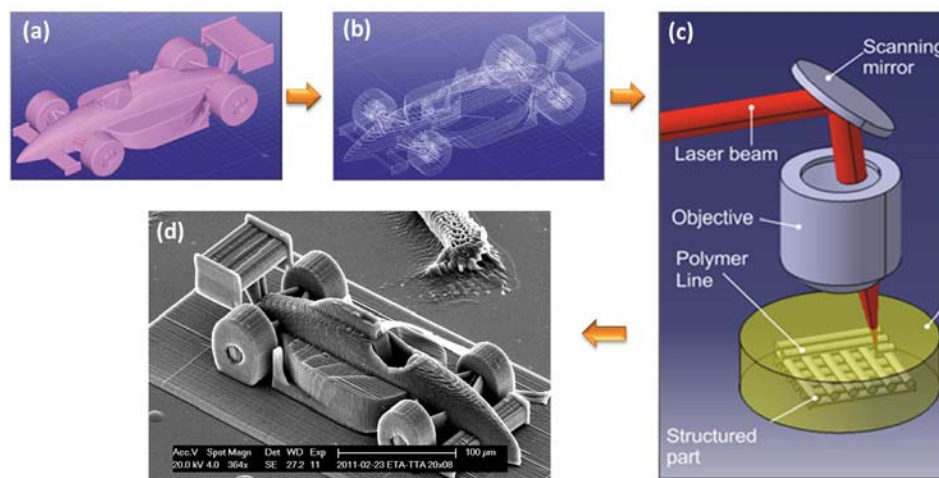
Fig 10 2PP fabrication process[23]

One important concern of 2PP is the highest resolution determined by a voxel, the smallest volumetric unit. The size and shape of a voxel could be accurately measured via an ascending scan method.[14] In this technique, a series of voxels are fabricated under identified conditions except with different heights ranging from submerged within the substrate to suspend above it. Truncation happens when the laser is focused too near the substrate surface (**Fig 11a** and A, B in **Fig 11b**); however, when the laser was focused too far above the substrate, the formed floating voxels would be washed away during developing (G in **Fig 11b**). Voxels with appropriate height, which are only loosely attached to the substrate, would topple over after washing (D, E, F in **Fig 10b**), giving a clear perspective of its true size and shape (**Fig 11c**).
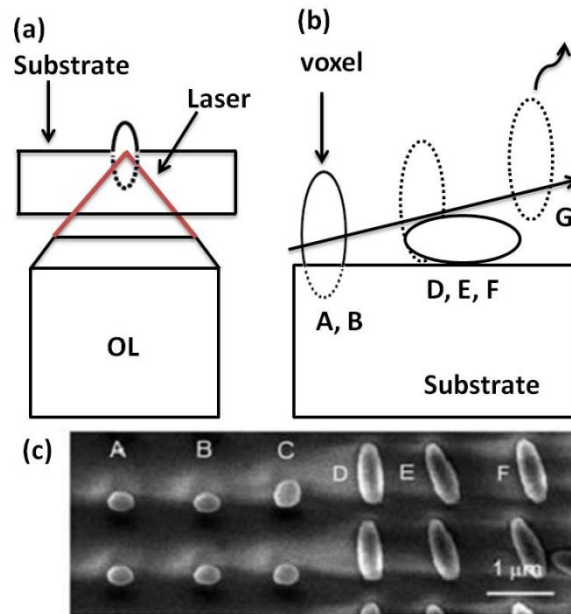
Fig 11 Schematic ascending scan method for achieving isolated and complete 3D voxels. (a) laser beam focusing that illustrates the substrate truncation effect, (b) voxels formed at different focusing level and (c) SEM image of voxels[14]

Voxels are generally ellipsoidal with two minor axes perpendicular to the optical axis which are about 3-5 times smaller than the major axis.[30] This shape is determined partially by the point-spread function of the light intensity near the focus. The smallest individual voxel under 800-nm excitation was 100 nm in diameter. Such value is considerably better than that predicted by the diffraction limit.[31] **Fig 12** shows the relationship of the polymerized volume, the voxel size and the laser intensity.[32] Photopolymerization occurs as soon as the density of active radicals exceeds a certain minimum concentration (P_{th}), but the fabricated structure is destroyed when the radical concentration is too high or thermal induced damage (P_{dam}) due to the high photon density. The size of voxel fabricated with laser intensity closed to P_{th} is smaller than that with higher energies. Using advanced techniques such as addition of radical quenchers[33] or repolymerization techniques,[34] it is even possible to improve the feature resolution to 65 nm and 22 nm, respectively.
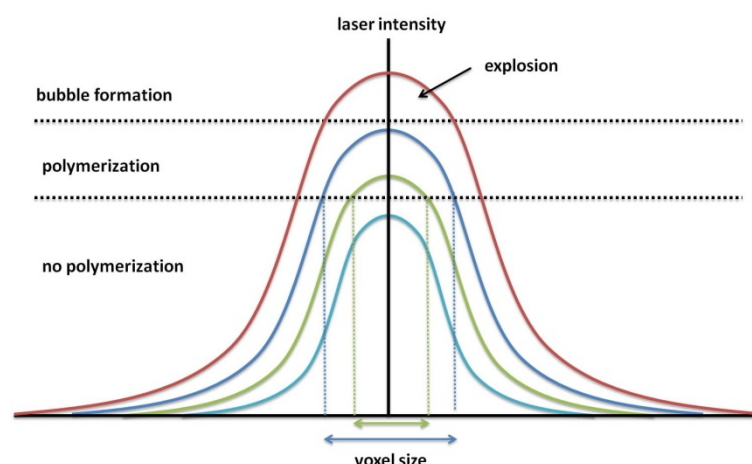
Fig 12 Relation between polymerized area, voxel size, and laser intensity[32]

Unlike TPM, which have been successfully commercialized and widely used in bioimagining, currently 2PP are mainly limited to academic research. In order to push 2PP into the market it is especially important to shorten the structuring time while maintaining the high resolution to obtain a higher throughput for mass production.[35] Therefore, high-power lasers are needed for fast writing speed. Further, lasers with high output intensities allow multipoint fabrication method in which the beam is split by using a microlens array to realize the simultaneous fabrication of periodic structures in a highly parallel fashion.[36]

On the other hand, a photoactive formulation, which mainly include multifunctional monomers and a PI, need to be optimized. Due to the accessibility, some efficient UV curing resins with premixed UV photoinitiators are directly applied in 2PP (**Table 1**). Most of the resin systems contain acrylate moieties, which would undergo free radical polymerization initiated by a proper photoinitiator. Acrylic resins have many attractive properties such as high activity, wide commercial availability and ease of handling.[31] SCR500, which contains a mixture of urethane acrylate oligomers and two type I UV photoinitiators (Irgacure 369 and Irgacure 184), is one frequently used acrylic photoresist in 2PP.[37] The main drawback of the acrylate formulation is the shrinkage after polymerization and during the developing process,[31] which would significantly reduce the fabrication accuracy.

One solution to address the shrinkage issue is to use SU-8, the most widely used epoxy photoresist in 2PP.[38] The resin composes eight epoxy groups per monomer and a triaryl sulfonium salt as a photoinitiator. The photoinduced cleavage of the photoinitiator

releases a strong Brønsted acid to initiate cationic polymerization of the epoxy groups. Since SU-8 remains a solidified state before and after laser exposure, the defects induced by the liquid-to-solid transition during the fabrication process could be minimized.[5] SU-8 is widely used for the fabrication of high-aspect-ratio structures. The handling of SU-8 generally requires additional processing steps like pre- and post-baking.[39]

Another strategy to reduce the shrinkage is to use the inorganic-organic hybrid photoresist ORMOCER, mainly based on sol-gel chemistry.[40] The resin has an inorganic (-Si-O-Si-) backbone functionalized with organic groups such as acrylates.[41] Such silicate-based materials can provide smooth 3D microstructures without shrinkage and deformation, making it quite suitable for making precise optical elements such as waveguides and photonic crystals.

Table 1 Common commercial resins used for 2PP[32]

Resin	Type of materials	Handling	Type of curing	Provider
SCR500	Urethane acrylate	Use directly	Free radical	Japan Synthetic Rubber Co.
Ormocer	Inorganic-organic hybrid	Use directly	Free radical & Sol-gel	Fraunhofer Institute Silicatforschung
IPG	Inorganic-organic hybrid	PI added	Free radical & Sol-gel	RPO. Inc
LN1	Urethane acrylate	PI added	Free radical	Sartomer
Nopcocure 800	Acrylic acid ester	Pre-exposure	Free radical	San Nopco
SU-8	Epoxy	Pre- and post-bake	Cationic	MicroChem
IP series	Inorganic-organic hybrid	Use directly	Sol-gel	Nanoscribe GmbH

Since the mentioned photopolymers are initially designed for the polymerization under one-photon excitation, their performance in 2PP is still limited. Recently, some real commercially available photoresists (IP-L (780), IP-G (780) and IP-Dip) for 2PP have been provided by Nanoscribe GmbH, Germany.[42] In combination with Nanoscribe's laser

lithography systems, the microstructures fabricated with these liquid and sol-gel negative-tone photoresists exhibit high resolution and high mechanical stability. The main drawback of the premixed commercial resins is that the specific composition is unknown; therefore the degree of freedom to adjust the formulation is limited.

Custom-made resins allow customers freely adjusting the formulation (different types of monomers, initiators and additives and ratios between these components) according to specific applications. Custom-made approach requires adequate raw materials candidates in the toolbox for selection to obtain the desired properties. In general, the monomers suitable for UV curing are also applicable for 2PP. However, the commercial UV photoinitiators, which have poor 2PA performance (detailed discussion in the following section), cannot meet the requirement of 2PP, especially for mass production demanding fast curing speeds and high throughput. Since efficient two-photon initiators (2PIs) allows high writing speeds, a low polymerization threshold, and therefore high-quality structures, to develop highly active 2PIs and further to make them commercially available is essentially important.

Up to now, a full understanding of the relationship of the molecular structure and the 2PA initiation has still remained a big challenge. An ideal efficient 2PI should possess a large 2PA cross section combined with high initiation efficiency, just like for normal UV photoinitiators.

Although 2PA active organic dyes were first reported in 1963,[43] the systematic study on structure-property relationships for the rational design of 2PA chromophores appeared until 1997.[17] Since 2PA is driven by intramolecular charge-transfer,[4] the presence of electron-donor (D) and/or electron-acceptor (A) groups are required. The D and A groups can be attached at terminal or central positions of the core structures. A proper combination of these components leads to dipolar (asymmetric), quadrupolar (symmetric), or octupolar structures (**Fig 13**). Moreover, the extent (i.e., path length) of conjugation, which leads to states with extended charge separation, has been proved to be essential for enhanced 2PA cross section.[9] In addition, good coplanarity could facilitate the intramolecular charge transfer process.[4] Increasing the number of conjugation paths, or connecting several linear paths to form a two-dimensional (2D) or a three-dimensional (3D) configuration has also been shown theoretically[44] and experimentally[45] to greatly increase 2PA responses.
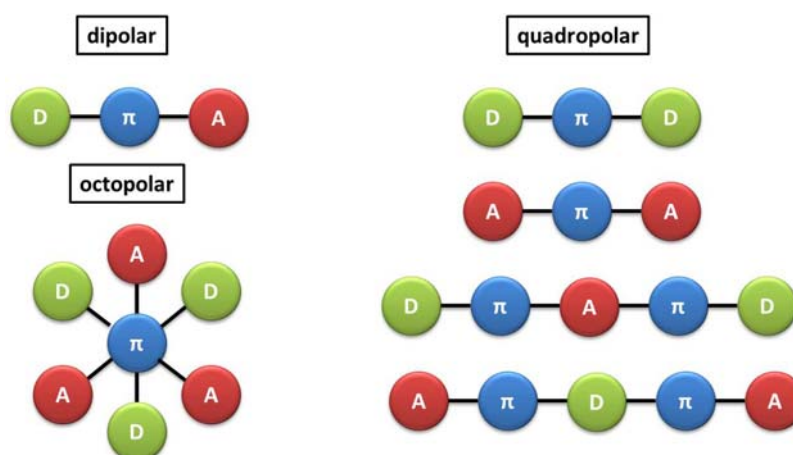
Fig 13 Schematics of various 2PA chromophores classified based on their substitution pattern (**D** = donor group, **π** = π-conjugated bridge, **A** = acceptor group)

A series of bis(styryl)benzene compounds listed in **Fig 14** clearly demonstrate the effect of the above factors on 2PA. Simple trans-stilbene compound **BS-1** only exhibits a small two-photon cross section of 12 GM at 514 nm, but the maximum two-photon cross section increase almost 10 times for its derivative **BS-2** with terminal dialkylated amino groups as electron donors.[17] A further enhancement was observed for **BS-3** when substituted the alkyl chains with diphenylamine moieties (also observed from **BS-8** to **BS-9**).[46] For electron donor groups, the disubstituted amino groups (dialkyl or diphenyl) are most popular choices due to their accessibility and the good balance between the oxidative stability and electron-donating capability of the amine.[4] N-substituted carbazoles[47] and pyrroles[48] could also serve as acceptable D groups.

When attaching nitrile groups as electron-acceptors to the central core to form a D-π-A-π-D structure, the 2PA cross section increases by almost a factor of two from **BS-7** to **BS-8**.[46, 49] Besides nitrile groups, the frequently used electron-withdrawing groups in 2PA include nitro,[50] sulfonyl,[51] triflyl (CF$_3$SO$_2$),[52] aldehyde (CHO),[53] phosphonate[50] and π-deficient heterocyclics,[54] as well as the related ionic analogues.[55]

Extension of conjugation length has a strong effect on 2PA. Extending the π-conjugated bridge leads to the enhancement of 2PA cross section, as shown for D-π-D chromophores from **BS-4** to **BS-6**. The value of σ^{2PA} increases from 230 GM to 410 GM going from 2 to 4 double bonds.[56] For longer chain lengths, σ^{2PA} is expected to approach saturation, because the terminal groups could become decoupled.[39] The prolonging conjugation length also results in a red shift of the 2PA peak. This shift allows chromophores to be optimized for different wavelengths, but the shifted 2PA spectra are not always desired

since it also leads to inefficient pumping at specific wavelength.[31] A similar trend is observed when the conjugation length increases from **BS-4** to **BS-7** by adding a phenyl unit.[46] Among various types of π bridges, ethynyl and vinyl groups are the most popular choices. Generally, triple-bond based systems are less conjugated than the corresponding double-bond based ones,[57] but this has little effect on 2PA.[9] The σ^{2PA} value of **BS-11** is only about 10% greater than that of **BS-13**.[58] However, for large molecules with steric congestion, such as meso-linked porphyrins, acetylenic systems tend to be more conjugated because the vinylene linker is prone to twist out of conjugation.[59] Moreover, the cis-trans isomerization of double bonds tend to attenuate the desired photochemical or photophysical processes.[60]
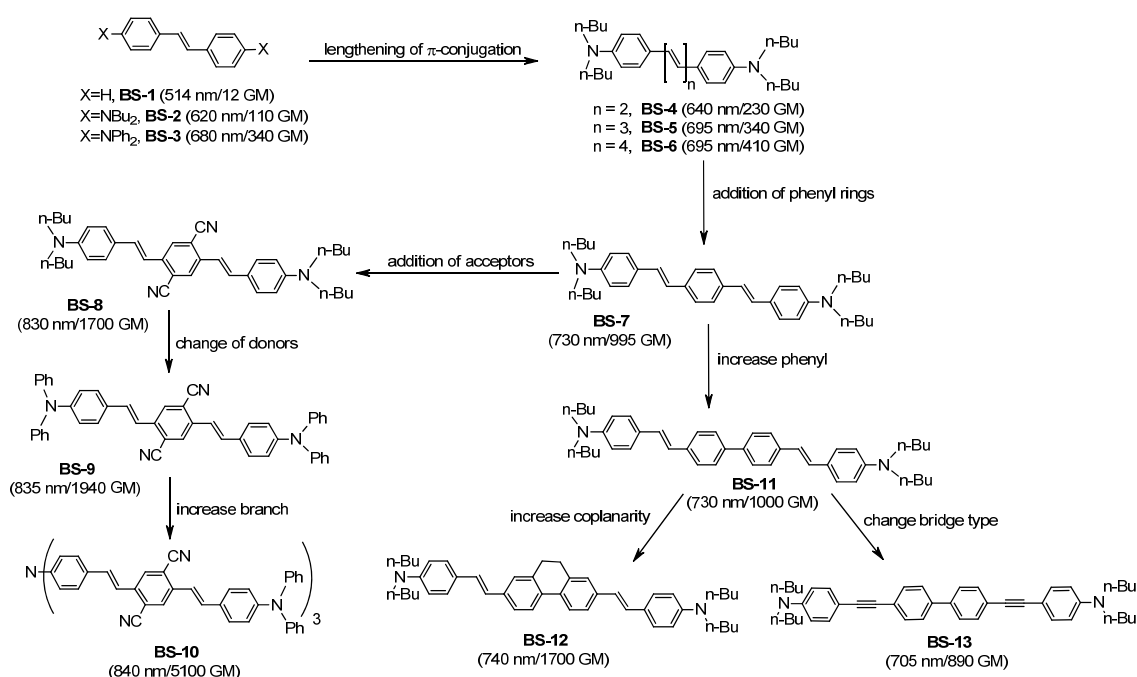
Fig 14 Structure-activity relationship results of bis(styryl)benzene-based compounds

A good planar geometry of a π system facilitates the electronic coupling and therefore maximizes π-orbital overlap to increase 2PA response. The σ^{2PA} of **BS-12** with rigid dihydrophenanthrene bridges increases by about a factor of 1.7 compared to that of **BS-11** with a flexible biphenyl bridge.[58] Therefore, fluorine, naphthalene and anthracene, which possess stereorigid carbon skeleton, are frequently used as π bridges to increase the coplanarity of the whole conjugated system.[31]

Increasing the dimensionality of the molecule via attaching multiple 2PA chromphores into a core is an effective strategy to obtained increased σ^{2PA}, as observed from **BS-9** to **BS-10**.[61] The enhancement is derived from the cooperative interaction between each arm

via electronic coupling or vibronic coupling.[62] A "saturation effect" is observed when increasing the number of arms.[63] Triphenylamine,[64] 1,3,5-triazine,[65] 1,3,5-trinitrilebenzene,[66] multi-annulene[67] and porphyrin derivatives[68] are frequently used candidates serving as a core.

Besides the above factors related to the intrinsic characters of the molecule structures, σ^{2PA} is more sensitive to the external microenvironment such as solvent polarity and hydrogen-bonding.[4] Generally the performance of a certain 2PA fluorophores is dramatically reduced in aqueous environment compared to in organic solvent.[69]

Although various 2PA active chromophores containing a planar π conjugated system with strong donor (D) and/or acceptor (A) groups have been synthesized within the last decade, most of these reported compounds are based on fluorescence dyes developed for imaging applications.[70] Therefore, despite high 2PA ability, only a few of these dyes are useful for 2PP due to their low photoinitiation ability.[71] Thus, it is of interest to develop novel efficient 2PIs possessing chromophores with high 2PA and chemical moieties which subsequently lead to efficient initiation for polymerization.

Objective

Two-photon photopolymerization has become a versatile technique for precise 3D microfabrications. An efficient 2PP process requires active 2PIs, which ensure high writing speeds, a low polymerization threshold and therefore high-quality structures. Previous work of our group has proven that 1,5-bis(4-(N,N-dibutylamino)phenyl) penta-1,4-diyn-3-one (**B3K**) containing a triple-bond π-bridge and a carbonyl group as electron withdrawing functional group serves as an efficient 2PI in comparison with typical one-photon UV PIs and other very potent 2PIs well known from the literature, such as E,E-1,4-bis[4'-(N,N-di-n-butylamino) styryl]-2,5-dimethoxybenzene (**R1**).[72] It is worth to mention that compared to **R1**, which shows strong fluorescence, the ketone-based PIs either show an undetectable or an extremely weak (Φem $< 5 \times 10^{-3}$) fluorescence emission. For efficient 2PIs, low fluorescence quantum yields are preferred as this is a requirement for a high population of the triplet state, which is usually the active state of the initiators producing radicals or ions for initiating the polymerization.
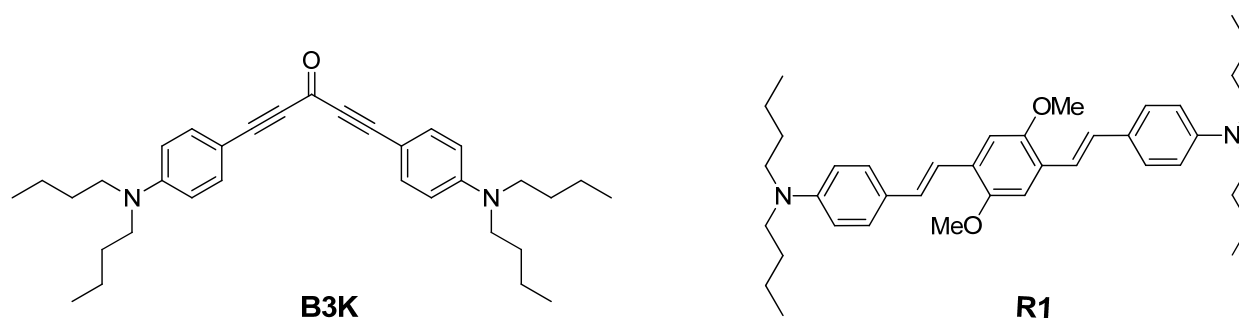
Based on the molecular structure of **B3K** containing triple bonds and cross-conjugated D-π-A-π-D lead structures, several aromatic ketone-based 2PIs, with expectation of strong 2PA due to the prolonged conjugation lengths and good coplanairties, should be investigated. Different aromatic ketones (benzophenone, fluorenone and anthraquinone) as acceptors in the central part of the π bridge and dialkylamino groups as electron-donor moieties can be used to study structure-activity relationships. Furthermore, the introduction of branched-alkyl chains at the end of the amino moieties should be considered for improved solubility.
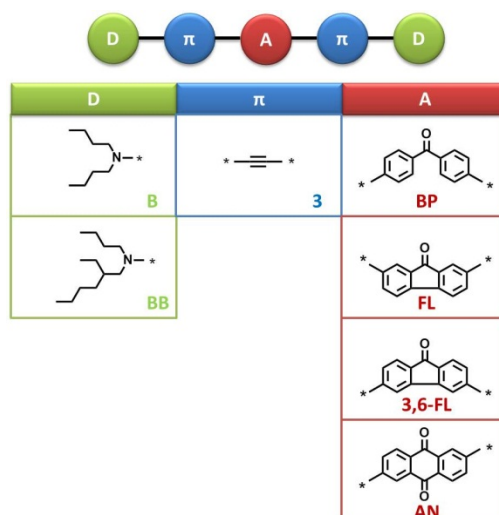
Beside initiation efficiency of 2PIs, the ease and cost of preparation are also critical factors from practical aspect. Aldol condensation has been proven to be a simple and economical synthetic route to prepare 2PA active benzylidene cyclopentanone compounds with D-π-A-π-D core structures. Since the size of the central ring significantly affects the photochemical and photophysical characteristics and thus the 2PA initiation efficiency, a series of linear and cyclic benzylidene ketone-based 2PIs containing double bonds and dialkylamino groups should be synthesized and their structure-activity relationships need to be systematically investigated to obtain efficient 2PIs.
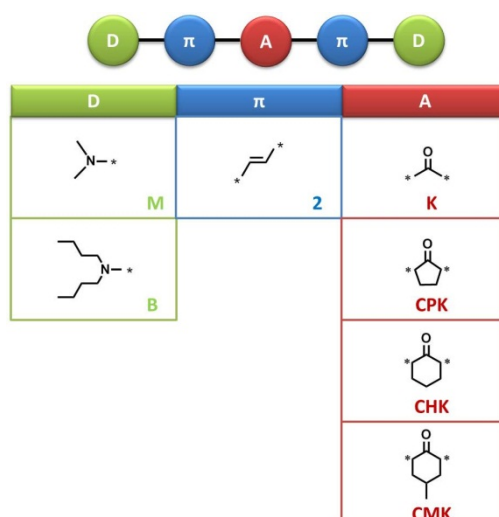
Furthermore, in order to expand the application range of 2PP to biofabrication, water-borne functionalities, such as carboxylic acid salts, should be introduced into the known core structures possessing high 2PA initiation efficiency to obtain efficient water-soluble 2PIs. The cytotoxicity tests of the hydrophilic 2PIs need to be performed since the project aims to realize the fabrication of 3D hydrogel scaffolds in the presence of the cells.

P2CK   FG= CH₂CH₂COONa

E2CK   FG= CH₂CH₂COONa
G2CK   FG= CH₂COONa
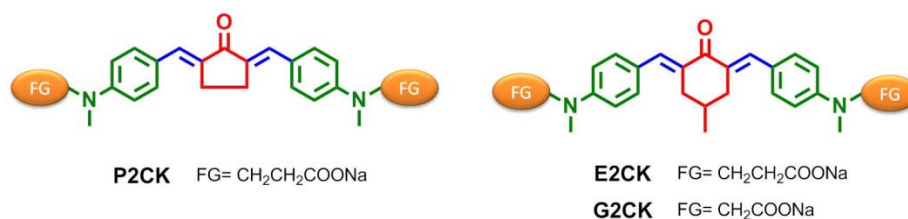
UV-vis absorption and emission measurements should be carried out to study the linear optical behaviors of the novel 2PIs. Moreover, two photon cross-section measurements via z-scan, as well as 2PP structuring tests need to be performed to evaluate the 2PA properties of the novel initiators.

Besides 2PP, another important application of multi-photon absorption (MPA) is multi-photon induced photografting (MPG), a powerful tool for 3D site-specific functionalization. Arylazides have been frequently used as efficient UV photografting agents to introduce functionalities onto the surfaces of the substrate. The concept should be transferred to 3D volumetric photografting under multi-photon excitation with a proper molecular design. To this end, commercial aromatic azides with long conjugation length, such as **BAC-M** with potentially strong MPA, should be investigated to prove the concept of MPG. Considering the inefficient 2PA of **BAC-M** at desired wavelength of 800 nm due to the absence of good electron donors, **AFA** series fluoroaryl azides with ''push-pull'' structures should be synthesized and investigated for enhanced grafting efficiency and reduced requiring energies. Moreover, desired functionalities, such as alkene and alkyne groups, should be introduced at the terminal amino groups for post-modification after MPG.
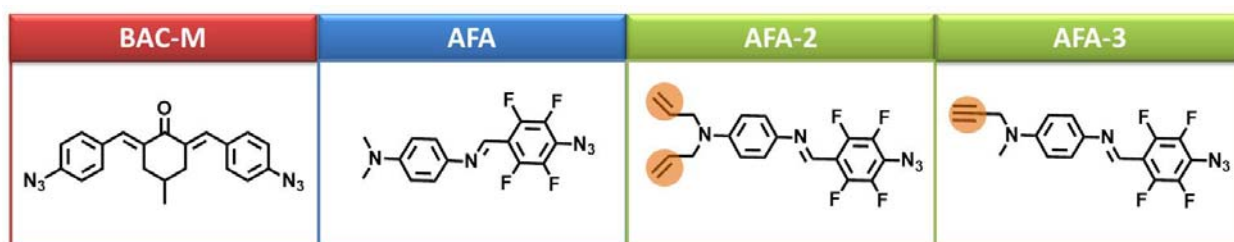
State of the art two-photon initiators (2PIs)

A 2PI is a photoactive molecule, which simultaneously absorbs two near-infrared photons upon nonlinear excitation to directly or indirectly generate free radicals or cations to induce the propagation of the monomers and finally realize polymerization. According to the difference of the initiating mechanism derived from the difference types of the active initiating species, 2PA photopolymerization are classified as 2PA free radical photopolymerization and 2PA cationic photopolymerization. Correspondingly, the 2PIs were classified into two types, namely free radical 2PIs and cationic 2PIs. Both types will be discussed in detail respectively.

Until now, most 2PP applications are based on free radical polymerization due to its ease of processing, fast polymerization rate and various selections of raw materials.[31] Therefore, major work has focused on the development of free radical 2PIs. Since high initiation ability is always the most important character for an efficient PI, to optimize the initiation systems for enhancing initiation efficiency has become the most popular direction of the development of the 2PIs. An ideal 2PI should have a large 2PA cross section at the desired wavelength to ensure sufficient efficiency of photon-absorption, high quantum yields of active radicals and high initiating efficiency of the formed radicals. Moreover, good compatibility of initiators with monomers and oligomers to ensure uniformly dispersion becomes important consideration. For efficient 2PP, a highly soluble photoinitiator of modest efficiency may be superior to a sparingly soluble initiator of high efficiency.

Some commercially available one photon radical PIs (**Table 2**), such as Irgacure 369[73] and Lucirin TPO-L[74], were used for 2PP at the initial stage. These Type I PIs undergo direct cleavage after 2PA to generate active free radicals to induce the polymerization (**Fig 15**). As these PIs have rather small σ^{2PA}, normally less than 40 GM,[75] and therefore poor absorption behavior, high excitation power and long exposure time, which often result in damage to the polymeric structures, are usually required. However, the limited 2PA cross section values of such photoinitiators are compensated by high quantum yields of radical formation to ensure acceptable initiation efficiency. These UV PIs are still being used in 2PP for practical reasons.
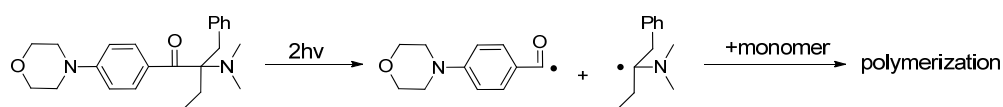
Fig 15 Photoinitiation mechanism of Irgacure 369[76]

Table 2 One-photon photoinitiators used in 2PP[77]

PIs	Chemical Structure	λ_{max} (nm)	σ^{2PA} (GM)
Irgacure 369		670	7
Irgacure 184		530	23
Irgacure 819		600	< 4
Irgacure OXE01		660	31
ITX		760	5
TPO-L		610	1.2

Incorporation of dyes as photosensitizers with commercial UV photoinitiators or amines as coinitiators is a practical method to increase the 2PA sensitivity. Belfield *et al.*[78] developed a commercially available 2PA photoinitiating system containing a visible light-absorbing dye 5,7-diiodo-3-butoxy-6-fluorone (H-Nu 470) and an arylamine N,N-dimethyl-2,6-diisopropylaniline. The proposed initiation mechanism involves an electron transfer from the amine to the dye under 2PA excitation, followed by proton transfer to generate active amine species to induce the polymerization (**Fig 16**). Adding a diaryliodonium salt as a coinitiator, the rate of polymerization can be accelerated by generating active phenyl radicals.[79]
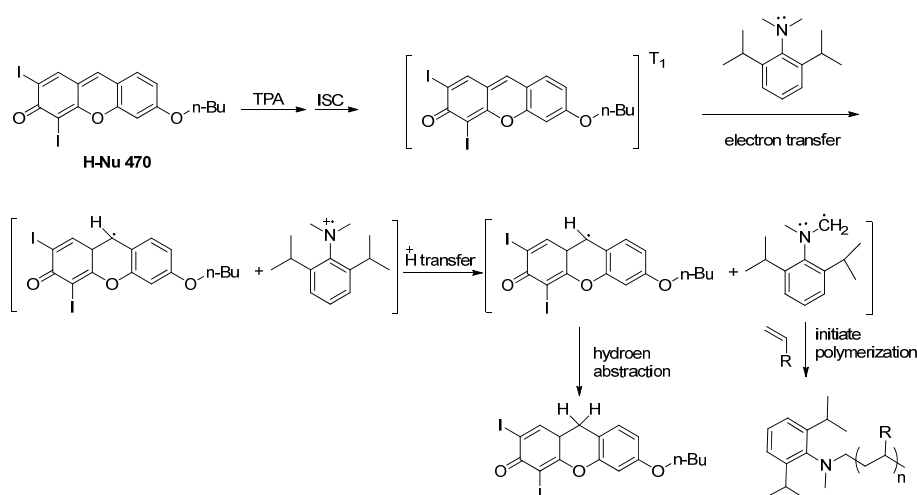
Fig 16 Initiation mechanism of dye/amine

Considering the 2PA cross section of fluorone dye is still limited, some real 2PA chromophores as photosensitizer were developed to increase the 2PA sensitivity of the initiation system.[80] In 2PA dye/amine system, both intersystem crossing quantum yield of the 2PA chromophore and the ability of hydrogen abstraction would affect the efficiency of the reaction. The hydrogen abstractability would be enhanced when the lowest triplet state T1 possesses a strong electronic n-π* feature.[81] However, chromophores with large 2PA cross sections usually comprise long conjugation length, which would extend the electronic delocalization and hinder the hydrogen abstraction process due to a concomitant strengthening of the π-π* character at the T1 state.[80] *Förster-type* energy transfer (ET) mechanism is one effective solution to such photophysical paradox. Fouassier *et al.*[82] reported a new photoinitiating system, where the two-photon absorption of a 2,7-bisaminofluorene moiety leading to the photoactivation of a camphorquinone subunit (**Jin 1**) through intramolecular energy transfer to induce polymerization in the presence of an amine as a coinitiator. The initiation efficiency of **Jin 1** is proved to be much higher than **Jin 0** which mainly undergoes electron transfer between the excited chromophore and monomers to generate active free radicals. Another method is introduction of a ketone moiety into a 2PA chromophore at a specific position. Malval *et al.* introduced a thioxanthone moiety into a 2PA chromophore with a chevron-shaped structure to prevent a total electronic delocalization and therefore enhance n-π* character at the T1 state (**Fig 17**).[80] High initiation efficiency was observed due to the improved hydrogen abstraction.
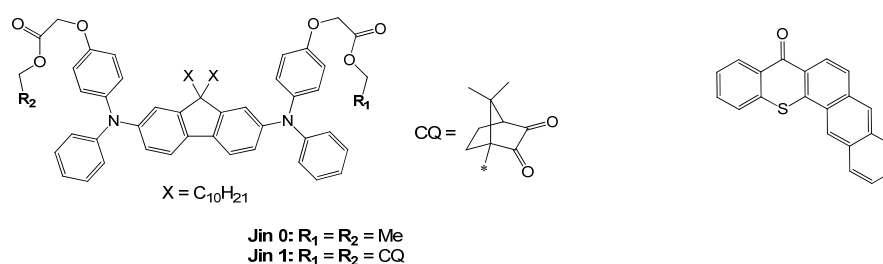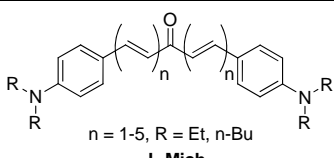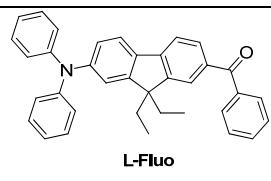
Fig 17 Chemical structures of 2PA dyes

The bimolecular systems suffer from some intrinsic limitations such as electron transfer efficiency between dyes and coinitiators or the back electron transfer, which would significantly decrease the initiation efficiency.

Until now, a full understanding of the relationship of the molecular structure and the two-photon initiation activity has still remained a big challenge. Fortunately, some core structures possess large 2PA cross section combined with high initiation efficiency have been reported thanks to the continuously theoretical and experimental efforts.[6, 9] Some "famous" examples, such as **fluorene**,[50, 78] **bis(styryl)benzene**,[72] **carbazole**[83] and **Michler's ketone**,[84] have been well summarized in Dr. Nicolas Pucher's PhD thesis.[85] More compounds are included in the reviews of Lin *et al.*,[86] Rumi *et al.*,[7] and Lee *et al.*[5] **Table 3** lists some representative core structures and the corresponding 2PIs.

Table 3 Representative core structures and the corresponding 2PIs.

Core Structures	2PIs
fluorene	
bis(styryl)benzene	
carbazole	

Michler's ketone	
Aromatic ketone	

All above 2PIs comprise dipolar or quadrupolar 2PA chromophores containing planar π systems with long conjugation length and strong donors and/or acceptors. The formation of the desired planar π systems usually requires multi-step synthesis and expensive catalysts. For example, double bonds are commonly introduced into existing π systems as bridges to extend the conjugation length. The desired products have mostly been realized by classical Wittig[87] or Horner-Wadsworth-Emmons (HWE) reaction[84] of non-commercial Wittig or HWE salts with corresponding aldehydes under strong alkaline conditions. A subsequent isomerization reaction with traces of iodine is generally required to convert undesired *cis* isomer to the desired trans product.[88] Another method to make double-bond bridges is the Heck coupling reaction, a palladium-catalyzed reaction of aryl halides with terminal alkenes.[89] The main drawback of the Heck coupling is the high price of palladium catalysts and difficulties associated with catalyst recycling.[90] Although quite common, double bond containing 2PIs tend to be less efficient than analogous triple-bond based PIs due to the deactivation derived from potential photoinduced *cis-trans* isomerization.[60] The Sonogashira coupling reaction is often employed to introduce alkyne groups into the backbone of the PIs under ambient condition with high yields.[91] Similar to the Heck reaction, such palladium-catalyzed coupling of aryl halides with terminal alkynes suffers from high costs. The needs for expensive catalysts or additional synthetic steps result in restrictively expensive 2PIs, which has been obstructive for the development of the promising 2PP technology.

To this regard, the core structure based on **benzylidene cyclopentanone**[92] (**Fig 18**) is particularly attractive because the formation of such D-π-A-π-D conjugated system is straightforwardly realized by aldol condensation with commercial precursors with low price. Such series of compounds could be used directly as 2PIs, but much higher activity was observed when used as photosensitizers in combination with 4,4'-dimethyl-diphenyliodinium hexafluorophosphate (Omnicat 820) in 2PP. In case of the usage as

photosensitizers, an enhanced performance was achieved when incorporating a coumarin-based moiety, which boosts the 2PA cross section and photosensitizing quantum yields.[92d] Interesting, the substitution position of the coumarin moieties has significant effect on the 2PA performance.[92c] Although **3-DAC** exhibits much larger 2PA cross section than **4-DAC**, the photosensitizing efficiency of **4-DAC** is higher than that of **3-DAC**. The results of electrochemical experiments indicated that the enhanced sensitizing efficiency of **4-DAC** derived from a lower electron transfer free energy with Omnicat 820. In order to increase the 2PA sensitivity, a multi-branched benzylidene cyclopentanone dyes with a triphenylamine core were synthesized.[92b]
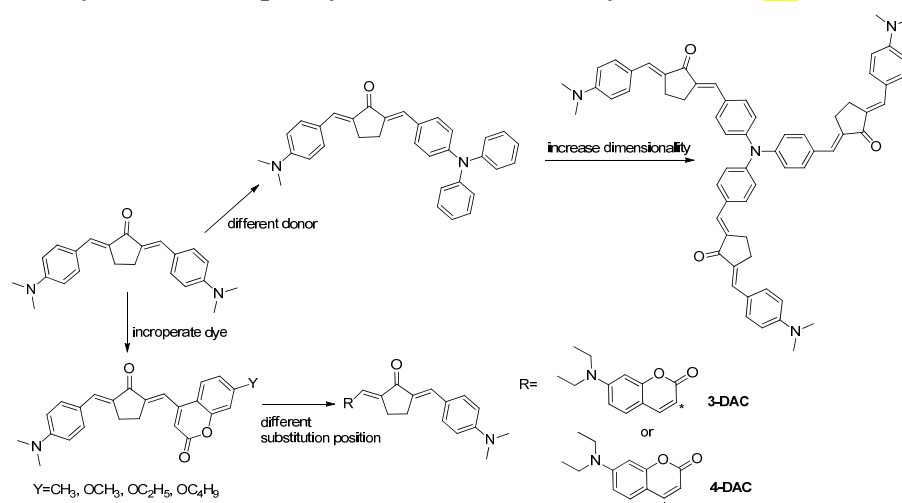
Fig 18 Structures of benzylidene cyclopentanone-based compounds

The proposed initiation mechanism of the 2PIs involves a two-photon induced intermolecular electron transfer from photoexcited chromophores to the functional monomer which produces a radical anion responsible for the subsequent polymerization (**Fig 19**).[93] Additionally, an intramolecular charge transfer (intra-CT) state in the excited state (intra-exciplex) is also proposed to be the precondition for the photopolymerization.[94] In the intra-exciplex, π-bridge becomes more electron-rich and the complex is prone to transfer its electron to the surroundings. Therefore, the initiation efficiency is not only associated with 2PA, but also the efficiency of electron transfer from the excited state of the initiators to the monomers.[93]
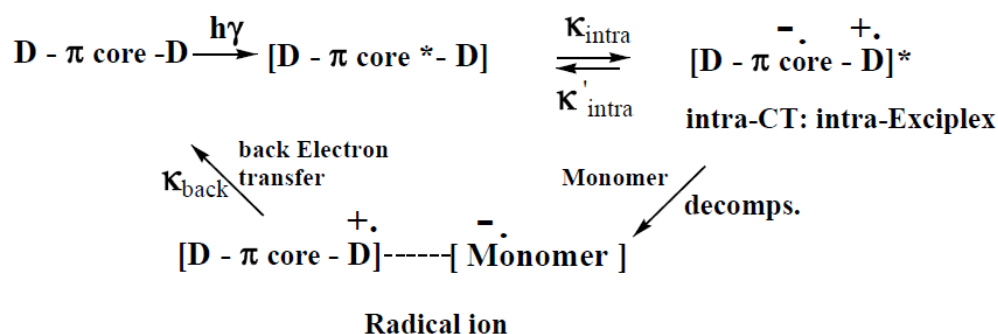
Fig 19 Intra- and intermolecular transfer process of common 2PIs from literature[94]

Similar to dye/coinitiator system, the initiation efficiency of such bimolecular photoreaction is limited due to the electron back process, especially in the viscous formulation. Some effective strategies to prevent electron back transfer, such as photoinduced cleavage,[95] have been widely used in UV curing. With a proper molecular design, these concepts should be transferred to 2PIs for improved initiation efficiency. Very recently, Farsari's group reported a series of novel cleavable 2PIs based on acylo-phosphine oxides (**Fig 20**).[96] The 2PIs with "push-pull" structures were straightforwardly synthesized in two steps with high yields. However, due to the lack of double/triple bonds as π bridges, the maximum σ^{2PA} among the investigated 2PIs is only 9 GM at 800 nm. The poor 2PA leads to high required laser powers of 20-40mW and low writing speed of 20 μm/s. As a side note, the strong absorption at about 400 nm might make these PIs promising candidates for photopolymerization with LED light (395 nm).
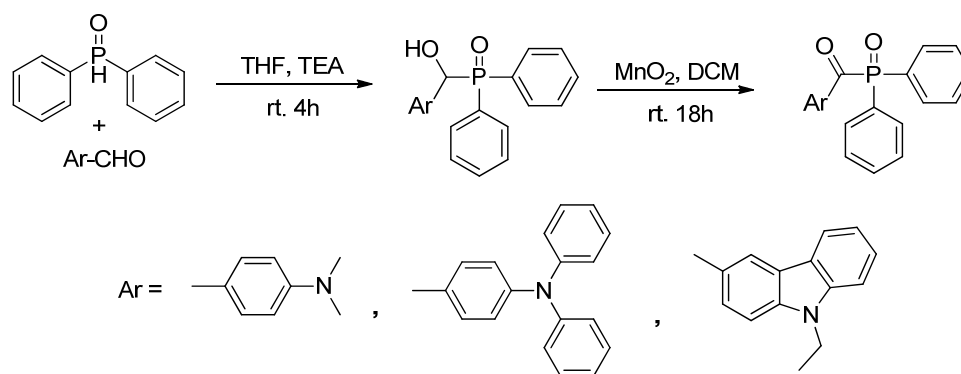
Fig 20 Synthesis scheme and structures of novel acylo-phosphine oxides

What should be kept in mind when designing a cleavable 2PI is that the extended conjugation can strengthen the π-π* character with detriment of the n-π* feature. The reduced population of n-π* state would significantly decrease the cleavage efficient to generate active radicals for the polymerization. Alternative initiation mechanism based

on photoinduced reduction of the metal species has been proposed. Kabouraki *et al.* reported on an organic-inorganic composite material, in which one of the components, a vanadium metallo-organic complex, initiates the polymerization under multi-photon excitation.[97] The involved vanadium (V) triisopropoxide oxide acted simultaneously as an inorganic network forming molecule and a radical supplier. The initiation process involves the self-generation of radicals via three-photon induced intramolecular reduction of the metal species from vanadium (V) to vanadium (IV). Spangenberg *et al.* demonstrated a new class of free radical 2PIs based on a cationic silver (I) complex incorporating 4,4'-diaminostyryl-2,2'-bipyridine derivatives (**DES**) as ligands.[98] The coordinated silver cation facilitated the intramolecular charge transfer process, which enhanced the σ^{2PA} of the complex with respect to that of the free ligand. The proposed mechanism involved the silver cation-promoted formation of radical cations (DES$^{\bullet+}$) under 2PA, which acted as an hydrogen abstractor and subsequently interacted with N-methyldiethanolamine (**MDEA**) to generate α-aminoalkyl radicals to induce the polymerization (**Fig 21**).
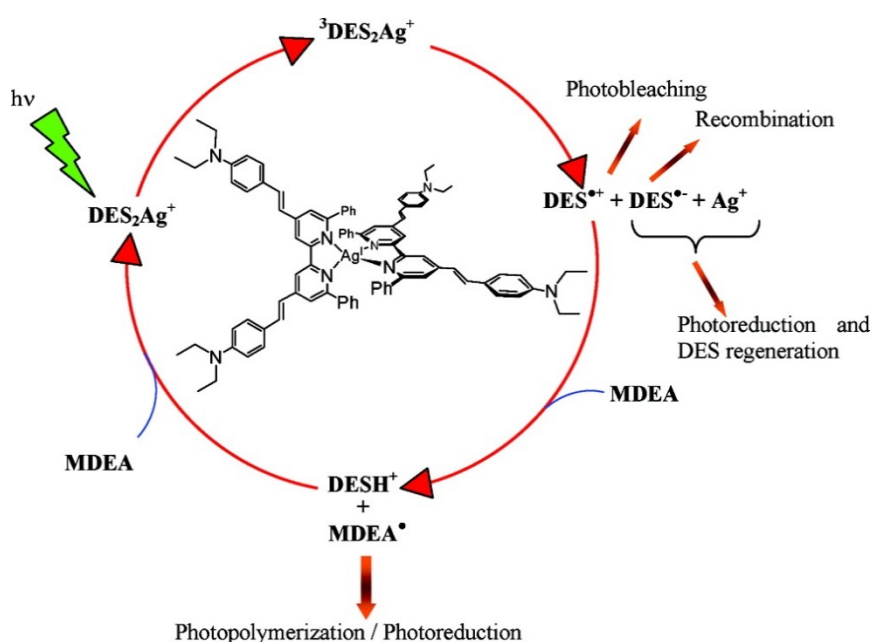
Fig 21 Initiation mechanism of the silver (I) complex[98]
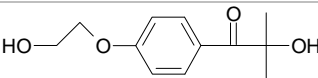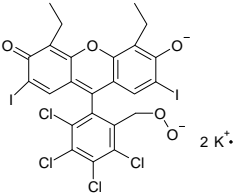
Besides increasing the initiation efficiency, another direction for the development of 2PIs is to tailor the properties of PIs for specific applications. One important functionalization is to increase the hydrophilicity of 2PA initiating systems for microfabrication of 3D scaffolds used in tissue engineering research. Originally commercial UV photoinitiator Irgacure 2959 was used for 2PP due to its reasonable hydrophilicity and low
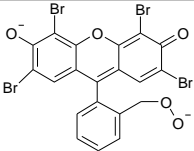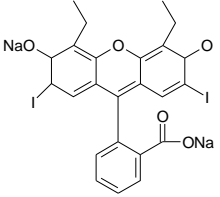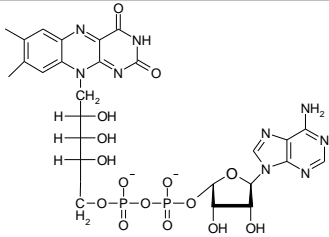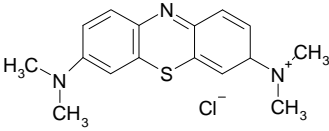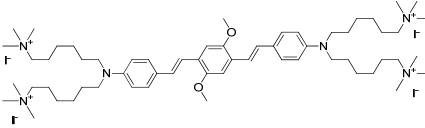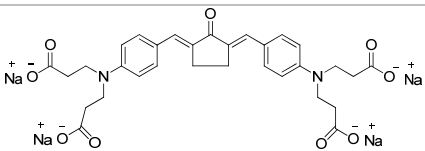
cytotoxicity,[99] but this initiator is only suitable with a 515 nm pulse laser, which tends to increase the risk for denaturing surrounding proteins.[100] Another strategy developed to improve water solubility of commercially available, hydrophobic initiators is based on the assistance of nonionic surfactants. Jhaveri *et al*. increased the water solubility of commercial hydrophobic initiators (Irgacure 651 and AF240) using a nonionic surfactant (Pluronic F127).[28] Though this approach facilitates the fabrication of hydrogel structures within an aqueous formulation via 2PP, large amounts of surfactant are needed to ensure adequate initiation efficiency and cell lysis becomes a concern.

Until now, the most popular hydrophilic initiation system for 2PP is a dye-amine combination. Due to suitable absorption at desired wavelength and easy accessibility, commercial hydrophilic xanthene dyes, such as rose bengal, eosin and erythrosine, were applied in 2PP with amines as co-initiators (

Table 4).[101] In this initiation system, the dye is excited by 2PA and subsequently intermolecular electron transfer followed by hydrogen transfer from the amine to the excited dye generates active amine radicals to induce polymerization.[102] The main drawbacks of such initiation system are the requirement of high laser intensities (~100 mW) and long exposure times (300–400 μs) due to the small 2PA cross section of the dye.[69] Additionally, some intrinsic limitations derived from bimolecular systems, such as electron transfer efficiency between dyes and coinitiators or the back electron transfer, would significantly decrease the initiation efficiency.[103] Rational design of unimolecular hydrophilic chromophores possessing high 2PA activity would effectively overcome these drawbacks. However, true water-soluble 2PIs are still very rare.

Table 4 Structure and σ^{2PA} (at 800 nm) of water-soluble 2PIs

Water-soluble initiator	σ^{2PA}	Chemical Structure	Monomers
Irgacure 2959[99]	N		Modified Gelatine
Rose Bengal[101a]	10		Firbinogen Fibronectin Concanavalin A BSA Cytoplasmic proteins

Eosin Y[101a]	10		Lypholized BSA
Erythrosin[101a]	10		
Flavin adenine dinucleotide (FAD)[104]	0.035		BSA
Methylene blue[105]	N		BSA Lypholized BSA
WSPI[106]	136		PEGDa
BSEA[69]	287		PEGDa

Some hydrophilic dyes, such as rose bengal[102a] and methylene blue[105, 107] can also be used to directly crosslink proteins under two-photon excitation. Since the protein itself fulfills the role of coinitiator and crosslinker at the same time, triethanolamine is not required and in fact appears to act as an inhibitor. Protein crosslinking without a coinitiator is believed to occur in one of two ways, both of which involve excitation of the dye to the T1 state. The excited dye can either abstract hydrogen directly from a protein molecule to induce protein crosslinking, or transfer energy to the ground state triplet molecular oxygen, producing singlet molecular oxygen.[102b] In the singlet oxygen mechanism, the active oxygen species continues to react with an oxidizable amino acid residue to generate an electron-deficient protein that may react with another protein's amino acid residue to form a covalent bond. The probability for this reaction depends on the type of amino acid residues on proteins. Protein crosslinking is thus different from a polymerization process. Two radicals have to be formed by 2PA to make one crosslink,

which makes the process rather inefficient compared to chain growth 2PP of synthetic materials. Furthermore, though Campagnola *et al*. improved rose bengal and benzophenone initiation adding coinitiators to form one molecule,[108] the 2PA activity of the dyes remained low. As a result, the fabrication process still requires very long exposure times and high energies.[28]

Since a full understanding of the relationship of molecular structure and two-photon properties still remains a big challenge, the most effective way to produce efficient water-soluble 2PIs is to introduce water-borne functional groups, such as quaternary ammonium cations[109] or carboxylic sodium salts,[70] into the known core structures possessing high 2PA initiation efficiency. One successful example is a distyrylbenzene chromophore with quaternary ammonium cations (**WSPI**), which has been proven to be a potent hydrophilic 2PI and was used to fabricate 3D hydrogel scaffolds in the presence of a living organism.[106] Following the same strategy, Wu's group reported a benzylidene cyclopentanone dyes with hydrophilic sodium carboxylate group at the terminal alkyl chains.[69] They applied the molecule alone or as sensitizer combined with triethanolamine for 2PP under aqueous condition. The same group also reported a series of polyethylene glycol-functionalized benzylidene cyclopentanone dyes.[110] Compared to the ionic water-borne moieties such as quaternary ammonium cations or carboxylic acid sodium salts, the nonionic functionality is non-pH influenced and the formation of the insoluble salts could be avoided when different sorts of cations exist in the same system. Although the cyclopentanone dyes with polyethylene glycol moieties were applied in two-photon excited photodynamic therapy, high initiation efficiency is expected due to the core structures possessing high 2PA activity.

Overall, compared to the development of the hydrophobic 2PIs, the optimization process of the hydrophilic 2PIs is still at a much slower pace. The reported water-soluble 2PIs definitely could not meet the rapidly growing demands of various biological applications. Therefore, to develop efficient 2PIs with good biocompatibility (excellent hydrophilicity and low cytotoxicity) will be a hot research topic in the near future.

Another important modification is to optimize 2PA initiating systems to obtain high spatial resolution, the main concern of 2PP. Since the popular applications of 2PP are based on free radical photopolymerization, in material aspect, active free radicals are determinative for the obtained lateral spatial resolution. The behaviors of the free radicals

are mainly influenced by laser intensity and exposure time. A low laser intensity combined with a short exposure time would generate free radicals in a more confined region and reduce the number and diffusion of the generated radicals. Using a highly active 2PI (**BPDPA**), Xing *et al.*[111] realized a single line writing with a lateral resolution of 80 nm using a laser power of 0.80 mW and a linear scan speed of 50 μm/s (**Fig 22**). Theoretical calculations indicated that dramatically better lateral resolution can be obtained with more efficient 2PIs and reduced laser power.
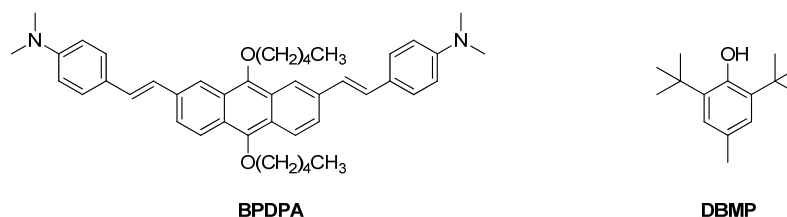
Fig 22 Structure of active 2PI and inhibitor

Another effective strategy to improve the spatial resolution is to use a radical quencher. When dynamic processes such as diffusion of radical and quencher are considered, free radical quenchers would effectively eliminate the diffused free radicals for a tighter confinement. With optimized concentration of quencher **DBMP** (**Fig 22**), less than 100-nm-width line in 2PP was achieved.[112] Nearly 20% improvement of the fabrication accuracy would reduce the dimension of polymerized objects in principle by the same percentage.[113]

In order to obtain a significant confining effect, a large amount of radical quenchers, compared to that of photoinitiator, were needed. Moreover, the intermolecular radical-quench reactions are intrinsically limited by diffusion. To overcome these problems, Duan's group[114] designed a functionalized molecule (**BNMBC**) by introducing a radical quenching moiety p-methoxybenzyl (**PhOMe**) to a reported efficient 2PI (**BNBC**) (**Fig 23**). Due to the high initiation efficiency and effective confining effect of radical diffusion, the volumes of polymer fibers fabricated by 2PP using **BNMBC** as a photoinitiator were 20%-30% smaller than those with **BNBC** as a photoinitiator. The covalent linking of the radical quenching group has also been proven to be more effective in quenching reactions when compared to the results of the formulation with physical mixture of the same molar ratio of the radical quencher.
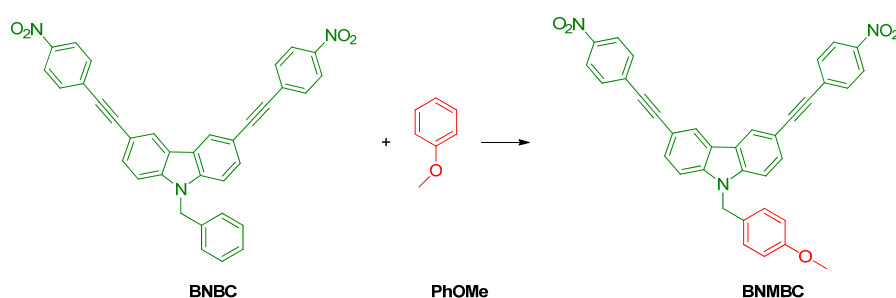
Fig 23 Synthesis scheme of **BNMBC**[114]

The addition of radical quenchers, however, could induce an increasing threshold in the 2PP. Another disadvantage of the quenching effect was the low mechanical strength of polymerized structures due to their short chain lengths.[112] Very recently, Sakellari *et al.*[115] proposed a new quench strategy based on a mobile amine monomer which would not only quench the radicals generated by excited photoinitiators but also react with other monomers to maintain the mechanical stability of the structure. By this method, woodpile structures with interlayer period 400 nm were fabricated. It is worth to mention that intrinsically low scan speed (20 μm.s^{-1}) is needed to allow diffusion of the quencher monomer into the writing area to ensure the impressive resolution. Using a faster diffusing quencher or a multiple scanning strategy might address the low writing speed issue.

Another "state-of-the-art" technique to improve the resolution of 3D lithography is stimulated-emission-depletion (STED). In STED, two laser beams are needed; a first laser with short pulse is used to bring fluorescent molecules to their excited state. Before fluorescence and ISC occurs, a second laser generally with longer wavelength to avoid one photon absorption is used to deplete the excited electronic state. The intensity and the wavelength, as well as the time delay of the depletion pulse significantly influence the deactivation efficiency.

Another important factor for efficient STED is the selection of the photoinitiator. The required photoinitiator should have large oscillator strength between the S_0 and the S_1 state and long lifetime of the singlet excited state, as well as good photoinitiation ability. Commercial cleavable photoinitiators used for 2PP, such as Irgacure 369,[116] Irgacure 1800,[116b] Irgacure 819,[116b] Darocur TPO[116] have been proven not suitable for STEP due to their inherently low oscillator strength of n-π* transition and short lifetime of the excited state.

The Type II photoinitiator isopropylthioxantone (**ITX**) has been successfully applied in STEP by Wegener *et al*,[116b] but further report from the same group pointed out that other mechanism rather than STED is the main depletion pathway.[117] Later, a better candidate (7-diethylamino-3-thenoylcoumarin) (**DETC**) (**Fig** 24) has unambiguously been shown to support STED. **DETC** has a large oscillator strength of 40550 L.mol^{-1}.cm^{-1}, which is comparable to the green-emitting fluorescent dyes. Besides as a triplet sensitizer, **DETC** can also be used as photoinitiator with low fluorescence quantum yields. Since keto-coumarins with various absorption and emission properties have been well developed, such series of compounds would become promising candidates for future optimized STED photoinitiators.

DETC   **MGC.HCl**
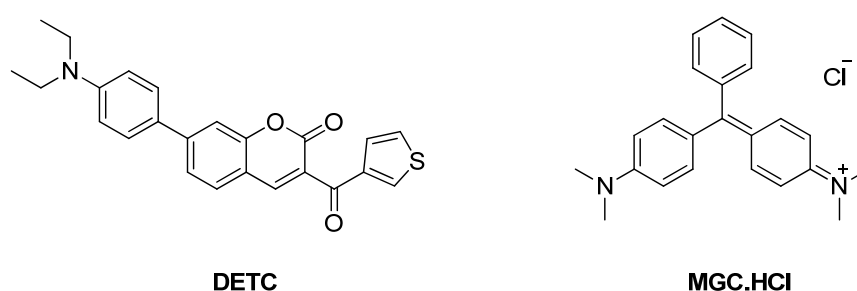
Fig 24 Structures of photoinitiators used in STEP and RAPID

Besides keto-coumarins, some special cationic dyes like **MGC.HCl** (**Fig** 24) have also been used in STEP experiments.[118] Interestingly, when tuning the pulse delay from 0 to 13 ns between the two beams, which should affect the inhibition in STEP, no significant effect was observed. The result was ascribed to the depletion of an intermediate state with longer lifetime, which is yet to be determined. The authors named this insensitive to pulse delays method resolution augmentation through photo-induced deactivation (RAPID). The intermediate with long lifetime allows the use of a much cheaper continuous-wave (cw) laser for depletion and makes a precise timing between excitation and depletion pulses unnecessary.[119]

The main disadvantage of STED and RAPID is the complicated laser setup required to provide very accurate beam control. Until now, only few research groups can implement such advanced technique.[116]

Beside 2PA induced free radical photopolymerization, another method for polymerization induced by 2PA is cationic photopolymerization. In this process, the photoinitiator undergoes homolytic cleavage under irradiation and generates strong Brønsted acid for initiating the polymerization. Although the majority of studies on 2PP

are based on free radical polymerization of (methyl) acrylates, cationic photopolymerization of epoxides and vinyl ethers exhibits some features important for microfabrication. One great advantage is the low shrinkage after polymerization, which facilitate repeatability for 3D writing.[14] The employed epoxide-based photoresists ease the developing process of complicated internal structures due to the low viscosity. In addition, the sensitivity of cationic polymerization to oxygen is much less than radical polymerization.[7] Photo acid generators (PAGs) can also realize the 2PA microfabrication in positive-tone resists, which promise to be a useful way to fabricate 3D microfluidic devices.[120]

As with free radical polymerization, some well-established one-photon PAGs were originally used under two-photon excitation conditions. For example, the commercially available diaryliodonium salts (**p.1**) (**Fig 25**), with 2PA cross section of only 16 GM under 530 nm,[77] was used to fabricate microstructures of lines in commercial diepoxide resins (Sartomer K-126) under 775 nm/150 fs excitation.[71] The main drawback of such system is the limited polymerization rate due to the low 2PA cross section of the onium salt. One method to improve 2PA sensitivity is to combine the 2PA sensitizers, such as coumarin **DEDC** (**Fig 25**),[121] with a commercial PAG with high quantum efficiency. The acid formation usually proceeds via photo-induced electron transfer (PET) from the excited sensitizer to the PAG.[122] However, the efficiency of the transfer process in bimolecular system is intrinsically limited by diffusion. In addition, the 2PA cross sections of the above sensitizers are still relatively small, thus high excitation energies are required.
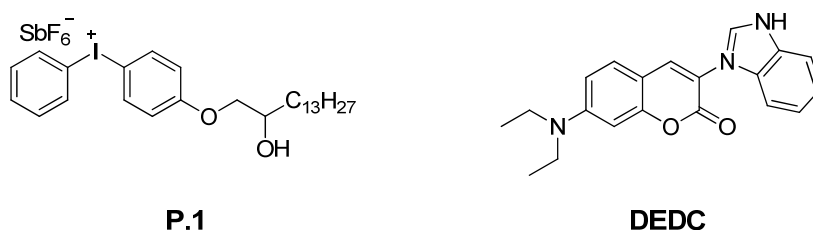
Fig 25 Strucutes of commercial diaryliodonium salts and 2PA sensitizers

An alternative to the bimolecular method is the integrated approach, which is based on the introduction of an acid-generate functionality into a two-photon active chromophore. Such strategy was firstly exemplified by Perry's group.[120] They reported a novel 2PA PAG, labeled **BSB-S2** (**Fig 26**), in which the sulfonium moieties were covalently attached to a bis[(diarylamino) styryl]benzene core. Such PAG exhibits both a large two-

photon absorption cross section of 690 GM at 710 nm and a high quantum yield for the photochemical generation of acid (φ_{H^+} = 0.5). The 2PA sensitivity of **BSB-S2** is nearly one order of magnitude greater than that of widely used commercial PAGs. Belfield's group developed a microwave-assisted method to form sulfonium salts, which contain fluorene as the core structure and stilbene motifs (2- and 7-positions) to extend the π-conjugation (**11**).[123] Although the molecular architecture of these sulfonium salts are similar to **BSB-S2** (A-π-A) and the 2PA induced intramolecular PET process is proposed to form acid, the quantum yield for acid generation significantly drops. Jin *et al*. assumed that the reduction of acid generation efficiency might be caused by the substituted position of the sulfonium moieties.[124] To verify such hypothesis, they designed and synthesized two positional isomers of a 4-alkoxystilbene substituted with a methyl (p-cyanobenzyl) sulfonium group (**EtO-PS** and **EtO-MS**) (**Fig 26**). The results demonstrated that a para-to-meta substitution of the sulfonium group strongly influences the photodissociation efficiency of the PAGs and leads to an increase of the quantum yield for acid generation by a factor of 2.4. This substantial effect was well corroborated by the increasing activity in cationic photopolymerization. Interestingly, the position of the sulfonium moiety hardly affects the two-photon absorption properties of these push-pull chromophores.[124]
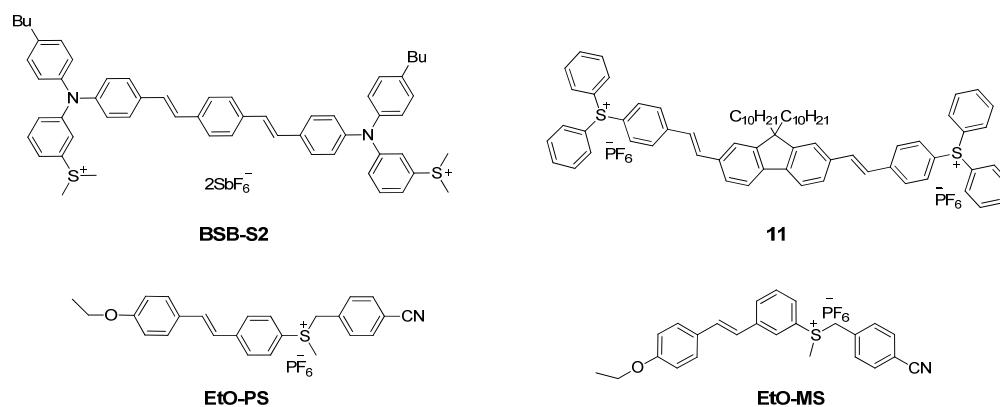
Fig 26 Strucutes of sulfonium salts as 2PA PAGs

Ober's group developed a series of non-ionic PAGs for two-photon lithography (2PL).[125] The improved solubility was achieved by introducing flexible joints between 2PA chromophores and photocleavable groups. In contrast to the ionic counterparts, those non-ionic PAGs were efficient in TPL for cationic as well as free radical induced microfabrication. However, relatively small 2PA cross sections (below 12 GM at 800 nm) required the addition of 2PA sensitizer **AF-69** to increase the 2PA sensitivity (**Fig 27**).
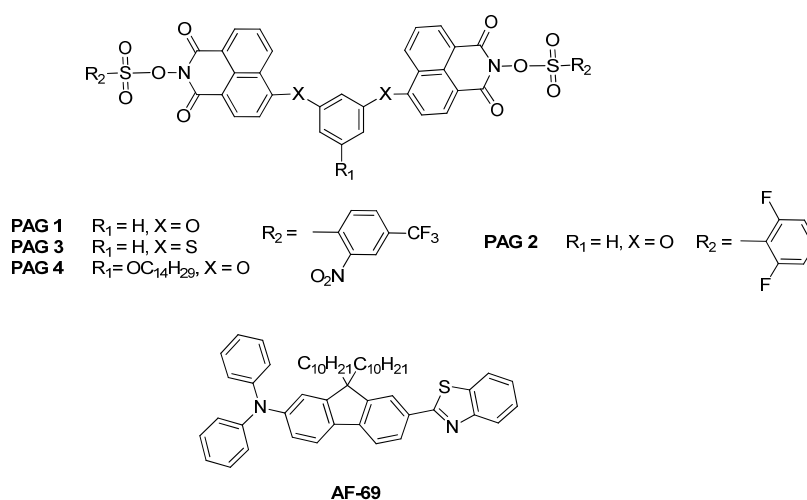
Fig 27 Structures of non-ionic 2PA PAGs and 2PA sensitizer.

The main disadvantage of cationic photopolymerization is the sensitivity to moisture, which is harmful to chain propagation process.[126] Compared to free radical photopolymerization, cationic photopolymerization also suffer from low reactivity, therefore decreased writing speed would be expected. Additional processing steps for epoxide photoresist, such as pre- and post-exposure baking, are usually required.[31]

Part I Novel 2PIs for 2PP

1 Aromatic ketone-based 2PIs

1.1 Molecular design of the aromatic ketone-based 2PIs

High initiation efficiency is always the most important character for an efficient 2PI. Initiation efficiency generally depends on 2PA cross section and the quantum yields of radical generation, as well as the initiating efficiency of the formed radicals. Until now, the behavior of the active radicals has been seldom investigated due to the small irradiated volume and complicated instrumental setup required.[94] The limited study on initiation mechanism can hardly provide useful guide for the molecular design. On the other hand, several molecular key features to ensure large 2PA have been well identified.[4] Therefore, the most straightforward way to obtain efficient 2PIs is to increase the 2PA of the photoactive molecules. Since intramolecular charge-transfer is the ''driving force'' for 2PA, electron-donor and electron-acceptor groups are required. In addition, long π conjugated bridges combined with good coplanarity which lead to states with extended charge separation, is critical in enhancing the efficiency of intramolecular charge transfer.[4]

Based on the molecular structure of **B3K** containing triple bonds and cross-conjugated D-π-A-π-D lead structures, several aromatic ketone-based 2PIs were proposed (**Fig 28**). Different aromatic ketones (benzophenone, fluorenone and anthraquinone) used as acceptors in the central part of the π bridge and dialkylamino groups as electron-donor moieties should be synthesized to study the structure-property relationship.

B3BP

B3FL

3,6-B3FL

BB3FL

B3AN

BB3AN

B3K

R1
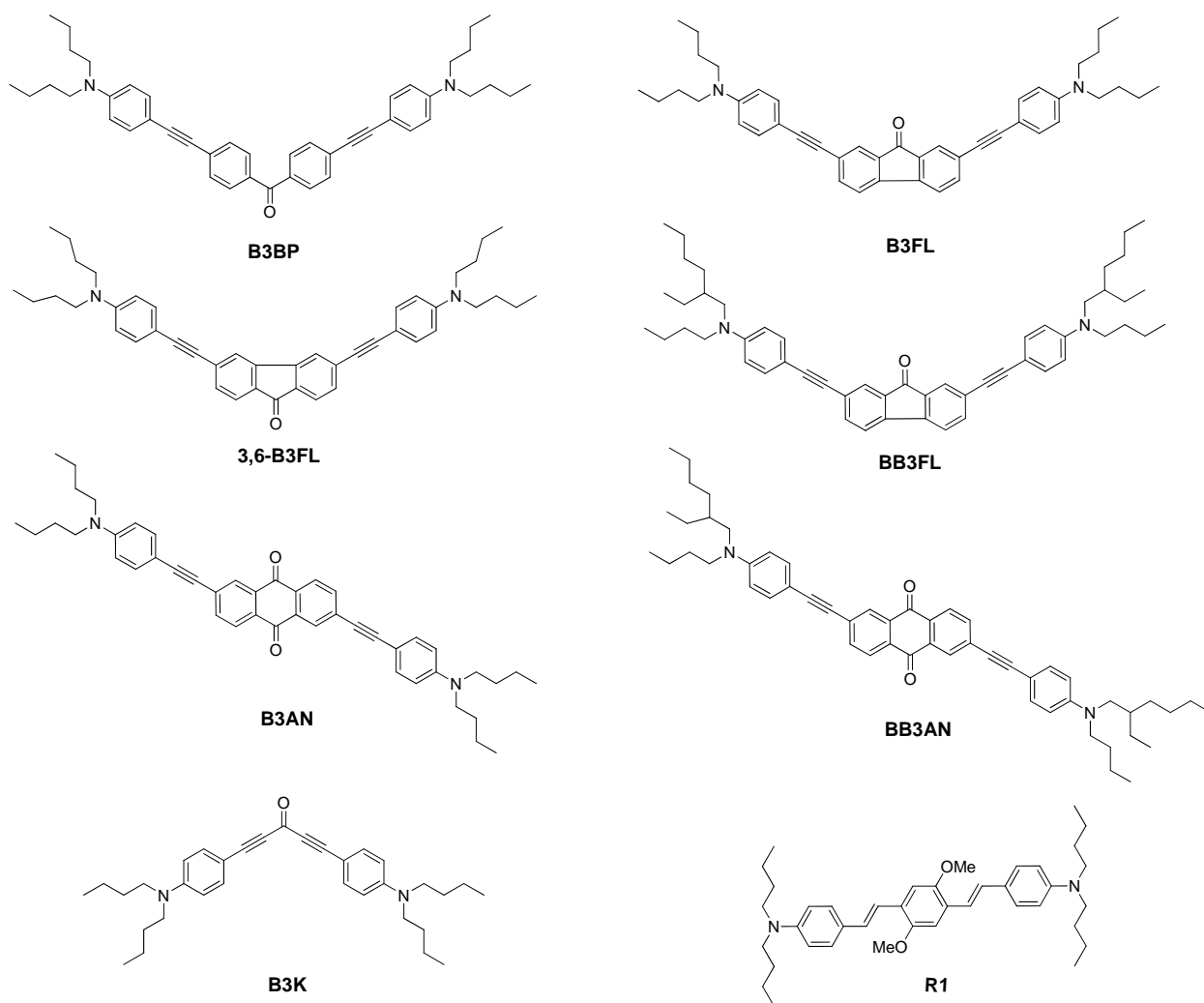
Fig 28 Proposed chemical structures of the novel 2PIs and the reference PIs

Benzophenone-based initiator **B3BP** should be prepared because compared to **B3K**, **B3BP** exhibits a longer conjugation length of the whole π system and therefore a higher σ^{2PA} can be expected. Structure-activity relationship tests in the recent literature showed that benzophenone-bearing dyes exhibited much larger σ^{2PA} than their analogues without a benzophenone unit.[127]

Additionally, 2PIs based on aromatic ketones with stereorigid carbon skeleton (**B3FL**, **3,6-B3FL** and **B3AN**) should be synthesized because of their good coplanarity, which facilitates the intermolecular charge transfer process and thus enhances the σ^{2PA}. Anthraquinone is used because of its excellent electron accepting ability and because its 2-, 6-positions can be easily modified by introducing π conjugated systems with electron donor groups resulting in a D-π-A-π-D type molecule. Recently, a double-bond containing anthraquinone compound was synthesized and exhibited a large two-photon cross section value of 1635 GM at 800 nm, as well as low fluorescence quantum yield.[83]

B3FL is of interest because 2,7-substituted fluorene cores are known to exhibit high thermal and photochemical stability.[128] Furthermore, the electron-withdrawing carbonyl group at C-9 stabilizes the LUMO of fluorene, making it remarkably electrophilic.[129] Substitution at positions 3 and 6 theoretically offers good electronic communication through the entire fluorenone skeleton.[129] In order to investigate the effect of different substituted positions on structure-reactivity relationships, both 2,7- and 3,6- substituted fluorenone compounds should be synthesized and investigated.

Moreover, the solubility in the monomers is an important issue for the efficiency of initiators. Therefore, long and branched-alkyl chains should be introduced at the terminal amino groups for improved solubility, as in fluorenone-based 2PI **BB3FL** and anthraquinone-based 2PI **BB3AN**.

1.2   Synthesis

The proposed synthesis route of the novel aromatic ketone-based 2PIs, which contain triple bonds and cross-conjugated D-π-A-π-D lead structures, are mainly based on Sonogashira reaction (**Fig 29**). Some distinct characters of Sonogashira coupling, such as high selectivity and ambient reaction condition with high yields, make it become a powerful tool to build conjugated structure comprising triple bonds as π bridges.[91] The coupling reaction mainly occurs between terminal alkyne and corresponding idodo- or bromo- derivatives in the presence of a palladium catalyst and trace of CuI. The desired 2PIs can be realized by coupling aryl alkynes containing different alkyl chains with corresponding dihalide aromatic ketones or by coupling aromatic iodo compounds with ketones containing two terminal alkyne groups. The first route was chosen because the synthesis strategy of alkylated aryl alkynes has been well developed by our institute.
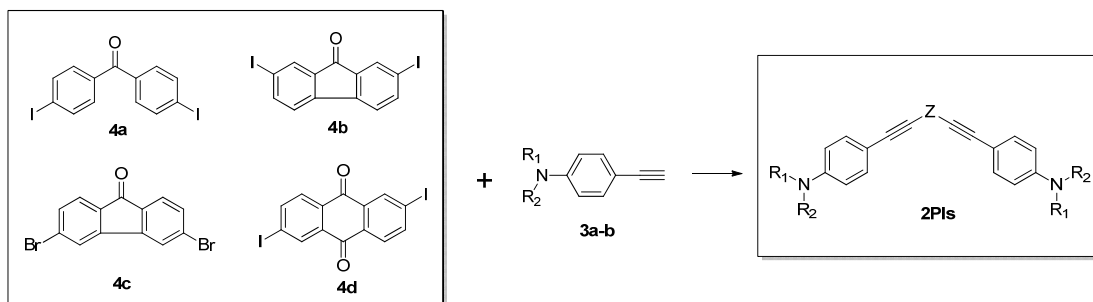
Fig 29 Proposed reaction scheme for the synthesis of the new 2PIs

1.2.1   Synthesis of alkyne precursors 3a and 3b

For the synthesis of the new initiators, there are two key intermediates **3a** and **3b** based on the *p*-amino aryl alkyne group containing different alkyl chains at the N-atom. These intermediates can be prepared by Sonogashira coupling reactions of the appropriate iododialkylamino benzenes with either (trimethylsilyl)acetylene or 2-methyl-3-butyn-2-ol followed by a subsequent cleavage of the protection groups in two steps.[130] Another way to prepare the terminal alkyne is a Wittig-type one pot synthesis starting from the corresponding aldehydes.[131] Although both methods have been proven to be suitable to obtain the terminal aryl acetylenes with high yields,[132] the former method was chosen because various alkyl chains can be easily realized for alternative PIs in further studies, while the counterpart aldehyde compounds are not always commercially available. Moreover, considering the relatively high price of (trimethylsilyl)acetylene, 2-methyl-3-butyn-2-ol is used instead for the synthesis of the alkyne precursors.
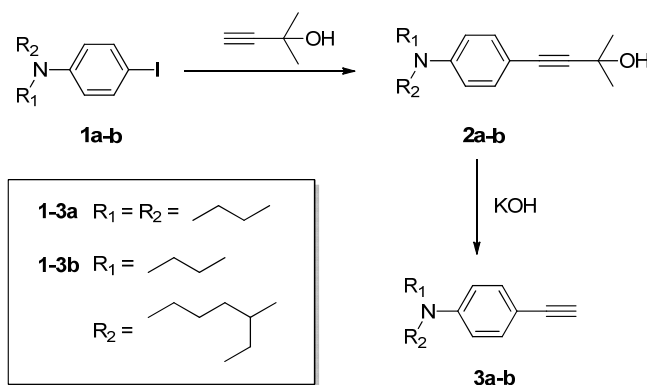
The 4-iodobenzeneamine with terminal alkyl chains can be prepared by iodination of the corresponding alkylated aniline,[133] halogen exchange[134] or alkylation of 4-iodobenzeneamine.[135] The last method was chosen because such synthesis route has been well developed in our institute. The synthesis of the butyl derivative **1a** was conducted as described by Pucher *et al.*[136]
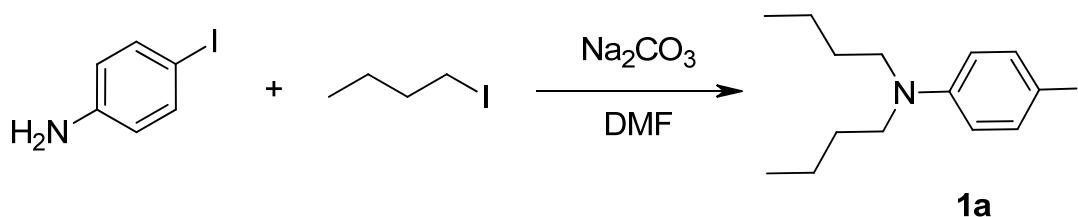
1.0 equivalent of 4-iodobenzeneamine reacted with 4.6 equivalents of 1-iodobutane in the presence of Na_2CO_3 as an acid acceptor. Excessive amount of 1-iodobutane and high temperature (95 °C) were needed to increase the yields of the desired dialkylated products. The final product **1a** was obtained as pale yellow oil with a good yield of 70% after a flash column chromatography (pure hexane).

The branched precursor **1b** was prepared using a very similar method to **1a**. Generally, iodinated alkanes are more active than corresponding bromides towards the alkylation. However, since the price of 2-ethylhexyl iodide (65.00 USD for 10 mL from Sigma-Aldrich) is much higher than that of 2-ethylhexyl bromide (37.30 USD for 100 g), the bromated alkane is used instead of its iodo analogues to prepare the branched precursor **1b**. Due to the relatively lower activity of the bromo derivative, potassium iodide and tetrabutylammonium bromide as a phase transfer catalyst were added to speed up the reaction.
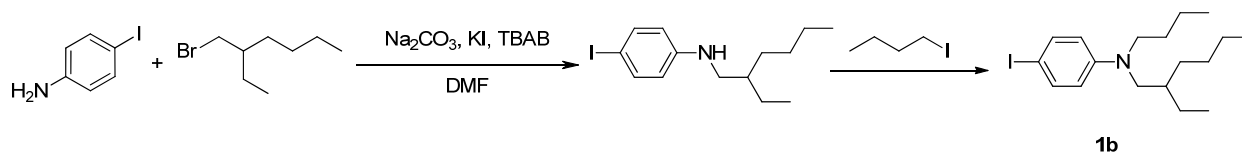
As a second substitution with the branched alkyl chain exhibited quite low yield (less than 15% from GC-MS) due to the steric hindrance, one butyl group was used instead. The product **1b** was obtained as colorless oil with satisfying a yield of 60% (2 steps) after a column chromatography.

The preparations of the protected alkynes **2a-b** were carried out in dry and degassed triethylamine under argon atmosphere due to the high sensitivity of the palladium catalyst. The Sonogashira coupling reaction of these 4-iodobenzeneamine derivatives with 2-methyl-3-butyn-2-ol were conducted as describe by Pucher *et al.*[136]
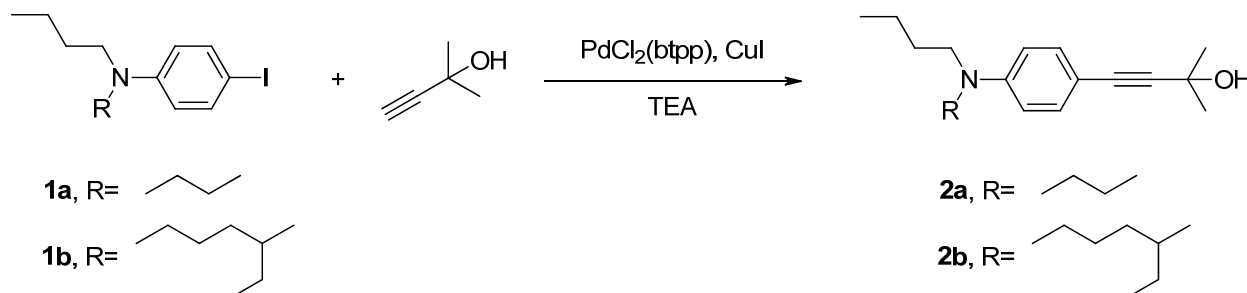
To a solution of 1.0 equivalent of 4-iodobenzeneamine derivatives in degassed and dry Et$_3$N under argon atmosphere, 2.5 equivalents of 2-methyl-3-butyn-2-ol, 0.2 equivalents of CuI and 0.2 equivalents of PdCl$_2$(btpp) were added. The reaction was stirred at 40 °C until the complete consumption of 4-iodobenzeneamine compounds (TLC analysis). After column chromatography, the protected alkyne products **2a** and **2b** were obtained in yields of 83% and 88%, respectively.

Finally, the deprotection reactions of **2a-b** were carried out in reflux toluene under an alkaline condition.[136]
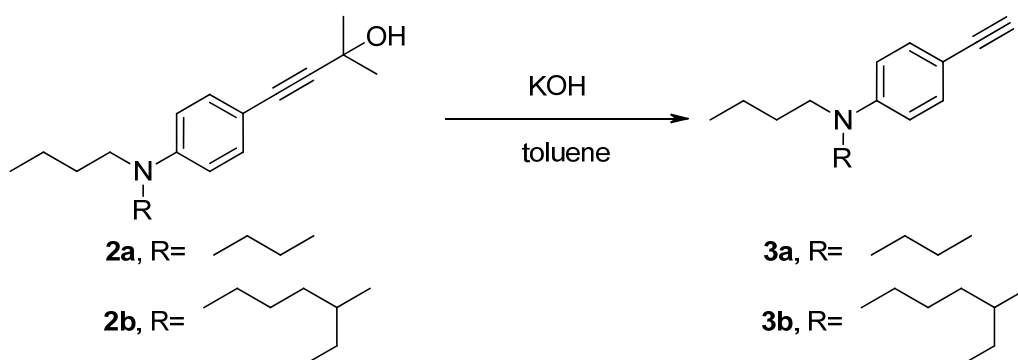
For the cleavage of the protecting group, 1.0 equivalent of protected alkynes was dissolved in toluene and 2.0 equivalents of powdered KOH were added. This suspension was stirred under reflux until the complete consumption of the protected alkynes (TLC analysis). In order to shift the equilibrium toward the products, the formed acetone was continuously removed. It is worth to mention that when running a column chromatography for purification, some unwanted reactions occurred between the crude products and the weakly acidic silica gel, which subsequently became green. The side reactions significantly reduce the column efficiency and the final yields. Adding small amount of triethylamine (1 %) into the eluents can address the issue and ensure good yields (80%) of the final terminal alkynes **3a-b**.

1.2.2 Synthesis of dihalide aromatic ketones 4a-d

Different strategies were employed to prepare the dihalide aromatic ketones **4a-d** for the coupling reaction with terminal alkynes **3a-b**. The bezophenone derivative **4a** can be prepared by iodination of diphenylmethane followed by oxidation to convert methylene

group to carbonyl group.[137] Another strategy for aromatic halogenation is based on diazonium salts which undergo dediazoniation induced by halides.[138] Aromatic halogen exchange reaction[139] and Friedel-Crafts acylation[140] have also been reported for the synthesis of **4a**. Considering the ease of preparation and the accessibility of the reagents, the first method as described by Novikov *et al.*[137] was chosen to prepare **4a** in one pot.
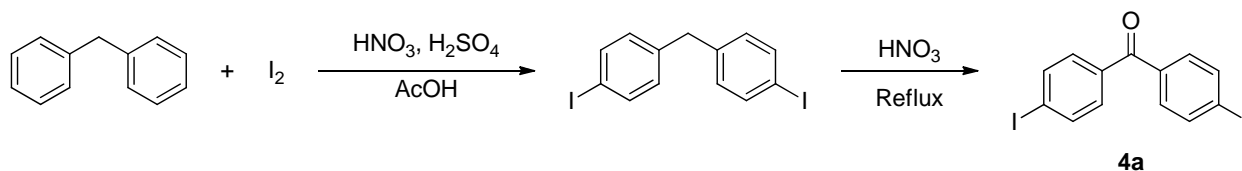
In the presence of a mixture of nitric acid (63%) and concentrated sulfuric acid (98%), diphenylmethane reacted with an equimolecular quantity of molecular iodine to obtain the desired 3,8-substituted diiodo compound. Without separation, the diiodized diphenylmethane was subsequently subject to oxidation with concentrate nitric acid to generate the 3,8-diiodinated benzophenone. The disappearance of the brown gas NO_2 indicated the completeness of the oxidation reaction. The diiodo product **4a** was obtained as white needle-shape crystal with satisfying yields of 70% after recrystallization from dioxane.

The most reported method to prepare 2,7-substituted diiodo precursor **4b** is direct diiodination of fluorenone with various iodinating agents like N-iodosuccinimide,[141] molecular iodine[142] and some synthesized iodides.[143] Other methods include diiodination of fluorene followed by oxidation[144] and dediazoniation of corresponding diazonium salts with potassium iodide.[145] Direct diiodination with molecular iodine as an iodinating agent as reported by Abashev *et al.*[146] was chosen because the synthesis route is simple and economical.
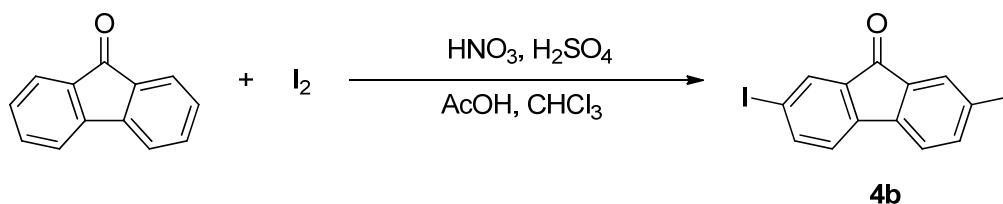
In the presence of a mixture of fuming nitric acid and concentrated sulfuric acid (98%), fluorenone was subject to diiodination with an equimolecular quantity of molecular iodine under reflux in glacial acetic acid. The orientation effect of carbonyl group can ensure the desired 2,7-disubstituted product. Since the molecular iodine can undergo

sublimation with elevated temperature and subsequently be condensed on the wall of the flask and the condenser during the reaction, small amount of chloroform was added to wash off the sublimed iodine under reflux to ensure adequate amount of iodine for the iodination. The diiodo product **4b** was obtained as yellow needles with satisfying yields of 73% after recrystallization from ethyl acetate.

Generally, aromatic iodides are more active than corresponding bromides towards Sonogashira coupling. However, no substance record of 3,6-diiodo-fluorenone has been found in literatures until now. Therefore, 3,6-dibromo-fluorenone **4c** was synthesized instead. Record of direct dibromination of fluorenone in the presence of [bis(acetoxy)iodo]benzene to prepare 3,6-dibromo-fluorenone was found in the query results of Reaxy. However, the query results were incorrect because the molecule recorded in the original paper is substituted at 2,7- not 3,6- positions.[147] Therefore, multiple steps to prepare 3,6-dibromo precursor **4c** were employed as described by Estrada *et al.*[129]
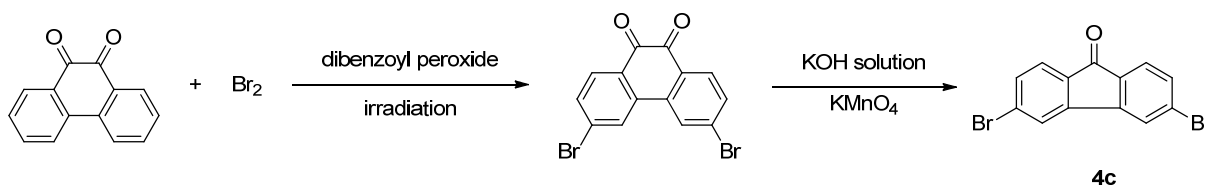
With assistance of dibenzoyl peroxide irradiated under a 100 W tungsten light bulb, 1.0 equivalent of 9,10-phenanthrenequinone was dibrominated with 2.9 equivalents of molecular bromine. The obtained 3,6-dibromophenanthrene-9,10-dione was then subject to elimination under basic condition to form the dibromo product **4c** (38% for 2 steps). Multiple recrystallizations in DMSO must be performed to remove trace amounts of 3,6-dibromophenanthrene-9,10-dione, which can be detrimental toward efficient Sonogashira couplings.[129]

2,6-diiodoanthraquinone **4d** were prepared via dediazoniation according to Stone *et al.*[148]
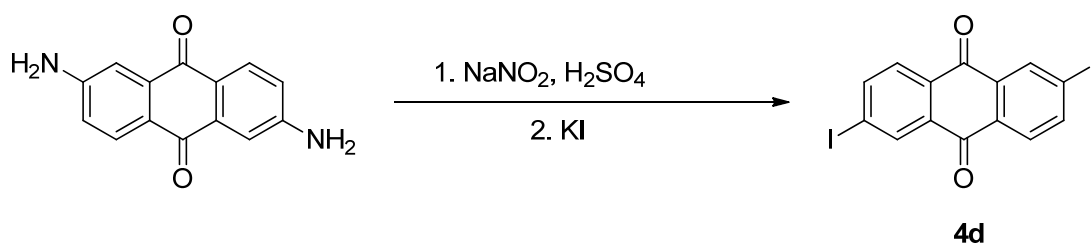
1.0 equivalent of 2,6-diaminoanthraquinone was used as a starting material to react with 2.0 equivalents of NaNO$_2$ in the presence of concentrated sulfuric acid to form diazonium salts under low temperature. The highly active diazonium intermediates serve as electrophilic agents reacting with potassium iodide followed by release of nitrogen to form the desired product. The diiodo product **4d** was obtained as light brown crystalline solid with satisfying yields of 60% after recrystallization from toluene.

1.2.3   Synthesis of novel 2PIs

On the basis of these intermediates, the final 2PIs were obtained by Sonogashira coupling reaction of the terminal alkyne derivatives **3a-b** with different aromatic ketone dihalides **4a-d**.[85]
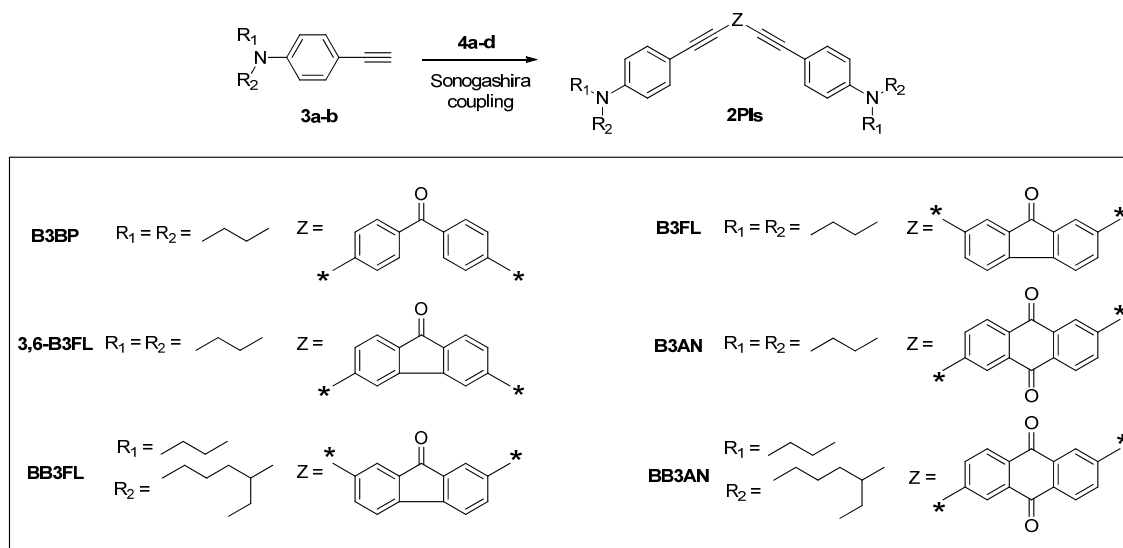
To a solution of 1.0 equivalent of aromatic ketone dihalides in degassed and dry THF/Et$_3$N mixture (1:1) under argon atmosphere, 2.5 equivalents of terminal alkyne, 0.2 equivalents of CuI and 0.2 equivalents of PdCl$_2$(btpp) were added. The coupling reactions conducted under room temperature only provided mono-substituted compounds as the main products. Therefore, reflux is needed to increase the yield of desired di-substituted compounds. Several eluent systems including PE/EE, PE/DCM, PE/chloroform, chloroform/methanol and PE/toluene with different ratio were investigated for the purification by column chromatography. PE/toluene has the best performance to give good solubility and separation ability. The final 2PIs were obtained with yields of 36-57% after column chromatography.

1.3   Linear photophysics

The linear optical properties of the novel 2PIs were studied in a close cooperation with Prof. Eric Vauthey and Dr. Arnulf Rosspeintner from the Physical Chemistry Department, University of Geneva. **Fig 30** depicts the absorption spectra of **B3AN**, **B3BP**, **B3FL** and **3,6-B3FL** in dichloromethane (also **Table 5** for some prominent values of the extinction coefficient). All 2PIs evaluated do not exhibit any linear absorption beyond 600 nm, which could thus interfere at the wavelength used in the z-scan experiments and the two-photon polymerization microfabrication. The absorption spectra of these novel 2PIs exhibit an intense low energy absorption band with the maximum molar extinction coefficient, ε, being in the range from 10^4 to 5×10^4 M^{-1} s^{-1}. The absorption bands show a slight hypsochromic shift with increasing solvent polarity (**Table 6**). A thorough solvatochromic analysis of these absorption bands, e.g. of Lippert-Mataga (LM) type is obscured because the absorption band is rather broad, slightly changes shape with the solvent and overlaps with the adjacent transitions. Any attempts of performing a LM analysis using simply the maxima of the absorption band resulted in suboptimal (i.e. nonlinear) LM plots. This might indicate that the nature of the transition is changing with the solvent, from a mainly local excitation in apolar solvents to a partial charge transfer absorption in polar solvents (or at least the amount of charge transfer character is changing).
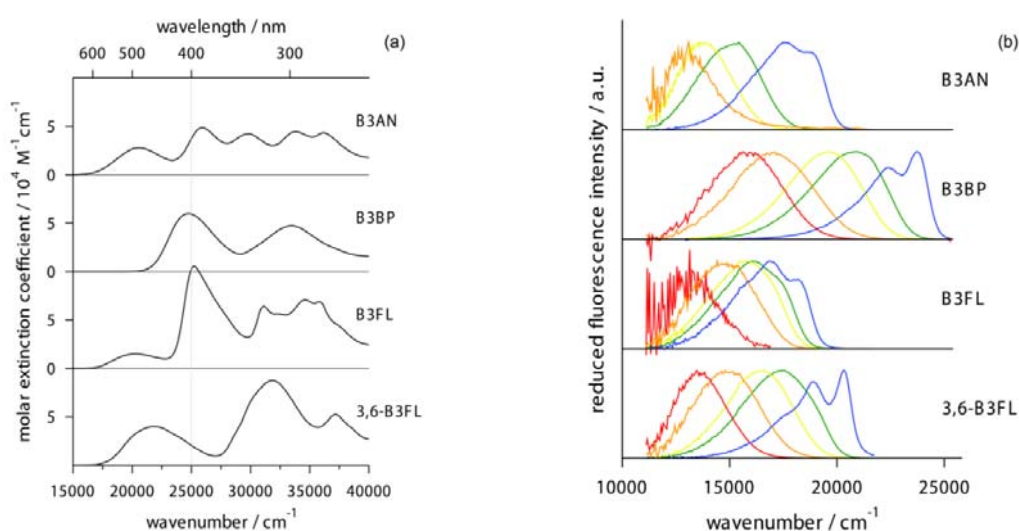
Fig 30 (a) Absorption spectra of **3,6-B3FL**, **B3FL**, **B3AN** and **B3BP** in dichloromethane .(b) Reduced fluorescence spectra of **3,6-B3FL**, **B3FL**, **B3AN** and **B3BP** in cyclohexane (blue), butyl ether (green), ethyl ether (yellow), butyl acetate (orange, for **B3BP** propyl acetate) and dichloromethane (red).

Table 5 Molar extinction coefficients of **3,6-B3FL**, **B3FL**, **B3AN** and **B3BP** in dichloromethane for the two lowest energy absorption maxima and the half wavelength of the 2PA cross section measurements (400 nm).

2PIs	λ (nm)	$10^{-3}\varepsilon$ ($M^{-1}cm^{-1}$)
B3AN	485 / 400 / 387	28 / 38 / 50
B3BP	405 / 400 / 300	60 / 60 / 50
B3FL	495 / 400 / 396	15 / 100 / 105
3,6-B3FL	460 / 400 / 315	40 / 20 / 85

Inspection of **Fig 30b** and **Table 6** shows that the situation is only slightly better concerning the interpretation of the emission spectra. The four 2PIs investigated (**B3AN**, **B3BP**, **B3FL** and **3,6-B3FL**) show a relative intense and structured fluorescence in apolar cyclohexane. By increasing the solvent polarity (from cyclohexane to dichloromethane), the emission spectra undergo more (for **3,6-B3FL** and **B3BP**) or less (**B3FL**) strong bathochromic shifts in the range of 0.5 to 1 eV. Additionally the emission spectra lose their vibronic structure upon increasing the solvent polarity. Since these trends are more or less prominent for certain 2PIs, it is worth emphasizing their differences: For both **B3AN** and **B3FL**, lifetime and emission quantum yield decrease monotonously with increasing solvent polarity. For **3,6-B3FL** the emission quantum yield and lifetime pass through a maximum for the ethers but hold a smaller value in cyclohexane. For **B3BP**, whose emission and absorption spectrum are also at higher energies than for the other PIs, the quantum yield and lifetime show no pronounced dependence with solvent polarity, except for the fact that these values in cyclohexane are rather low.

Table 6 Basic photophysical properties of **3,6-B3FL**, **B3FL**, **B3AN** and **B3BP** in six solvents at 25 °C. The properties comprise the energies of the maximum of the reduced fluorescence spectrum ν_f, the lowest energy maximum of the reduced absorption spectrum ν_a, the fluorescence quantum yield $_{em}$ and the fluorescence lifetime τ. Additionally the dielectric constant, ε, and refractive index, n, of the solvent are given.

solvent	ε	n	ν_f (eV)	ν_a (eV)	$\Phi_{em} 10^{-3}$	τ (ns)
			B3AN			
CX	2.01	1.4235	2.18	2.67	520	4.3
BE	3.08	1.3968	1.87	2.64	130	2.3

EE	4.20	1.3495	1.71	2.66	17	0.6
BA	5.01	1.3918	1.62	2.61	0.7	-
DC	8.93	1.4210	-	2.53	-	-

B3BP

CX	2.01	1.4235	2.95	3.16	70	0.1
BE	3.08	1.3968	2.57	3.15	340	1.7
EE	4.20	1.3495	2.43	3.16	430	1.8
PA	6.00	1.3828	2.11	3.13	230	1.7
DC	8.93	1.4210	1.96	3.05	160	1.8

B3FL

CX	2.01	1.4235	2.10	2.61	440	4.6
BE	3.08	1.3968	1.99	2.57	150	2.3
EE	4.20	1.3495	1.98	2.57	110	2.0
BA	5.01	1.3918	1.84	2.54	15	0.5
PA	6.00	1.3828	1.80	2.52	11	0.4
DC	8.93	1.4210	1.65	2.49	0.7	-

3,6-B3FL

CX	2.01	1.4235	2.52	2.93	210	0.8
BE	3.08	1.3968	2.17	2.87	650	3.6
EE	4.20	1.3495	2.04	2.83	680	4.1
BA	5.01	1.3918	1.84	2.77	90	0.9
PA	6.00	1.3828	1.81	2.76	44	0.9
DC	8.93	1.4210	1.69	2.68	12	0.3

Abbreviations: CX-cyclohexane, BE-butyl ether, EE-ethyl ether, BA-butyl acetate, PA-propyl acetate, DC-dichloromethane

On the basis of the present data, which comprise only steady-state and subnanosecond time-resolved emission experiments, the following tentative conclusions may be drawn. A charge transfer state is populated either via direct excitation, or indirectly, via excitation of a locally excited state.[149] The current data does not allow speculations of possible populations of the triplet state of the PIs. Femtosecond time resolved transient absorption and emission spectroscopy might help shed light onto the photophysics and possible mechanism(s) of photoinitiation for these 2PIs.

1.4   Z-scan measurement (σ^{2PA})

To investigate the 2PA properties of the new PIs, an open aperture z-scan analysis was performed to determine the σ^{2PA} at 800 nm, also the wavelength for 2PP tests. The z-scan analyses were performed in a close cooperation with Prof. Wolfgang Husinsky and Dr. Aliasghar Ajami from the Institute of Applied Physics (TU Vienna). Detail information of the z-scan analysis can be found in Dr. Aliasghar Ajami's PhD thesis.[150] Since our previous σ^{2PA} results of **R1** and **B3K** were obtained in THF, the same solvent was used for the 2PA characterization of the novel 2PIs for a better comparison. A nonrecycling flow cell was used for the measurements because of the strong photodegradation of some PIs during the tests (especially the ketone-based PIs). **Fig 31** shows the photo-degradation of **BB3FL** as a representative example at two different z-scans: without flow and with 4 mL/h flow rate. The previous results indicate that a flow rate of 4 mL/h is sufficient for all 2PIs to wash the irradiated sample out of the focal volume in a reasonable time.[136]
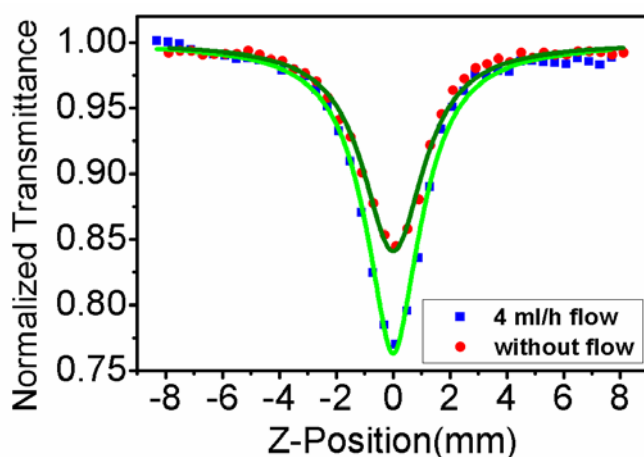
Fig 31 Photodegradation effect of **BB3FL** at different volumetric flow rates (0 and 4 mL/h)

The experimental data were fitted using the adopted equations of Sheik-Bahae *et al*.[151] in order to obtain the σ^{2PA} (**Fig 32**a). To exclude excited-state absorption and to verify that a pure σ^{2PA} is determined, the measurements were repeated at different peak intensities and the calculated parameter q_0 scales linearly with intensity (**Fig 32b**).[151] All calculated σ^{2PA} values are given in **Table 7**.
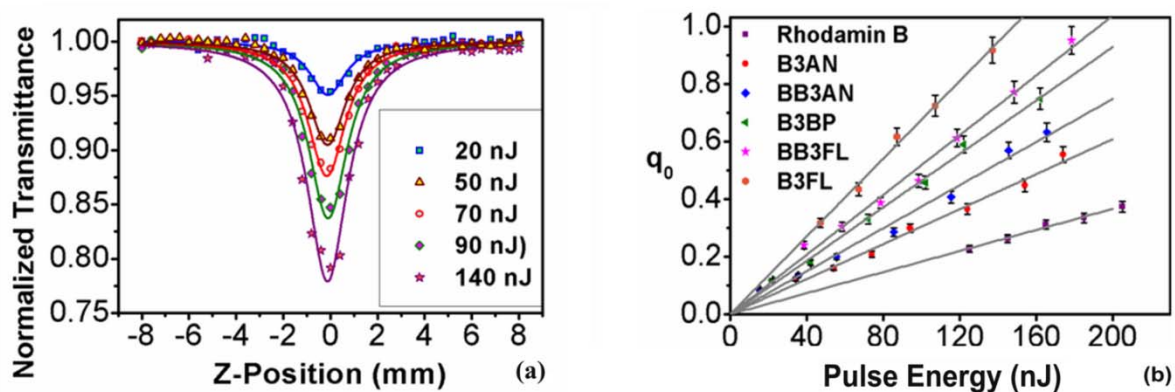
Fig 32 (a) Experimental z-scan data (dots) and fitting curves (full lines) for **B3FL** at different pulse energies. (b) q_0 plotted vs. intensity for the investigated 2PIs.

Table 7 2PA cross section values of PIs in THF by z-scan measurement at 800 nm

2PIs	σ^{2PA} (GM)
R1	328
B3K	238
B3BP	336
B3FL	440
B3AN	235
3,6-B3FL	308
BB3FL	385
BB3AN	250

The cross section value of the reference compound **R1** is in good agreement with our previous result[132] and the literature,[152] verifying the reliability of the experimental setup. With longer conjugation length, benzophenone-based initiator **B3BP** shows a larger cross section value than **B3K** of 238 GM, which is almost equal to that of **R1**. By changing the acceptor group in **B3BP** from a benzophenone group to an anthraquinone moiety as in **B3AN**, the value decreases to 235 GM. The reduction may be due to the relatively lower absorption in one-photon spectra at about 400 nm, which indicates that the two-photon absorption peaks in 2PA spectra are shifted in wavelength away from 800 nm. As expected, the substitution of the butyl group at the amine by branched alkyl chains alters the two photon cross section only marginally.

Interestingly, the 3,6-substituted fluorenone-based PI **3,6-B3FL**, which theoretically should facilitate an intramolecular electron transfer process, exhibits a lower cross

section value compared to the 2,7-substituted analogue **B3FL**. An explanation can be given by the red-shift-induced low 2PA absorption at the given wavelength. Among the aromatic ketone derivatives, **B3FL** had the highest 2PA cross section value of 440 GM. One reason is the excellent coplanarity of the stereo rigid fluorenone carbon frame and the suitably strong absorption around 400 nm, which ensures the considerable 2PA at 800 nm.

Due to the instrumental limitation, we obtained the σ^{2PA} values only at 800 nm from the z-scan measurement. These values serve important references for optimizing 2PP from practical aspect because Ti-sapphire lasers with 800 nm emission are the most popular excitation sources used in 2PP fabrication system. Recently, a new 2PA setup, which can provide the whole 2PA spectra at a wide range of wavelengths, has been built by Dr. Arnulf Rosspeintner. The two-photon excited fluorescence spectra of some 2PIs in THF are shown in **Fig 33**. The linear absorption spectra of the 2PIs are also included for a comparison between 1PA and 2PA.
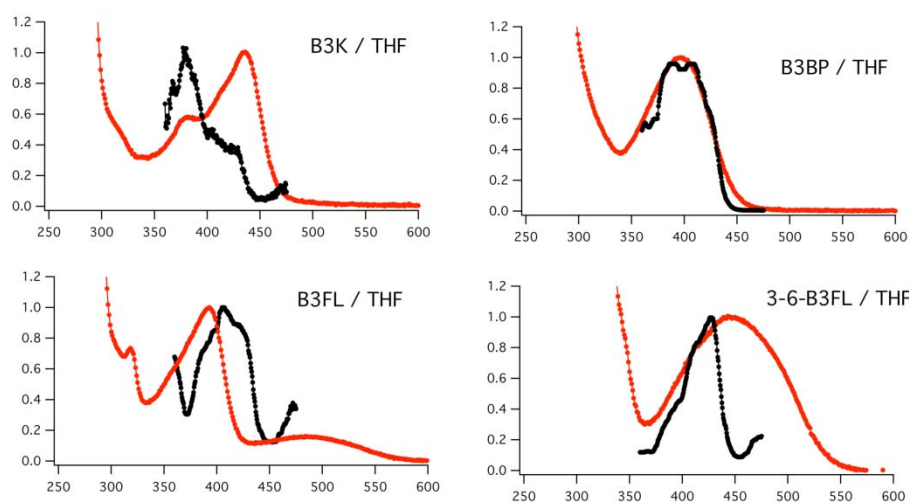
Fig 33 Linear absorption spectra (red) and two-photon excited fluorescence spectra at half-wavelength (black) of 2PIs in THF

As mentioned in Introduction section, there is no direct correlation between the 1PA maxima and the 2PA maxima ($\lambda^{2PA}_{max} \neq 2 \times \lambda^{1PA}_{max}$) for the PIs with centrosymmetric geometry. For **B3BP**, the spectra of 1PA and 2PA (at half-wavelength) fit well to each other. However, the shape and maxima of the absorption peaks are totally different for the other three investigated 2PIs. Blue-shift of λ^{2PA}_{max} (at half-wavelength) is observed for **B3K** and **3,6-B3FL**, while λ^{2PA}_{max} of **B3FL** exhibits red-shift. Moreover, λ^{2PA}_{max} (at

half-wavelength) of **B3K** and **3,6-B3FL** lie beyond 400 nm, which lead to a weak 2PA at 800 nm. The results can well explain their relatively small σ^{2PA} values measured by z-scan at 800 nm. For **B3BP** and **B3FL**, 2PA maximum peaks are much closed to 800 nm. Since **B3FL** has a stereo rigid fluorenone carbon frame to ensure excellent coplanarity, its σ^{2PA} is larger than **B3BP**.

Although σ^{2PA} is the most popular parameter used to evaluate the 2PA chromophores, it gives only information about the nonlinear absorption behavior (similar to the extinction coefficient, ε, of one-photon absorption in Lambert-Beer's law). A large σ^{2PA} indicates more efficient photon absorption, which might also lead to deactivation processes such as fluorescence emission or thermal conversion. Therefore, the measurement of σ^{2PA} alone is not sufficient for assessing the initiation efficiency of the initiators. Thus, 2PP structuring tests were performed in a close cooperation with Prof. Jürgen Stampfl and Dr. Klaus Cicha from the Institute of Materials Science and Technology (TU Wien) to further characterize the new 2PIs.

1.5   2PP test

There are several methods to estimate the initiation efficiency of initiators in 2PP. The three most popular are voxels,[14] lines,[153] or more complicated 3D structures. Single voxels enable easy evaluation of the minimal resolution and the actual voxel dimensions.[14] Structuring single lines is a more straightforward measurement compared to voxel tests and enables the determination of the P_{th}, as well as the estimation of the voxel dimensions.[154] Here, more complicated 3D shapes fabricated under various laser intensities and writing speeds are chosen for the evaluation. Such a method is more practical since broad ideal processing windows are critical for high throughput in mass production. In order to estimate the activity of the 2PIs, defined test structures (lateral dimension: 50 × 50 μm, 10 μm hatch-distance, 0.7 μm layer-distance, 20 layers) were written into the monomer formulation by means of 2PP. The laser intensity was screened in a range of 1-32 mW (measured after passing the 100× microscope objective). A 1:1 mixture of trimethylolpropane triacrylate (TTA) and ethoxylated (20/3)-trimethylolpropane triacrylate (ETA) (**Fig 34**) as an acrylate-based test resin with the same molar PI concentration of 6.3× 10^{-6} mol PI/g resin was used since good results had been previously achieved under these conditions.[155]
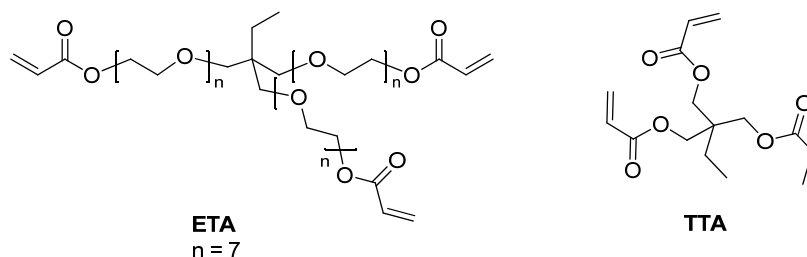
Fig 34 Chemical structures of monomers used for the 2PP structuring tests

The full processing windows of the 2PIs are shown in **Fig 35**. Different color and their corresponding numbers indicate the quality of the structures (**Fig 36**). At write speeds beyond the ideal processing window, the initiation threshold is not reached and incompletely connected structures are obtained after developing. Above that, class A defines excellent structures with fine hatch-lines (green area) and class B good structures with thick hatch-lines (compared to class A) or slightly contorted structures (yellow area). Generally, broader "perfect" processing windows (class A and B) and lower laser intensities are desired in terms of high throughput in mass production because this allows a splitting of the initial laser beam for parallel processing with multiple laser heads at high feed rates, while thermally induced decomposition of the material can be avoided. Samples rated as class C (red area) have shapes that can be identified but with small mistakes (e.g. holes, exploded regions caused by overexposure). Parts structured with laser intensities rated as class D no longer show acceptable results (blue area). The shapes are no longer identifiable with completely missing walls and/or vast holes.

(a)   (b)   (c)   (d)
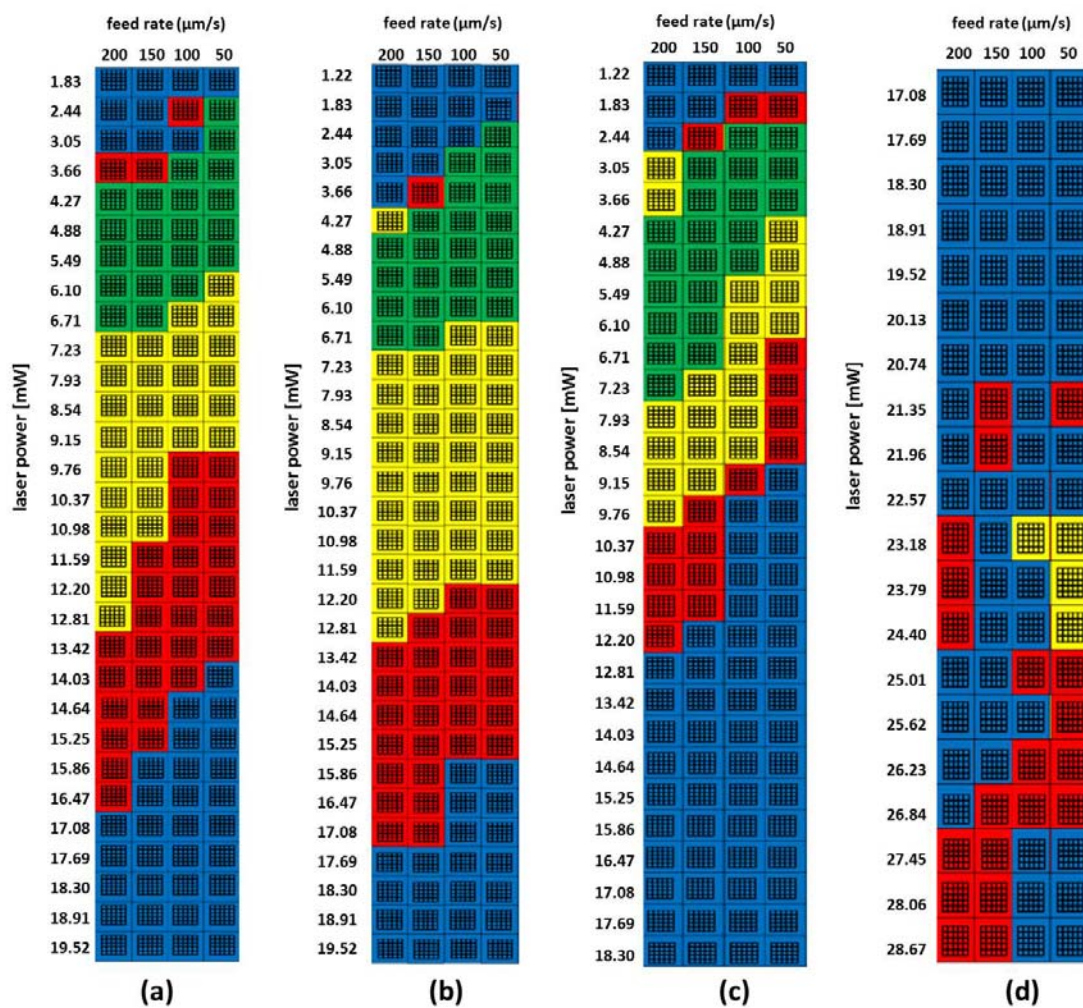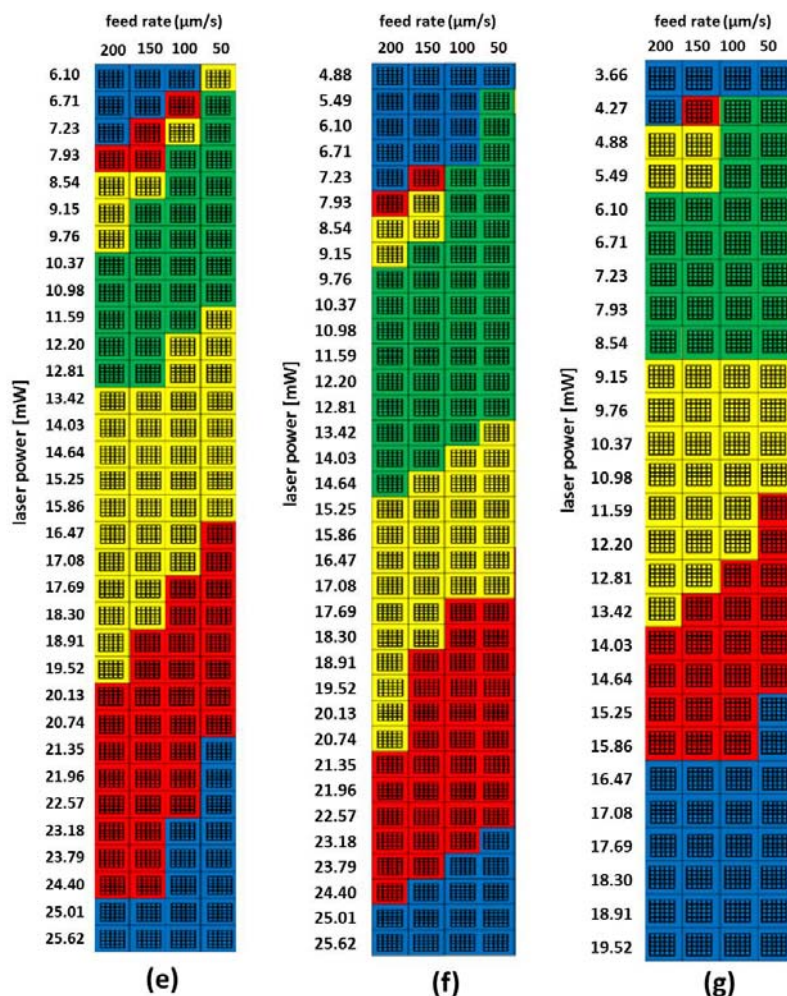
Fig 35 Processing Windows of PIs with different feed rate and laser power.
(a) **R1**; (b) **B3K**; (c) **B3BP**; (d) **BB3AN**; (e) **3,6-B3FL**; (f) **B3FL**; (g) **BB3FL**
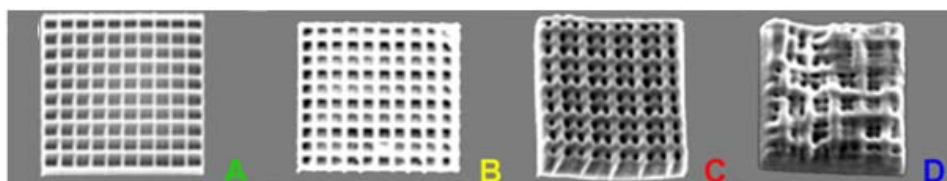
Fig 36 Classification of the structures by the typical quality of their shapes

In order to quantitively evaluate the initiation efficiency of the 2PIs, the processing windows with different laser intensities and a constant writing speed are investigated as representatives (**Fig 37**). Feed rate of 50 μm/s is chosen because with this speed, formulations containing **R1** and **B3K** as 2PIs can provide nice microstructures under very low laser intensities, which can serve as good references for the evaluation.
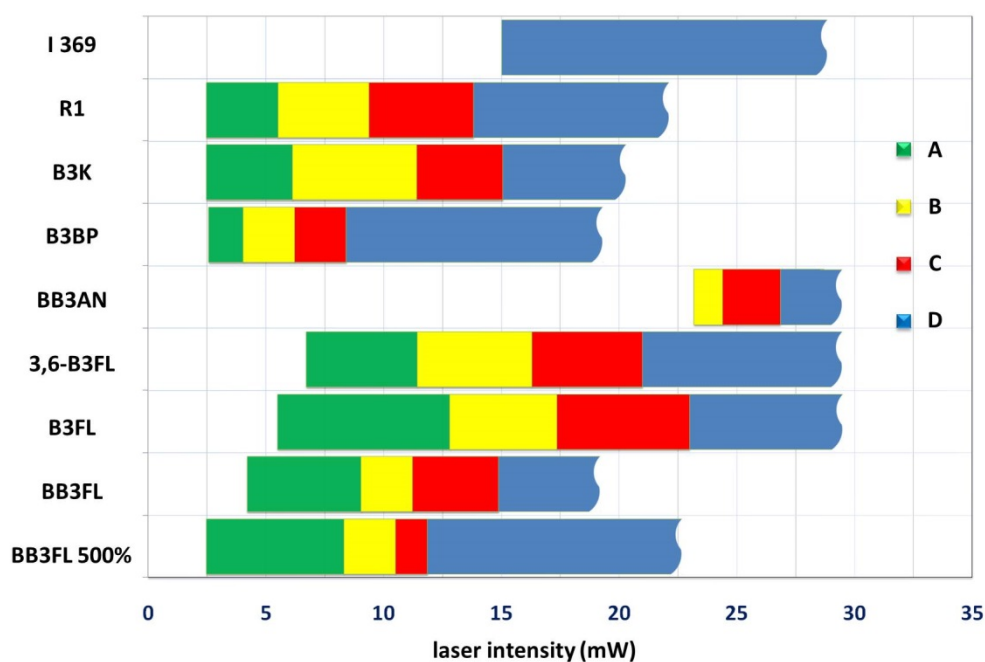
Fig 37 2PP screening tests (PI concentration: 6.3×10^{-6} mol PI/g resin; writing speed: 50 μm/s).

The well-known reference initiator **R1** can be used to build nicely shaped structures at a low laser intensity of 2.44 mW. Nice structures can also be obtained by **B3K** with the same threshold energy but with slightly broader ideal processing windows. On the other hand, the commercially available PI **Irgacure 369** shows no good results at 800 nm at the given PI concentration (6.3×10^{-6} mol PI/g resin), which is in good agreement with the small 2PA cross section.[156]

The benzophenone-based initiator **B3BP** gives nice structures at similarly low laser intensities as **R1**, but its ideal processing window is significantly smaller. By changing the acceptor group in **B3BP** from a benzophenone group to an anthraquinone moiety as in **B3AN**, the solubility is dramatically decreased. In the structuring tests, no comparable result with **B3AN** can be obtained due to its poor solubility. The introduction of branched-alkyl chains at the end of the amino moieties of the anthraquinone-based initiator **BB3AN** could, to some extent, resolve the solubility problem. However, high laser intensities are required to obtain good structures in a small area. This might be explained by the relatively small 2PA cross section and the significantly lower solubility in the resin.

The fluorenone-based initiators (**3,6-B3FL**, **B3FL** and **BB3FL**) show very good results in the tests. The ideal processing windows are broader than that of the references, but the required laser intensities are slightly higher. Despite the lower cross section compared to that of **B3BP**, the ideal window of **3,6-B3FL** is much broader. This might be explained by the stereo rigidity of the carbon frame of fluorenone, which increases the coplanarity of the entire molecule and thus facilitates the electron transfer process. The triple bonds attached at the 2- and 7- positions of **B3FL**, exhibit much broader ideal processing windows than those of **3,6-B3FL**, which is in good agreement with the z-scan values. By changing the alkyl side chains from butyl to branched alkyl chains of **BB3FL**, the ideal processing windows (class 1 and 2) become smaller. The difference may be explained by the lower migration ability of the 2PI with the increase of its molecule size. The lower laser intensity required for **BB3FL** might be attributed to the increased solubility. It is worth mentioning that the introduction of branched-alkyl chains significantly improves the solubility of the fluorenone-based PIs, which enables the preparation of a sample with fairly a high concentration (3.2×10^{-5} mol PI/g resin). The **BB3FL** sample with a high concentration can reduce the required laser intensity to as low as 2.44 mW. **B3FL** turns out to be the best performing initiator in our tests having the broadest ideal structuring process window at low concentration (6.3×10^{-6} mol PI/g resin) and good solubility in the resin.

Additionally, more complex 3D structures (**Fig 38**) were inscribed into the material volume using **B3FL** (6.3×10^{-6} mol PI/g resin) as initiator. These shapes demonstrate perfectly the advantages of 2PP compared to other rapid prototyping techniques. High spatial resolution, which is otherwise inaccessible, and complex 3D structures with massive overhangs such as the London Tower Bridge (**Fig 38**c) and the St. Stephen's Cathedral of Vienna (**Fig 38**d) can be easily obtained.
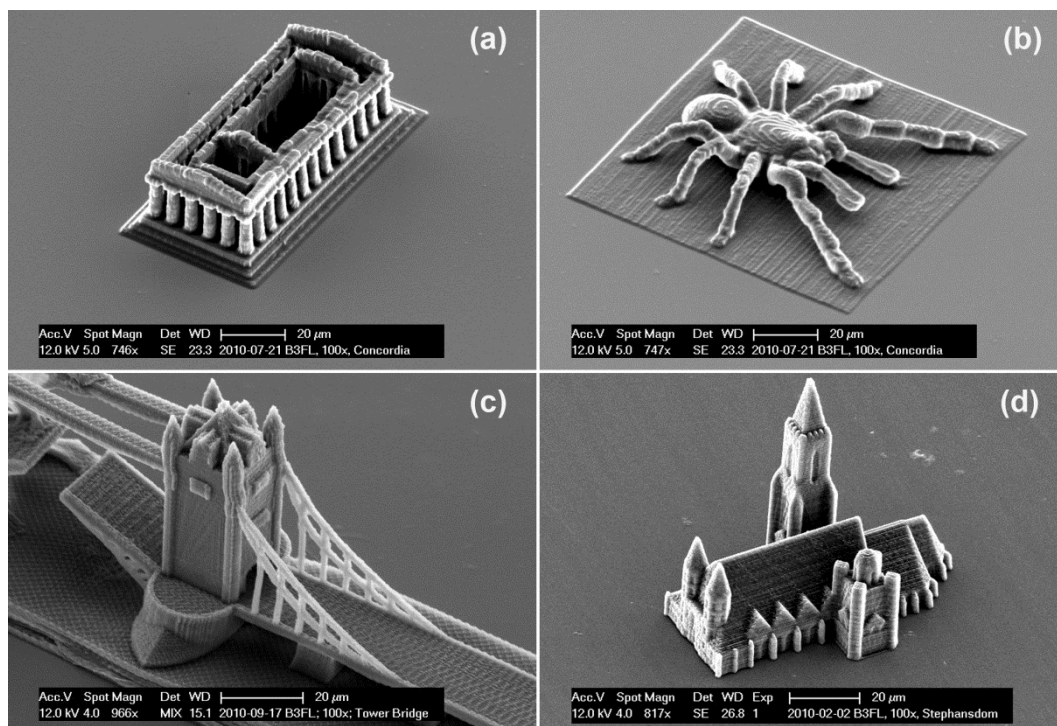
Fig 38 3D structures (resin ETA/TTA 1:1, **B3FL** as initiator): (a) Concordia Temple; (b) Tarantula Spider; (c) detail of the London Tower Bridge; (d) St. Stephen's Cathedral.[157]

1.6   Double bonds conversion via FTIR microscopy

2PP structuring tests can provide some important information like maximum resolution, threshold energy of polymerization and the processing windows. These parameters are valuable references for optimizing the microfabrication process. The evaluation standard of 2PP is based on the optical appearance of the microstructures. For practical applications, it is also critical to study the degree of the photopolymerization and to evaluate the mechanical properties of microstructures fabricated by 2PP. However, due to the small sample size (micrometer scale) and long fabrication times (typical feed rate between 100 μm/s and 1 mm/s), traditional characterization methods for photopolymerization, such as photo-differential scanning calorimetry (DSC)[158] and photorheology,[159] cannot be directly used to characterize 2PP. To address such issue, Dr. Cicha developed a quantitative way using FT-IR microscopy to study the degree of the 2PP process by double bonds conversion (DBC).[160]

B3FL, which has the best performance in 2PP structuring tests, and **R1**, a potent 2PI reported in literature,[72] were chosen for the screening. The same resin formulations as

used in 2PP are employed for the DBC tests for comparison. The formulations containing **B3FL** and **R1** as initiators were named as formulation A and B, respectively. A pure potassium bromide plate was molded and fixed on a substrate that can be mounted in the 2PP setup (**Fig 39a**). An array of woodpile structures was fabricated on the potassium bromide plate (**Fig 39b**). More detailed information of the sample preparation and 2PP microfabrication could be found in the published paper.[160]
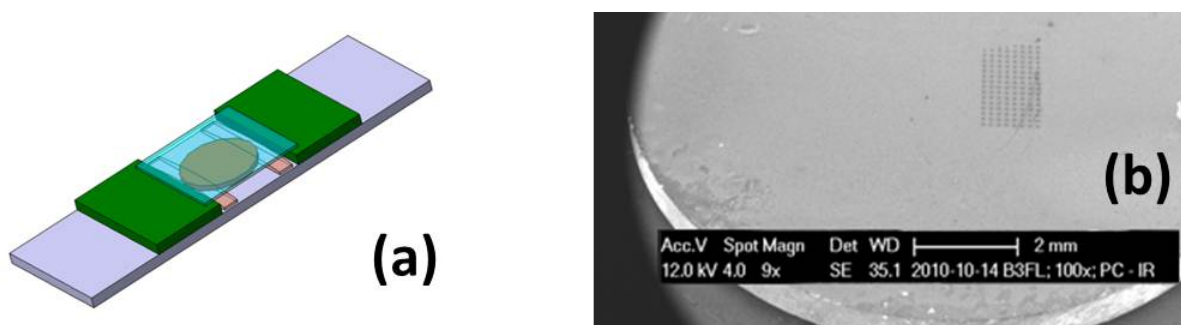
Fig 39 (a) sample holder (b) fabricated array of woodpile structures on KBr-plate

Since it's difficult to exactly determined the thickness of the IR samples (2PP structure, monomer droplet, UV cured sample), the carbonyl peak (1730 cm^{-1}), which remains constant during the polymerization process, was used as a reference to study the change of the target double-bond peak (810 cm^{-1}). The DBC of the 2PP structures fabricated using formulation B containing **B3FL** as an initiator under different laser power and writing speed is shown in **Fig 40**. Compared to the writing speed, the laser power exhibits a higher influence on the double-bond conversion. The lower threshold energy level (LTEL), defined as below which the microstructure could not be clearly identified, was 23 mW. At this laser-power level a DBC of approximately 57% was determined (depending on the structuring speed). The DBC level increased up to 65% when increasing the laser power to 115% of the LTEL. However, when the laser power increased above 175% of the LTEL, the DBC level remains nearly constant. The structuring speed influenced the DBC only at low laser intensities. When the laser intensity increased above 125% of the LTEL, the DBC was independent to the structuring speed.
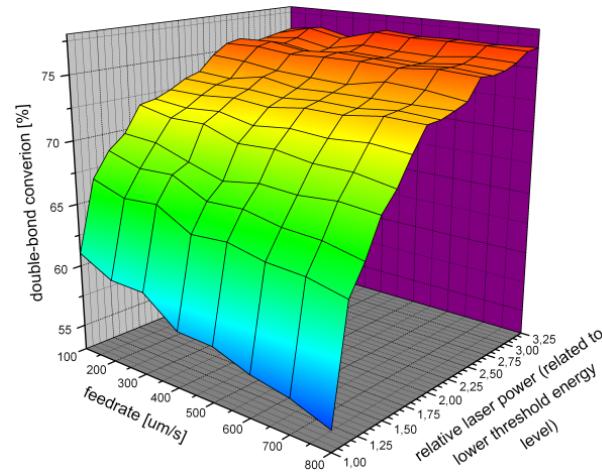
Fig 40 Double-bond conversion of formulation containing **B3FL**.[160]

Fig 41 shows the DBC comparison of formulations A and B. The fitting results show the dependency of the DBC to the square of the laser intensity, which means the polymerization is activated under 2PA. The final DBC for the two material systems is comparable. Although **B3FL** has a better performance than **R1** in 2PP structuring tests, the DBC of formulation B with **R1** increases faster than that of formulation A with **B3FL**. This indicates that formulation with **R1** seems to have a more abrupt on/off (polymerization) behavior. Generally high DBC with a laser power close to the LTEL is favored because it can provide microstructures with high resolution with high mechanical stability.
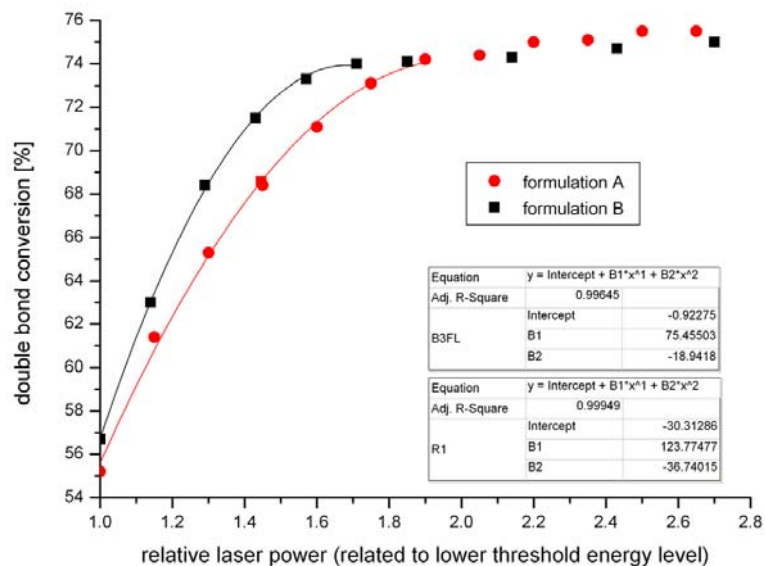
Fig 41 DBC comparison of formulations with different photoinitiators and 2nd order fitting function of rising DBC values.[160]

1.7   Mechanical properties via nanoindentation

FT-IR microscopy provides a quantitative method to evaluate different 2PA active formulations via comparing DBC. The main drawback of the approach is the time consuming analysis and interpretation of the measured IR-spectra. Moreover, DBC only indicates the degree of the photopolymerization, lacking the direct information about the mechanical properties of the microstructures. To this regard, a novel evaluation method based on nanoindentation technique was developed by Dr. Klaus Cicha and Dr. Thomas Koch from the Institute of Materials Science and Technology.

The screening samples for 2PP are the same as those used in DBC study. An array of cantilevers (80 μm × 15 μm × 10 μm), attached to the top of a prismatic base structure with a lateral length of 50μm and a height of 80μm, were fabricated with the building parameters (hatch distance 0.25μm, layer distance 0.6μm) to achieve fully solid structures (**Fig 42**). The structuring speed was held constant at 650μm/s while the laser power was varied and increased in 1mW steps. To compare the results of the two different formulations and to enable the comparison with previous work, the laser power was put in relation to LTEL. More detailed information of 2PP microfabrication and nanoindentation can be found in the published paper.[161]
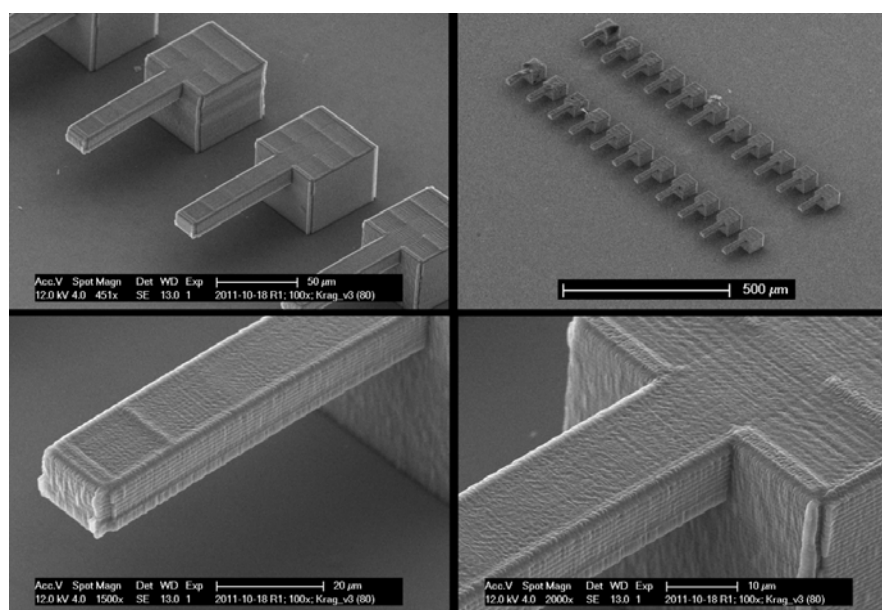
Fig 42 SEM-images of the micro-cantilevers[161]

Testing the micro-cantilever built with the two different formulations gives results presented in **Fig 43**. Increasing the laser power leads to an approximately linear increase of the Young's modulus. Formulation A (with **B3FL**) starts with a Young's modulus of approximately 1200MPa and reaches 1650MPa at the doubled LTEL. In comparison formulation B (with **R1**) shows a better result. The Young's modulus starts with 1400MPa and strongly increases to 2650MPa at the doubled LTEL. These findings backup the results gained from the FTIR-measurements where formulation B shows a better performance, though the differences are not that tremendous compared to the results of the Young's modulus measurements.
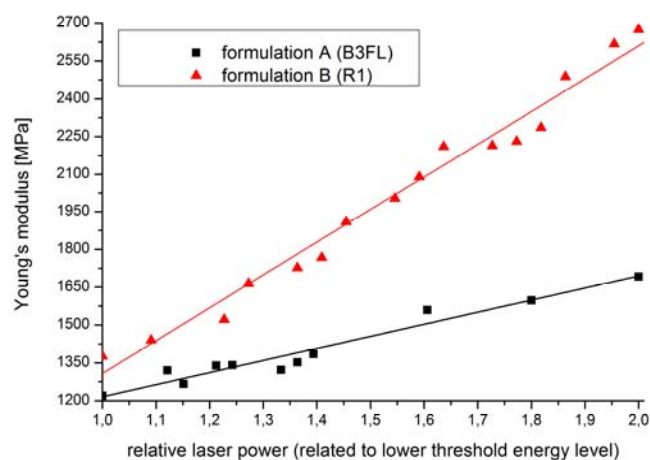
Fig 43 Young's modulus of both formulations vs. relative laser power.[161]

2   Benzylidene ketone-based 2PIs

2.1   Molecular design of the benzylidene ketone-based 2PIs

Beside initiation efficiency of 2PIs, the ease and cost of preparation are also critical factors from practical aspect. Most efficient 2PIs, which contain planar π systems with long conjugation length and strong donors and/or acceptors, are synthesized via classical Wittig,[87] Horner-Wadsworth-Emmons (HWE),[84] Heck[89] or Sonogashira coupling reaction.[91] These synthesis routes need expensive catalysts or multiple synthetic steps and thus result in restrictively expensive 2PIs. These adverse factors have been obstructive for the development of the promising 2PP technology.

Aldol condensation reaction is another powerful tool to build the desired long conjugated system. Wu's group reported the synthesis of a series of benzylidene cyclopentanone dyes and successfully applied them as 2PIs in 2PP.[162] The D-π-A-π-D core structures of benzylideneketone dyes can be simply built in one step via aldol condensation. Although a few studies on the structure-property relationship of benzylidene ketone dyes have been carried out by changing the terminal donor groups[162a, 163] and extending the conjugation length,[164] the effects of the central ketone with different size rings on 2PA behavior as photoinitiators have not been systematically studied. In fact, the size of the central ring significantly affects the photochemical and photophysical characteristics, such as fluorescence emission.[165] Central cyclohexanone compounds possess much weaker fluorescence than their cyclopentanone counterparts.[166] To be effective as a 2PA initiator, low fluorescence quantum yields are preferred as this leads to a higher population of the active state for initiating the polymerization.[154] On the other hand, the method to explore the effect of rings with different sizes is more simple and practical than previously reported ones because various cycloketones are commercially available at relatively low costs. Combining the synthetic merits of the aldol condensation reaction with a systematic study on the central ring effect of benzylidene ketones on 2PP should elucidate relevant routes to design and synthesize highly efficient 2PIs in a simple and economical way. Therefore, a series of linear and cyclic benzylidene ketone-based 2PIs containing double bonds and dialkylamino groups should be synthesized to systematically study the structure-property relationship (**Fig 44**).
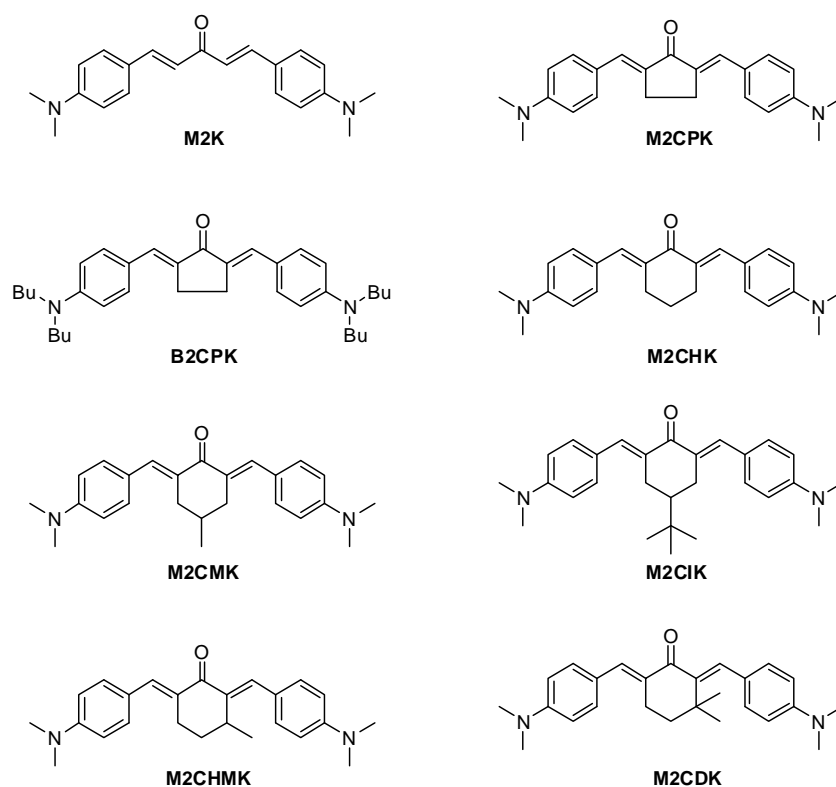
Fig 44 Chemical structures of 2PIs

2.2   Synthesis

The synthesis of the linear and cyclic benzylidene ketone-based 2PIs is quite straightforward. The desired D-π-A-π-D structure with dialkylamino groups as donors, vinyl as π-conjugated bridges and carbonyl as acceptors can be prepared in one step via classical aldol condensation reactions between N-substituted benzaldehydes and corresponding ketones (**Fig 45**), both of which are commercially available and inexpensive. Aldol condensation is an effective method for carbon-carbon double bond formation between various carbonyl compounds. Compared to other methods used in synthesizing 2PA chromophores, such as Heck and Sonogashira coupling reaction, aldol condensation is more practical and economical. Those features are important for industrial preparation with large scale. The reaction can be catalyzed with strong bases or acids[167] and complexes of metal (II) ions.[168] For ease of preparation and reduced costs, sodium hydroxide was used as catalyst for the condensation.
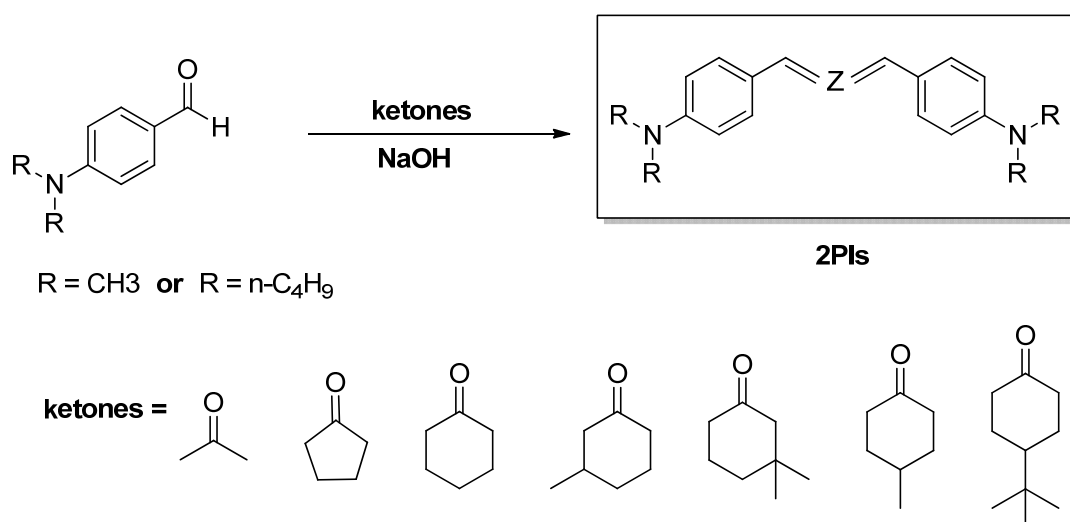
Fig 45 Reaction scheme for the synthesis of the 2PIs

The mechanism of aldol condensation under alkaline condition is shown in **Fig 46**.[169] At room temperature, one equivalent of the corresponding ketone (4-methylcyclohexanone, for example) is deprotonated at the α-position within a saturated sodium hydroxide solution. The resonance-stabilized enolate interacts with one equivalent of the aldehyde to form an alkoxide compound. Again, the base then deprotononates the α-carbon to form an enolate, which is subsequently subject to dehydration to form a α, β-unsaturated carbonyl. The mono-substituted product undergoes the same enolate formation and subsequent dehydration to form the di-substituted product.
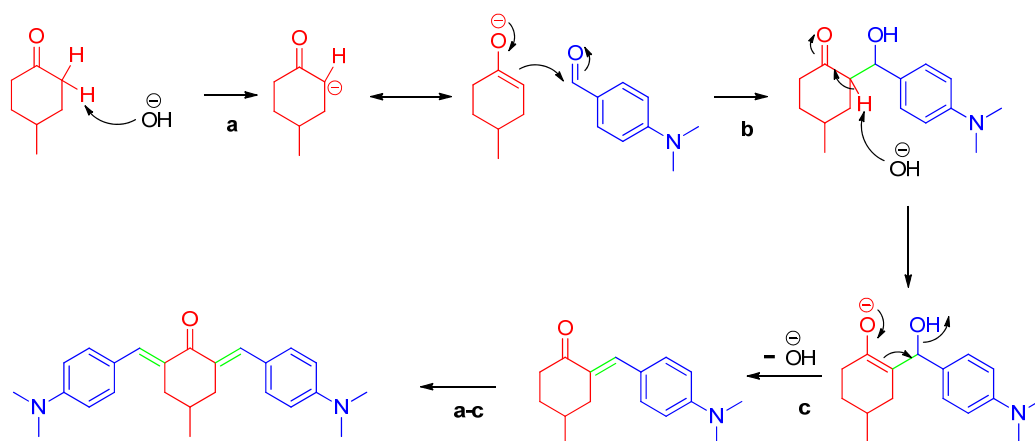
Fig 46 Mechanism of aldol condensation[169]

The linear and cyclopentanone-based 2PIs **M2K**, **M2CPK** and **B2CPK** were prepared by Dr. Nicolas Pucher during his PhD study.[85] 1.0 equivalent of freshly distilled ketones (acetone or cycloketones) dissolved in EtOH reacted with 2.0 equivalents of the aldehydes in the presence of 1.0 equivalent of sodium hydroxide (saturated solution). The

reaction was performed at room temperature in dark. The generated products generally precipitated due to the limited solubility in EtOH. High yields of 79% and 92% were obtained for **M2K** and **M2CPK**, respectively. The yield for **B2CPK** (57%) is much lower than that of its methyl substituted analogue **M2CPK**. One reason may be the stronger electron-donating ability of the butyl group, which reduces the electrophilic activity of the aldehyde group. Another possibility is the equilibrium shift of the coupling reaction due to the better solubility of **B2CPK**. By increasing the size of the central ring from cyclopentanone to cyclohexanone, the yields decreased to 45% and 40% for **M2CHK** and **M2CMK**, respectively. Reduced yield may derive from a steric hindrance effect of (4-methyl) cyclohexanone, which is obstructive for the nucleophilic addition reaction. The steric hindrance effect became much more significant when preparing **M2CIK**, **M2CHMK** and **M2CDK**, which contain (4-isobutyl) cyclohexanone, (3-methyl) cyclohexanone and (3,3-dimethyl) cyclohexanone, respectively. The yields greatly decreased to less than 1% due to the steric hindrance of the substituted groups on the cyclohexanone rings. The considerable low yields excluded these three compounds for the further investigation.

Unlike classical Wittig or HWE reactions, which usually generate *cis-* and *trans-* isomer mixtures, exclusively all-*trans* products were obtained in the aldol condensation reactions. The trans-configurations were confirmed by ^{1}H NMR where the proton signals for the CH= group in cycloketone compounds appear at 7.50-7.77 ppm. The chemical shifts of *E*-isomers are usually higher than 7.2 ppm, while the characteristic peaks for the Z isomers appear at ~6.8 ppm.[170] A coupling constant of 15.72 Hz for double bond protons was found, which is typical for the trans- isomers in the case of **M2K**.

It should be mentioned that the cross-conjugated dienones have been found to undergo spontaneous isomerization in solution under the scattered light irradiation. The size of the central ring was demonstrated to affect the degree of isomerization. The amount of the Z, E and Z, Z isomers increases when increasing the size of the cyclic rings from C5 to C8.[170]

2.3   Quantum-chemical calculations

In a close cooperation with Prof. Tom Scherzer and Dr. Sergej Naumov from Leibniz Institute of Surface Modification (IOM), Germany, quantum-chemical calculations were

carried out to theoretically study structure-property relationship of the 2PIs. Detailed information of the calculation results can be found in the published paper.[171] Here, more attention is paid to the optimized most stable structures, which indicate the coplanarity of the molecules and thus the degree of conjugation of the whole π systems.

The structure of reference compound **R1** is not planar. Due to the large NBu_2 groups with a strong pyramidality at the N atom (dihedral angle is about 26°), the aromatic rings on both sides are rotated by about 9° relative to the plane of the central ring. **B3FL** shows only a slight deviation from planarity due to the distortion from the large NBu_2 groups with strong pyramidality at the N atom (dihedral angle is about 22°). **M2K** and **M2CPK** have a planar geometry with only a small distortion at the NMe_2 groups (pyramidality with the dihedral angle = 15° in case of **M2CPK**). In contrast to **M2CPK**, the optimized structure of **B2CPK** is no longer planar, but shows a strong deformation at the cylopentane ring. This is apparently due to the strong distortion induced by the large NBu_2 groups. The two aromatic rings are twisted with respect to each other by about 41°. **M2CHK** and **M2CMK** have very similar structures, which are not planar due to the cyclohexane ring. However, the two aromatic rings are perfectly planar within the same plane.

2.4   Linear photophysics

Fig 47a depicts the absorption spectra of novel 2PIs in dichloromethane. All of them exhibit a rather intense ($\varepsilon > 5 \times 10^4$ $M^{-1}cm^{-1}$) and broad absorption band with the position of the maximum ranging from 430 (**M2CHK**, **M2CMK**) up to 480 nm (**B2CPK**). In addition a weaker band (with ε around 2×10^4 $M^{-1}cm^{-1}$) is found at 260 to 270 nm. An even weaker band can be tentatively identified in the region of 320 nm.
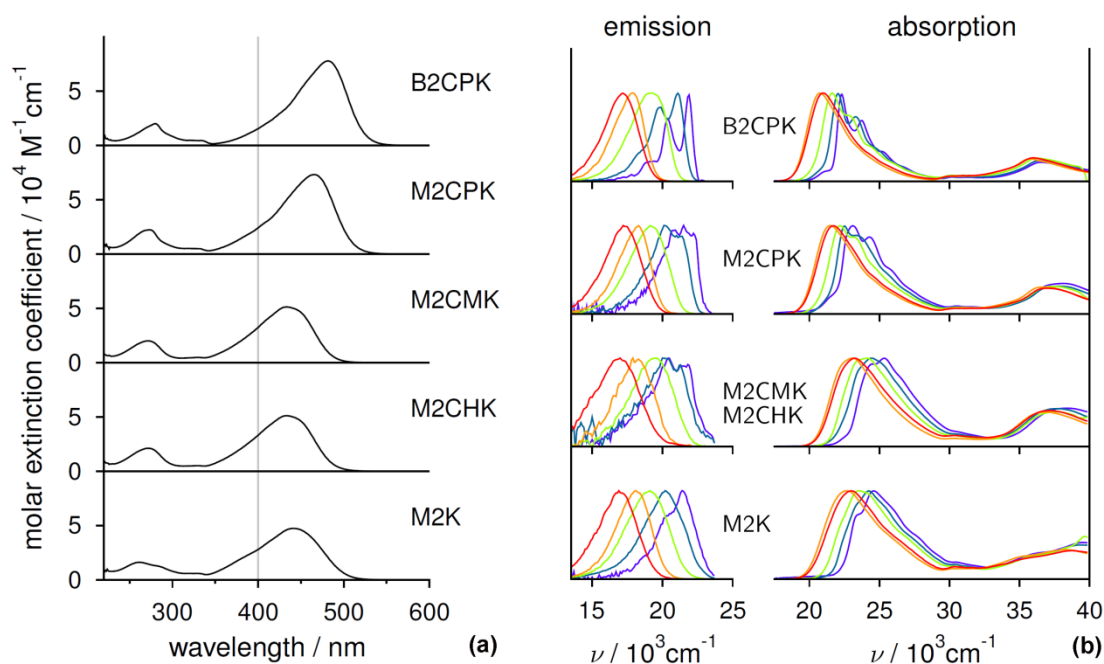
Fig 47 (a) Absorption spectra of the five PIs measured in dichloromethane. Note that the spectra of **M2CMK** and **M2CHK** are identical. (b) Normalized absorption (right) and corrected emission (left) spectrum for the five PIs in cyclohexane (violet), n-butyl ether (blue), propyl acetate (green), dichloromethane (orange) and acetonitrile (red).

The lowest energy absorption band of the five PIs allows relating structural molecular aspects to position and intensity of this band. Firstly, there is a slight trend of the maximum position of the absorption band on the type of the central acceptor group (cyclohexyl < linear < cyclopentyl). Additionally, the maximal molar extinction coefficient for the cyclopentyl PIs is significantly larger (by approx. 50%) than the one for the other three PIs (**Table 8**). Interestingly, methyl-substitution in the para position to the keto-group on the central cyclohexanone ring does not affect the photophysics (bandshapes, quantum yields, lifetimes) of the molecule. In fact, all measured photophysical properties for **M2CMK** and **M2CHK** are identical. Comparison of **B2CPK** and **M2CPK** shows, that substitution on the amino nitrogen with alkyl chains with increasingly electron donating character shows the expected bathochromic effect on the position of the lowest energy absorption band.

Table 8 Maximum molar extinction coefficients, ε_{max}, ($\pm 10\%$) of the investigated initiators in dichloromethane for the lowest energy absorption maximum (at λ_{max}).

2PIs	λ_{max} / nm	ε_{max} / 10^3 M^{-1} cm^{-1}
M2K	441	47

M2CPK	466	71
B2CPK	481	78
M2CHK	432	51
M2CMK	432	51

Fig 47b (and **Table 9**) shows the solvent dependence of the absorption and emission spectra of all five studied 2PIs. Both absorption and emission spectra show a pronounced red-shift and loss of vibronic structure upon increasing the solvent polarity. The latter is a common solvent dependence for optical spectra, while the former can be rationalized recurring to dipole moment changes between ground and electronically excited states. The emission quantum yields are strongly solvent dependent. Upon increasing the solvent polarity and thus decreasing the S_1-S_0 energy gap, the quantum yield in all PIs strongly increases. These observations are in striking contrast to the behaviour of references **R1** and **B3FL**. **R1** shows an almost solvent independent high emission quantum yield in the range from 0.59 to 0.79 in cyclohexane and acetonitrile, respectively.[136] **B3FL** on the other hand shows the opposite solvent dependence for the emission quantum yield.[172]

Table 9 Emission properties of 2PIs in five different solvents.

Solvent	DK	n	Φ_f	τ_f (ns)
		M2K		
cyclohexane	2.0	1.4235	6.2×10^{-4}	-
n-butyl ether	3.1	1.3968	7.1×10^{-3}	-
n-propyl acetate	6.0	1.3828	7.3×10^{-2}	0.20
dichloromethane	8.9	1.4210	1.5×10^{-1}	0.58
acetonitrile	35.9	1.3410	1.1×10^{-1}	0.76
		M2CPK		
cyclohexane	2.0	1.4235	2.4×10^{-3}	-
n-butyl ether	3.1	1.3968	2.4×10^{-2}	-
n-propyl acetate	6.0	1.3828	9.7×10^{-2}	0.56
dichloromethane	8.9	1.4210	1.4×10^{-1}	0.59
acetonitrile	35.9	1.3410	1.4×10^{-1}	0.68
		B2CPK		
cyclohexane	2.0	1.4235	1.2×10^{-2}	0.35
n-butyl ether	3.1	1.3968	7.2×10^{-2}	0.37
n-propyl acetate	6.0	1.3828	1.2×10^{-1}	0.46

dichloromethane	8.9	1.4210	2.0×10^{-1}	0.72
acetonitrile	35.9	1.3410	2.0×10^{-1}	0.80
M2CHK/				
M2CMK				
cyclohexane	2.0	1.4235	1.6×10^{-4}	-
n-butyl ether	3.1	1.3968	5.5×10^{-4}	-
n-propyl acetate	6.0	1.3828	4.6×10^{-3}	-
dichloromethane	8.9	1.4210	9.5×10^{-3}	-
acetonitrile	35.9	1.3410	2.2×10^{-2}	0.2

Φ_f is the fluorescence quantum yield and τ_f the fluorescence lifetime. DK and *n* are the dielectric constant and refractive index of the solvent at 25°C, respectively, from reference.[173]

2.5   Z-scan measurement

To investigate the 2PA properties of the new PIs, an open aperture z-scan analysis was performed to determine the 2PA cross sections at 800 nm. Since the solubility of the **M2CPK** and **M2CHK** are limited in THF, chloroform was used instead as solvent for the 2PA characterization. All calculated σ^{2PA} values are given in **Table 10**.

Table 10 2PA cross section, σ^{2PA} of the 2PIs in chroloform at 800 nm

2PIs	σ^{2PA} /GM
M2K	349/269[a]
M2CPK	466
B2CPK	327
M2CHK	352
M2CMK	191

[a]measured in THF.

Since intramolecular charge-transfer is utilized as the "driving force" for 2PA, strong electron-donor and electron-acceptor groups are required. In addition, long π-conjugated bridges and good coplanarity, which lead to states with extended charge separation, are critical in enhancing the efficiency of intramolecular charge transfer. The investigated benzylidene ketone-based 2PIs comprise typical D-π-A-π-D core structures with C_{2v} symmetry, where dialkylamino groups act as donors, vinyl as π-conjugated bridges and

carbonyl as acceptors. The open chain acetone-based PI **M2K** exhibits a large σ^{2PA} of 349 GM. When changing the acceptor group in **M2K** from an acetone group to a cyclopentanone moiety as in **M2CPK**, the value even increases to 466 GM. The enhancement may be due to a relatively higher molecular rigidity as well as a higher degree of conjugation compared to **M2K**.[122] Substitution of the N-methyl groups by butyl groups as in **B2CPK** led to a reduced σ^{2PA} of 327 GM. An explanation can be given by the red-shift-induced low 2PA absorption at the given wavelength. Another reason, as indicated in quantum chemical calculations, is the deformation of the central cylopentanone ring in **B2CPK** due to the strong distortion induced by the large NBu_2 group. The non-planar nature of the ring can decrease the conjugation and therefore lead to weak 2PA.

When increasing the size of the central ketone from cyclopentanone to cyclohexanone as in **M2CHK**, the σ^{2PA} value drops to 352 GM. The reduction in 2PA absorption might be explained by the non-planarity of the six membered ring, as indicated in quantum chemical calculations. The non-coplanarity property can lead to a decrease in the degree of conjugation. Interestingly, although the linear absorption spectrum of **M2CHK** is identical to that of **M2CMK**, methyl substitution at the 4-position on cyclohexanone dramatically reduces the σ^{2PA} of **M2CMK** to 191 GM. The above results indicate that not only the size of the central ring but also the ring-substitution can significantly affect the 2PA behavior of the benzylideneketone-based initiators.

2.6 2PP test

Defined woodpile structures (lateral dimension: 50×50 μm, 5 μm hatch-distance, 0.7 μm layer-distance, 20 layers) were written into the monomer formulation by means of 2PP to evaluate the activity of the 2PIs. The laser intensity was screened in a range of 1-27.82 mW (measured after passing the 100× microscope objective). The same formulation as used in chapter 1 containing a 1:1 mixture of TTA and ETA with the same molar PI concentration of 6.3×10^{-6} mol PI/g resin was employed for a better comparison. The full processing windows of the investigated 2PIs are shown in **Fig 48**.
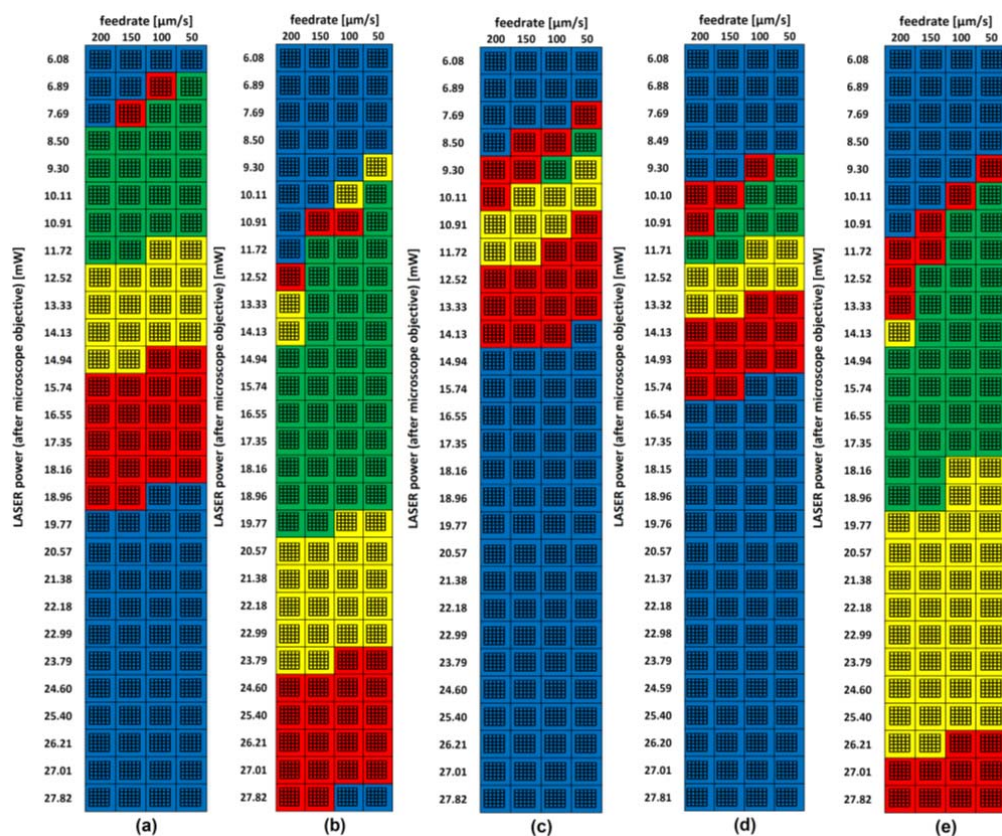
Fig 48 Processing Windows of 2PIs with different feed rate and laser power.
(a) **R1**; (b) **B3FL**; (c) **M2K**; (d) **B2CPK**; (e) **M2CMK**.

In order to quantitively evaluate the initiation efficiency of the 2PIs, the processing windows with different laser intensities and a constant writing speed of 50 μm/s were investigated as representatives (**Fig 49**). The evaluation standard is the same as the one used in chapter 1.
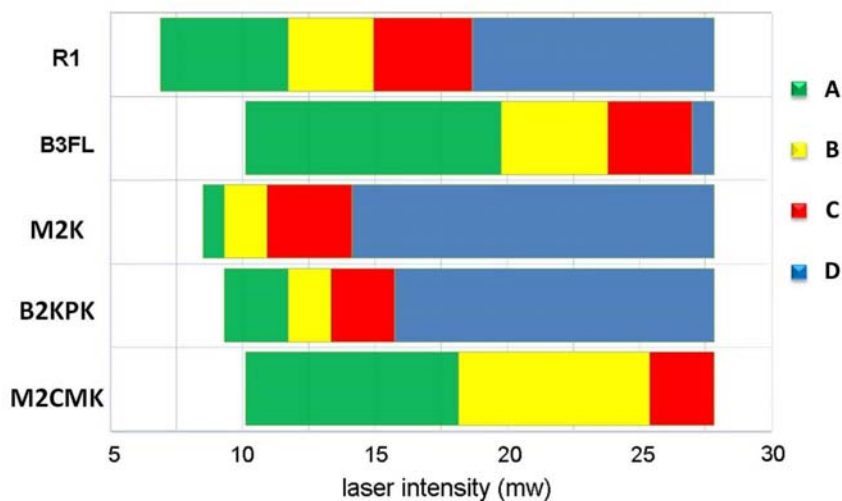
Fig 49 2PP screening tests of 2PIs
(PI concentration: 6.3×10^{-6} mol PI/g resin; writing speed: 50 μm/s).

The reference PI **R1** can be used to build nicely shaped structures at low laser intensities. On the other hand, the 2-,7-substituted fluorenone-based PI **B3FL** exhibits excellent performance in the 2PP test. Although slightly higher laser intensity is required for **B3FL** compared to **R1**, the ideal processing windows of **B3FL** are much broader than that of **R1**. The higher efficiency of such a triple-bond containing PI may derive from the larger σ^{2PA}, the exclusion of photo induced cis-trans isomerization and the lower fluorescence quantum yield.

The acetone-based initiator **M2K** gives nice structures at lower laser intensity than **B3FL**, but its ideal processing windows are significantly smaller. One reason is the relatively smaller 2PA cross section of **M2K**. Another main reason for the low efficiency of **M2K** lies in its strong fluorescence emission, which deactivates the active triplet state. In addition, the photochemical *cis-trans* isomerization can also reduce the initiation efficiency as well. By changing the acceptor group in **M2K** from an acetone group to a cyclopentanone moiety as in **M2CPK**, the solubility in the resins is dramatically decreased. An attempt to improve its solubility by adding drops of various organic solvents finally failed because of the heterogeneous solution obtained. Therefore, no comparable result with **M2CPK** in the structuring tests can be obtained due to its poor solubility. The substitution of the N-methyl groups by butyl groups in the cyclopentanone-based initiator **B2CPK** resolves the solubility problem. The ideal processing windows of **B2CPK** are slightly broader than those of **M2K**. The improvement may derive from the rigidity of the ring, which confines the rotation of the double bonds and thus reduces isomerization deactivation.

When increasing the size of the central ketone from cyclopentanone to cyclohexanone as in **M2CHK**, the solubility improves to some extent due to its non-planar molecular structure. The PI readily dissolved in the resin with the assistance of a few drops of chloroform. However, some precipitate formed when removing the last traces of solvent at 40 °C under vacuum. Therefore, similar to **M2CPK**, no comparable result for **M2CHK** can be obtained. By changing the electron acceptor from cyclohexanone to 4-methylcyclohexanone as in **M2CMK**, the solubility significantly improves. The enhancement is attributed to increased steric hindrance, which facilitates the dispersion of PI in the resin. Surprisingly, although **M2CMK** exhibits the smallest ^{2PA} among the investigated PIs, the ideal processing windows are much broader than those of other benzylidene ketone PIs and reference PI **R1**. The initiation efficiency is dependent not

only on ^{2PA}, but also on the quantum yield of active radical formation. Although initiator **M2CMK** possesses the smallest ^{2PA}, its fluorescence quantum yield is 5-10 times smaller than that of its analogues. Low fluorescence quantum yields are essential for efficient photoinitiators as this leads to less radiative deactivation and a higher population of the active state for initiating the polymerization. Such considerable enhancement was also observed by Duan's group[83] while studying the photoinitiation efficiency of other similar C_{2v} symmetrical 2PIs. For initiator **M2CMK**, high radical formation quantum yields tend to compensate its low 2PA cross section to ensure high initiation efficiency. The kind of compensation is common for some traditional UV photoinitiators, such as Irgure 369[174] and Lucirin TPO-L,[175] which are still used in 2PP. The activity of **M2CMK** in 2PP tests is as high as that of **B3FL**. It should be mentioned that **M2CMK** can be simply prepared in one step while the synthesis of **B3FL** required four steps and involved an expensive palladium catalyst. More complex 3D structures (**Fig 50a** and **b**) were inscribed into the material volume with an acrylate-based formulation containing **M2CMK** (0.2 wt %) as initiator.
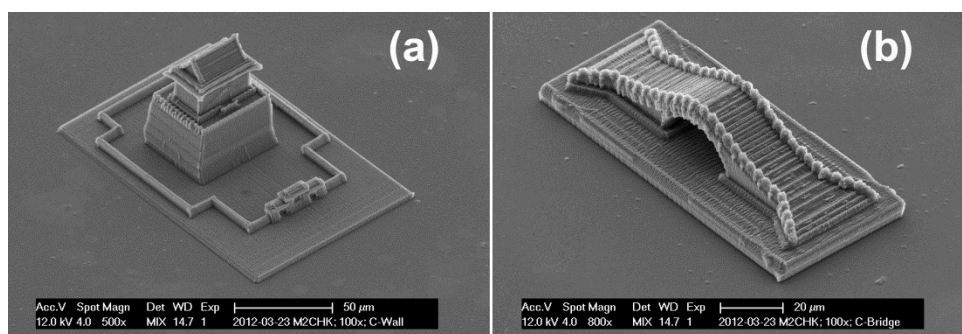
Fig 50 (a) Ancient tower in oriental style; (b) Chinese Jade Belt Bridge

Recently, a new 2PP micro-processing system Mipro has been designed by Dr. Jan Torgersen from Prof. Jürgen Stampfl's group. With improved mechanism of the mirrors, the focal point of laser can move with a high speed and precision (detailed information of Mipro can be found in Dr. Jan Torgersen's PhD thesis[23]). With the same formulation containing **M2CMK** as an initiator, only 4 minutes are required for fabricating a 3D racing car model, which is of $285 \times 130 \times 50$ μm^3 in dimensions and consists of 100 layers at an average of 200 polymer lines each (**Fig 51**). Taking the time used for positioning the mechanics, the focal point is traced in the resin at well above 80 mm/s. Due to inertia limitations of the experimental setup, the scanning speed is limited for this specific CAD structure. Using **M2CMK** as initiator, a 300 μm wide cube, sliced into layers of equidistant polymer lines, can be fabricated within acrylate-based formulations

at the speed of several m/s. This is remarkable since previously reported scanning speeds are below 10 mm/s.[101b]
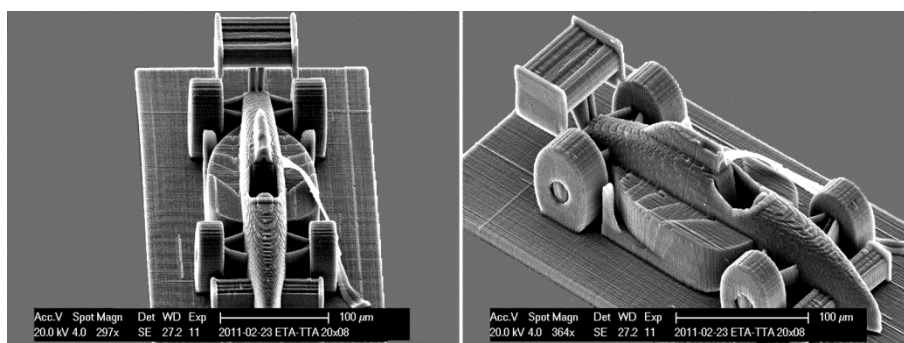
Fig 51 3D racing car model fabricated with 2PP

3   Water-soluble 2PIs

3.1   Molecular design of water-soluble 2PIs

The precise microfabrication of hydrogels with arbitrary predesigned shapes has become critical for construction of biosensors[176] and the creation of soft scaffolds[177] for tissue engineering. Among various microfabrication techniques, 2PP attracts considerable attention due to its unique capacity for direct 3D writing with high resolutions.[72] Moreover, the long wavelength of the excitation source offers the advantages of deeper tissue penetration with reduced risk for unintended photodamage,[20] making 2PP especially suitable for various biological applications.[177]

Ideal 2PIs for biofabrication should possess high initiation efficiency, sufficient hydrophilicity and good biocompatibility, especially low cytotoxicity, which is critical for cell encapsulation. Since a full understanding of the relationship of molecular structure and two-photon properties still remains a big challenge, the most effective way to produce efficient water-soluble 2PA PIs is to introduce water-borne functional groups, such as quaternary ammonium cations or different carboxylic sodium salts, into the known core structures possessing high 2PA initiation efficiency. One successful example is a distyrylbenzene chromophore with quaternary ammonium cations (**WSPI**), which has been prepared by Dr. Nicolas Pucher during his PhD study (**Fig 52**)[85] and been used as a potent hydrophilic 2PI to fabricate 3D hydrogel scaffolds in the presence of a living organism.[106] **B3FL** has been proven to be efficient 2PIs in chapter 1. Following the same strategy, the feasibility to introduce water-borne functionalities into the core structure of **B3FL** to obtain water-soluble 2PIs should be investigated.

Introducing quaternary ammonium cations as water-borne functionalities into the **B3FL** core structure has some disadvantages. First of all, due to the high sensitivity of the water-borne functionality, the introduction is generally realized at the very late steps via substitution of corresponding iodo intermediate with trimethylamine. Since the water-solubility of quaternary ammonium cations is limited, multiple substitutions are generally required to ensure enough hydrophilicity. However, uncompleted substitution often occurs, which makes the final purification more difficult. More importantly, the precursor with iodo groups attached at the terminal alkyl chains can induce some unwanted coupling reactions under Sonogashira reaction condition when constructing **B3FL** core

structures. To this end, carboxylic sodium salts become appealing due to their significantly improved hydrophilicity compared to quaternary ammonium cations, which makes the multiple substitutions unnecessary and thus can provide an easy purification. Moreover, several effective strategies have been developed to introduce carboxylic acid (or salts) groups, such as hydrolysis of nitrile, oxidation of alcohol and hydrolyzation of ester. These methods can provide more options when designing the synthesis routes and thus increase the possibility to obtain the desired products. The proposed water-soluble 2PI based on **B3FL** core structure as **WS-B3FL** is shown in **Fig 52**.

WSPI   **WS-B3FL**
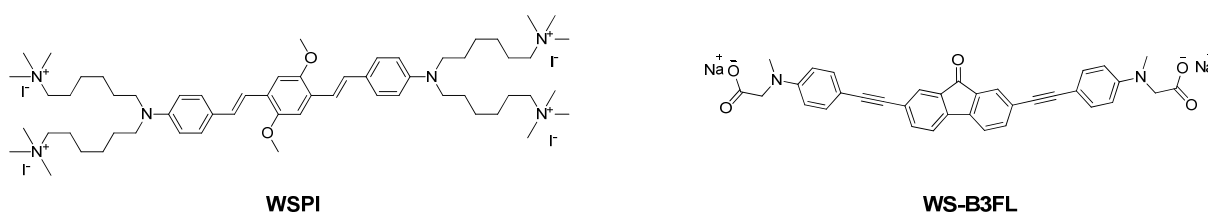
Fig 52 Chemical structure of **WSPI** and the proposed water-soluble 2PI

Similar to **B3FL, M2CMK** with very high initiation efficiency in 2PP tests is another attractive core structure. Since the formation of the conjugated molecule via straightforward aldol condensation does not require any expensive transition metal catalyst, the preparation of benzylidene cycloketone-based water-soluble 2PIs should be more economical, which allows large scale preparation and possible commercial applications. Wu's group reported a benzylidene cyclopentanone dye with four hydrophilic sodium carboxylate groups at the terminal alkyl chains.[69] They applied the molecule as a water-soluble 2PI or as sensitizer combined with triethanolamine for 2PP under aqueous condition. In chapter 2, different sizes of the central rings have been proven to have significant effect on their activity as initiators in 2PP. Therefore, higher initiation efficiency would be expected when expanding the central ring from cyclopentanone to cyclohexanone. On the other hand, since the project aims to realize the fabrication of 3D hydrogel scaffolds in the presence of living cells, cytotoxicity of 2PIs becomes a major concern. The singlet oxygen quantum yields of chromophore with cyclohexanone are much lower than that of its cyclopentanone analogue.[178] Lower singlet oxygen quantum yields mean lower photoinduced cytotoxicity, which is critical for cell encapsulation. In order to study the ring effect on 2PA behaviors and cytotoxicity under aqueous condition, **P2CK** with a five member ring and **E2CK** with a six member ring should be prepared and investigated (**Fig 53**).
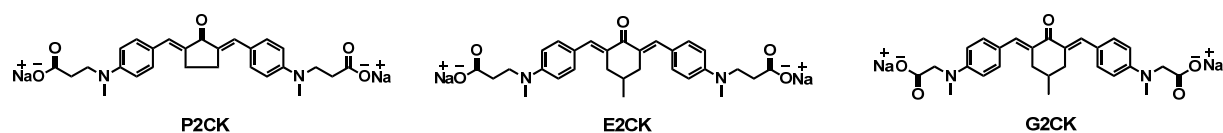
Fig 53 Proposed structures of the benzylidene cycloketone-based hydrophilic 2PIs

Besides studying the central ring effect, to explore alternative mechanism to ensure high initiation efficiency is of interest. Such exploration is critical because the aqueous environment generally reduces the 2PA considerably, therefore deactivates the initiation process. Currently reported 2PIs exclusively undergo intermolecular electron transfer mechanism between photoexcited chromophores and monomers, which subsequently produce active radicals for the polymerization.[94] Such bimolecular photoreaction suffers from the back electron transfer process, especially in the viscous formulation.[103]

Photoinduced decarboxylation of N-phenylglycine (NPG) has been well developed as a promising strategy to solve the problem derived from back electron transfer in UV photopolymerization.[179] The initiation mechanism involves electron transfer between excited sensitizers and NPG, followed by decarboxylation to generate active amine species for polymerization.[179] Recently, phenylthioacetic acid sodium salts were described as efficient photoinitiators for UV curing within water-based formulations.[180] Therefore, incorporation of phenylglycine sodium salts groups into the 2PA chromophore as in **G2CK** (**Fig 53**) should be investigated to explore the possibility of 2PA induced decarboxylation with a purpose to develop an efficient mechanism to facilitate the 2PP process. It should be mentioned that, the waster-soluble 2PIs **WS-B3FL** with phenylglycine sodium salts moieties can also potentially undergo 2PA induced decarboxylation via the same mechanism as described above.

3.2   Synthesis

For the synthesis of **WS-B3FL**, three synthesis routes were proposed according to different methods to introduce carboxylic acid (salt) groups (**Fig 54**).
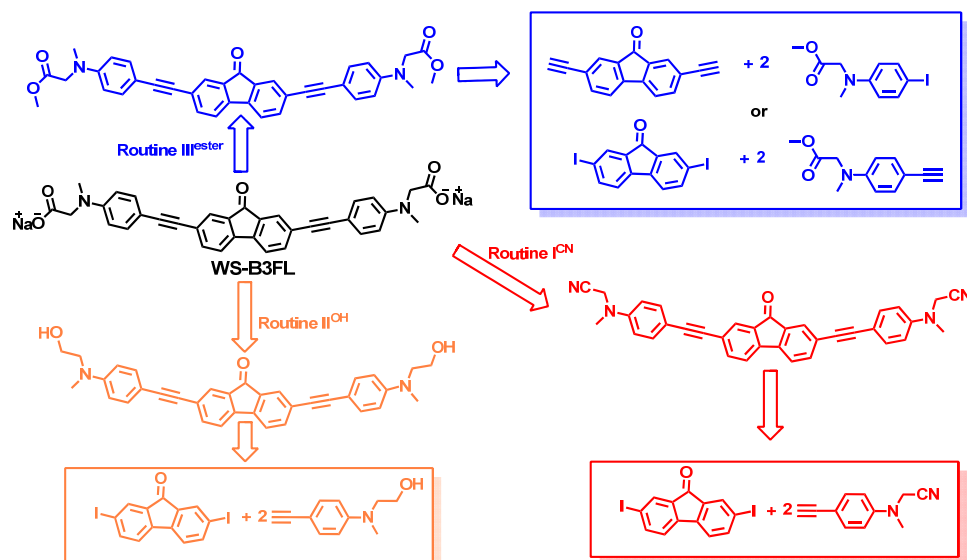
Fig 54 Retrosynthesis of the WS-B3FL

In route I^{CN}, nitrile groups undergo hydrolysis to form corresponding carboxylic acid salts. Such route is quite appealing because according to the literature,[181] the nitrile-containing aryl alkyne precursor can be prepared in one step. The ease of synthesis makes it possible to provide partners with larger quantities of initiators and for possible commercial applications. The risk of the route is the unknown effect of the terminal nitrile groups on the Sonogashira coupling reaction.

In route II^{OH}, oxidation of the terminal alcohol gives the desired carboxylic acid. Since the synthesis of the terminal hydroxyl-containing aryl alkyne has been well developed[182] and the presence of hydroxyl groups do not exhibit any negative effect on the Sonogashira coupling,[183] the synthesis route to obtain the hydroxyl-containing fluorenone intermediate is quite feasible. Such intermediate is very versatile because besides converting hydroxyl groups to carboxylic acid via oxidation, other functional groups such as acrylate can be introduced to prepare self-polymerizable 2PIs or polymeric 2PIs. The risk of the route II^{OH} is that the long conjugation system containing triple bonds as π bridges is apt to be oxidized. Therefore, model oxidation reaction should be conducted to check the stability of **B3FL** core structure before synthesizing the precursors for the coupling reactions.

In classical route III^{ester}, the ester groups undergo hydrolysis to form corresponding carboxylic acid salts. The proposed synthesis route is quite straightforward. The coupling reaction can be realized between aryl alkynes containing ester group and diiodo-

fluorenone or between aromatic iodo compounds with ester group and fluorenone containing two terminal alkyne groups.

For the preparation of benzylidene cycloketone-based hydrophilic 2PIs, two synthesis routes were proposed according to the order of introducing the water-borne functional groups into the core structure (**Fig 55**).
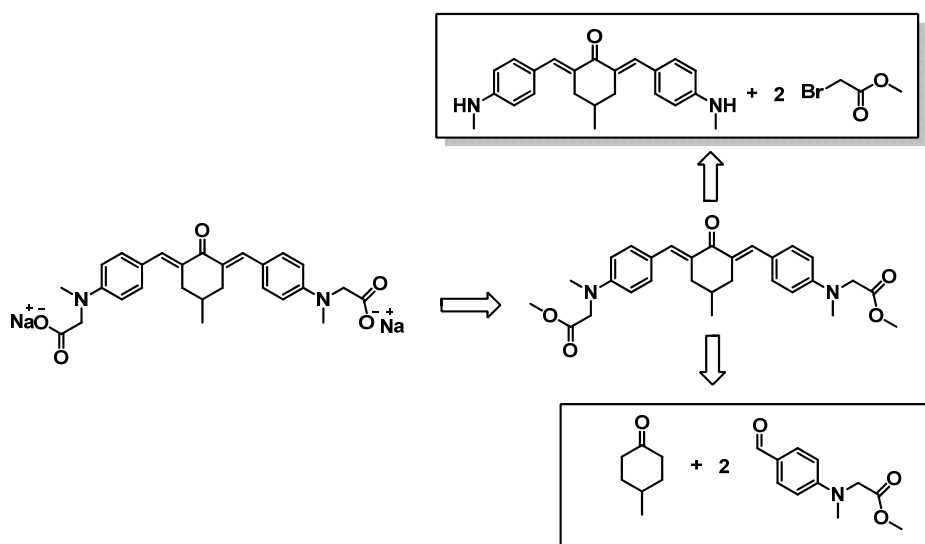
Fig 55 Retrosynthesis of the benzylidene cycloketone-based water-soluble 2PIs

In route I^{after}, the ester groups, which would be subject to hydrolysis to give carboxylic acid salts, were proposed to be introduced after the aldol condensation. The secondary aromatic amine intermediate is very attractive because it allows introducing various functionalities via alkylation. The disadvantage is that the condensation of secondary aromatic amines with cycloketones is synthetically unknown.

In route II^{before}, the benzene aldehyde with ester groups is prepared and then used to couple with corresponding cycloketones via aldol condensation. Since a very similar compound containing cyclopentanone with four terminal carboxylic sodium salts has been reported by Wu *et al*. using a similar synthesis strategy,[69] the formation of desired benzylideneketone via route II^{before} is quite feasible.

3.2.1   Synthetic route I^{CN} to give WS-B3FL

The retrosynthetic analysis revealed that this route is very attractive because the key precursor nitrile-containing aryl alkyne can be prepared in one step according to Han *et al.*[181] by oxidation of tertiary amines in the presence of inexpensive and non-toxic iron salts without designed ligands. Although the effect of the terminal nitrile groups attached to an alkyl chain on the Sonogashira coupling reaction is synthetically unknown, several reports has proven that the Sonogashira coupling can be realized between aromatic nitrile compound and corresponding iodo compounds.[184]

Attempt to prepare the α-aminonitrile compound was conducted as described by Han *et al.*[181]
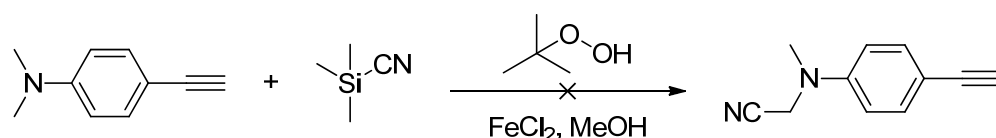
Under an atmosphere of dry N_2, 2.0 equivalents of trimethylsilyl cyanide and absolute MeOH were added successively by syringe to a flask charged with 1.0 equivalent of 4-ethynyl-N,N-dimethylbenzenamine (synthesized by Dr. Nicolas Pucher and freshly purified by column chromatography before using) and 0.1 equivalent of $FeCl_2$. To the mixture was added dropwise 2.5 equivalents of *tert*-butyl hydroperoxide (5.5 M in decane). The color of the solution changed from green to dark red. The solution was heated to 50 °C until the complete consumption 4-ethynyl-N,N-dimethylbenzenamine (monitored by TLC). Unfortunately, the desired product was not formed from the results of GC-MS and ^{1}H-NMR after column chromatography. Using different reaction conditions ($FeCl_3$ instead of $FeCl_2$, temperature, starting material addition order) did not provide the desired product.

In order to verify the feasibility of the reaction condition, dimethylaniline was used as substrate instead of 4-ethynyl-N,N-dimethylbenzenamine for the α-cyanation. The result of GC-MS indicates the formation of the mono α-aminonitrile under the identical reaction condition. Therefore, the unsuccessful α-cyanation is caused by the substrate. The reason might be that the alkyne group become labile in the presence of the oxidant.[185]
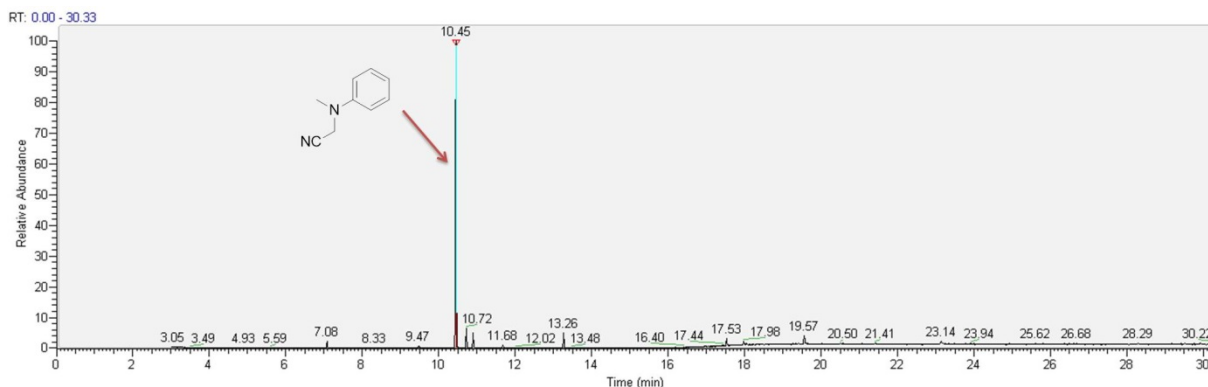
3.2.2 Synthetic route II^OH to give WS-B3FL

In route II^{OH}, the introduction of carboxylic acid is realized by oxidation of the terminal alcohol groups. Since the synthesis of the terminal hydroxyl-containing aryl alkyne has been well developed[182] and several reports have proven the feasibility of the Sonogashira coupling in the presence of hydroxyl groups attached to the alkyl chains,[183] the key step of route II^{OH} is the final oxidation of the terminal alcohol to provide the desired carboxylic acid. Therefore, model oxidation reaction should be conducted to check the stability of **B3FL** core structure before synthesizing the precursors for the coupling reactions.

Generally, oxidation of primary alcohols can provide corresponding carboxylic acids. The most common and economical oxidants include potassium permanganate ($KMnO_4$) and Jones reagent. $KMnO_4$ is not suitable for the model oxidation of **B3FL** because of its strong oxidative capacity, which can potentially destroy the C=C and C≡C bonds. To this end, Jones reagent becomes appealing because the carbon-carbon double bonds and triple bonds are not affected under the Jones oxidation condition. Therefore, the model oxidation of **B3FL** was conducted as describe by Sniady *et al*. using Jones reagent as the oxidant.[186] To a solution of 1.0 equivalent of **B3FL** in acetone, 1.5 equivalents of Jones reagent was added dropwise by syringe at 0 °C. The solution changed from red to green when adding Jones reagent. The result of TLC after 10 min showed that **B3FL** had been completely consumed. Therefore, **B3FL** with long conjugation length cannot stand the applied Jones oxidation condition. Optimizing the concentration of the Jones reagent might provide the possibility for the selective oxidation. However, the optimization

required the preparation of Jones reagent with various concentrations. Considering the serious toxicity of chromium trioxide, no further effect was made on such route.

3.2.3 Synthetic route III^{ester} to give WS-B3FL

The proposed synthesis route III^{ester} is classical and quite straightforward. The carboxylic acid salts are expected to be formed via hydrolysis of the ester groups. Theoretically, the coupling reaction can be realized between aryl alkynes containing ester group and diiodo-fluorenone or between aromatic iodo compounds with ester group and fluorenone containing two terminal alkyne groups. The later method was chosen because when preparing the aryl alkyne precursor containing ester groups with 2-methyl-3-butyn-2-ol, the subsequent deprotection needs to be performed in the presence of KOH. The ester groups would be hydrolyzed under the strong alkaline condition.
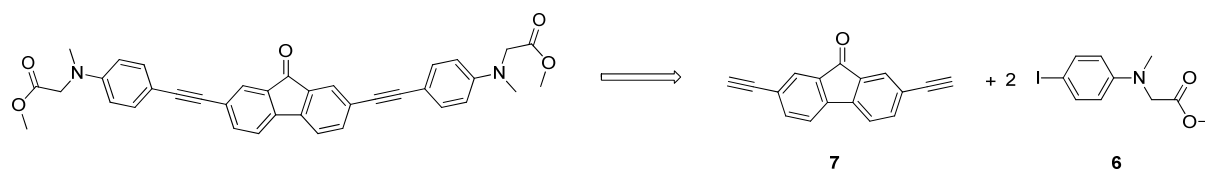
3.2.3.1 Synthesis of iodo precursor 6

The iodo precursor **6** was prepared by iodination of N-methyl aniline, followed by alkylation to introduce the ester group.
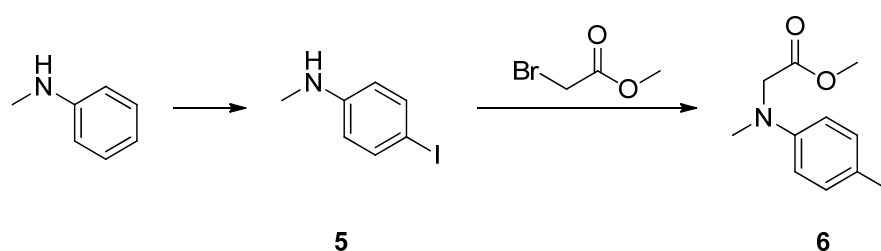
The mono-substituted aniline **5** can be prepared by alkylation of iodo-aniline with methyl iodide.[187] In such method, the unwanted di-alkylation cannot be avoided and thus leads to more difficult purification. Another more general method is iodination of the N-methyl aniline with various iodinating reagents, such as N-iodosuccinimide[188] and NaI or molecule iodine in the presence of oxidant.[189] Considering the reagent accessibility, the iodination was conducted as described by Sosnowski *et al*.[190]
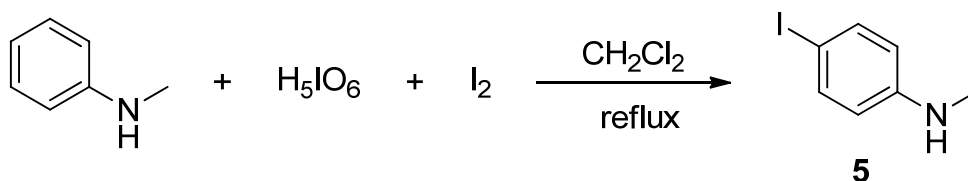
1.0 equivalent of H_5IO_6 and 2.7 equivalents of finely powdered diiodine were suspended with stirring in CH_2Cl_2 (25 mL). Then, 7.0 equivalents of N-methylaniline were added and the solution was heat to reflux until N-methylaniline was completely consumed (monitored by GC-MS analysis). The desired mono-substituted aniline precursor **5** was obtained as yellow oil with a yield of 60 % after column chromatography

The alkylation of the mono-substituted aniline **5** with methyl bromoacetate was conducted with a very similar procedure as described by Parisel *et al.*[191]
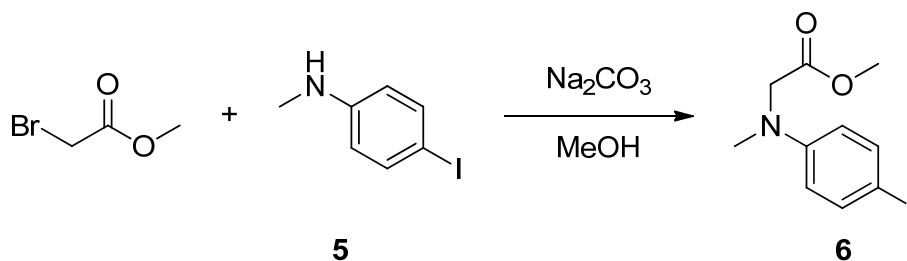
1.1 equivalents of methyl bromoacetate were added to a solution of 1.0 equivalent of the mono-substituted aniline **5** in MeOH. The reaction mixture was stirred at 80 °C until **5** was completely consumed (monitored by GC-MS analysis). The desired ester **6** was obtained as yellow oil with a yield of 80 % after column chromatography.

3.2.3.2 Synthesis of alkyne precursor 7

The reported synthesis route of the terminal alkyne precursor **7** was exclusively prepared by Sonogashira coupling reactions of 2,7-diiodo fluorenone with (trimethylsilyl)acetylene followed by a subsequent cleavage of the protection group in two steps.[192] 2-Methyl-3-butyn-2-ol is also frequently used to introduce terminal alkyne group, but with much lower price compared to (trimethylsilyl)acetylene. Therefore, the attempt to prepare the dialkyne **7** with 2-methyl-3-butyn-2-ol was conducted for economical reason. The Sonogashira coupling reaction of 2,7-diiodo fluorenone with 2-methyl-3-butyn-2-ol proceeded smoothly, but the desired product was not formed after deprotection. The reason might be that the carbonyl group becomes labile under the strong alkaline condition for the deprotection.
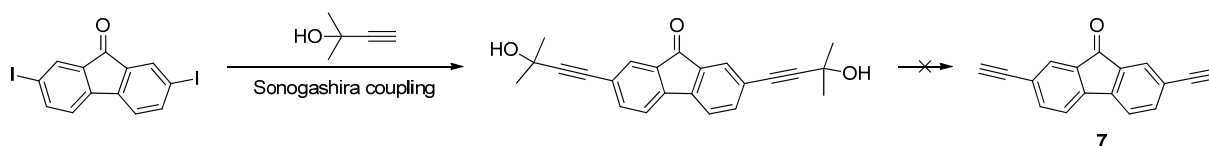
Therefore, (trimethylsilyl)acetylene was used for the Sonogashira coupling reactions to prepare the dialkyne **7** as described by Rodriguez *et al* in two steps.[193]
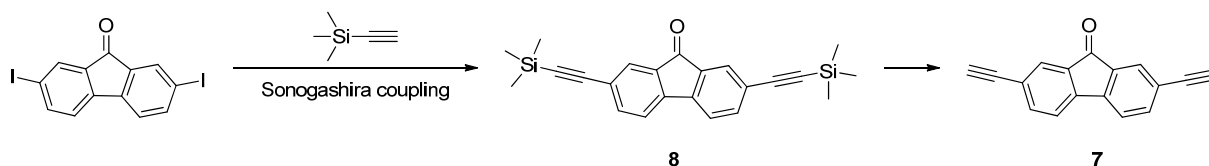
To a solution of 2,7-diiodo-fluorenone in degassed and dry THF/Et$_3$N mixture (1:1) under argon atmosphere, 2.5 equivalents of (trimethylsilyl)acetylene, 0.2 equivalents of CuI and 0.1 equivalents of PdCl$_2$(btpp) were added. The reaction was stirred under room temperature until the complete consumption of 2,7-diiodo-fluorenone (TLC analysis). The crude product was extracted and purified by column chromatography to give the protected dialkyne **8** as yellow powder with a satisfying yield of 62%.

Subsequently the terminal alkyne **7** was generated by deprotection. For the cleavage of the protecting group, the protected dialkyne **8** was dissolved in absolute methanol and 5 equivalents of powdered K$_2$CO$_3$ were added. This suspension was stirred under room temperature until the complete consumption of **8** (TLC analysis). The crude product was washed and subsequently purified by column chromatography to give the desired terminal dialkyne **7** as orange powder in a good yield of 70%.

3.2.3.3   **Attempt of coupling reaction via Sonogashira reaction**

The Sonogashira coupling reaction of the iodide **6** with the terminal alkyne **7** was conducted using the classical reaction condition.[192a]
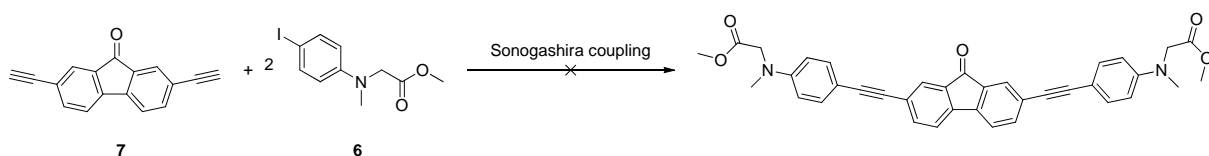
Under argon atmosphere, 1.0 equivalent of the terminal alkyne **7** and 2.5 equivalents of the iodide **6** dissolved in degassed and dry THF/Et$_3$N mixture (1:1). Then 0.2 equivalents

of CuI and 0.1 equivalents of PdCl$_2$(btpp) were added. The reaction was stirred under room temperature until the complete consumption of **7** (monitored with TLC). ^{1}H-NMR was performed for the characterization after column chromatography. However, the result of ^{1}H-NMR indicates that no desired product was formed.

In order to verify the feasibility of the reaction condition, the iodide **1a** was used as substrate instead of the iodide **6** for the coupling reaction. The results of TLC and ^{1}H-NMR indicate the formation of **B3FL** under the identical reaction condition. Therefore, the unsuccessful coupling is caused by the substrate **6**. The ester group might complex with the palladium catalyst and induces the unwanted reactions.
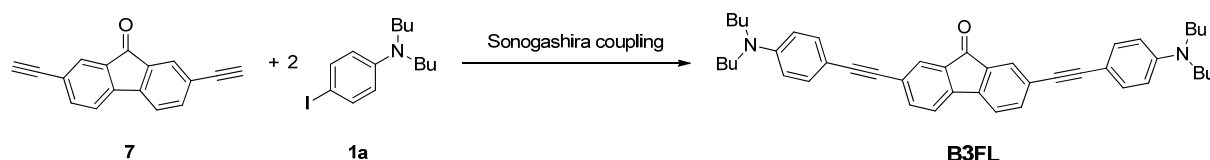
3.2.4 Synthetic route I$^{\text{after}}$ for benzylidene cycloketone-based 2PIs

In route I$^{\text{after}}$, the ester groups were proposed to be introduced after the aldol condensation. The mono-substituted amine intermediate is very appealing because various functionalities can be introduced to the amino groups via alkylation. The proposed synthesis of the intermediate is based on the aldol condensation of N-methylaminobenzaldehyde **9** with commercially available cycloketones.
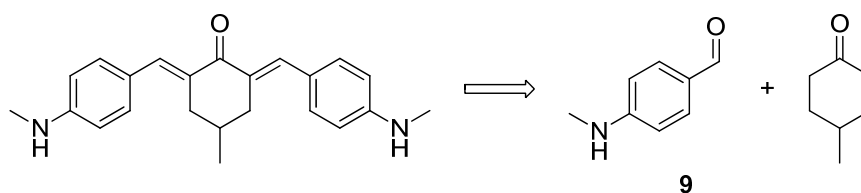
3.2.4.1 Synthesis of mono-substituted amine precursor *9*

Several strategies have been developed to prepare the key aniline precursor **9**. The method reported by Goswami *et al*. involves an amide formation via alkylation and subsequent rearrangement of the amide in the presence of alkali to provide the

corresponding amine.[194] The linear synthesis route requires multiple steps and suffers from the low yield (less than 10% for 3 steps).
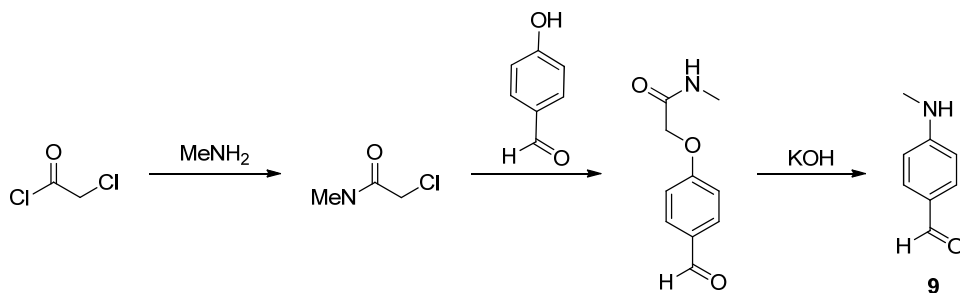
Jiao *et al.* reported a facile and practical Ullmann amination of aryl halides with aqueous methylamine catalyzed by copper powder. The reaction was conducted in air at high temperature, giving N-arylamines as sole products in good yields.[195] Such method is quite appealing because of its simpleness. Another direct synthesis is reported by Blaser *et al.* via an improved Vilsmeier-Haack reaction of N-methylformanilide with an equimolecular quantity of oxalyl chloride.[196] This one-pot synthesis is straightforward but needs a more complicated workup process compared to the Ullmann amination. For the ease of preparation, the first attempt to prepare the aniline precursor **9** was performed using Ullmann amination as described by Jiao *et al.*[195]
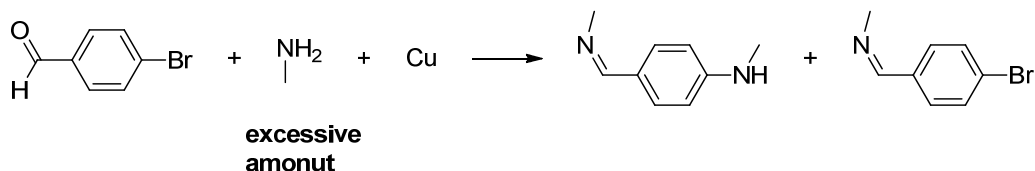
A mixture of 1.0 equivalent of 4-bromobenzaldehyde, 5.0 equivalents of methylamine (30% aqueous solution), 0.05 equivalents of copper powder and a stirring bar were sealed in a 30 mL screwed tube and stirred at 100 °C for 13 h. After workup, GC-MS was performed to analyze the crude reaction mixture.

The desired product cannot be directly observed from GC-MS because of the imine formation of the aldehyde group on the aniline precursor **9** with the excessive amounts of methylamine. The methylamine also reacted with aldehyde groups on the starting materials to form the corresponding Schiff base. Moreover, the content ratio of the two Schiff base indicates that the rate of imine formation of 4-bromobenzaldehyde with methylamine is faster than that of the Ullmann amination of 4-bromobenzaldehyde with methylamine under the employed reaction condition.
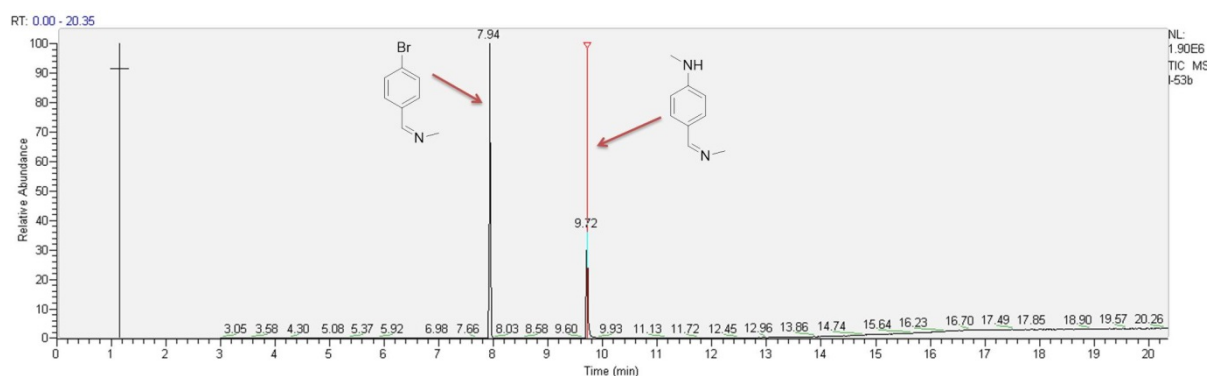
Since the Ullmann amination cannot provide the desired aniline product **9**, improved Vilsmeier-Haack reaction was conducted as described by Blaser *et al.*[196]
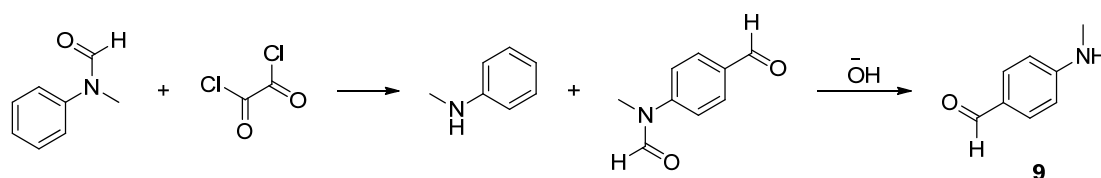
2.0 equivalents of oxalyl chloride were slowly added to 1.0 equivalent of N-methylformanilide while maintaining the temperature between 40-50 °C. The solution was stirred at room temperature for 12 h. Then the solution was dissolved in water and alkalized with 6N sodium hydroxide solution. The by-product N-methylaniline was removed by steam distillation and the residual solution was extracted with CH$_2$Cl$_2$. After removing the solvent, the residual red oil was distilled (185-187 °C/15mm) to give the desired mono-substituted aniline **9** as light yellow oil with a satisfying yield of 36%.

3.2.4.2   **Attempts of coupling via aldol condensation**

Until now, the benzylideneketone compounds with mono-substituted amino groups were exclusively reported by patents without detailed information of the preparation.[197] Therefore, the synthesis was conducted using the classical aldol condensation condition. 1.0 equivalent of the 4-mehtylcyclohexanone, 2.0 equivalents of **9** and 1.0 equivalent of NaOH were dissolved in EtOH. The reaction was stirred in dark at room temperature.

9
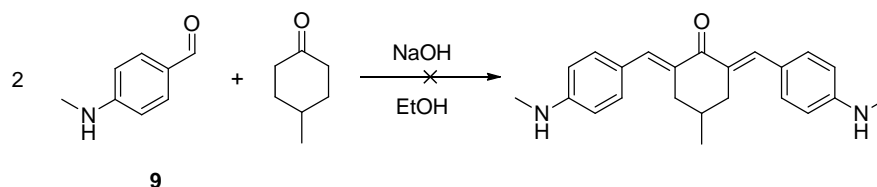
The results of TLC and ^{1}H-NMR indicated that the desired condensation reaction did not occur. Elevating the temperature up to 80 °C and prolonging the reaction time up to 48 h did not make any improvement. The reason for the unsuccessful condensation might be the lability of secondary amine under strong alkaline condition, which can induce some unwanted reaction between amine and ketone groups.

3.2.5   Synthetic route I^{before} for benzylidene cycloketone-based 2PIs

In route II^{before}, the benzene aldehyde with terminal ester groups are prepared and then used to couple with corresponding cycloketones via aldol condensation. Since the cycloketones are commercially available, the aldehydes with terminal ester groups become the key precursors for the aldol condensation.

10 R = CH$_2$COOCH$_3$

11 R = CH$_2$CH$_2$COOCH$_3$
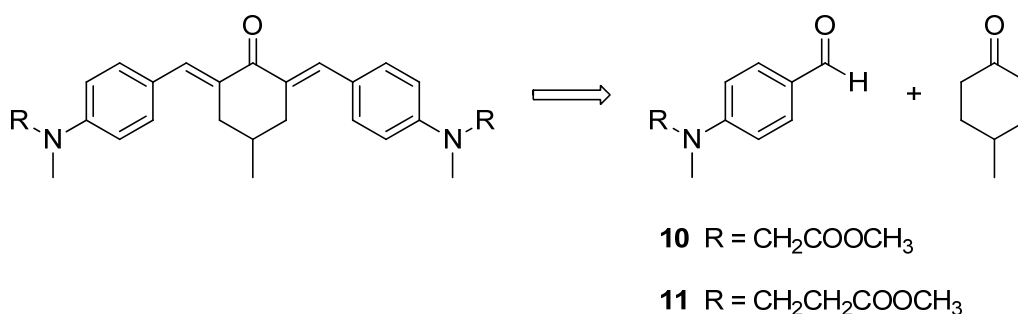
3.2.5.1   Synthesis of benzaldehyde precursor 10

The key aldehyde precursor **10** for the preparation of **G2CK** were synthesized in two steps with a very similar procedure as described by Zheng *et al.*[198]

12
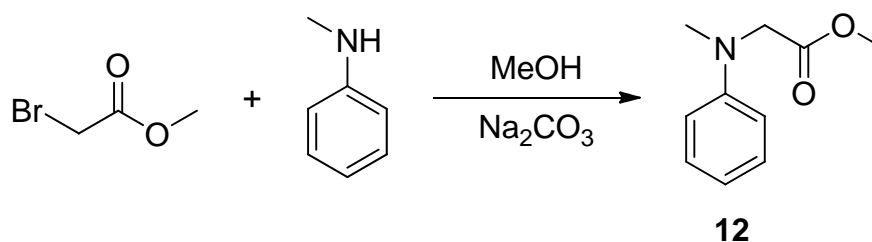
1.0 equivalent of N-methylaniline reacted with 1.1 equivalents of methyl bromoacetate under reflux in the presence of sodium carbonate as an acid acceptor. Methanol rather

than other alcohol was used as the solvent to prevent the interesterification. Purification by column chromatography gave the aniline precursor **12** as light yellow oil with a good yield of 85%.

Then aldehyde group was introduced to the *para*-position of the aniline **12** via Vilsmeier–Haack reaction to prepare the aldehyde precursor **10**. Vilsmeier–Haack reaction is a powerful method to produce an aryl aldehyde or ketone via substitution of amide with phosphorus oxychloride and an electron-rich arene.
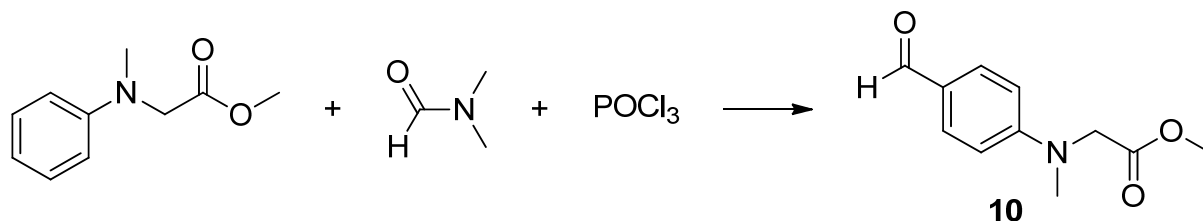
Phosphorous oxychloride were added dropwise to dry DMF at 0 °C and kept stirring for 30 min to form a substituted chloroiminium ion, also called the Vilsmeier reagent. Then an equimolecular quantity of **1a** was added to react with the generated electronphlic chloroiminium ion. The reaction was subsequently heated to 75 °C due to the limited electronphilicity of the Vilsmeier reagent. The initially formed product was an iminium ion, which subsequently underwent hydrolyzation to obtain the desired aromatic aldehyde **10** with good yields of 60% after column chromatography.

3.2.5.2   **Attempt of coupling via aldol condensation of 10 and cycloketone**

In order to verify the feasibility of the aldol condensation of the aromatic aldehyde **10** with cycloketone, 2.0 equivalents of **10** was added into MeOH solution containing 1.0 equivalent of 4-methycyclohexanone.
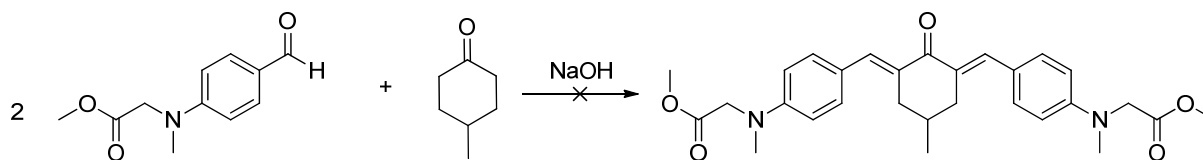
Considering that the ester groups can be hydrolyzed in the presence of NaOH, excessive amount of base (3.0 equivalents) was added. The reaction was performed at room temperature and monitored by TLC. After 48 h, no new spot was observed on TLC plate. The result of ^{1}H-NMR indicated that no aldol condensation occurred. Adjusting the

amount of base, prolonging the reaction time and increasing the reaction temperature did not make any improvement.

The unsuccessful aldol condensation might be caused by the unsuitability of the used solvent because the successful condensation of cyclopentanone with benzaldehyde containing terminal carboxylic sodium salts has been reported using water as solvent.[69] Therefore, the hydrophilic benzaldehyde with terminal carboxylic sodium salts need to be prepared for the condensation under aqueous condition.

3.2.5.3 Synthesis of hydrophilic benzaldehyde 13

The hydrophilic benzaldehyde precursor **13** with carboxylic acid sodium salt was obtained by hydrolyzation of the ester group of **10** in the presence of NaOH. Excessive amount of base (3.0 equivalents) was used to ensure the completeness of the hydrolyzation.
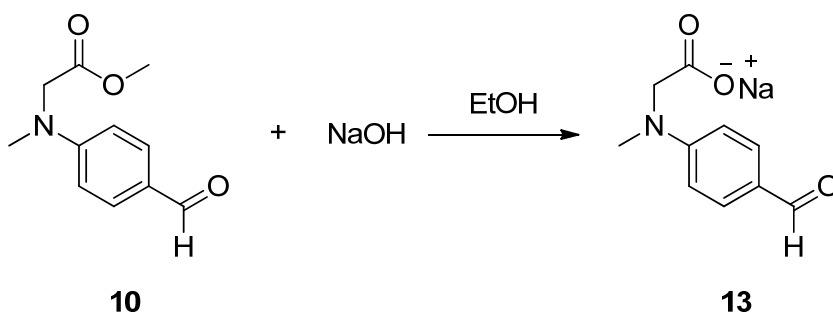
3.2.5.4 Synthesis of hydrophilic benzaldehyde 14

Another important hydrophilic precursor **14** for the preparation of **P2CK** and **E2CK** can be synthesized using the similar strategy for the preparation of **13**. Such synthesis route is universal since ester group can be introduced to the terminal amino group with various lengths of alkyl spacers.
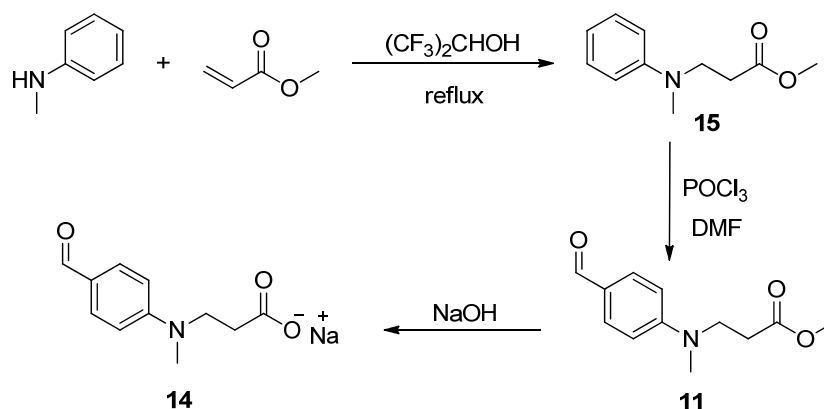
Another more straightforward method is applied specifically for the preparation of benzaldehyde **14** only with ethylene as the spacer. The approach is based on the hydrolysis of nitrile to form carboxylic acid group.[199]
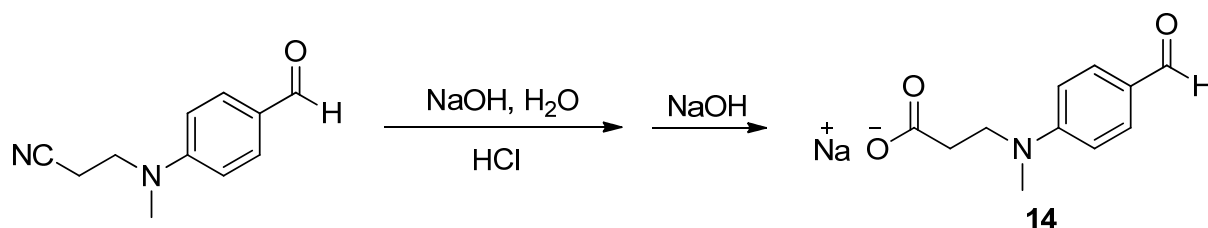
1.0 equivalent of 3-((4-formylphenyl)-(methyl)-amino) propanenitrile was suspended in water containing 5.0 equivalents of NaOH. The reaction mixture was refluxed until the complete consumption of the nitrile compound (monitored by TLC). The suspended reaction mixture became clear as the hydrophobic nitrile group was converted to hydrophilic carboxylic acid sodium salt. After filtration, dilute HCl solution was added into the filtrate to precipitate the formed propionic acid. Purified by simply washing with water gave the product as yellow powder with a high yield of 90%. The sodium salt precursor **14** can be obtained by neutralizing the propionic acid with NaOH aqueous solution before starting the aldol condensation.

3.2.5.5   Synthesis of water-soluble 2PIs

The water-soluble 2PIs were prepared via a classical aldol condensation reaction between the hydrophilic benzaldehyde precursors (**13** and **14**) and corresponding ketones (cyclopetanone and 4-methylcyclohexanone).
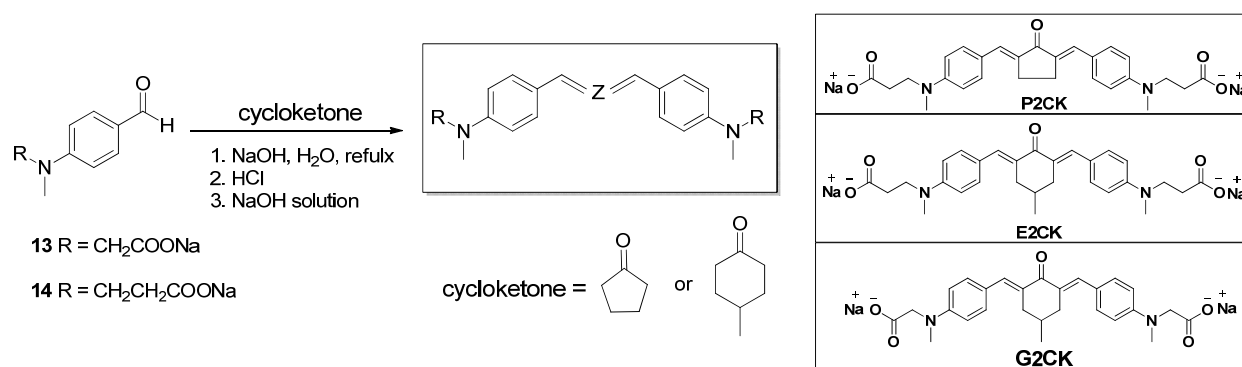
In an orange light room, 1.0 equivalent of potassium hydroxide, 2.0 equivalents of the benzaldehyde compounds and 1.0 equivalent of the freshly distilled cycloketones were dissolved in water. The reaction was stirred at 80 °C for 4 h and then EtOH and diluted HCl were added consequently until no precipitate formed. The red solids were collected by centrifugation and dried in vacuum. The obtained solids can be purified by washing with small amount of cold MeOH. But such method can induce about 20% loss of the product. Improved purification was developed by Daniel Bomze from our institute. The five member ring compound can be purified by recrystallization from 2-propanol, while the six member ring compounds can be purified by column chromatography using chloroform with small amount of acetic acid as eluent. The purified acids were neutralized with 0.1M NaOH until pH 8.5 was reached (monitored with pH meter). The undissolved solids were filtered off and water was removed via freeze-drying to yield desired products.

Satisfying yields of 50 % were obtained for **P2CK**. By increasing the size of the central ring from cyclopentanone to 4-methylcyclohexanone, the yields decreased to 33% and 30% for **G2CK** and **E2CK**, respectively. Reduced yields may derive from sterical hindrance of the cyclohexanone ring, which is obstructive for the nucleophilic addition reaction. Such an effect was also observed for the synthesis of analogous hydrophobic cyclohexanones in chapter 2.

3.3   Z-scan measurement of the water-soluble 2PIs

To investigate the 2PA properties of the new PIs, an open aperture z-scan analysis was performed to determine the 2PA cross sections at 800 nm with the same PI concentration of 1.0×10^{-2} mol.L^{-1}. Water was used as solvent for the 2PA characterization of all the investigated PIs. All calculated σ^{2PA} values are given in **Table 11**.

Table 11 2PA cross section values of 2PIs in water by z-scan measurement at 800 nm

2PIs	σ^{2PA} (GM)
P2CK	176
G2CK	163
E2CK	201

The investigated 2PIs comprise typical D-π-A-π-D core structures with C_{2v} symmetry, where alkylamino groups act as donors, vinyl as π-conjugated bridges and cycloketones as acceptors. Due to the long conjugation length and the presence of strong electron donor and acceptor groups, as well as good coplanarity derived from the cyclopentanone ring, the σ^{2PA} of **P2CK** is 176 GM at 800 nm in water. Such a value is substantially smaller than that of its hydrophobic analogue (466 GM in chloroform[200]). The reduction may be largely attributed to the solvent-effect on 2PA behavior. Various experimental and theoretical results demonstrated that 2PA significantly depends on the surrounding medium and that the relation of 2PA behavior to solvent polarity may in fact be non-monotonic[201]. However, the σ^{2PA} of hydrophilic 2PA chromophores measured in water always drops considerably compared to that of their hydrophobic counterparts in organic solvents.[69] The exact mechanism still remains unclear at the present stage but the specific solute-solvent interactions such as hydrogen bonding or changes in the chromophore geometry and/or multichromophore aggregation are likely.[202]

When expanding the central ketone from cyclopentanone to 4-methylcyclohexanone as in **G2CK**, the σ^{2PA} value slightly dropped to 163 GM. The reduction in 2PA absorption might be attributed to the non-planarity of the six-member ring, which leads to a decrease in the degree of conjugation. Interestingly, only a minor drop in σ^{2PA} of **G2CK** is observed compared to its hydrophobic counterpart with a σ^{2PA} of 191 GM.[200] It seems that the solvent-effect on 2PA behavior is not as significant for **G2CK** as for **P2CK**. One possibility is the stereo hindrance, derived from the non-planarity of the 4-methylcyclohexanone, which generally reduces aggregation. By extending the alkyl spacers from methylene to ethylene as in **E2CK**, the σ^{2PA} increases to 201 GM. This enhancement might derive from the stronger electron donating ability of amino groups with longer alkyl chains. Another reason might be the red-shift-induced large 2PA absorption at the given wavelength.

3.4   2PP test

Some general evaluated methods such as single-line writing,[83] in which the width of lines and threshold energies are used to quantify writing efficiency, is not suitable to characterize the 2PP here when considering the swelling property of hydrogels in water. Therefore, more complicated 3D shapes fabricated under various laser intensities and writing speeds as described in the previous chapters are used to assess the efficiency. Defined lattices (lateral dimension: 50 × 50 μm, 10 μm hatch-distance, 5 μm layer-distance, 40 layers) were written into the hydrophilic formulation by means of 2PP to evaluate the activities of the PIs. A mixture of 50 wt% of polytheleneglycol diacrylate (PEGDa, 700 Da) and 50 wt% of DI water with the same PI concentration of 2 wt% was used. Since the molecular weights of the three investigated 2PIs are very closed to each other, the slight difference in molar concentration would not significantly affect the 2PP results. Mass concentration is much more frequently used than molar concentration in practice. Good results have been previously obtained for such a formulation.[106]

In the experiments, the laser power was varied from 60 to 410 mW using increments of 50 mW for each element. Writing speed was adjusted from 1 to 100 mm/s. After fabrication and subsequent development, the whole structure array can be visualized via focal laser scanning microscopy (LSM). The green fluorescence of the microstructures comes from the buried 2PIs and the photoproducts after initiation. LSM images of all initiators with full processing windows are shown in **Fig 56**. Different levels of fluorescence denote differences in the density of the polymer network.[106]
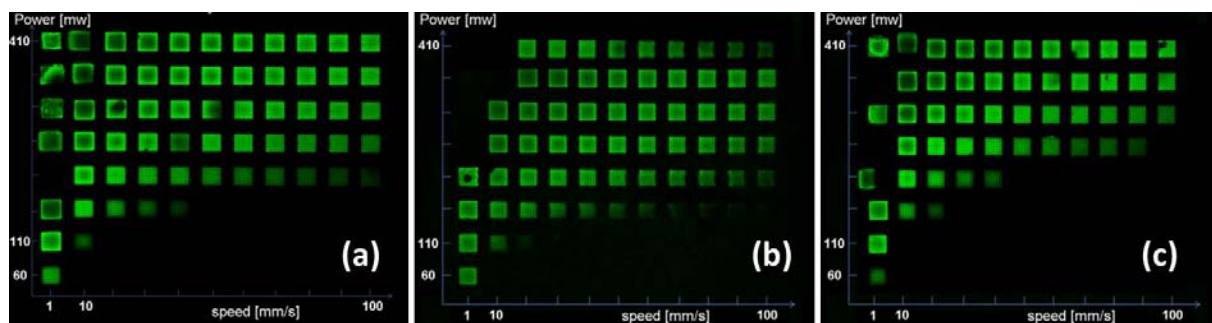
Fig 56 LSM images of the microstructures fabricated with different feed rate and laser power: (a) **E2CK**; (b) **G2CK**; (c) **P2CK**.

In order to quantitively assess the 2PA initiation efficiency of the initiators, three classes are employed to represent the quality of the structures (**Fig 57**). Class A (green area) defines excellent structures with well recognized straight lines and class B (yellow area)

good structures with thick hatch-lines (compared to class A) or slightly contorted wavy lines. Structures rated as class C (red area) have identified shapes but with slight mistakes (e.g., holes, burst regions due to overexposure) or with thick lines growing together.
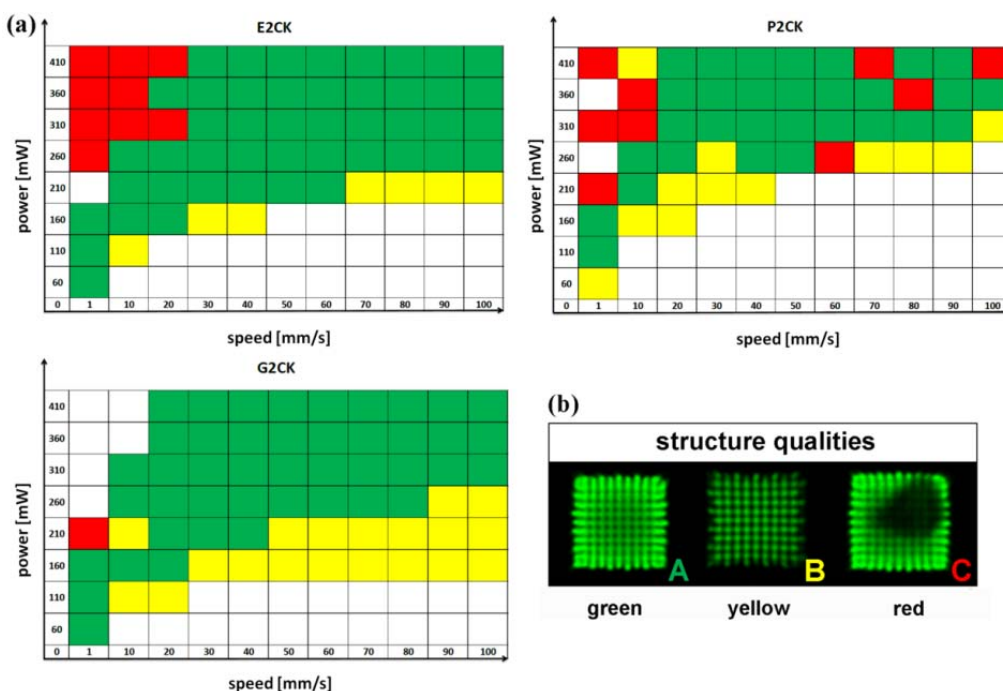
Fig 57 (a) Processing windows of investigated initiators in 2PP screening tests; (b) Classification of the structures by the typical quality of their shapes.

Both **E2CK** and **P2CK** contain a D-π-A-π-D core structure although the central cycloketone ring differs in size. In chapter 2, the hydrophobic initiator **M2CMK** with a central 4-methylcyclohexanone ring has already been proven as a very efficient 2PI in 2PP tests.[200] Via introduction of carboxylic sodium salts as hydrophilic moieties, the hydrophilic initiator **E2CK** also exhibits high initiation efficiency in photoactive formulation with 50 wt% of DI water. The threshold power of **E2CK** is 110 mW at a writing speed of 10 mm/s, which is found to be not sufficiently intense to trigger polymerization in a similar formulation containing the benzylidenecyclopentanone-based initiator **P2CK**. Such a trend is more significant as writing speed is increased: at the highest applied writing speed of 100 mm/s, the threshold energy is 210 mW for **E2CK**, whereas 100 mW of additional power is required when processing with **P2CK**. Besides lower threshold energies, the ideal processing windows (class A) of **E2CK** are larger than those of **P2CK**. One possible explanation for this enhancement is the larger 2PA cross section of **E2CK** (201 GM) compared to that of **P2CK** (176 GM). Another more likely reason is the central ring effect, which significantly affects the fluorescence emission. Central cyclohexanone compounds possess much weaker fluorescence than

their cyclopentanone counterparts.[203] Low fluorescence quantum yields are essential for efficient photoinitiators as they lead to less radiative deactivation and a higher population of the active state for initiating the polymerization.[99] The effect of ring geometry on initiation efficiency has been confirmed when studying the 2PP behavior of a series of hydrophobic benzylidene ketones with different central rings in chapter 2. In comparison to the five-member ring based initiator **P2CK**, the six-member ring analogue **E2CK** should also show higher initiation efficiency in the water-borne formulation. Although **P2CK** offers smaller processing windows than **E2CK,** it is still substantially better performing than conventional xanthene dyes which exhibits at least 5 times smaller processing windows with the identical parameters.

G2CK and **E2CK** share the same benzylidenecyclohexanone core structures but with different alkyl chain spacers. The processing windows of **G2CK** are very similar to those of **E2CK**. Notably, when writing speed is increased above 20 mm/s, both **G2CK** and **E2CK** permit fabrication employing laser power as high as 410 mW without destruction of the microstructures. Good resistance to high laser power can also allow fast writing speed but with sufficient energy to induce polymerization. Delicate microstructures of hydrogels can be obtained even at a fabrication rate as high as 100 mm/s. To the best of our knowledge, it is the fastest writing speed up to now for 3D hydrogel microfabrication via 2PP. Enhanced writing speeds are critical for high throughput in mass production, especially when processing scaffolds with large size.

With the same formulation containing **G2CK** as initiator, 3D objects based on a CAD model (insert in **Fig 58**a) with intended dimensions of $200 \times 170 \times 94 \ \mu m^3$ can be easily fabricated. The array of fabricated hydrogel frogs along with a detailed view of an individual frog object is shown in **Fig 58**.
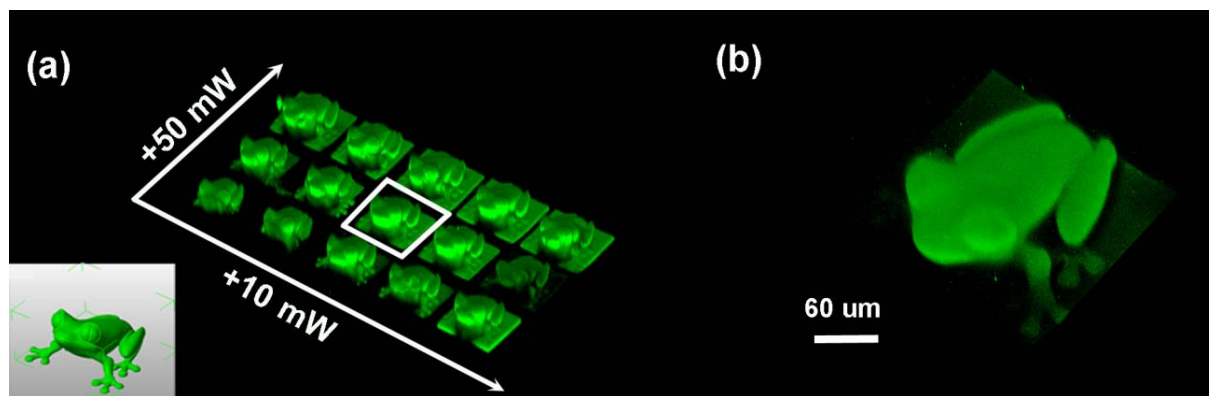
Fig 58 Fabrication of a CAD frog in a 1:1 PEGDa : DI water hydrogel formulation containing 2 wt% of **G2CK** using a 20× NA 0.8 objective, (a) Fabricated array at 15 mm/s with different laser powers (100-240 mW), stacked 3D LSM image, insert is the CAD model; (b) Detailed view of the LSM image of the white marked structure.

3.5   Photoinduced decarboxylation

In **G2CK**, the introduction of phenylglycine sodium salts groups is not only as hydrophilic functionalities, but also with intention to enhance the initiating efficiency via 2PA induced decarboxylation mechanism. The previous results from our group indicated that *ortho-* and *para-* substituents with electron-donating functionalities on the aromatic moiety or N-alkyl substitution of NPG can significantly accelerate the decarboxylation.[103] Therefore, the attached methyl group to the amino moiety is expected to facilitate the decarboxylation process. However, in 2PP tests, the processing windows of **G2CK** are very similar to those of **E2CK**. Such results implicates that no or very slow decarboxylation of **G2CK** occurred under the defined 2PP conditions**.**

The possible reason for the unsuccessful decarboxylation might be the strong electrostatic force between carboxylic acid ions and sodium cations. Such assumption seems reasonable because to the best of our knowledge, there is no report on the decarboxylation of the NPG sodium salts. However, NPG with tetrabutylammonium cations, which have weaker electrostatic force compared to sodium cations, has been proven to undergo decarboxylation smoothly.[179] Moreover, Bartoszewicz *et al*. demonstrated that the counter-ion significantly affect the decarboxylation efficiency.[204] Therefore, sodium cations in **G2CK** were replaced by tetrabutylammonium cations to obtain a new water-soluble 2PI **T2CK** to verify the above assumption.

Although 2PA induced reactions and 1PA induced reactions might differ in the initial excitation stage, the subsequent photophysical and photochemical processes are expected to be the same.[205] Therefore, the mechanism study under one-photon excitation can also provide useful information to understand the photo behaviors under 2PA. Photolysis experiments were carried out as described by Yagci *et al.*[206] in order to qualitatively study the possibility of photoinduced decarboxylation of **T2CK**. 1 mL of **T2CK** solution with a concentration of 1.28×10^{-2} M in water was placed in a transparent glass vial and connected via a curved needle to another vial containing K_2CO_3 solution (1.12×10^{-2} M) and one drop of phenolphthalein (**Fig 59**). Sunlight was used as irradiation source because the absorption of the 2PA chromophore lies within the visible light region at about 430 nm (measured in chapter 2), also because sunlight can penetrate into the transparent glass to provide enough energy for the photolysis reaction. If the decarboxylation occurred, the released CO_2 would diffuse through the needle and neutralize K_2CO_3; the pink would become lightened or even disappeared. It should be mentioned that the CO_2 in the air might also slowly penetrate into the vial, react with K_2CO_3 and induce the decoloration. Therefore, a control experiment without 2PIs was also conducted to evaluate the effect of the CO_2 from the air. The vials were irradiated under sunlight for 2 days. The temperature of the vial was not significantly changed during the irradiation.

After irradiation, the intensive pink before photolysis experiment becomes much lightened, while the color remains nearly unchanged in the control samples (**Fig 59**). The results indicate that under one-photon excitation, **T2CK** can undergo decarboxylation in water without monomers. On the other hand, when replacing **T2CK** to **G2CK** and conducting the photolysis experiment under identical condition, the intensive pink remains unchanged, even with a prolonged irradiation time up to one week. Such results demonstrate the very low possibility of photoinduced decarboxylation of **G2CK** under the testing condition.
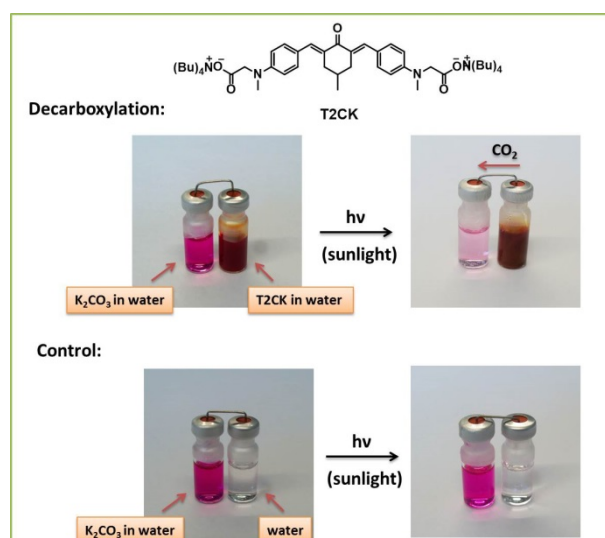
Fig 59 Photolysis experiment of T2CK

Photolysis experiment only provides the information of the photo reactions in pure solvent under one-photon excitation. Therefore, 2PP tests should be performed to further study the two-photon behaviors of **T2CK**, or more specifically the possibility of 2PA induced decarboxylation and its effect on the initiation efficiency of the polymerization.

Fig 60 shows the processing windows of **G2CK** and **T2CK** at a constant writing speed of 10 mm/s but with different laser powers. Since the molecular weight of **T2CK** (945.45 g/mol) is nearly two times larger than **G2CK** (506.57 g/mol), the same molar concentration of 1.97×10^{-5} mol/g resin (a mixture of 1:1 of PEGDa and DI water) was used for the 2PP tests. The tests were also conducted with a lower molar PI concentration of 3.94×10^{-6} mol/g resin (denoted as T2CK 0.2 and G2CK 0.2) to determine the lowest possible PI concentration under these conditions.
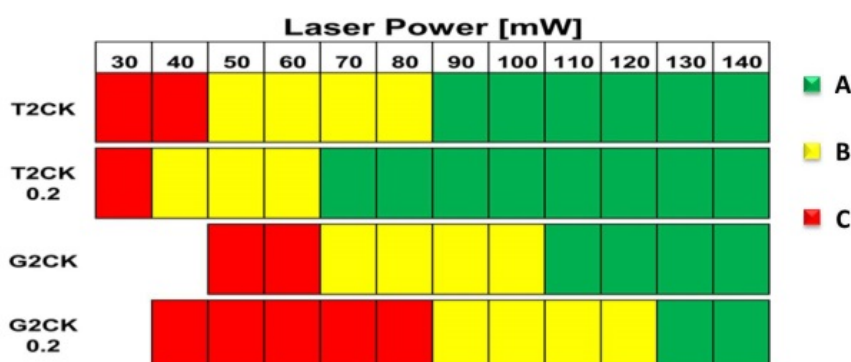
Fig 60 Processing windows of **T2CK** and **G2CK** with different concentrations (writing speed: 10 mm/s)

In both high and low concentrations, **T2CK** requires much less energy than **G2CK** to obtain nice microstructures. Moreover, the processing windows of **T2CK** are much broader than those of **G2CK** within the investigated range of the laser powers (30-140 mW). The lower required energy and broader processing widow indicate that **T2CK** is much more efficient than **G2CK**. Since **T2CK** and **G2CK** share the same 2PA chromophore, their nonlinear absorption behavior should be identical. The difference of initiation efficiency should derive from the subsequent photo reactions after 2PA. The results of photolysis experiment and 2PP (compared to **E2CK**) indicate the low possibility of photoinduced decarboxylation for **G2CK**. Therefore, the most reported initiation mechanism, which involves two-photon induced intermolecular electron transfer from photoexcited chromophores to the monomer which produces a radical anion responsible for the subsequent polymerization, is very likely to occur on **G2CK**. Such bimolecular photoreaction suffers from the back electron transfer process and thus provides low initiation efficiency. On the other hand, the higher initiation efficiency of **T2CK** demonstrates a more effective initiation mechanism through which the 2PI can induce a more efficient polymerization. The results of photolysis experiment indicate that **T2CK** is very likely to undergo 2PA induced decarboxylation. The proposed initiation mechanism of **T2CK** under 2PA excitation is shown in **Fig 61**.
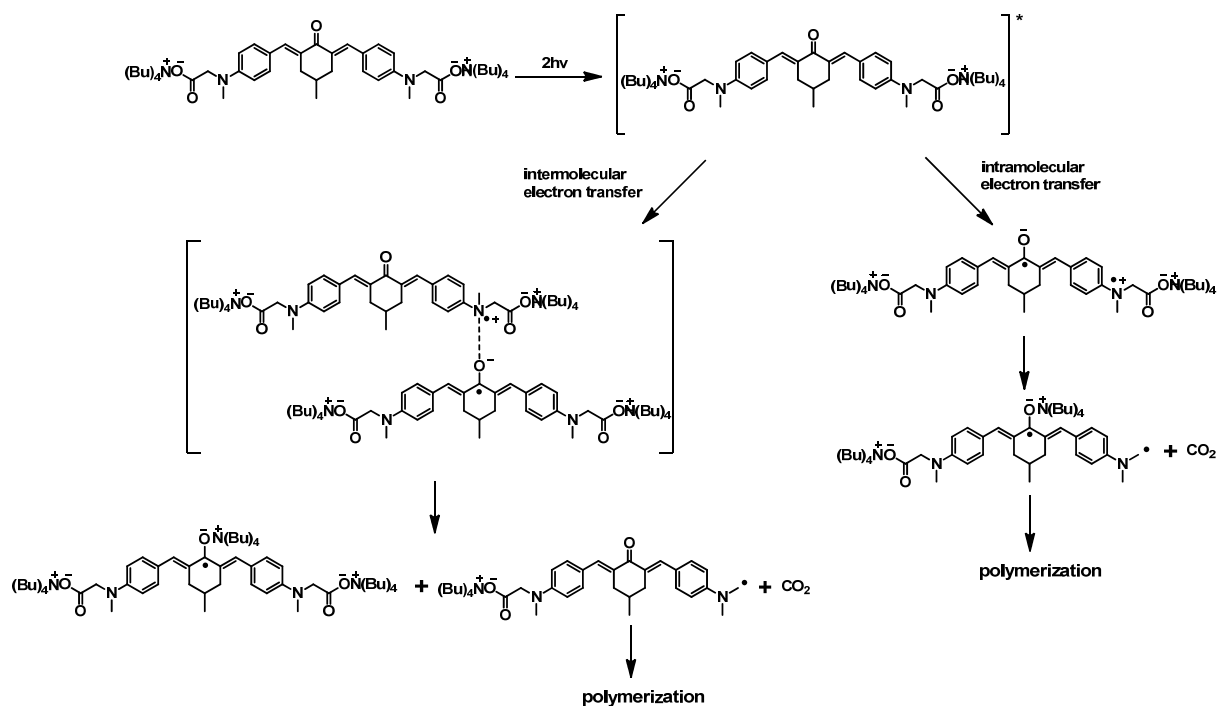
Fig 61 Proposed initiation mechanism of **T2CK** under 2PA

After 2PA, the excited **T2CK** molecule can undergo either intermolecular or intramolecular electron transfer to form positively charged amine radical ions and negatively charged ketone radical ions. Then a very fast decarboxylation occurs, leading to the formation of the [ketone$^{\cdot-}$-----$^{+\cdot}$N(Bu)$_4$] ion pair and very active amine radicals which induce the subsequent polymerization. Since decarboxylation can effectively prevent back electron transfer, high quantum yields of active radicals and thus efficient polymerization can be obtained. A very similar mechanism has been reported by Bartoszewicz *et al*. when studying the photopolymerization using a photoinitiation system containing benzophenone and phenylthioacetic acid tetraalkylammonium salts.[204]

3.6   Cytotoxicity test

In a close cooperation with Prof. Wolfgang Holnthoner and his co-workers Severin Mühleder from Ludwig Boltzmann Institute for Experimental and Clinical Traumatology, Austria, the influence of different PIs on cell viability was determined with two different cell types. More detailed information of the sample preparation and testing can be found in the recent publication.[207] MG63 osteosarcoma cells and outgrowth endothelial cells (OEC) were exposed to PIs dissolved in PBS for 10 and 30 minutes. Only **G2CK** had a significant effect ($p = 0.0411$ (10 min); $p = 0.0087$ (30 min)) on the viability of MG63 cells while the effects of the other PIs were comparable to the control (**Fig 62**a). In addition to MG63, we analyzed the PIs using primary endothelial cells, which, in contrast to MG63 cells, show physiological behaviour when cultured *in vitro*. When increasing the incubation time from 10 min to 30 min, a significant drop of the viable cell number were observed with 4-methylcyclohexanone-based initiators **G2CK** ($p = 0.022$) and **E2CK** ($p = 0.0022$). The dark cytotoxicity of cyclopentanone-based initiator **P2CK** is as low as that of the reference I2959 for 10 min. When the incubation time was prolonged to 30 min, **P2CK** also reduced cell viability ($p = 0.026$), but to a much less degree than the other two 2PIs (**Fig 62**b).
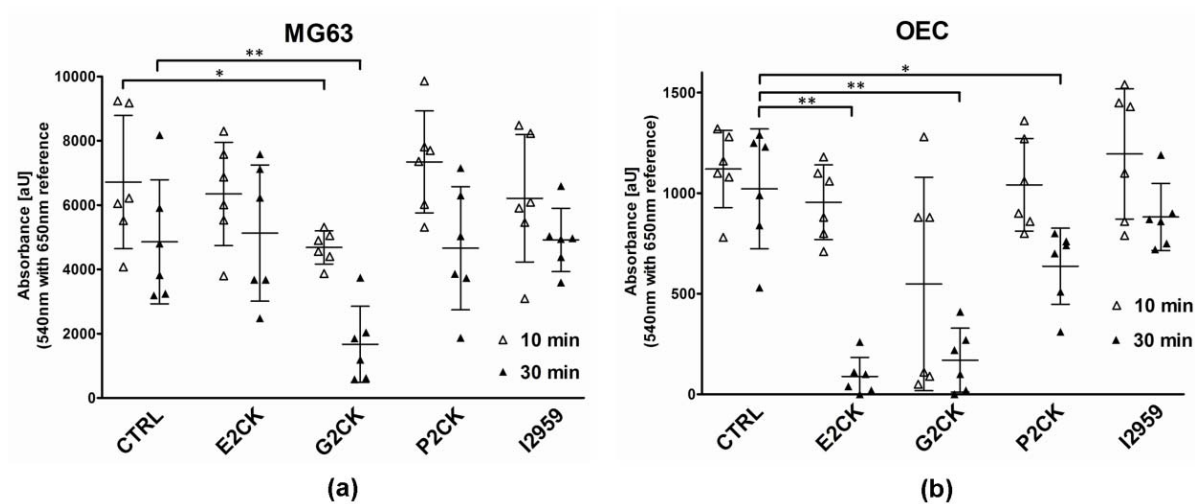
Fig 62 Cytotoxicity of synthesized photoinitiators in two different cell types. (a) In MG63. (b) In OEC; aU: arbitrary units; *p < 0.05 ; **p < 0.01

Part II Novel arylazides for multiphoton grafting

State of the art photografting

Photografting is an effective method which enables the covalent immobilization of functional groups onto a polymer surface under irradiation. Photografting can be conducted in liquid, vapor and bulk and on different substrates.[208] UV light is frequently used as irradiation source to realize surface graft polymerization, often with assistance of a suitable photoinitiator or photosensitizer. Norrish type II photoinitiators like benzophenone, rather than Norrish type I initiators, are more frequently used because the former ones provide higher grafting efficiency, while the latter ones lead to higher polymerization yield and faster reaction rate, but lower grafting efficiency.[209]

Compared to other modification methods, photografting provides many advantages such as rapid reaction rate, mild reaction condition, low price of processing and simple equipment required.[208] Moreover, the photografting patterns can be customer-made by standard photolithographic procedures[210] and spatial and temporal control of the photografting process can be realized simply by tuning the exposure dose.[211] Due to these distinct characters, photografting has been widely used to tailor physical-chemical properties of surfaces, such as wettability,[212] adhesiveness,[213] biocompatibility,[214] and antifouling.[215]

Due to the limited penetration ability of UV light, most studies on photografting focus on two dimensional patterning of surfaces. However, capability to produce 3D patterns decorated with biomolecules is very attractive for tissue engineering because it provides the possibility to tailor the in vitro model much closer to the real 3D appearance of the natural extracellular matrix.[216] To this end, multiphoton grafting (MPG) becomes appealing due to its unique character of real 3D writing capability with high resolution, which enables immobilization of functional molecules within a 3D volume in a straightforward fashion.

True 3D patterning within UV-polymerized PEGDa-based hydrogels via MPG has been reported by Hahn *et al.*[217] In their work, the hydrogel matrix was firstly soaked in a photoreactive solution which contained functionalized acrylates and a suitable photoinitiator. Then under MPG, selective immobilization of functional molecules was

achieved by means of photoinitiator-assistant copolymerization with acrylate groups of the hydrogel matrix (not consumed during the initial UV polymerization). Biochemical patterning was visualized by copolymerization a fluorescently labeled monoacrylate derivative with the residual acrylate groups within the hydrogel matrix (**Fig 63**).
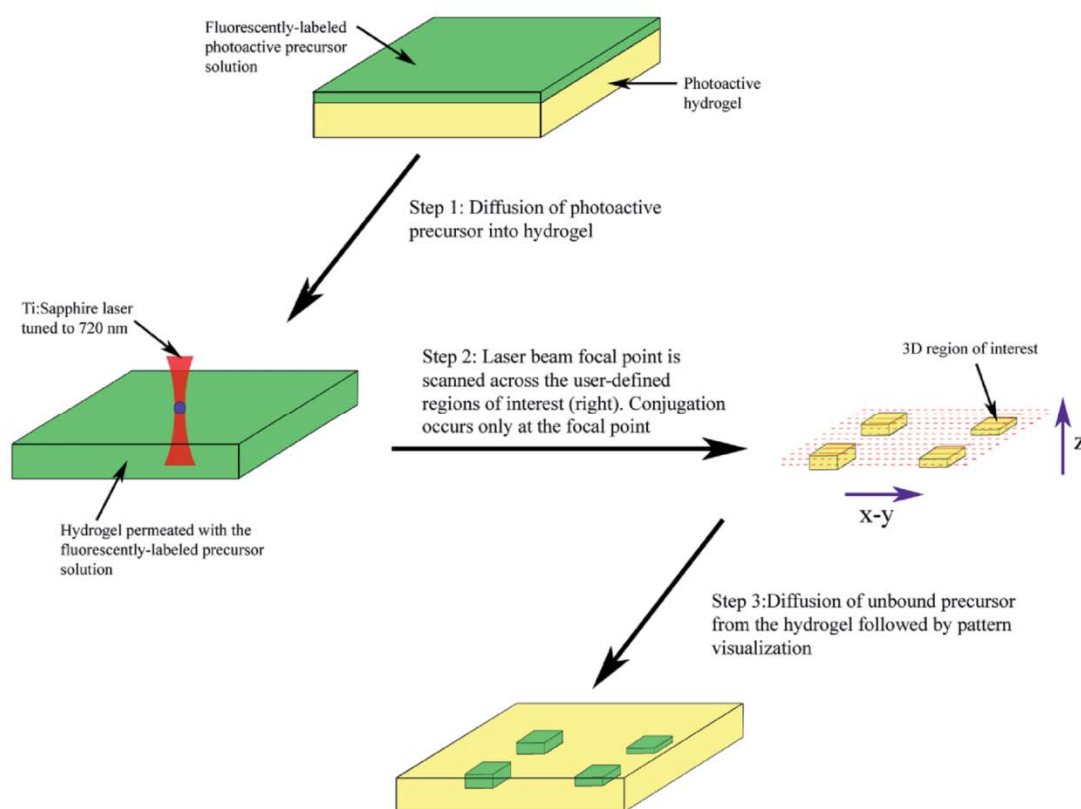
Fig 63 Procedure for multiphoton induced photografting of residual acrylate groups with fluorescent molecules[218]

Another polymerization-based grafting strategy to obtain functionalized 3D microstructures was reported by Wegener *et al.*[219] In such method, 3D microstructures with desired shapes were firstly fabricated via 2PA induced thiol-ene polymerization. Since the thiol groups were not completely consumed during the polymerization process, the thiol-contained microstructures were subsequently grafted with different functionalized maleimides via thiol-Michael addition reaction (**Fig 64**). Very similar strategy has also been used to realize selective metallization of 3D structures fabricated via 2PP.[220]
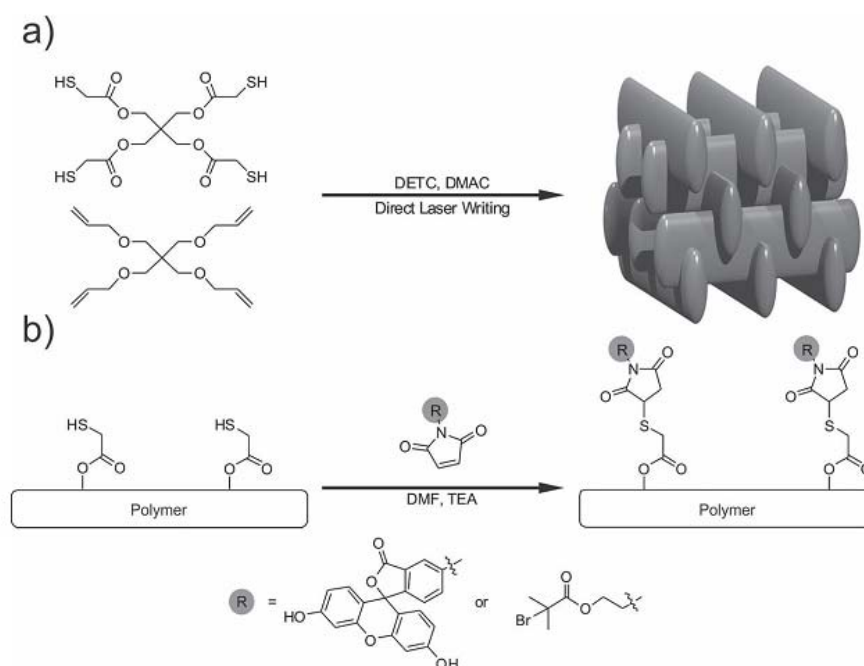
Fig 64 Procedure for 2PA induced thiol-ene polymerization and subsequent grafting of residual thiol groups with fluorescent molecules[219]

2PA induced uncaging is another efficient strategy developed by Shoichet *et al.* to realize 3D patterning.[221] In this method, an agarose hydrogel functionalized with coumarin-caged molecules was synthesized and subsequently underwent photocleavage under two-photon excitation (**Fig 65**).   The functionalities--primary amine or thiol groups are selectively distributed within the 3D hydrogel matrix after photouncaging and can be used for postmodification with biofunctionalized molecules.[221b]

Multiphoton excitation localizes photochemical modification in 3D space

Gel contains "latent" patterned volumes of free thiol groups

Thiol-reactive molecules are selectively immobilized in the patterned volumes
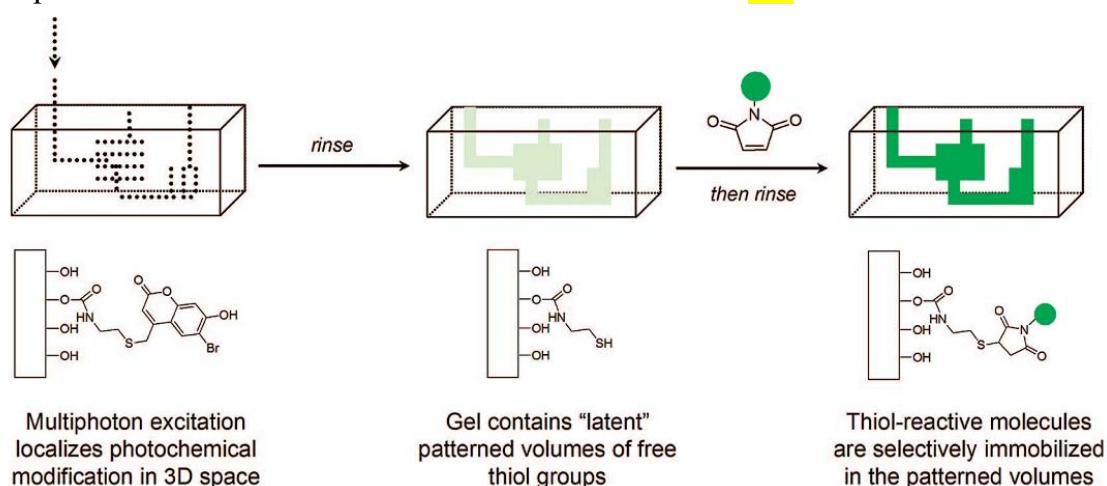
Fig 65 Procedure for two-photon uncaging and postmodification of active thiol groups with fluorescent molecules[221a]

Very recently the same group successfully realized simultaneous 3D protein patterning using combination of two-photon uncaging and orthogonal chemistry of peptide binding (**Fig 66a**).[222] In the presence of thiol-reactive proteins, pulsed laser beams selectively activate the caged thiol groups which subsequently react with barnase containing maleimide moieties via thiol-Michael addition reaction. Using the same method, the second potent maleimide-streptavidin was site-specifically immobilized within the same agarose hydrogel matrix. Finally, the patterned matrix is soaked in a mixture of fusion proteins, barstar-SHH and biotin-CNTF, which specifically bind to barnase and streptavidin, respectively (**Fig 66b**).
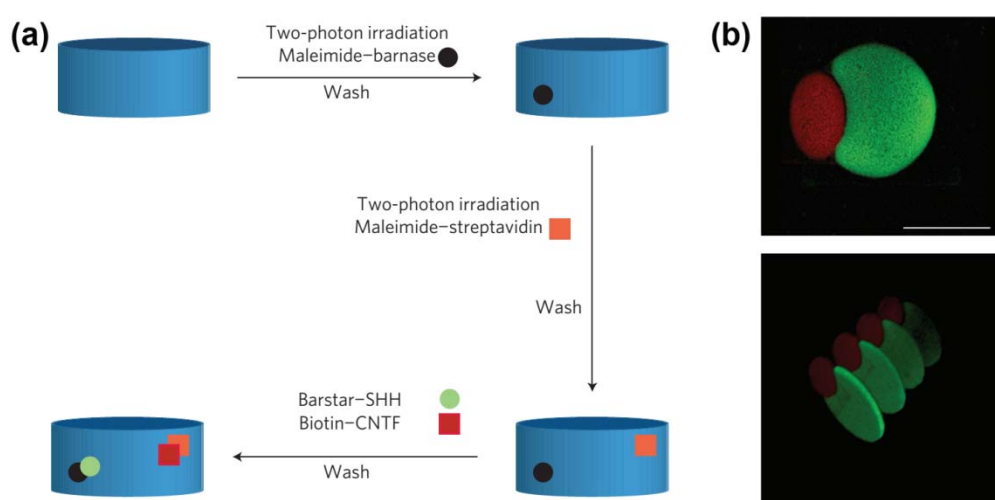
Fig 66 (a) Procedure for simultaneous 3D protein patterning using combination of two-photon uncaging and orthogonal chemistry of peptide binding; (b) 3D patterns containing two fluorescent proteins[222]

Compared to photoinitiator-assistant copolymerization which involves free radicals during the polymerization process, two-photon uncaging is potentially more precise since the functional groups are bonded to the matrix and thus cannot diffuse. However, the involved chemistry is rather inefficient due to the limited mobilization of the active species. Moreover, the relatively small 2PA cross section of the coumarin chromophore used as "cage" can also reduce the uncaging efficiency, which limits the wide applicability of the method.

Besides the two abovementioned techniques, multiphoton chemistry of arylazides would be another potentially promising strategy for MPG. Arylazides have been frequently used as efficient UV photografting agents to introduce functionalities onto the surfaces of the substrate.[223] The photografting process of arylazides stars with photoinduced dissociation

of the N-N bond from the excited singlet state followed by the generation of nitrogen and nitrene species. The highly reactive nitrene intermediate could undergo various reactions.[224] Three main processes are of relevance to photografting: (I) rearrangement to the corresponding seven-membered ketenimine; (II) C-H or N-H insertion; and (III) relaxation via intersystem crossing (ISC) to the triplet phenylnitrene (**Fig 67**). Both (I) and (III) are deactivations for efficient photografting process (II). Several studies have proven that the introduction of halogen atoms such as F on the aromatic ring greatly suppresses the ring expansion because the substituted halogen moieties raise the energy barrier of the ring-expansion reaction and significantly prolong the lifetime of the corresponding halogenated singlet nitrenes, which thus increase the yields of the insertion reactions.[225]
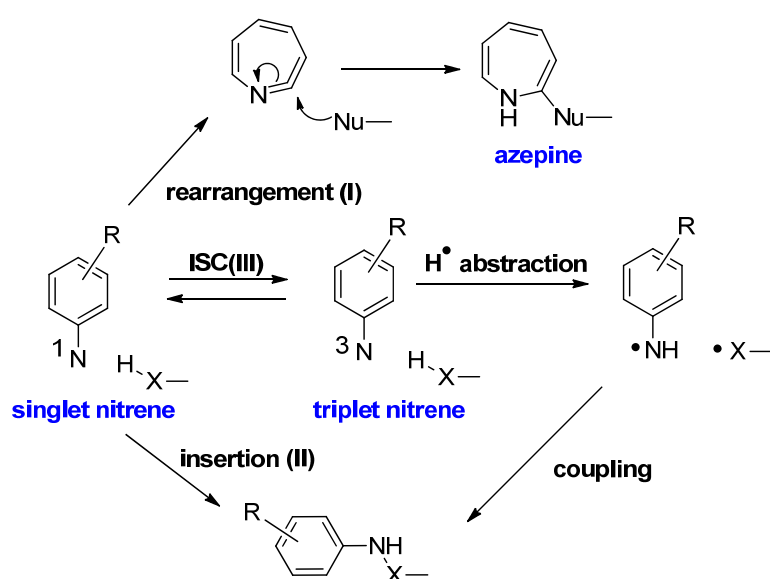
Fig 67 Possible reaction pathways for the arylnitrenes [224]

Compared to photopolymerization-based and photouncaging-based grafting techniques, photografting of arylazides which involves a single-molecule insertion mechanism is potentially: i) more efficient, but less precise than uncaging; and, ii) more precise, but less efficient than chain-growth mechanisms. Therefore, MPG of arylazides would for sure become a valuable candidate in the toolbox for 3D patterning. Although currently extensive studies focus on 2D surface photografting of arylazides under UV excitation, the concept can be transferred to 3D volumetric photografting under multi-photon excitation with a proper molecular design. Efficient MPG process requires a suitable arylazide comprising a large multi-photon absorption (MPA) cross section combined with high photografting efficiency. Chromophores with large MPA cross section are characterized by a planar π conjugated system containing electron donor and acceptor

groups.[5] However, the synthesis of arylazides with complex structures possessing large MPA has still remained a great challenge until now due to the high sensitivity and thermal instability of azides.[226]

4 Multiphoton grafting with commercial arylazides

4.1 Selection of commercial arylazides for MPG

Considering the challengeable synthesis of aromatic azides with complex structures, it is advisable to select commercial aromatic azides with proper molecular structures to prove the concept of MPG. The selection criterion is based on the principles well known from 2PA, which includes planar π-conjugated systems containing strong donor and/or acceptor groups.[5] Therefore, three arylazides derivatives from Sigma-Aldrich become interesting candidates (**Fig 68**).
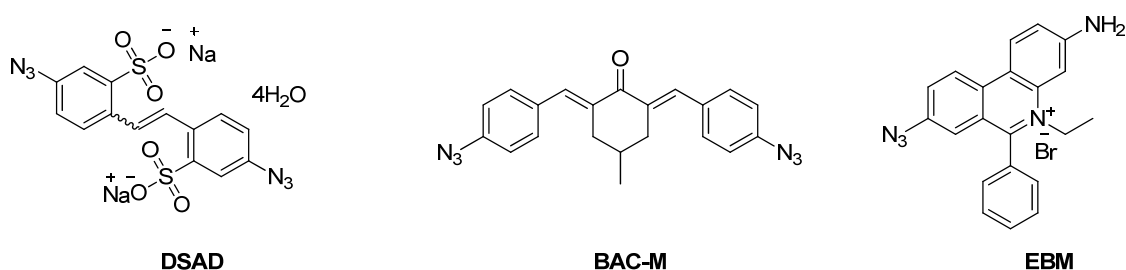
Fig 68 Chemical structures of commercial arylazides

DSAD comprise an A-π-A core structure, where azide and sulfonate groups act as acceptors and vinyl group as a π-conjugated bridge. Sulfonate groups on the aromatic rings can provide excellent hydrophilicity, which enables the grafting process under aqueous conditions. Such character makes **DSAD** quite appealing for biological applications. The disadvantage of the molecule is the lack of efficient electron donors, like alkylated amino groups, which would limit its multiphoton absorption at the desired wavelength used for MPG (800 nm).

Similar to **DSAD**, **BAC-M,** containing an A-π-A-π-A core structure, also lacks electron donors, but with longer conjugation length. Moreover, the benzylidene cycloketone derivatives have been used as efficient PIs and photosensitizers under multiphoton excitation;[162b] therefore, **BAC-M** is expected to be an efficient multiphoton absorber.

EBM is frequently used as a photoactive stain to covalently bind to nucleic acids.[227] The molecule contains a D-π-A core structure, where the amine group acts as a donor, the polyaromatic ring as a π-conjugated bridge and the azide group as an acceptor. The

maximum linear absorption was reported at 530 nm,[228] which indicates the 2PA peak lies at about 1060 nm due to the asymmetric molecular geometry. Such wavelength is far beyond the one used for our screening (at 800 nm). Moreover, the price of **EBM** (5 mg for 243.50 USD from Sigma-Aldrich) is much higher than that of **DSAD** (10 g for 59.50 USD) and **BAC-M** (5 g for 79.80 USD). Therefore, as a proof-of-concept, **DSAD** and **BAC-M** were purchased for the tests.

The preliminary screening results shows that only the successful MPG of **BAC-M** was confirmed with the current instrumental setup. The inefficiency of **DSAD** might be caused by its short conjugation length, which limits the multiphoton absorption at 800 nm and the subsequent grafting process. Another reason might be that the wavelengths of the LSM used for excitation are not fit to the photoproducts of **DSAD** and thus the photografting patterns cannot be visualized via LSM. Therefore, only **BAC-M** was selected for the following detailed investigation.

4.2   Z-scan measurement of BAC-M

The efficiency of 3D grafting process depends on the nonlinear absorption probability. **Fig 69a** depicts the UV-vis absorption spectrum of **BAC-M** with a concentration of 1.0×10^{-5} mol L^{-1} in acetonitrile. The evaluated compound does not exhibit any linear absorption beyond 430 nm and is completely transparent in the near infrared range. A weak absorption around 400 nm could allow the possibility of 2PA. The 3PA peak generally appears at a wavelength shorter than three times the linear absorption peak,[42] but the possibility of 3PA is significantly lower than that of 2PA. Therefore, in order to determine the order of nonlinearity as well as multi-photon absorption cross section, an open aperture z-scan experiment was performed.

Fig 69b shows the results of a z-scan measurement for **BAC-M** using 100 fs pulses having the energy of 160 nJ. The green solid line shows the fitting curve with an assumption of two-photon absorption; whereas the red one assuming the three-photon absorption (The detail information of the fitting process is included in Dr. Ajami Aliasghar's PhD thesis[150]). The Comparison of the two fit curves clearly indicates that 3PA occurs in **BAC-M**.
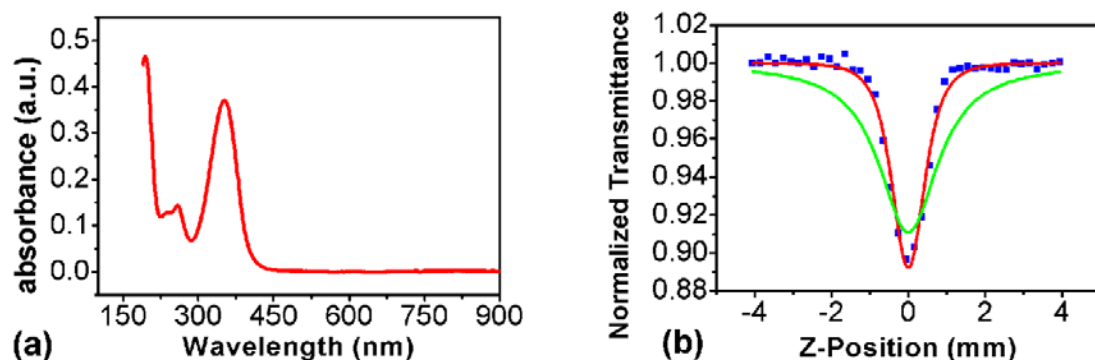
Fig 69 (a) UV-vis absorption spectra of the **BAC-M** in acetonitrile with a concentration of 1.0×10^{-5} mol.L^{-1}; (b) Results of the z-scan characterization of **BAC-M** solution. The red line is the fit curve assuming 3PA and the green one is the fit curve assuming 2PA.

In order to verify this finding the nonlinear absorption was fitted to the z-scan data with different pulse energies (**Fig 70a**). From each fitting curve the value of the variable P_0^2 is extracted. If 3PA occurs in **BAC-M** solution, the P_0^2 should scale linearly with intensity square (E_p^2). **Fig 70b** shows the extracted values of P_0^2 as a function of E_p^2. The linear behavior provides an additional proof, indicating that the 3PA is indeed the predominant nonlinear absorption in **BAC-M**. From the fit curve in **Fig 70b** a value of 1.19×10^{-78} cm^6 s^2 was obtained for the 3PA cross section of **BAC-M**.
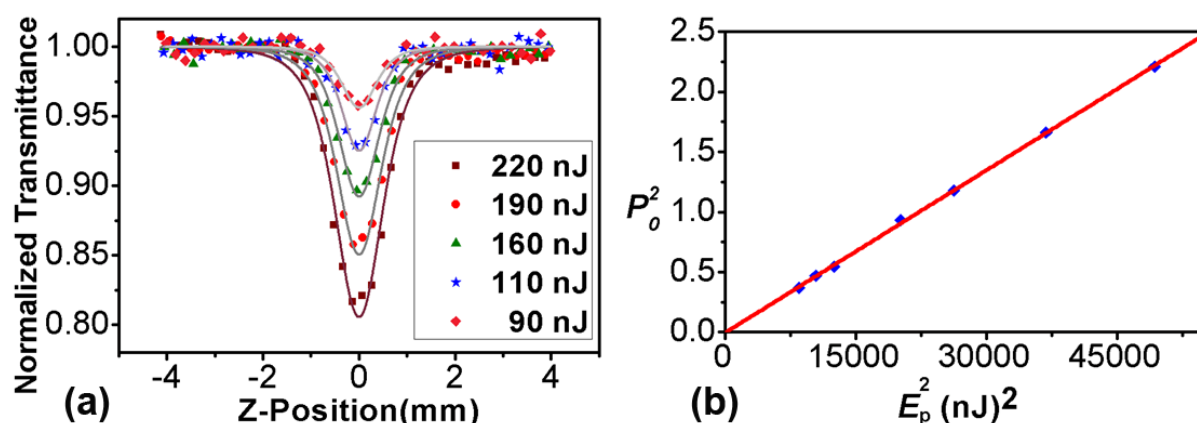
Fig 70 (a) Z-scans measurement of **BAC-M** at different pulse energies with the assumption of 3PA; (b) extracted values of P_0^2 plotted versus E_p^2.

It should be mentioned that the multiphoton cross section only give the information of the amount of energy that can be absorbed by the photoactive molecule. The absorbed energy

can induce fluorescence or can be converted to thermal energy, both of which are deactivation processes for efficient photografting.

4.3   Photografting of BAC-M under 3PA

Multiphoton grafting tests were performed in a close cooperation with Dr. Aleksandr Ovsianikov and his colleague Evaldas Stankevičius from the Institute of Materials Science and Technology (TU Wien) and **Fig 71a** shows the 3PA photografting strategy investigated. The cylindrical PEGDa-matrix, which is produced via UV photopolymerization, swells in **BAC-M** solution with a concentration of 2 wt%. THF was firstly selected as a solvent because it provides good solubility for **BAC-M**. However, the relatively low-boiling point solvent is prone to evaporate during the grafting process, especially with laser beams of high power, and thus affects the photografting efficiency. Therefore, DMF, with higher boiling point and good solubility, is used instead. The PEGDa-matrix needs to be kept in **BAC-M** solution for at least 24 h to ensure homogeneous distribution of **BAC-M** molecules within the matrix before starting MPG.

Although multiphoton induced reactions and one photon induced reactions might differ in the initial excited state, the subsequent grafting process is expected to be the same.[229] Multiphoton induced photolysis of the azide causes the dissociation of the N-N bond from the excited singlet state, followed by the generation of nitrogen and nitrene species.[230] The highly reactive nitrene intermediate could undergo various reactions and **Fig 71b** depicts the desired one: direct immobilization on the matrix by insertion into a C-H bond. This single step process is very universal because it is applicable to a wide variety of matrices containing C-H or N-H bonds.[229] PEGDa-based hydrogels were chosen as a model substrate here because of its excellent biocompatibility and wide applications in tissue engineering.[169] Since the PEGDa-network is transparent in NIR region, the laser beams used for writing are able to deeply penetrate inside the matrix and induce the photografting reactions within 3D volume of the hydrogels. Moreover, since the two-photon interaction is only confined within the small focal point, immobilization of **BAC-M** on the PEGDa matrix could be performed with the high spatial resolution. By moving the laser focus within the sample, arbitrary 3D patterns of immobilized molecules can be "recorded".

After grafting, the matrix is washed with DMF to remove the unreacted azide. Since the main final photolytic product ketocyanine dye exhibits strong fluorescence,[231] the produced patterns can be observed directly via LSM upon excitation at 555 nm. Such strategy is more straightforward compared to previously reported one which required additional fluorescence dye-bounding acrylate monomers with assistance of a suitable photoinitiator for characterization.[217]
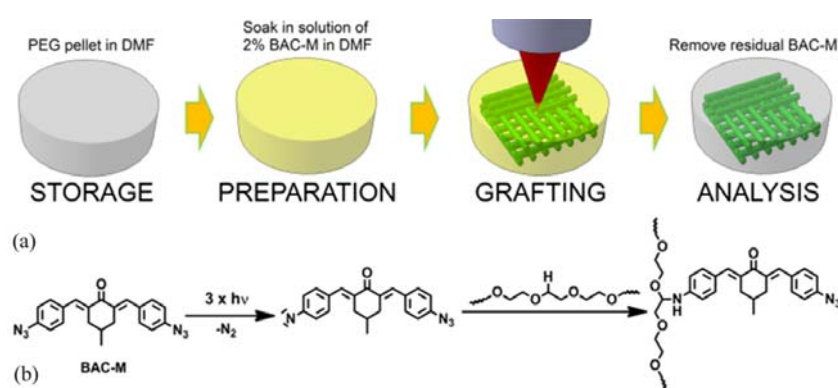
Fig 71 Schematic representation of the 3PA grafting procedure; (b) 3PA induced decomposition and subsequent insertion of **BAC-M** into a PEGDa matrix

Fig 72 shows an array of squares produced at different laser power and scanning speed parameters. **BAC-M** is found to have a large processing window from 30 mW to over 450 mW for laser power range at scanning speeds from 5 to over 550 mm s^{-1}. No patterns are observed at 20 mW and below, while the top laser power of 450 mW and speed of 550 mm s^{-1} are the limits of the current experimental setup. The fluoresce intensity of the photografting patterns, indicating the level of immobilization, directly correlated to both laser power and scanning speed. Higher laser power combined with lower scanning speed provides more energy in the excited focal volume to produce "brighter" patterns.
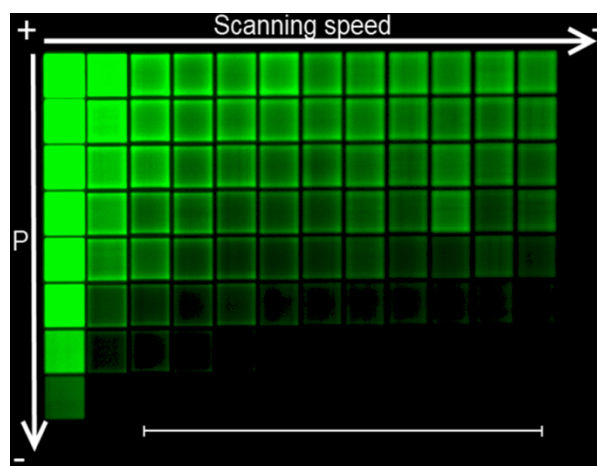
Fig 72 An array of squares produced by 3PA induced photografting at different laser power (100-30 mW; step = -10 mW) and scanning velocity (5-555 mm s^{-1}; step = +50 mm s^{-1}); scale bars: 500 μm.

4.4   Post modification of the patterned matrix

There are two different pathways for the introduction of functional groups. One method is to functionalize the aromatic azide prior to the photografting. This approach requires the synthesis of specific compounds for every application. Another more universal approach is the post-modification of the immobilized functional groups after photografting. Considering the stability of the biocompatible hydrogel matrix and the small volume of the grafted areas, the reactions used for postmodification should be conducted under mild conditions with high yields. To this end, click chemistry become very appealing due to its unique characters. Besides meeting the abovementioned two requirements, its fast reaction rate and outstanding orthogonal reactivity make click reactions quite attractive for various biological applications.[232] Three types of functionalities, namely ketone, vinyl and azide group, covalently attached within the 3D matrix after photografting can be taken into account for the postmodification via oxime, thiol-ene and copper(I)-catalyzed azide-alkyne cycloaddition (CuAAC) click reaction, respectively.

4.4.1   Attempt of postmodification via oxime click reaction

Oxime click chemistry, involving the reaction between an alkoxyamines group and an aldehyde or ketone, can be realized under mild conditions without additional catalysts.[233]

In contrast to Schiff base which is apt to undergo the dissociation of the C=N bond under acidic condition, the O-hydroxylamine compound is quite stable since the equilibrium favors the oxime. Therefore, oxime bond formation has become a promising method to produce site-specific conjugates.[234]

A model reaction between **M2CMK** and hydroxylamine hydrochloride were conducted to verify the feasibility of oxime formation. After photografting, the azide groups of **BAC-M** are converted to the alkylated amino groups. Therefore, the molecular structure of the photoproduct after insertion is very similar to **M2CMK**. The reactivity of **M2CMK** to hydroxylamine hydrochloride should indicate the reactivity of the produced patterns.

Until now, there is only one Japanese patent reporting an oxime compound 2,6-bis-(4-amino-benzylidene)-cyclohexanone oxime, which has very similar structure to the desired product, but the detail information of the synthesis is missing.[235] Therefore, the model reaction was carried out using the general method as described by Zhang *et al.*[236]
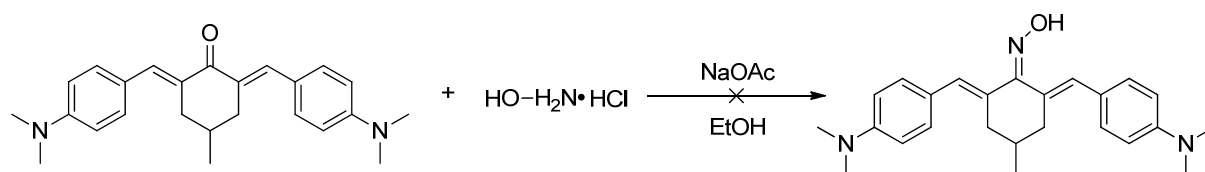
1.0 equivalent of **M2CMK** and 1.5 equivalents of hydroxylamine hydrochloride were dissolved in ethanol and then 1.5 equivalents of sodium acetate were added to deprotect the hydrochloride salts to release the hydroxylamine. The solution was stirred at room temperature and TLC was used to monitor the process of the reaction. Even after 24h, there was no new spot formed on the TLC plate. Then the solution was heated to 60 °C for 24h and still no new spot was observed. Considering that the weakly acidic property of the silica gels coated on TLC plate can potentially induce the dissociation of the C=N bond when running TLC, ^{1}H-NMR measurement was used to identify the final product after workup. The ^{1}H-NMR spectrum of the product is identical to that of **M2CMK**, indicating no new compound was formed.

In order to verify the feasibility of the reaction condition, bezophenone was used as substrate instead of **M2CMK** for the oxime reaction. A new spot with greater R_f value compared to bezophenone was observed on TLC plate when the reaction conducted for

2h under room temperature. After 24h, the spot of the raw material cannot be observed, indicating the completeness of the reaction. The result of ^{1}H-NMR confirmed the feasibility of the oxime formation between bezophenone and hydroxylamine. Therefore, the unsuccessful oxime formation between **M2CMK** and hydroxylamine hydrochloride is caused by the inertia of **M2CMK**. The inefficiency might be derived from the conjugated effect and the strong electron donating ability of the dimethyl amino groups, which would reduce the electrophilicity of the carbonyl group. The unsuccessful result was also reported by Dommock *et al* when trying to prepare a similar compound 2,6-dibenzylidenecyclohexanones oxime with similar reaction condition.[237] They attributed the failure to the steric hindrance of a second phenylmethylene group to the attacking nucleophile. They also demonstrated that when using primary amines rather than a mixture of the amine hydrochloride and sodium acetate, the desired product was obtained but with only a yield of 3%. Reaction of substituted 2,6-dibenzylidenecyclohexanones with a 4-molar excess of hydroxylamine hydrochloride in the presence of sodium under reflux gave the oxime but with unwanted structures.[237-238]

R = H, Me, Cl
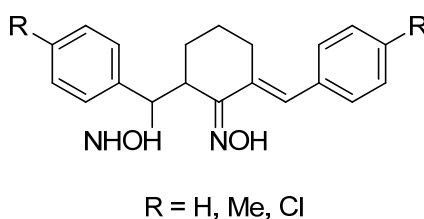
In summary, the oxime formation is not suitable for the postmodification of the immobilized ketone groups on the patterned matrix due to the low yield and the required harsh reaction condition (reflux), which would destroy the hydrogel matrix.

4.4.2 Attempt of postmodification via thiol-ene click reaction

Thiol-ene chemistry, the hydrothiolation reaction of thiols with reactive C=C bonds, or simply "enes", are usually conducted under radical condition.[239] The reaction proceeded under mild base or nucleophilic catalysis is generally called thiol-Michael addition. Both types of reactions well meet the criteria of "click" reaction.[240] The mechanism of radical thiol-ene reaction involves direct addition of a thiyl radical, which is formed with assistance of a suitable photoinitiator under irradiation, to the vinyl groups. The generated carbon-centered radical then undergoes chain transfer to a second thiol group to give the thiol-ene addition product. An analogous mechanism is applies to the thiol-Michael addition by replacing the radicals with corresponding anionic species.[241]

It has to be mentioned that when employing the immobilized vinyl groups for the postmodification with thiol-ene reaction, the residual double bonds from the PEGDa matrix can be involved and thus have to be deactivated before the grafting procedure. Another way to avoid the interference of the residual double bonds is to use other transparent hydrogels without vinyl groups, like agarose,[221a] as matrix for the photografting.

Again, **M2CMK** with a similar molecular structure to the final photoproduct was chose as a model substrate to react with alkylthiols in order to verify the feasibility of thiol-ene reaction. According to the literature,[170] the C=C bond on 2,6-dibenzylidenecycloketone compounds can undergo various types of reactions, such as cycloaddition,[242] bromination[243] and oxidation.[244] However, to the best of our knowledge, there is no report on the thiol-ene reaction involving the double bonds of the dibenzylidenecycloketone derivatives. Therefore, the model reaction was conducted using the general method as described by Killops *et al.*[245] Considering that the radical thiol-ene reaction is generally extremely rapid at ambient temperature,[239] the model reaction was directly carried out in a transparent NMR tube and monitored by ^{1}H-NMR.
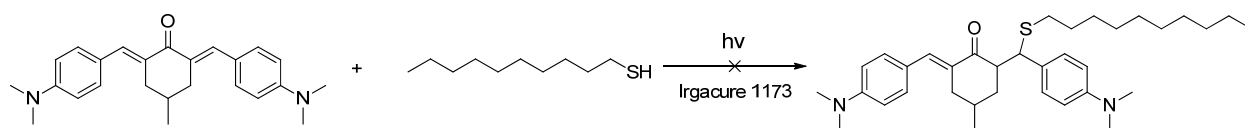
1.0 equivalent of **M2CMK**, 2.0 equivalents of 1-decanethiol and 0.2 equivalents of a photoinitiator were dissolved in 0.7 mL of DMSO-d_6. Liquid Darocur 1173 was used as photoinitiator due to its good solubility and suitability to induce thiol-ene reaction.[246] The mixture was shaken to ensure homogeneity and then under irradiation for 10 min. Then ^{1}H-NMR measurement was performed for the characterization. If the thiol-ene reaction occurs, the double bonds would be consumed. Since the aromatic rings of **M2CMK** are not affected during the reaction, the consumption of the double bonds would change the integration ratio between the protons of vinyl groups and those of the aromatic rings. Before the reaction, the ratio mentioned above is 1:2:2.

The ^{1}H-NMR results showed that after irradiation, the integration ratio still remained unchanged as 1:2:2, which indicated that the desired thiol-ene reaction did not occur. The inertia of the vinyl groups of **M2CMK** may be derived from the conjugated effect. Hoyle *et al*. listed the reactivity order of the general "enes" and conjugated enes were proven to

be less reactive.[247] The low reactivity is caused by the relatively stable intermediate carbon-centered radicals, which reduce the hydrogen abstraction rates from the second thiol molecule.[239] Another reason for the inefficiency of the vinyl groups of **M2CMK** is the steric hindrance. In general, terminal enes are much more reactive towards hydrothiolation compared to internal ones.[247] Moreover, several studies demonstrated that the reduced reactivity of internal enes is not entirely due to steric effects, the reversibility of the addition to *cis* C=C bonds forming a conjugated system and the isomerization accompanied also deactivate the wanted reaction.[248]

Therefore, the proposed postmodification of the immobilized vinyl groups via thiol-ene reaction cannot be taken into account due to the inertia of the internal C=C bonds.

4.4.3   Postmodification via CuAAC click reaction

CuAAC, a 1,3-dipolar cycloaddition between an azide and a terminal or internal alkyne to give a 1,2,3-triazole reaction, is by far the most widely used click reaction.[232] The reaction is catalyzed by commercial copper(I) derivatives such as cuprous bromide or iodide, or a mixture of copper(II) like copper(II) sulfate and a reducing agent (e.g. sodium ascorbate) to produce Cu(I) in situ. Addition of amines is needed to stabilize the unstable Cu(I) species. Since copper is believed to be cytotoxic and excessive copper intake would induce some side effects, in order to apply the click reaction into living systems, some copper-free alternatives, such as Staudinger ligation[249] or strain-promoted [3+2] heterocycloadditions,[250] have been developed.

In spite of the wide application of CuAAC, the reaction has yet to fulfill the requirements for micropatterns on flat surfaces[251] or within 3D scaffolds,[252] which demand very high spatial and temporal control. Using light as a CuAAC reaction trigger is an effective strategy to realize spatiotemporal control. Bowman's group reported micropatterns of hydrogels fabricated by using standard photolithographic techniques via in-situ generation of Cu(I) through photo-induced reduction.[253] Since such system involved multiple species, some side effects hindering the spatially resolved character could not be avoided. Popik, Locklin, and co-workers employed surfaces functionalized with cyclopropenone-masked dibenzocyclooctynes for the light activated immobilization of azides using the catalyst-free click chemistry.[254] However, a complex synthetic procedure is required for the preparation of cyclopropenone precursor, which restricts its broader

applications. More importantly, completely spatial control, especially in 3D, is limited for these mentioned approaches due to the inherent limitation of traditional photolithographic techniques. Therefore, if the postmodification of the immobilized azides groups via CuAAC can be successfully realized here, it will become the first example of 3D CuAAC with fully spatiotemporal control.

BAC-M has two azide groups on the aromatic rings. Under multiphoton excitation, both one and two azide groups can insert into the C-H bond within the matrix. Therefore, the residual azide functionality on the patterned matrix after photografting can be used for postmodification. **BAC-M** was selected as the model substrate to verify the feasibility of the CuAAC reaction. Unlike oxime formation and thiol-ene reaction of **M2CMK**, which are seldom reported, successful CuAAC reaction of **BAC-M** has been well proven.[255] Therefore, more attention should be paid to the molecular design of the model alkyne precursor for a better characterization after postmodification.

Considering the small area of the grafted pattern, the general methods like NMR and IR are not suitable for the characterization. Other effective approaches to characterize the micropatterns such as AFM and SEM can only provide the information of the surface morphology. The most frequently used method is to introduce suitable fluorophore to visualize the 3D micropatterns.[217] However, there are some difficulties when applying such approach in our case. Firstly, due to the complex photo reactions of arylazide during the grafting, it is hard to find a model compound to provide an analogue absorption and emission spectra of the grafting patterns. Secondly, the grafted patterns already exhibit strong fluorescence due to the inclusion of the ketocyanine dye. Moreover, the emission of the grafted patterns can be observed at the four wavelengths (405, 488, 555 and 639 nm) used for LSM excitation. The broad absorption range and unknown emission spectrum make it difficult for the selection of suitable fluorophores.

Energy-dispersive X-ray spectroscopy (EDX) is an efficient analytical technique for the elemental analysis of a sample. The characterization capabilities of EDX are based on the fundamental principle that each element has a unique atomic structure allowing unique set of peaks on its X-ray spectrum.[256] Therefore, with a proper molecular design of the model precursor, such method can be used for the characterization of the patterns after postmodification.

For the EDX measurement, the model precursor should have an element other C, H, O and N which are already included into the patterned matrix. Moreover, the precursor should also contain a terminal alkyne group for the CuAAC reaction with the residual azide groups on the matrix. Based on the above consideration, a bromo-containing alkyne **15** was designed and synthesized via alkylation with a similar procedure as described by Lasek *et al.*[257] with a high yield of 92%.
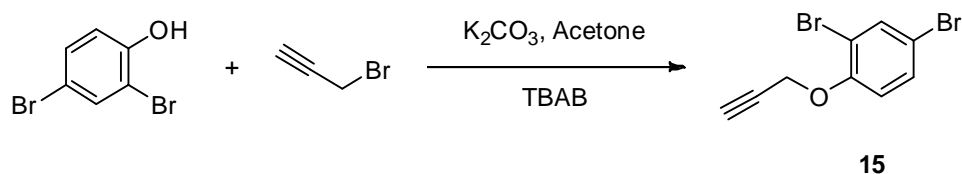
Before conducting the postmodification of the patterned matrix, a model reaction between **BAC-M** and the terminal alkyne **15** was performed under the reaction conditions as suggested by Gallardo *et al.* to verify the feasibility of the CuAAC reaction.[258]
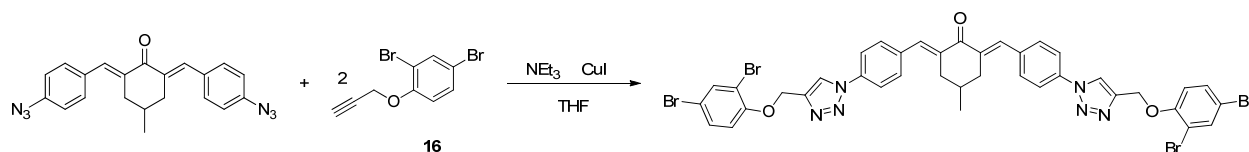
1.0 equivalent of **BAC-M** and 2.0 equivalents of the terminal alkyne **16** were dissolved in degassed THF containing 5.0 equivalents of TEA and 1.0 equivalent of CuI. The reaction was performed under room temperature in dark due to the photosensitivity of **BAC-M**. After 24h, the orange precipitates were collected and washed with water, acetone and chloroform, respectively, before the ^{1}H-NMR measurement.
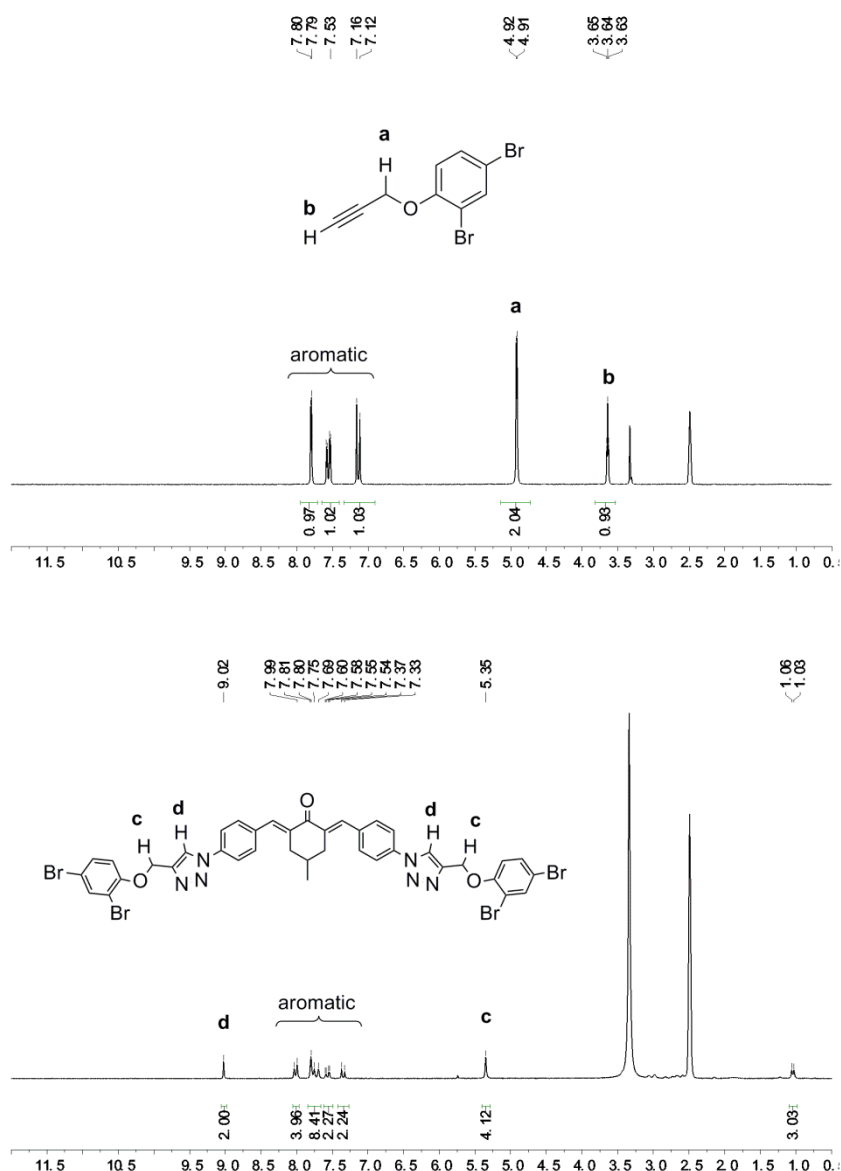
Fig 73 [^1]H-NMR spectra of **16** (up) and the product after CuAAC reaction (down)

The [^1]H-NMR spectra were recorded in DMSO-d$_6$ (**Fig 73**). After the reaction, the chemical shift of protons on the methylene group next to oxygen altered from 4.91 ppm (proton **a**) to 5.35 ppm (proton **c**). The disappearance of the alkyne proton **b** and the characteristic peak formed at 9.02 ppm (proton **d**) indicated the formation of triazole rings between aryl azide and dibromo-alkyne. Attempt to use [^13]C-NMR for further characterization of the product failed due to the poor solubility of the product with large molecular size. Even increasing the scan number up to 10000 cannot provide identifiable signals.

Based on the encouraging result of the model reaction, postmodification of the patterned matrix was performed under the similar condition of model reaction except replacing **BAC-M** with the grafted pellet. The successful immobilization was verified by EDX screening of the Br content on the grafted area. Since EDX is only capable of analyzing a thin layer of material, a larger and denser grafted pattern was produced on and a few micrometers into the surface of the sample for this purpose. After postmodification with the Br-containing alkyne **16**, the line scan through the functionalized area yielded a Br distribution profile reproducing the shape of the photografted pattern (**Fig 74**). The quantitative evaluation of the Br content was performed by EDX scanning of the equal grafted and control areas. The weight content of Br, calculated relative to the primary elements of the sample (C and O), was 5 ‰ on the grafted area and 0.5 ‰ outside the pattern. Despite the low relative concentration of Br on the sample, the tenfold increase of its content indicates the selective functionalization of the grafted area by means of the CuAAC reaction.
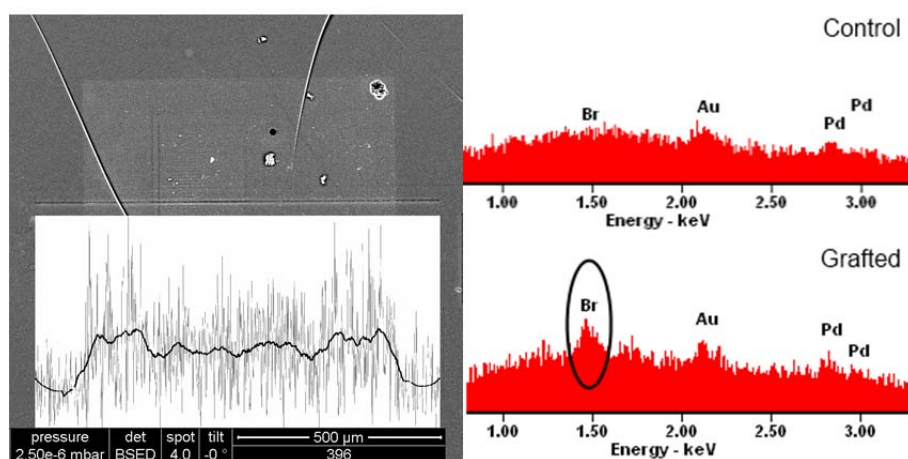
Fig 74 EDX analysis of sample photografted and subsequently functionalized with Br-containing compound. A line scan through the photografted pattern (light area in the SEM image) shows the distribution of Br.

The disadvantage of EDX method is that it can only analyse the element content of the patterns produced on the surface or a few micrometers into the surface, lacking the information of the volumetric element content. Another problem is that the patterned hydrogel matrix after postmodification must be completely dried under vacuum before the EDX measurement. The evaporation of the solvent can easily induce the crack of the pellet.

5   AFA series for photografting under 2PA

5.1   Molecular design of novel arylazide for photografting under 2PA

In chapter 4, **BAC-M** has been used to prove the concept of selective functionalization of 3D PEGDa matrix under 3PA. The obtained results encourage us to explore more aromatic azides for 3D photografting. Due to the lack of efficient electron donor groups, the activation of **BAC-M** needs to be realized under 3PA, which means more laser energies are needed compared to the excitation under 2PA. Within the same laser power range, more required energy means narrower processing windows. On the other hand, high laser power required also limits the writing speed because with constant laser power, faster writing speed generally provides less energy, which cannot induce the desired reactions. Therefore, to develop novel aromatic azides with strong 2PA is of interest.

Since a full understanding of the relationship of molecular structure and two-photon properties still remains a big challenge, the most effective way to produce 2PA active aromatic azides is to introduce azides groups to chromophores with large two-photon cross sections. In the strategy used to prepare water-soluble 2PIs, the water-borne functionalities should be attached at the terminal of the long alkyl chains to avoid changing the electronic structure of the core structures. However, the introduced azide groups should be involved into the whole conjugated system to ensure efficient use of the absorbed energy to induce the subsequent desired photochemical reactions. Both **B3FL** and **R1** have been proven to be efficient two-photon absorbers in chapter 1. Therefore, two arylazide candidates with core structures of conjugated fluorenone and distyrylbenzene were proposed (**Fig 75**).
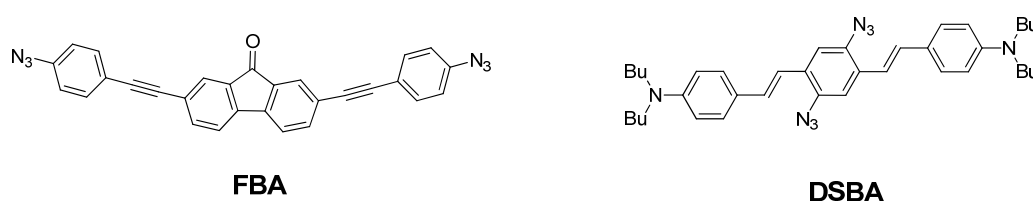
Fig 75 Proposed structures of the arylazides

The proposed preparation of fluorenone-based azides **FBA**, which includes the coupling reaction between 4-ethynylphenyl azide and 2,7-diiodo-fluorenone, seems quite feasible

because Tomioka *et al.* has reported the synthesis route of 4-ethynylphenyl azide and further demonstrated the successful Sonogashira coupling reaction with corresponding iodide.[259] Similar to **BAC-M**, however, there is no efficient electron donor, which would limit the 2PA at 800 nm. Considering the potentially limited 2PA performance, such molecule was not taken into account.

The distyrylbenzene-based candidate **DSBA** is attractive because the azide groups are attached into the central benzene ring and play dual roles: electron acceptors and functionalities for photografting and postmodification. Unlike **FBA** without electron donors, **DSBA** comprises a D-π-A-π-D core structures with dialkylamino groups as donors and vinyl as π-conjugated bridges, which can ensure large 2PA at 800 nm. Moreover, the distyrylbenzene derivatives with central electron-drawing groups, which can facilitate intramolecular electron transfer process, have been proven to exhibit larger 2PA cross sections compared to the analogues with D-π-D-π-D structures.[46] The main disadvantage of the molecule is its complex synthesis. In the proposed synthesis route (**Fig 76**), the highly sensible azide groups should be introduced at last step via the substitution of the central amine groups with azides. The central amines should derive from the reduction of the corresponding nitro groups.
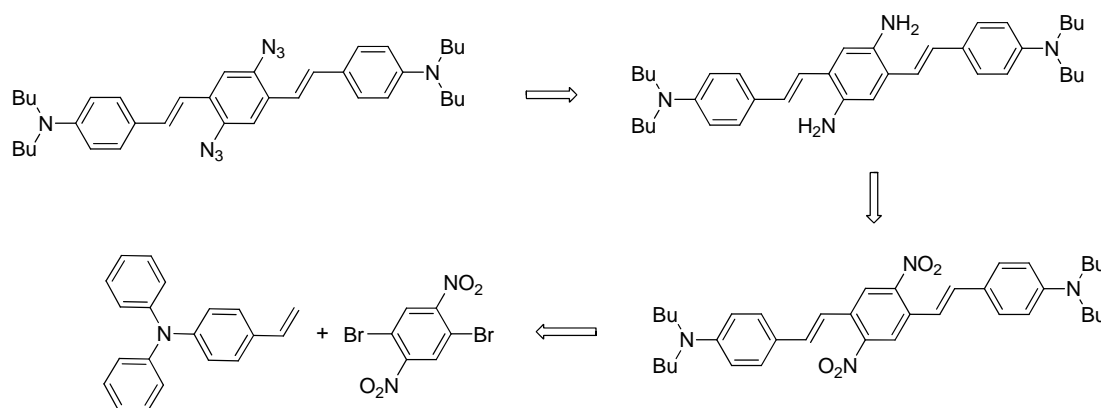
Fig 76 Proposed synthesis route of DSBA

A conjugated molecule with very similar structure to the desired nitro-containing precursor except with triphenyl rather than dibutyl-aniline has been reported by Nielsen *et al.* [260] The reported D-π-A-π-D structure was realized by Heck coupling reaction but with a very low yield of 10%. Considering the preparation of the precursors for the coupling, the synthesis of **DSBA** contains at least 6 steps. Moreover, when introducing azide groups at the last step, only the di-substituted product is of interest because for the mono-substituted molecule, no azide group left for the postmodification after photografting. Considering the challengeable synthesis route and low yield of the

coupling reaction, new 2PA absorber should be explored to obtain the desired 2PA active arylazides but with a simple preparation.

Pentafluorobenzene connected with an alkylated aminophenol through a vinyl bridge is another promising 2PA absorber.[261] Several studies demonstrate that using C=N bond instead of C=C as a conjugated bridge does not significantly alter the 2PA property,[262] but provides a much simple synthesis. Since the fluorine atom at *para-* position can be easily substituted by azide group,[263] novel arylazides with D-π-A core structures were proposed (**Fig 77**).
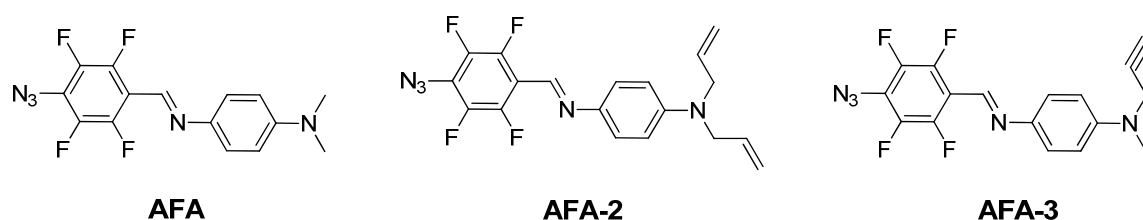
Fig 77 Proposed structures of the AFA series compounds

The electron-drawing ability of an azide is reported as strong as a fluorine atom,[226] therefore, high 2PA activity of the aromatic azide is expected. Amino groups and fluorinated aromatic azide are used as D and A, respectively. Beside the strong electron drawing ability of fluoroaryl azide, such compound offers high grafting efficiency because of the selective formation of singlet nitrene intermediates which exclude potential deactivations derived from intramolecular rearrangement [264]

The simple synthesis provides the possibility to incorporate not only azides group, but also other functionalities for postmodification after photografting. Since click chemistry has been proven as an effective strategy for the postmodification in Chapter 4, amino groups with terminal vinyl and alkyne as in **AFA-2** and **AFA-3** are of interest. Both **AFA-2** and **AFA-3** uses azide groups for photografting and subsequently terminal alkene groups of **AFA-2** and alkyne groups of **AFA-3** are used for post-functionalization via thiol-ene and CuAAC reactions, respectively. Therefore, high photografting efficiency means more functional groups for the subsequent click reaction. However, in the case of **BAC-M**, there is a compromise between the amount of azide groups for photografting and post-modification because azide groups are involved in both processes.

5.2   Synthesis

The proposed synthesis route of **AFA** series compounds is quite straightforward (**Fig 78**). The formation of the Schiff base can be realized between the azidotetrafluorobenzaldehyde with aromatic amines under mild condition. Since the preparation of azidotetrafluorobenzaldehyde has been well developed,[263] the key point is to synthesize the corresponding amines with desire functional groups.
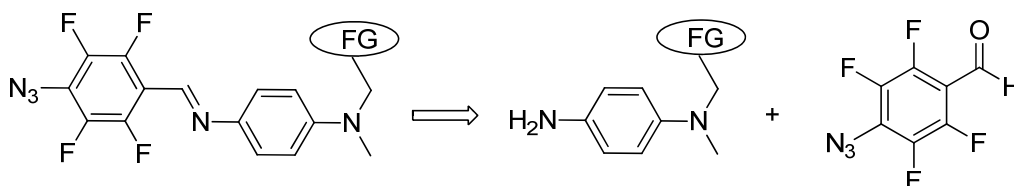
Fig 78 Proposed synthesis route of AFA series compounds

5.2.1   Synthesis of 4-azido-2,3,5,6-tetrafluorobenzaldehyde (16)

The precursor azidotetrafluorobenzaldehyde was synthesized as described by Keana *et al.*[263]
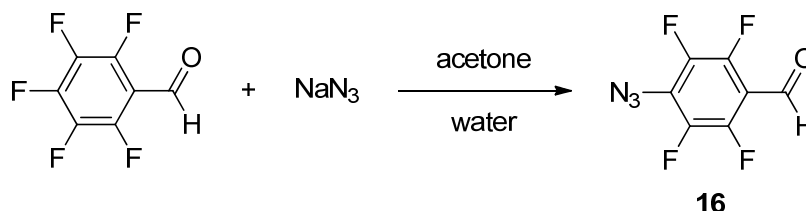
1.0 equivalent of pentafluorobenzaldehyde reacted with 1.1 equivalents of the nucleophilic reagent sodium azide under reflux acetone/water mixture to give the desired aldehyde **16** with high yield (80%) after sublimation (25 °C/0.1 mm). It is reported that no ortho-isomer was detected with such synthesis procedure[264] and the characteristic data are in well agreement with the previous reports.[265] The characteristic peak of azide group at 2118 cm^{-1} in infrared spectra indicates the product with the desired functional group. In ^{19}F NMR, the integration results confirm the exclusive *para*-substituted product.

5.2.2   Synthesis of N,N-diallyl-benzene-1,4-diamine (18)

The amine precursor **18** with terminal vinyl groups for the synthesis of **AFA-2** was prepared in two steps.
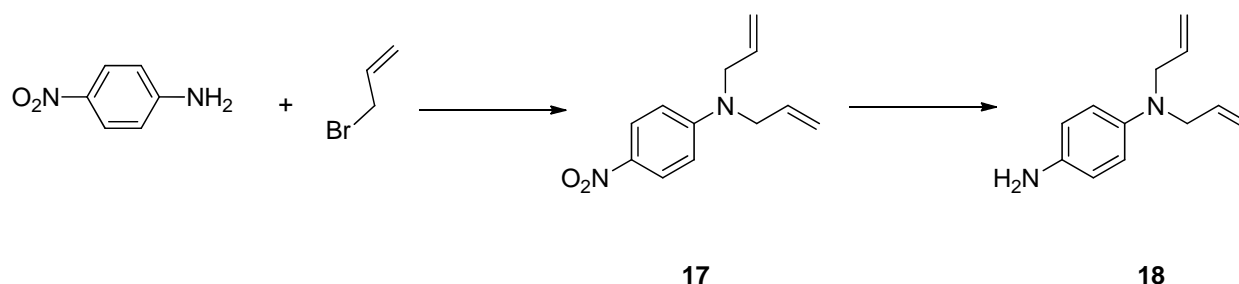
The nitro precursor **17** can be prepared by substitution of 4-fluoro-1-nitrobenzene with di-2-propenylamine via addition-elimination mechanism.[266] The strong electron drawing property of the nitro group combined with good leaving-group ability of the fluoride ion facilitates the nucleophilic aromatic substitution. However, the reported preparation procedure required long reaction time (10h) and high temperature (100 °C).[266] Another synthesis route is based on the alkylation of 4-nitro-phenylamine with 3-bromo-propene in the presence of a strong base. The alkylation is conducted under room temperature with fast reaction rate. Due to the ease of preparation and the accessibility of the reagents, the nitro precursor **17** was synthesized via alkylation as described by Ramachary *et al.*[267]
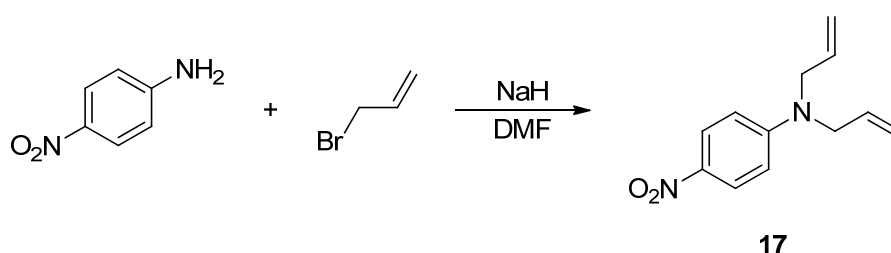
1.0 of equivalent of 4-nitro-phenylamine was deprotonated by sodium hydride in dry DMF. Then excessive amount of 3-bromo-propene (3.0 equivalents) was added to ensure the di-substitution. A high yield of 80% was obtained after column chromatography.

Conversion of nitro group on **17** to amine to prepare **18** was realized by reduction. One effective method to reduce the aromatic nitro group is catalytic hydrogenation using palladium-on-carbon as the catalyst.[268] The reduction can be conducted under mild condition with easy workup because the catalyst can be simply filtered off after the reaction. The disadvantage of the approach is the relatively high price of the metallic catalysts. Moreover, the catalytic hydrogenation can potentially reduce the vinyl and alkyne groups[268] and thus the reduction condition needs to be optimized. Another more economical reduction method is metal reduction, in which $SnCl_2$ and Fe are frequently

used as reducing agents.[269] In contrast to hydrogenation, metal reduction does not affect the C=C and C≡C bonds, but requires harsh reaction conditions (strong acidic environment and high temperature). For the ease of synthesis and economical reason, the nitro precursor **17** was reduced using $SnCl_2$ to prepare the amine **18** as descript by Larch *et al.*[270]
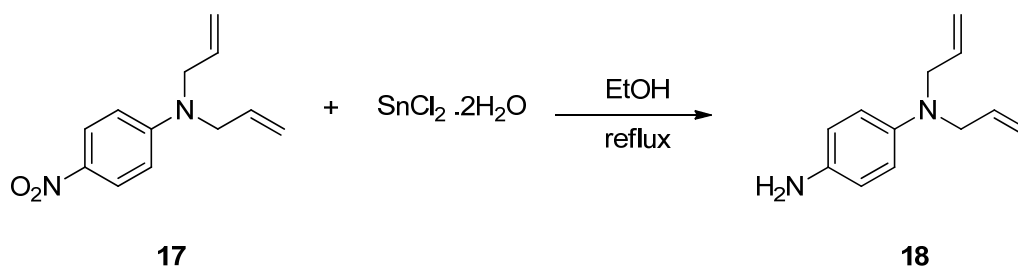
Under argon protection, 1.0 equivalent of the nitro compound **17** was treated with 5.0 equivalents of tin (II) chloride dihydrate in EtOH under reflux. The reaction was quenched by adding NaOH solution when **17** was completely consumed (monitored by TLC). In the workup, when neutralizing the residual $SnCl_2$ with NaOH solution, the formed very fine powder of tin hydroxide is difficult to filter off, even with Büchner funnel under reduced pressure. The issue can be addressed by centrifugation to remove the slurry precipitate. The crude product was purified by column chromatography to give the amine precursor **18** as orange oil with a yield of 50%.

5.2.3   Synthesis of amine precursor (20)

Attempt to introduce two alkyne groups to the 4-nitro-phenylamine using the similar synthesis strategy of **17** is not successful. The reason might be the weak acidity of the alkyne group, which can react with sodium hydride and thus destroy the reagents.
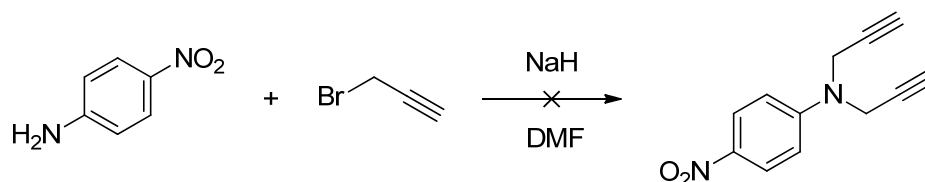
Therefore, only one alkyne group was introduced by substitution of 4-fluoro-1-nitrobenzene with N-methylpropargylamine via addition-elimination mechanism as describe by Wolfe *et al.*[271]

19
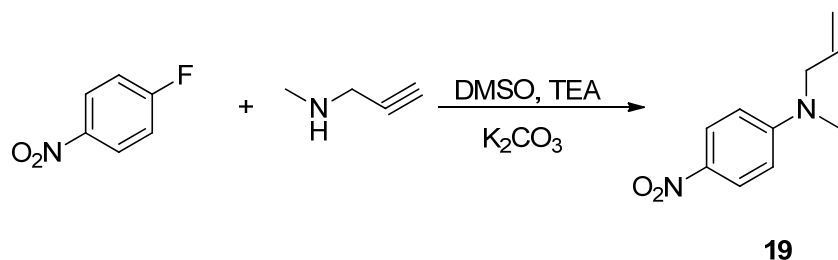
1.0 equivalent of 4-fluoro-1-nitrobenzene reacted with 1.0 equivalent of N-methylpropargylamine in the presence of potassium carbonate as an acid acceptor. The mixture was stirred overnight at 50 °C. The crude product was washed with water and 2-propanol to obtain the alkyne **19** as yellow solid with a high yield of 75%.

Using the similar reduction procedure of the amine **18**, the nitro group was successfully converted to amine with excessive amount of tin (II) chloride dihydrate as a reducing agent. Considering that the amine group of **20** can be easily oxidized and the nitro precursor **19** has no negative effect on the further Schiff base formation, the product **20** (> 95% purity from NMR) was used for the next step without further purification.

19   **20**
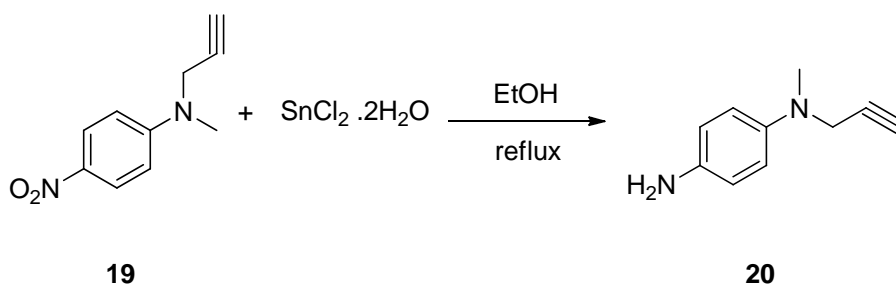
5.2.4   Synthesis of novel fluoroaryl azides

The fluoroaryl azides were prepared via forming imine bonds between 4-azidotetrafluorobenzaldehyde and equal equivalent of corresponding amine precursors. The reactions were carried out in dry toluene under room temperature. The impurities could be simply washed away with appropriate cold solvents to obtain the final products with satisfying yields from 50% to 66%. Cold acetone was used as washing solvent for **AFA** but it was not suitable for **AFA-2** and **AFA-3** due to their improved solubility derived from the longer terminal alkyl chain. Therefore, cold ether was used instead.
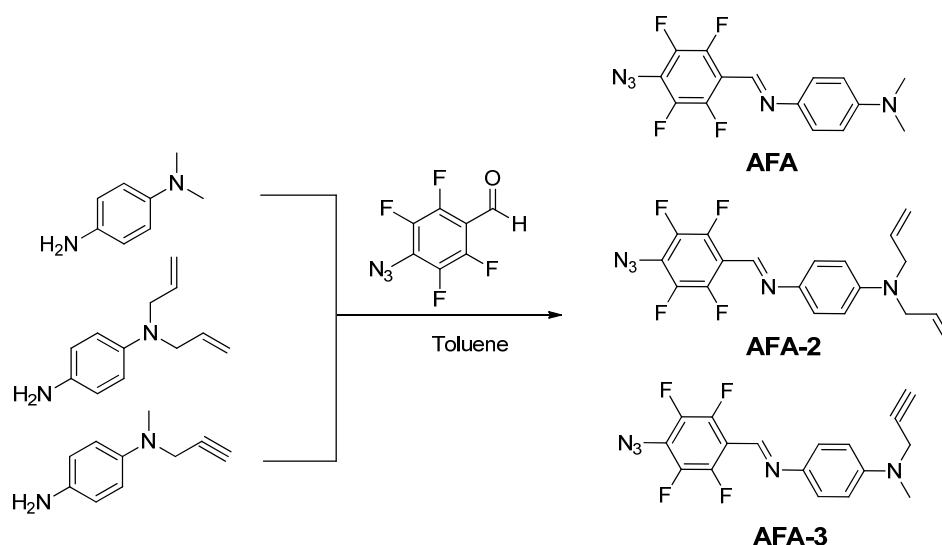
5.3   Z-scan of AFA series compounds

Since the electron-drawing ability of an azide is reported as strong as a fluorine atom,[226] the absorption spectra of **AFA** should be very similar to its core structure. The maximum UV absorption peak of the core structure lies at about 397 nm,[272] which indicates a high possibility of 2PA at 800 nm. It is not the case for **BAC-M** with a linear absorption at about 365 nm, which has been proven to be three-photon active at 800 nm. Therefore, in order to determine the order of nonlinearity as well as multi-photon absorption cross section, an open aperture z-scan experiment was performed at 800 nm in DMF with the same concentration of 1.0×10^{-2} mol. L^{-1}. The z-scan result of **BAC-M** was also included for comparison.

In the z-scan method, the absorbance caused by the third-order nonlinearities such as 2PA is proportional to the input intensity while the one resulted from the fifth-order nonlinearities such as 3PA is quadratic to the input intensity [273]. From z-scans of **AFA** shown in **Fig 79,** the maximum transmittance (at focus) behaves linearly with pulse energy which is an indication of 2PA process. The maximum transmittance in z-scan of **BAC-M** increases quadratically with pulse energy signifying the predominance of 3PA process in this compound. The slope of fitting curves shown in **Fig 80b** also confirm the predominance of 2PA process in **AFA** and 3PA in **BAC-M**.(the detailed information of the fitting is described in Dr. Aliasghar Ajami's PhD thesis[150]). The σ^{2PA} values of **AFA** series compounds are listed in **Table 12**. Since the introduction of functional groups -

terminal vinyl and alkyne- does not significantly alter the electronic structure of the whole molecules, the σ^{2PA} values nearly remain unchanged.
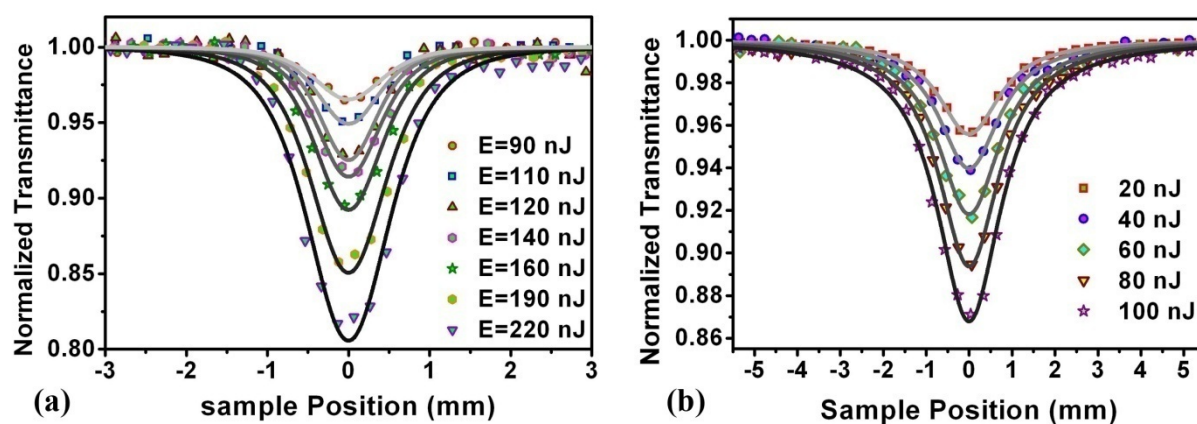
Fig 79 Experimental z-scan data (dots) and fitting curves (full lines) for (a) **BAC-M** and (b) **AFA** at different pulse energies

Table 12 2PA cross section values of arylazide in DMF by z-scan measurement at 800 nm

Arylazide	σ^{2PA}(GM)
AFA	178
AFA-2	176
AFA-3	164

Fig 80a shows two z-scans of **AFA** and **BAC-M** with the same transmittance. It indicates that the intensity required to cause a certain absorbance via a 2PA process is much lower than that of a 3PA process. It also illustrates the main advantage of a two-photon absorber over a three-photon absorber. The transmittance change versus intensity is faster in case of 3PA comparing to 2PA leading to achieve higher spatial resolution in MPG using three-photon grafting molecules. These two major differences between a two-photon absorber and a three-photon absorber (i.e. lower intensity threshold for starting 2PA but higher structural resolution using a three-photon absorber in MPG) are practically illustrated by performing photografting patterning tests using **AFA** and **BAC-M** (see next section).
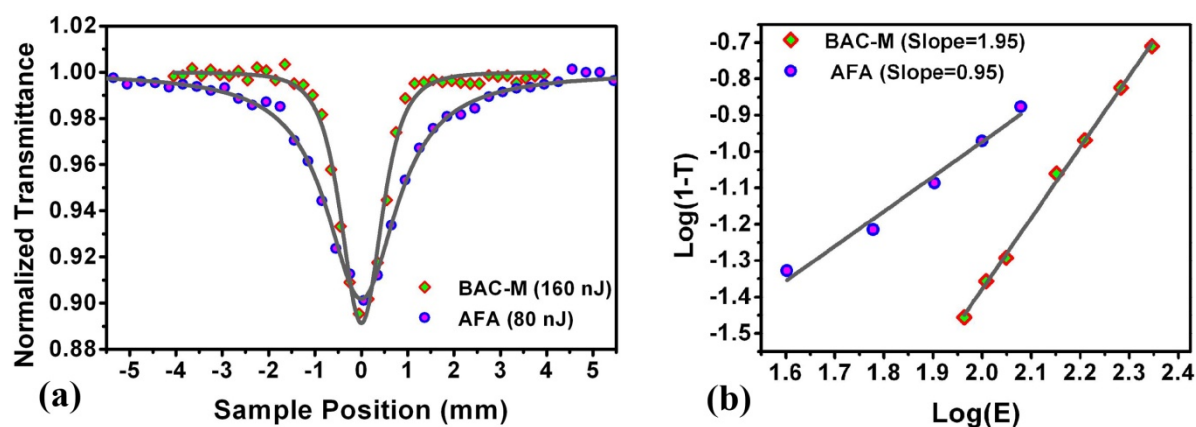
Fig 80 (a) Z-scans of BAC-M and AFA with the same transmittance. (b) Log(1-*T*) versus Log(*E*) for both compounds indicating that **BAC-M** is a three-photon absorber but **AFA** is a two-photon absorber[150]

5.4 Comparison of photografting under 2PA and 3PA

The photochemistry of **AFA** under two-photon excitation is proposed as shown in **Fig 81a**. Photolysis of the azide causes the dissociation of the N-N bond from the excited singlet state followed by the generation of nitrogen and nitrene species, which are directly immobilized on a PEGDa-network by insertion into a C-H bond. After grafting, the products still contain "push-pull" features, which exhibit certain fluorescence. Therefore, grafted patterns can be directly visualized via LSM. **Fig 81b** shows an LSM image of a 3D lockyball pattern [274] produced with **AFA** (0.5%) at the average power of 330 mW and scanning speed of 500 mm/s.
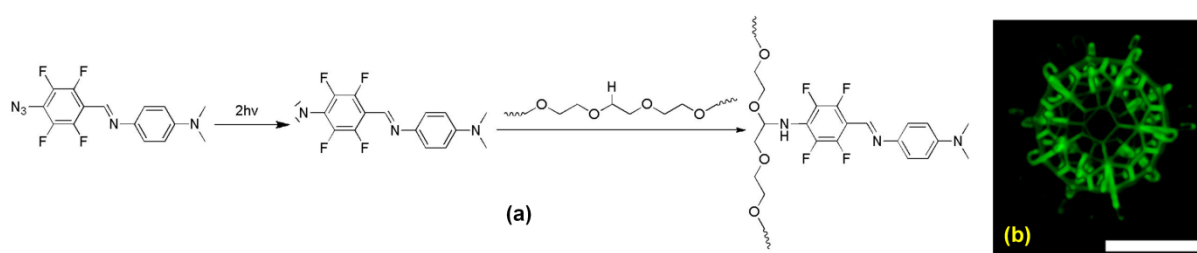
Fig 81 Grafting process: (a) 2PA-induced photolysis of **AFA**, followed by an insertion reaction within the PEGDa-based matrix; (b) fluorescent image of a photografted lockyball [274]. Scale bar is 200 μm.

Both **AFA** and **BAC-M** contain active arylazide groups for photografting. Since the activation of **AFA** is under two-photon excitation, while **BAC-M** has proven to be three-

photon active, it is of interest to compare the photografting behavior of these aromatic azides under different order of excitation. **Fig 82a** and **c** show the processing windows of both arylazides using different average laser powers and scanning speeds. The probability of 3PA is lower than that of 2PA; as a consequence higher laser intensity is required for the activation of **BAC-M** compared to **AFA**. This difference in the threshold is confirmed by the fact that the MPG processing window of **AFA** is much broader than that of **BAC-M**, allowing creation of photografted patterns with lower intensity and with higher writing speed using **AFA**. However, the observed fluorescence intensities of grafted patterns of **BAC-M** under high laser intensities and low scanning speed are greater than those of **AFA** with the identical parameters. This difference can be explained by the photografting products of **BAC-M**, which contain the ketocyanine chromophore with strong fluorescence[275]. Notably, the levels of immobilization can be spatially controlled by simply altering the irradiation exposure time or laser intensity during the photopatterning process**.** Such controlled 3D spatial gradients cannot be generated by conventional photolithographic methods. The ability to produce biochemical and biomechanical gradients in 3D is important to numerous bio-technology applications.[218]
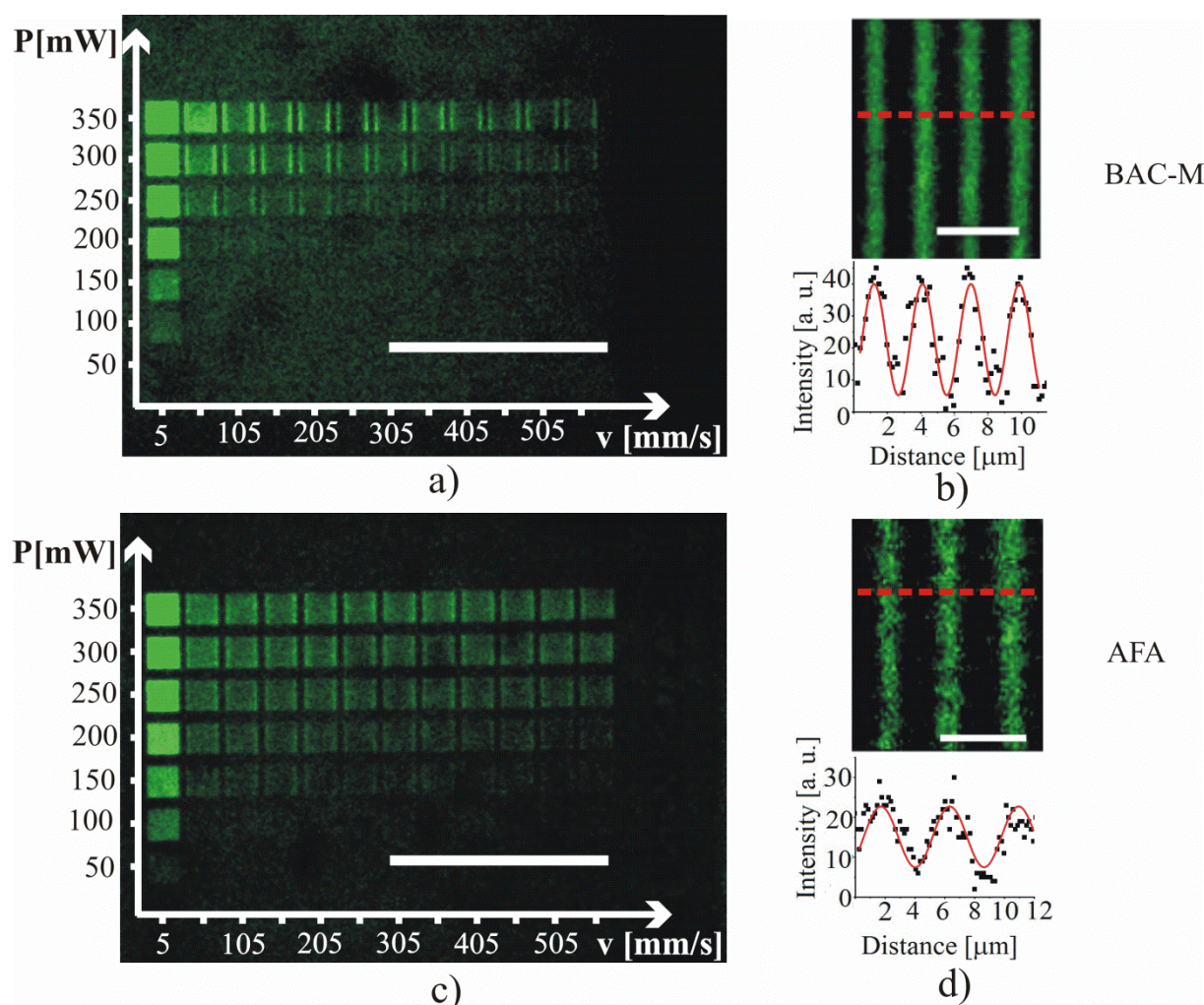
Fig 82 An array of multi-photon grafted patterns produced at the different scanning speed and average laser power: (a) **BAC-M** and (c) **AFA**. The scale bar is 500 μm. Comparison of achievable resolution; the distance between lines is: (b) 3 μm for **BAC-M** and (d) 4.5 μm for **AFA**. The scale bar is 5 μm.

The achievable resolution for **BAC-M** and **AFA** patterns produced at fixed grafting parameters (the average laser power of 350 mW and laser scanning speed of 5 mm/s) and molar concentration of azides molecules (14 mmol/L) was also compared (**Fig 82**). It was evaluated that the width of single lines produced by using the above mentioned laser power and scanning parameters is around 2.5 μm for **BAC-M** and around 4.1 μm for **AFA**. The resolvability of lines is confirmed by the according fluorescence intensity distribution. At a smaller distance the separate lines could not be distinguished. **BAC-M** shows a better spatial resolution than **AFA**. Since the immobilization of **BAC-M** molecule proceeds via 3PA process and of **AFA** via 2PA process, the initial activation volume is expected to be smaller for **BAC-M**.

In summary, the processing window of **AFA** is much broader than that of **BAC-M** due to less energy required for 2PA excitation, but patterns with higher resolutions can be produced with **BAC-M** because of better confinement of 3PA. The choice of the appropriate molecules for 3D grafting should depend on the specific applications.

AFA-2 and **AFA-3** have very similar molecular structures to **AFA**. Z-scan measurements have proven that the introduction of the functionalities does not significantly affect the 2PA behavior of the **AFA** series compounds. In 2PA photografting tests, the width of single lines and the resolvability of lines produced by **AFA-2** are around 3.1µm and 4.0 µm, respectively, while the corresponding values for **AFA-3** are around 3.6 µm and 4.5 µm (**Fig 83**). The obtained values of **AFA-2** and **AFA-3** are very comparable to those of **AFA**, indicating that the photografting behaviors are marginally affected by the introduced functional groups.
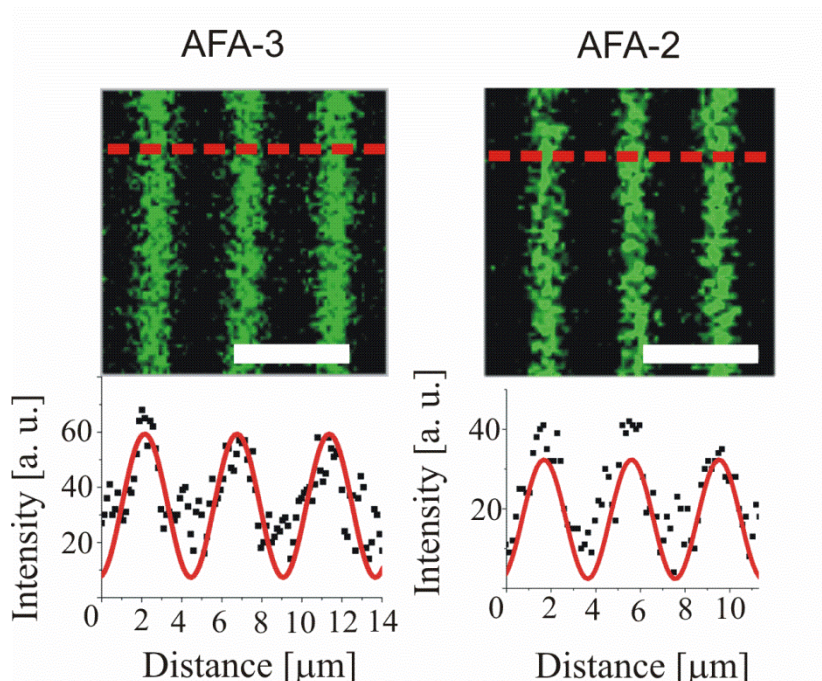
Fig 83 Comparison of achievable resolution; the width of single lines and the distance between lines are: 3.1µm and 4.0 µm for **AFA-2** and 3.6 µm and 4.5 µm for **AFA-3**. The scale bar is 5 µm.

5.5 Stability of the grafted patterns

After photografting, the immobilized chromophores still contain C=N bonds, which are potentially hydrolysable under acidic conditions. In order to evaluate the stability of the

clickable patterns, the 2PA functionalized pellets (using **AFA-3** for the photografting agent) were transferred from DMF to aqueous solutions with different pH value and incubated under room temperature for 24h. Then the pellets were re-immersed into DMF for 24 hours before LSM observation. Considering the swelling property of the hydrogel matrix, the solvent DMF should be removed and refilled every 2 hours (for 6 times) to ensure sufficient solvent exchanging between water and DMF. Since the PEGDa pellet contains ester and ether groups, both strong acidic or alkaline conditions can induce the decomposition of the matrix. Therefore, the stability tests were performed with limited pH values ranging from 3 to 10, at which the matrix has been proved to be stable for that period of time. If hydrolyzation of the photografting patterns occurred, the intensity of the fluorescence would shift due to the change of the electronic structure of the immobilized molecules derived from the hydrolysis of C=N bond. Actually, under excitation at 555 nm, no fluorescence was observed for the model patterns obtained by UV photografting of 4-azido-2,3,5,6-tetrafluorobenzaldehyde. Therefore, decreasing fluorescence was expected if immobilized molecules underwent hydrolyzation process. As shown in **Fig 84**, the unchanged intensities of fluorescence indicate that 2PA grafting patterns exhibit remarkable stability under investigated pH values. Considering most biological applications are performed under mild conditions in buffer solutions, the 2PA photografting patterns demonstrate sufficient stability to fulfill the requirement.
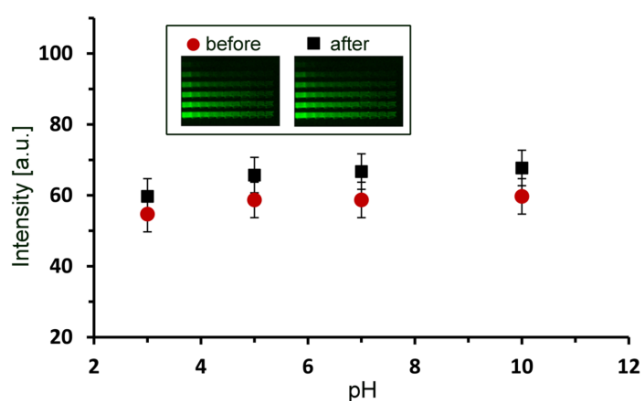
Fig 84 Fluorescence intensity before and after the stability tests under different pH value; insert are LSM images of the fluorescent patterns before (left) and after (right) the tests at pH=7

5.6   Post modification of AFA-3

When using **AFA-3** for the 2PA photografting, the alkyne groups are selectively immobilized within the 3D hydrogel matrix. Due to the distinct characters of the CuAAC click reactions, various functionalized molecules with azide moiety can be conjugated onto the formed "clickable" patterns containing alkyne functionalities produced by 2PA grafting. Azide MegaStokes dye 673 was selected as a model precursor for the click reaction because the strong fluorescence emission of the dye lies at a long wavelength of 673 nm, at which the fluorescence of the "clickable" patterns produced by 2PA grafting could not be observed. Therefore, an excellent differentiation of the fluorescent patterns before and after click reaction could be achieved. The good hydrophilicity of the dye[276] allows the click reaction performing in PBS solution (pH 7.4) in the presence of $CuSO_4$-sodium-ascorbate and triethylamine.

MegaStokes dye 673
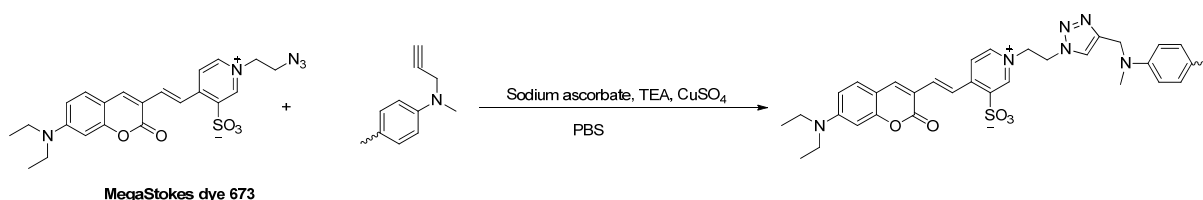
Before click reaction, the complex 3D patterns (yin yang) obtained via 2PA grafting exhibited green fluorescence (**Fig 85a**). The color of the fluorescent pattern changed from green to red indicating the successful 3D site-specific immobilization of the azide-fluorophores via CuAAC click reaction (**Fig 85b**).
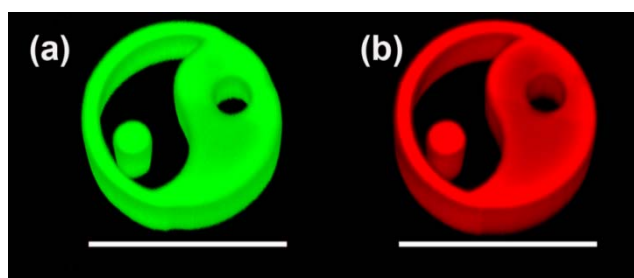
Fig 85 Laser scanning microscopy (LSM) images of the 3D photografted patterns: (a) before click reaction (λ_{exc} = 488 nm); (b) after click reaction (λ_{exc} = 555 nm). Scale bar: 100mm.

Experimental

1 Aromatic ketone-based 2PIs

1.2 Synthesis of Aromatic-ketone based 2PIs

1.2.1 Synthesis of alkyne precursors 3a and 3b

1.2.1.1 Synthesis of *N,N*-dibutyl-4-iodobenzeneamine (1a)[132]

[219.03]   [184.02]   [331.24]
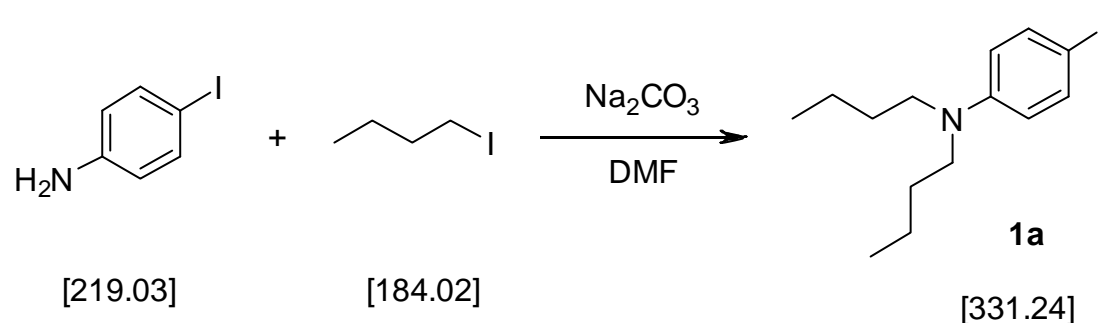
Reagents	MW [g/mol]	[g]	[mL]	[mmol]	[eq.]
4-iodobenzeneamine	219.03	9.81		44.8	1.0
1-iodobutane	184.02	28 +10		206.5	4.6
sodium carbonate	105.99	8.5+5.2		129.3	2.9
DMF			125		

Procedure

To 9.81 g (44.8 mmol) of freshly recrystallized colorless crystals of 4-iodobenzeneamine and 28 g (152.2 mmol) of 1-iodobutane dissolved in 125 mL DMF, 8.5 g (80.2 mmol) of Na$_2$CO$_3$ as base were added and the mixture was heated to 95 °C. After 45 h no full conversion was detected (monitored by TLC and GC-MS analysis) so that additional 10.0 g (54.34 mmol) of 1-iodobutane and 5.2 g (49.06 mmol) of sodium carbonate were added and the temperature was increased to 110 °C. After 52 h still no full conversion was given, but nevertheless the reaction mixture was allowed to cool to room temperature and subsequently poured into water (300 mL) and extracted with DCM (3 × 140 mL). The combined organic layers were washed with water (2 × 70 mL) and brine (1 × 70 mL) and subsequently dried over Na$_2$SO$_4$. The solvent was evaporated in vacuum and a flash

column chromatography (pure hexane) afforded 10.3 g of the product **1a** as pale yellow oil.

Yield

70 % of theory (95% of lit<mark>[132]</mark>)

Analysis

TLC (hexane):	R_f = 0.36
^{1}H-NMR (200 MHz, CDCl$_3$):	δ (ppm) = 7.43 (d, J = 9.13 Hz, 2H, ar-H2+H6), 6.43 (d, J = 9.13 Hz, 2H, ar-H3+H5), 3.24 (t, J = 7.52 Hz, 4H, 2×N-C$\underline{H}_2$), 1.66-1.45 (m, 4H, 2×CH$_2$-C$\underline{H}_2$-CH$_2$), 1.45-1.23 (m, 4H, 2×CH3-C$\underline{H}_2$), 0.96 (t, J = 7.12 Hz, 6H, 2×C$\underline{H}_3$-CH$_2$).
^{13}C-NMR (50 MHz, CDCl$_3$):	δ (ppm) = 147.7 (ar-C4), 137.7 (ar-C2+C6), 114.1 (ar-C3+C5), 75.4 (ar-C1), 50.85 (N-$\underline{C}$H$_2$), 29.3(CH$_2$-$\underline{C}$H$_2$-CH$_2$), 20.4 (CH$_3$-$\underline{C}$H$_2$), 14.1 ($\underline{C}$H$_3$-CH$_2$).
GS-MS analysis:	(m/z) = 231.96, 245.94, 287.98, 331.01.

1.2.1.2   Synthesis of N-butyl-N-(2-ethylhexyl)-4-iodoaniline (1b)
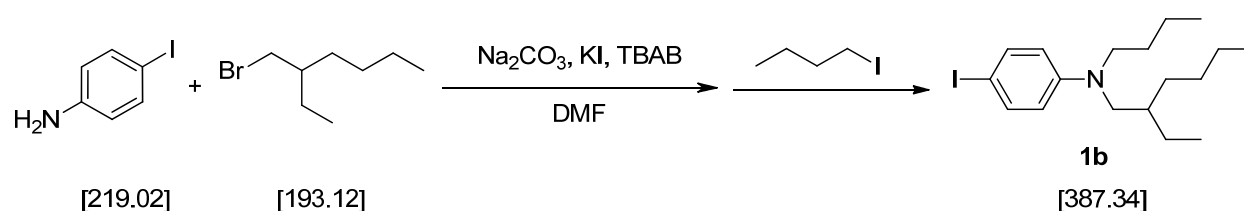
Reagents	MW [g/mol]	[g]	[mL]	[mmol]	[eq.]
4-iodobenzeneamine	219.03	21.91		100	1
3-(bromomethyl)heptane	193.12		50	300	3
sodium carbonate	105.99	41.46		300	3
potassium iodide	166	8.31		50	0.5
TBAB	322.37	1.99		6	0.06
1-iodobutane	184.02		34	300	3

DMF   300

Procedure

To a solution of 21.91 g (100 mmol) of 4-iodoaniline in 300 mL degassed dry DMF under argon atmosphere, 50 mL (300 mmol) of 3-(bromomethyl)heptane, 41.46 g (300 mmol) of Na_2CO_3 powder, 8.31 g (50 mmol) of potassium iodide and 1.99 g (6 mmol) of tetrabutylammonium bromide (TBAB) were added and the reaction mixture was stirred at 110 °C until 4-iodoaniline was completely consumed (GC-MS analysis). Then 34 mL (300 mmol) of 1-iodobutane were added, and heating was continued for 3 days. Afterwards, the solution was poured onto 500 mL of water and extracted by ethyl acetate until the aqueous layer was colorless. The combined organic layers were washed with water (3 × 200 mL) and brine (2 × 100 mL), dried over Na_2SO_4, filtered and concentrated. Purification by column chromatography (hexane) yielded 23.26 g of the product **1b** as colorless oil.

Yield

60 % of theory (two steps)

Analysis

TLC (hexane): $R_f = 0.46$

^{1}H-NMR (200 MHz, CDCl$_3$):   δ (ppm) = 7.39 (d, J = 8.9 Hz, 2H, ar-H2+H6), 6.40 (d, J = 9.0 Hz, 2H, ar-H3+H5), 3.23 (t, J = 7.4 Hz, 2H, N-C$\underline{H}_2$-CH$_2$), 3.08 (d, J = 7.3 Hz, 2H, N-C$\underline{H}_2$-CH), 1.66-1.60 (m, 1H, CH$_2$-C$\underline{H}$-CH$_2$), 1.58-1.11 (m, 12H, CH$_3$-C$\underline{H}_2$+CH$_3$-C$\underline{H}_2$+CH$_3$-C$\underline{H}_2$+CH$_2$-C$\underline{H}_2$-CH$_2$+CH$_2$-C$\underline{H}_2$-CH$_2$+CH-C$\underline{H}_2$), 1.04-0.74 (m, 9H, C$\underline{H}_3$-CH$_2$+C$\underline{H}_3$-CH$_2$+C$\underline{H}_3$-CH$_2$).

^{13}C-NMR (50 MHz, CDCl$_3$):   δ (ppm) = 147.9 (ar-C4), 137.5 (ar-C2+C6), 114.4 (ar-C3+C5), 75.4 (ar-C1), 55.2 (N-C$\underline{H}_2$-CH), 51.6 (N-C$\underline{H}_2$-CH$_2$), 37.4 (CH$_2$-C$\underline{H}$-CH$_2$), 30.7 (CH-C$\underline{H}_2$-CH$_2$), 28.7 (N-CH$_2$-C$\underline{H}_2$), 28.3 (CH-CH$_2$-C$\underline{H}_2$), 23.9 (CH-C$\underline{H}_2$-CH$_3$), 23.2 (CH3-C$\underline{H}_2$-CH2-CH2-CH), 20.3 (CH3-C$\underline{H}_2$-CH2-CH2-N), 14.1 (C$\underline{H}$3-CH$_2$-CH2-CH2-CH), 14.0 (C$\underline{H}$3-CH$_2$-CH2-CH2-N), 10.8 (CH-CH$_2$-C$\underline{H}_3$).

GS-MS analysis: (m/z) = 119.37, 231.79, 246.24, 288.09, 387.04.

EA: [calculated for $C_{18}H_{30}IN$]: C, 55.81; H, 7.81; N, 3.62.
                        [found]: C, 55.96; H, 7.33; N, 3.51.

1.2.1.3   Synthesis of 4-(4-(N,N-dibutylamino)phenyl)-2-methylbut-3-yn-2-ol (2a)[132]

[331.24]   [84.12]   [287.45]
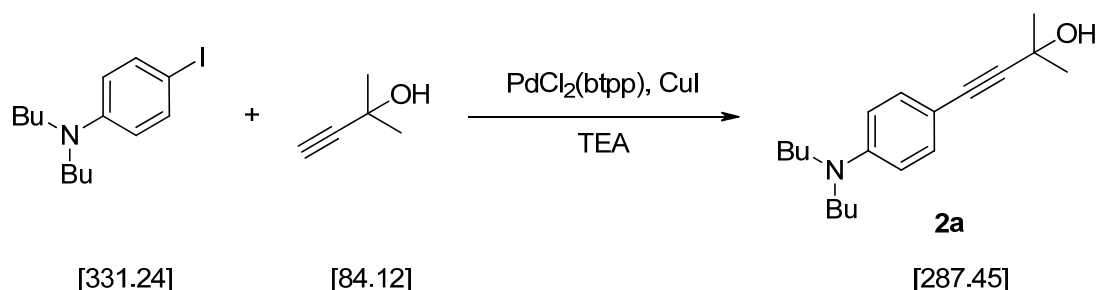
Reagents	MW [g/mol]	[g]	[mL]	[mmol]	[eq.]
iodide **1a**	331.42	3.43		10.36	1.0
2-methyl-3-butyn-2-ol	84.12	1.21		14.37	1.38
PdCl$_2$(btpp)	701.89	0.15		0.2	0.02
copper(I) iodide	190.45	0.04		0.2	0.02
dry triethylamine			100		

Procedure

To a solution of 3.43 g (10.36 mmol) of iodide **1a** in 100 mL of degassed dry triethylamine under argon atmosphere, 1.21 g (14.37 mmol) of 2-methyl-but-3-yn-2-ol, 0.04 g (0.20 mmol) of copper(I)iodide and 0.15 g (0.21 mmol) of bis(triphenylphosphine)palladium(II) dichloride (PdCl$_2$(btpp)) were added and the reaction mixture was stirred at 40 °C. The progress of the reaction was monitored by TLC and GC-MS analysis. After the entire conversion of **1a**, the red colored solution was filtered off, the solid residue was washed with ethyl acetate (3 × 100 mL) and the volatile compounds were removed in vacuum. The crude product was dissolved in 100 mL of ethyl acetate and extracted with water (3 × 100 mL) and brine (1 × 100 mL). The combined organic layers were dried over Na$_2$SO$_4$, filtered and concentrated. Purification by column chromatography (PE:EE = 20:3) yielded 2.47 g of **2a** as light yellow, highly viscous liquid.

Yield

83 % of theory (95% of lit[132])

Analysis

TLC (PE:EE = 10:1): $R_f = 0.42$

^{1}H-NMR (200 MHz, CDCl$_3$): δ (ppm) = 7.24 (d, J = 8.80 Hz, 2H, ar-H2+H6), 6.53 (d, J = 9.00 Hz, 2H, ar-H3+H5), 3.26 (t, J = 7.72 Hz, 4H, 2×N-C$\underline{H}_2$-CH$_2$), 2.11 (s, 1H, O$\underline{H}$), 1.60 (s, 6H, 2×C-C$\underline{H}_3$) 1.64-1.48 (m, 4H, 2×CH$_2$-C$\underline{H}_2$-CH$_2$), 1.43-1.25 (m, 4H, 2×CH3-C$\underline{H}_2$), 0.95 (t, J = 7.24 Hz, 6H, 2×C$\underline{H}_3$-CH$_2$).

^{13}C-NMR (50 MHz, CDCl$_3$): δ (ppm) = 148.1 (ar-C4), 132.9 (ar-C2+C6), 111.2 (ar-C3+C5), 108.2 (ar-C1), 91.3 (C≡$\underline{C}$-C), 83.3 (ar-$\underline{C}$≡C), 65.8 ($\underline{C}$-OH), 50.7 (N-$\underline{C}$H$_2$), 31.8 (C-$\underline{C}$H3), 29.4 (CH$_2$-$\underline{C}$H$_2$-CH$_2$), 20.4 (CH$_3$-$\underline{C}$H$_2$), 14.1 ($\underline{C}$H$_3$-CH$_2$).

GS-MS analysis: (m/z) = 57.1, 115.1, 141.2, 169.2, 170.2, 184.2, 185.3, 226.3, 227.3, 269.4.

1.2.1.4 Synthesis of 4-(4-(butyl-(2-ethylhexyl)amino)phenyl)-2-methylbut-3-yn-2-ol (2b)
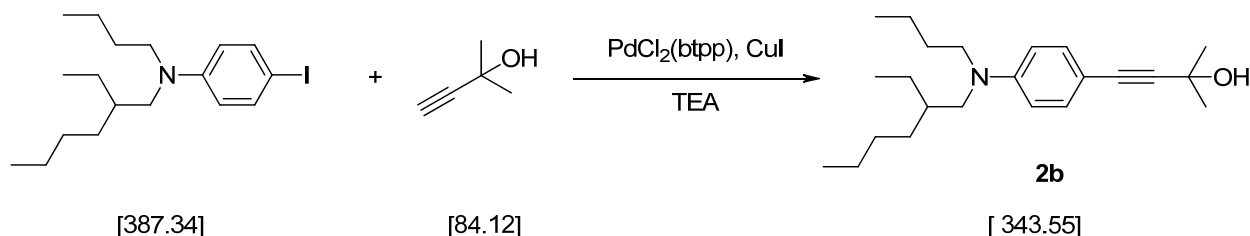
Reagents	MW [g/mol]	[g]	[mL]	[mmol]	[eq.]
iodide **1b**	387.14	5.6		14.4	1.0
2-methyl-3-butyn-2-ol	84.12	3.37		40	2.7
PdCl$_2$(btpp)	701.89	0.11		0.14	0.01
copper(I) iodide	190.45	0.03		0.14	0.01
dry triethylamine			100		

Procedure

To a solution of 5.6 g (14.4 mmol) of iodide **1b** in 100 mL of degassed dry triethylamine under argon atmosphere, 3.37 g (40 mmol) of 2-methyl-but-3-yn-2-ol, 0.03 g (0.14 mmol) of copper(I)iodide and 0.11 g (0.14 mmol) of bis(triphenylphosphine)palladium(II) dichloride (PdCl$_2$(btpp)) were added and the reaction mixture was stirred at 40 °C. The progress of the reaction was monitored by TLC and GC-MS analysis. After the entire conversion of **1b**, the red colored solution was filtered off, the solid residue was washed with ethyl acetate (3 × 100 mL) and the volatile compounds were removed in vacuum. The crude product was dissolved in 100 mL of ethyl acetate and washed with water (3 × 100 mL) and brine (1 × 100 mL). The combined organic layers were dried over Na$_2$SO$_4$, filtered and concentrated. Purification by column chromatography (PE:EE = 5:1) yielded 4.19 g of **2b** as orange, highly viscous liquid.

Yield

88 % of theory

Analysis

TLC (PE:EE = 5:1):	R$_f$ = 0.35
^{1}H-NMR (200 MHz, CDCl$_3$):	δ (ppm) = 7.22 (d, J = 8.9 Hz, 2H, ar-H2+H6), 6.52 (d, J = 8.9 Hz, 2H, ar-H3+H5), 3.26 (t, J = 7.4 Hz 2H, N-C$\underline{H}_2$-CH$_2$), 3.13 (d, J = 7.3 Hz, 2H, N-C$\underline{H}_2$-CH), 2.06 (s, 1H, O$\underline{H}$), 1.70-1.58 (m, 1H, CH$_2$-C$\underline{H}$-CH$_2$), 1.58 (s, 6H, 2×C-C$\underline{H}_3$), 1.43-1.11 (m, 12H, CH$_3$-C$\underline{H}_2$+CH$_3$-C$\underline{H}_2$+CH$_3$-C$\underline{H}_2$+CH$_2$-C$\underline{H}_2$-CH$_2$+CH$_2$-C$\underline{H}_2$-CH$_2$+CH-C$\underline{H}_2$), 0.95-0.83 (m, 9H, C$\underline{H}_3$-CH$_2$+C$\underline{H}_3$-CH$_2$+C$\underline{H}_3$-CH$_2$).
^{13}C-NMR (50 MHz, CDCl$_3$):	δ (ppm) = 148.2 (ar-C4), 132.7 (ar-C2+C6), 111.5 (ar-C3+C5), 108.1 (ar-C1), 91.2 (C≡$\underline{C}$-C), 83.1 (ar-$\underline{C}$≡C), 65.7 ($\underline{C}$-OH), 55.1 (N-$\underline{C}$H$_2$-CH), 51.4 (N-$\underline{C}$H$_2$-CH$_2$), 37.5 (CH$_2$-$\underline{C}$H-CH$_2$), 31.7 (C-$\underline{C}$H3), 30.6 (CH-$\underline{C}$H$_2$-CH$_2$), 28.7 (N-CH$_2$-$\underline{C}$H$_2$), 28.4 (CH-CH$_2$-$\underline{C}$H$_2$), 23.9 (CH-$\underline{C}$H$_2$-CH$_3$), 23.1 (CH3-$\underline{C}$H$_2$-CH2-CH2-CH), 20.2 (CH3-$\underline{C}$H$_2$-CH2-CH2-N), 14.1 ($\underline{C}$H3-CH$_2$-CH2-CH2-CH), 13.9 ($\underline{C}$H3-CH$_2$-CH2-CH2-N), 10.7 (CH-CH$_2$-$\underline{C}$H$_3$).
GS-MS analysis:	(m/z) = 141.01, 184.36, 226.21, 325.16.

EA: [calculated for $C_{23}H_{37}NO$]: C, 80.41; H, 10.86; N, 4.08. [found]: C, 80.23; H, 10.98; N, 4.21.

1.2.1.5 Synthesis of 4-(ethynyl)-N,N-dibutylbenzeneamine (3a)[132]

2a [287.45]

3a [229.37]
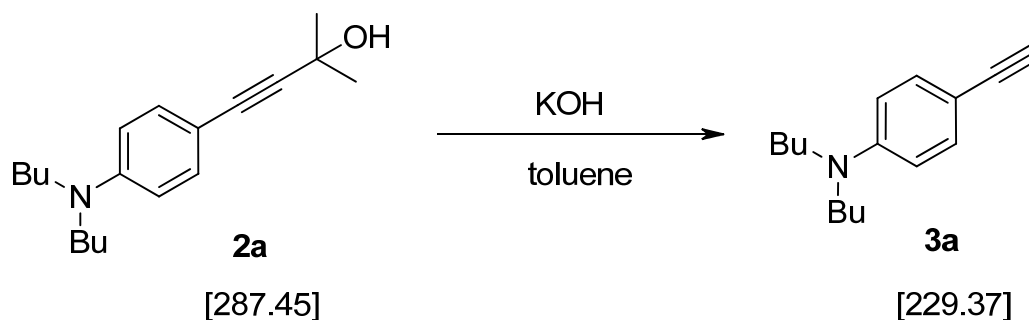
Reagents	MW [g/mol]	[g]	[mL]	[mmol]	[eq.]
alcohol **2a**	287.45	2.22		7.71	1
dry KOH powder	56.11	0.58		10.42	1.35
dry toluene			100		

Procedure

0.58 g (10.42 mmol) of dry KOH powder was added to a solution of 2.22 g (7.71 mmol) of alcohol **2a** in 100 mL of dry and degassed toluene under argon atmosphere. The suspension was heated to reflux and the acetone formed was continuously removed (the progress of the reaction was monitored by TLC and GC-MS). The mixture was then cooled to room temperature. The solid residue was filtered off and the solution was washed with water (3 × 100 mL) and brine (1 × 100 mL). The combined organic layers were dried over Na_2SO_4, filtered off and the solvent was evaporated. The crude product was purified by column chromatography (PE:EE = 40:1, with 1% triethylamine) giving 1.43 g of **3a** as pale yellow, highly viscous oil.

Yield

81 % of theory (93% of lit[132])

Analysis

TLC (PE:EE = 40:1): $R_f = 0.72$

^{1}H-NMR (200 MHz, CDCl$_3$):	δ (ppm) = 7.33 (d, J = 9.00 Hz, 2H, ar-H2+H6), 6.54 (d, J = 9.00 Hz, 2H, ar-H3+H5), 3.27 (t, J = 7.72 Hz, 4H, 2×N-C$\underline{H}_2$), 2.96 (s, 1H, C≡C$\underline{H}$), 1.64-1.49 (m, 4H, 2×CH$_2$-C$\underline{H}_2$-CH$_2$), 1.44-1.26 (m, 4H, 2×CH3-C$\underline{H}_2$), 0.96 (t, J = 7.23 Hz, 6H, 2×C$\underline{H}_3$-CH$_2$).
^{13}C-NMR (50 MHz, CDCl$_3$):	δ (ppm) = 148.3 (ar-C4), 133.4 (ar-C2+C6), 111.2 (ar-C3+C5), 107.5 (ar-C1), 85.2 (Ar-$\underline{C}$≡CH), 74.5 (Ar-C≡$\underline{C}$H), 50.78 (N-$\underline{C}$H$_2$), 29.4 (CH$_2$-$\underline{C}$H$_2$-CH$_2$), 20.4 ($\underline{C}$H$_3$-CH$_2$), 14.1($\underline{C}$H$_3$-CH$_2$).
GS-MS analysis:	(m/z) = 101.1, 130.1, 144.1, 186.2, 229.3

1.2.1.6 Synthesis of N-butyl-N-(2-ethylhexyl)-4-ethynylbenzeneamine (3b)

3a
[343.55]

KOH
toluene

3b
[285.47]
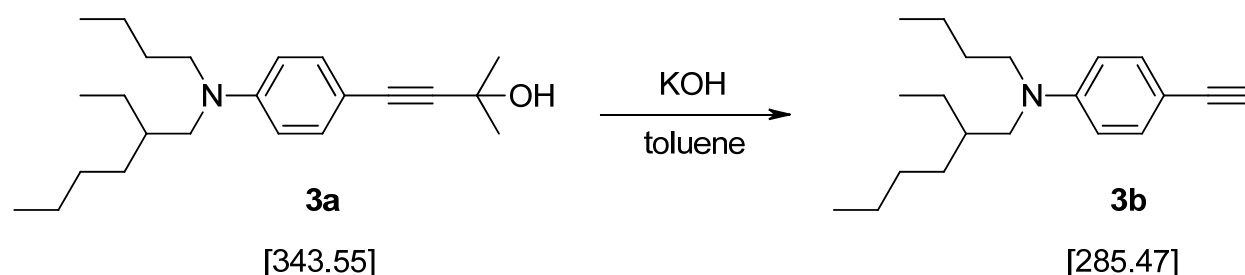
Reagents	MW [g/mol]	[g]	[mL]	[mmol]	[eq.]
alcohol **2b**	343.55	1.5		4.37	1
dry KOH powder	56.11	0.56		10	2.28
dry toluene			50		

Procedure

0.56 g (10 mmol) of dry KOH powder was added to a solution of 1.5 g (4.37 mmol) of alcohol **M2K** in 50 mL of dry and degassed toluene under argon atmosphere. The suspension was heated to reflux and the acetone formed was continuously removed (the progress of the reaction was monitored by TLC and GC-MS). The mixture was then cooled to room temperature. The solid residue was filtered off and the solution was washed with water (3 × 100 mL) and brine (1 × 100 mL). The combined organic layers were dried over sodium sulfate, filtered off and the solvent was evaporated. The crude

product was purified by column chromatography (PE:Chloroform = 5:1 with 1% triethylamine) giving 0.99 g of **3b** as pale yellow, highly viscous oil.

Yield

80 % of theory

Analysis

TLC (PE:Chloroform = 5:1): $R_f = 0.33$

^{1}H-NMR (200 MHz, CDCl$_3$):   δ (ppm) = 7.36 (d, $J = 8.9$ Hz, 2H, ar-H2+H6), 6.60 (d, $J = 8.9$ Hz, 2H, ar-H3+H5), 3.34 (t, $J = 7.4$ Hz, 2H, N-C$\underline{H}_2$-CH$_2$), 3.20 (d, $J = 7.3$ Hz, 2H, N-C$\underline{H}_2$-CH), 2.98 (s, 1H, C≡C$\underline{H}$), 2.02-1.71 (m, 1H, CH$_2$-C$\underline{H}$-CH$_2$), 1.69-1.21 (m, 12H, CH$_3$-C$\underline{H}_2$+CH$_3$-C$\underline{H}_2$+CH$_3$-C$\underline{H}_2$+CH$_2$-C$\underline{H}_2$-CH$_2$+CH$_2$-C$\underline{H}_2$-CH$_2$+CH-C$\underline{H}_2$), 1.12-0.63 (m, 9H, C$\underline{H}_3$-CH$_2$+C$\underline{H}_3$-CH$_2$+C$\underline{H}_3$-CH$_2$).

^{13}C-NMR (50 MHz, CDCl$_3$):   δ (ppm) = 148.5 (ar-C4), 133.3 (ar-C2+C6), 111.5 (ar-C3+C5), 107.6 (ar-C1), 85.1 (Ar-$\underline{C}$≡CH), 74.5 (Ar-C≡$\underline{C}$H), 55.2 (N-$\underline{C}$H$_2$-CH), 51.5 (N-$\underline{C}$H$_2$-CH$_2$), 37.5 (CH$_2$-$\underline{C}$H-CH$_2$), 30.7 (CH-$\underline{C}$H$_2$-CH$_2$), 28.8 (N-CH$_2$-$\underline{C}$H$_2$), 28.5 (CH-CH$_2$-$\underline{C}$H$_2$), 24.1 (CH-$\underline{C}$H$_2$-CH$_3$), 23.2 (CH3-$\underline{C}$H$_2$-CH2-CH2-CH), 20.3 (CH3-$\underline{C}$H$_2$-CH2-CH2-N), 14.1 ($\underline{C}$H3-CH$_2$-CH2-CH2-CH), 14.0 ($\underline{C}$H3-CH$_2$-CH2-CH2-N), 10.8 (CH-CH$_2$-$\underline{C}$H$_3$).

GS-MS analysis: (m/z) = 100.96, 130.04, 143.99, 186.06, 285.15.

EA: [calculated for C$_{20}$H$_{31}$N]: C, 84.15; H, 10.95; N, 4.91. [found]: C, 84.33; H,10.75; N, 4.83.

1.2.2   Synthesis of dihalide aromatic ketones 4a-d

1.2.2.1   Synthesis of bis(4-iodophenyl)methanone (4a)[137]
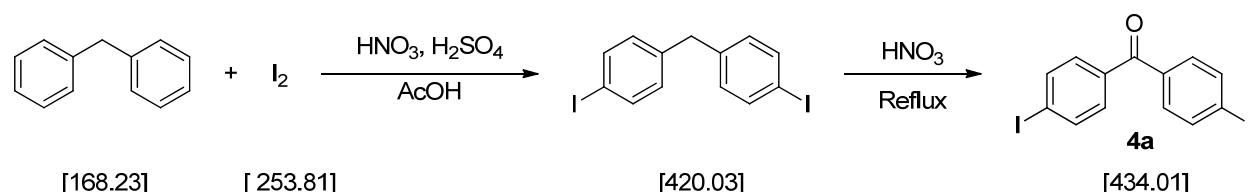
Reagents	MW [g/mol]	[g]	[mL]	[mmol]	[eq.]
diphenylmethane	168.23	11.85		70.44	1.0
iodine	253.81	17.90		70.53	1.0
HNO_3 (63%)			6.5		
HNO_3 (50%)			37		
H_2SO_4 (98%)			15		
AcOH			70		

Procedure

11.85 g (70.44 mmol) of diphenylmethane and 17.90 g (70.53 mmol) of molecular iodine were dissolved in 70 mL of glacial acetic acid. The solution was stirred at 40 °C and a mixture of 6.5 mL nitric acid (63%) and 15.0 mL of concentrated sulfuric acid (98%) was added dropwise. Then the reaction mixture was heated under reflux and 37 mL nitric acid (50%) was added. The solution was heated until the formation of brown gas stopped. The mixture was cooled down and the precipitate was filtered off, washed with water until neutral washings, dried in vacuum, and recrystallized from dioxane to give 21.4 g of **4a** as white needle-shape crystal.

Yield

70 % of theory (140% of lit[137])

Analysis

TLC (PE:EE = 10:1): $R_f = 0.65$

m.p: 233-235 °C (lit[137]: 234-235 °C)

^{1}H-NMR (200 MHz, CDCl$_3$): δ (ppm) = 7.84 (d, J = 8.2 Hz, 4H, ar-H3+H5+H8+H10), 7.47 (d, J = 8.3 Hz, 4H, ar-H2+H6+H7+H11).

^{13}C-NMR (50 MHz, CDCl$_3$): δ (ppm) = 195.5 (C=O), 137.7 (ar-C3+C5+C8+C10), 136.4 (ar-C1+C12), 131.3 (ar-C2+C6+C7+C11), 100.4 (ar-C4+C9).

1.2.2.2   Synthesis of 2,7-diiodo-9H-fluoren-9-one (4b)[146]

| [180.20] | [253.81] | | [432.00] |
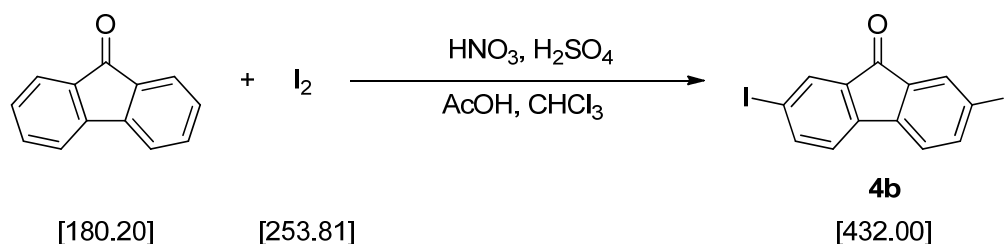
Reagents	MW [g/mol]	[g]	[mL]	[mmol]	[eq.]
fluorenone	180.20	7.51		41.62	1.0
iodine	253.81	10.62		41.84	1.0
fuming HNO_3			4		
H_2SO_4 (98%)			2		
$CHCl_3$			3		
AcOH			100		

Procedure

A solution of 7.51 g (41.62 mmol) of fluorenone and 10.62 g (41.84 mmol) of molecular iodine in a mixture of 100 mL of glacial acetic acid and 3 mL of chloroform (to wash off sublimed iodine) was heated under reflux. Subsequently, a mixture of 2 mL of concentrated sulfuric acid and 4 mL of fuming nitric acid was added dropwise, and the mixture was heated until the formation of brown gas stopped. The reaction mixture was cooled down and the precipitate was filtered off, washed with water until neutral washings, dried in vacuum, and recrystallized from ethyl acetate to give 13.29 g of **4b** as yellow needles.

Yield

73 % of theory (97% of lit[146])

Analysis

TLC (PE:EE = 20:1): $R_f = 0.35$

m.p: 202-204 °C (lit[146]: 205-206 °C.)

^{1}H-NMR (200 MHz, Acetone):   δ (ppm) = 8.01 (dd, *J* = 7.8, 1.5 Hz, 2H, ar-H4+H9), 7.92 (d, *J* = 1.4 Hz, 2H, ar-H2+H11), 7.64 (d, *J* = 7.9 Hz, 2H, ar-H5+H8).

^{13}C-NMR (50 MHz, Acetone):   δ (ppm) = 190.9 (<u>C</u>=O), 143.4 (ar-C6+C7), 142.9 (ar-C4+C9), 134.8 (ar-C1+C12), 133.5 (ar-C2+C11), 122.1 (ar-C5+C8), 94.4 (ar-C3+C10).

1.2.2.3   Synthesis of 3,6-dibromophenanthrene-9,10-dione[277]

| [208.21] | [159.81] | [366.00] |
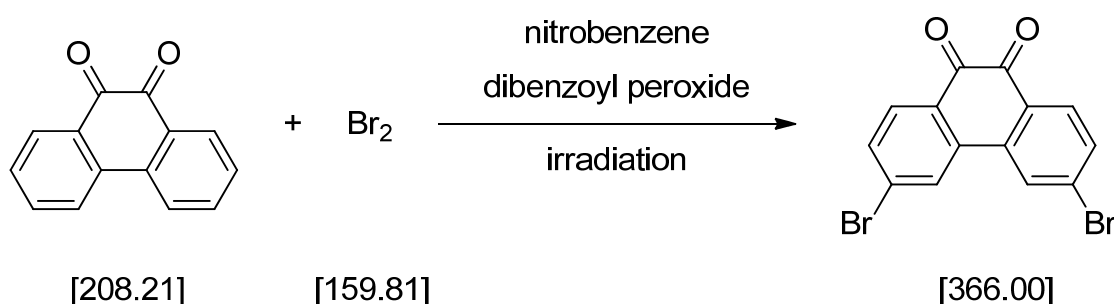
Reagents	MW [g/mol]	[g]	[mL]	[mmol]	[eq.]
9,10-phenanthrenequinone	208.21	7.03		33.4	1.0
dibenzoyl peroxide	242.23	0.35		1.4	0.04
bromine	159.81		5	97.6	2.9
nitrobenzene			50		

Procedure

A mixture of 7.03 g (33.4 mmol) of 9,10-phenanthrenequinone and 0.35 g (1.4 mmol) of dibenzoyl peroxide in 50 mL of nitrobenzene was irradiated with a 100 W tungsten light bulb at a distance of 10 cm. Over the course of 0.5 h, 5 mL of molecular bromine (97.6 mmol) was dripped in. The starting material slowly dissolved and soon precipitation of product started. Irradiation and stirring were continued for a further 5 h. The reaction mixture was kept at room temperature overnight, suspended in 50 mL of Et$_2$O, filtered and thoroughly washed with Et$_2$O. The dibrominated compound was obtained as 6.41 g of ocher yellow crystals.

Yield

52 % of theory (67% of lit[129])

Analysis

TLC (PE:EE = 20:3): $R_f = 0.52$

m.p: 284-287 °C (lit[277]: 285-286 °C.)

^{1}H-NMR (200 MHz, CDCl$_3$):   δ (ppm) = 8.10 (d, *J* = 2.0, 2H, ar-H5+ H8), 8.05 (d, *J* = 8.3 Hz, 2H, ar-H2+H11), 7.65 (dd, *J* = 8.3 Hz, 2.0 Hz, 2H, ar-H3+H10).

^{13}C-NMR (50 MHz, CDCl$_3$):   δ (ppm) = 178.8 (C=O), 135.9 (ar-C6+C7), 133.4 (ar-C5+C8), 132.6 (ar-C2+C11), 132.0 (ar-C1+C12), 129.9 (ar-C3+C10), 127.4 (ar-C4+C9).

1.2.2.4   Synthesis of 3,6-dibromo-9H-fluoren-9-one (4c)[278]
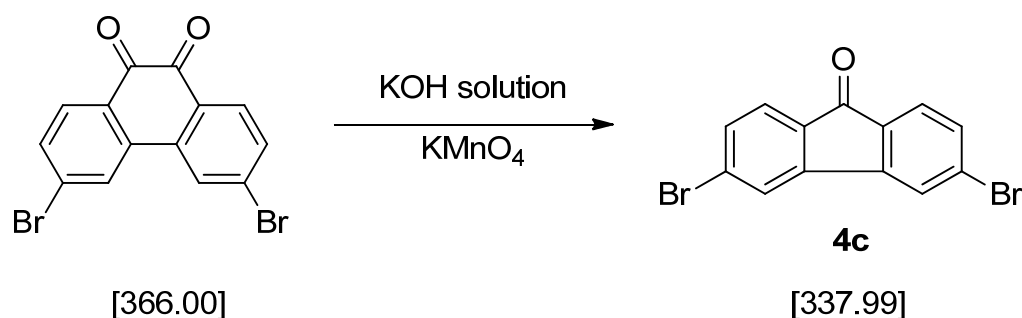
Reagents	MW [g/mol]	[g]	[mL]	[mmol]	[eq.]
dibromophenanthrenone	366.0	19.30		52.73	1.0
KOH	56.11	90		1604	30.4
KMnO$_4$	158.03	47		297.4	5.6
H$_2$O			35+20		

Procedure

A warm saturated potassium hydroxide solution was prepared by dissolving 90 g KOH in 35 mL of water. Then 19.30 g of crude 3,6-dibromophenanthrene-9,10-dione (52.73 mmol) were added and the thick suspension was heated under reflux for 1 h. Over the course of 2.5 h, the mixture was refluxed and treated with 47 g KMnO$_4$ in small portions. A supplemental addition of 20 mL of water was required to enable continued stirring of

the reaction mixture. After an additional 2 h of refluxing, the reaction was cooled overnight, cautiously acidified with 30% H_2SO_4 (evolution of CO_2) and the remaining oxidizing agent reduced with $NaHSO_3$ solution. The beige precipitate was filtered, washed thoroughly with water then with acetone. After air drying, the substance was purified by recrystallization from DMSO, removing the solvent adhering to the surface of the crystals after filtration with acetone then $CHCl_3$. The product was obtained as 10.05 g of light yellow crystals.

Yield

56 % of theory (81% of lit[129])

Analysis

TLC (PE:Chloroform = 10:1):	R_f = 0.63
m.p:	320-323 °C (lit[279]: 320-323 °C.)
^{1}H-NMR (200 MHz, CDCl$_3$):	δ (ppm) = 7.71 (d, J =1.5 Hz, 2H, ar-H5+H8), 7.58 (d, J =7.9 Hz, 2H, ar-H2+H11), 7.52 (dd, J = 7.8, 1.4 Hz, 2H, ar-H3+H10)
^{13}C-NMR (50 MHz, CDCl$_3$):	δ (ppm) = 189.5 ($\underline{C}$=O), 145.2 (ar-C6+C7), 133.4 (ar-C5), 133.8 (ar-C1+C12), 130.5 (ar-C2+C11), 126.6 (ar-C3+C10), 124.3 (ar-C4+C9).

1.2.2.5   Synthesis of 2,6-diiodo-9,10-anthraquinone (4d)[148]
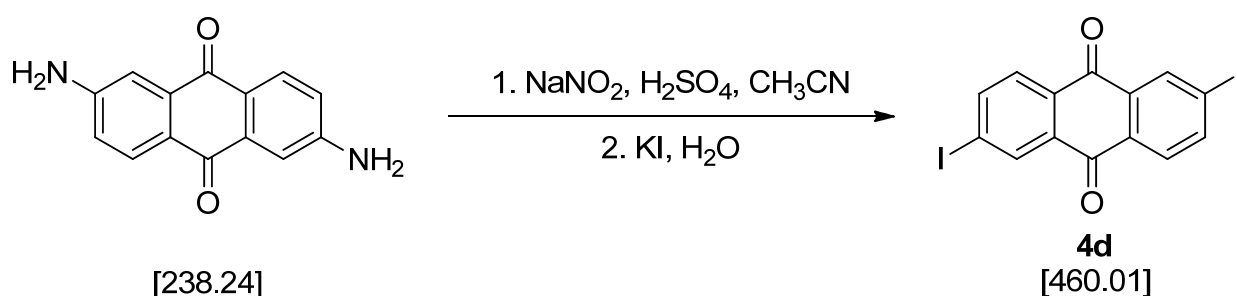
Reagents	MW [g/mol]	[g]	[mL]	[mmol]	[eq.]
2,6-diaminoanthraquinone	238.24	10.02		42	1.0
sodium nitrite	69	5.81		84.11	2.0

potassium iodide	166	20.01		120.51	2.86
H_2SO_4 (98%)			11		
acetonitrile			20		
H_2O			15 + 50		

Procedure

10.02 g of 2,6-diaminoanthraquinone (42 mmol) were dissolved in 20 mL acetonitrile and subsequently 11 mL of concentrated sulfuric acid was added. The resulting slurry was cooled to 0 °C in an ice bath and then a precooled solution (0 °C) of sodium nitrite (5.81 g, 84.11mmol) in water (15 mL) was slowly added. The reaction mixture was then stirred for 30 min at 0 °C and then added to a round bottom flask containing a solution of potassium iodide (20.01 g, 120.51 mmol) in water (50 mL) cooled to 0 °C. Then the solution was allowed to warm to room temperature with stirring for 1 h. The product was then recovered by filtration. The filtrate was washed with water until neutral washings, dried in vacuum, and recrystallized from toluene to give 11.59 g light brown crystalline solid.

Yield

60 % of theory (92% of lit[148])

Analysis

TLC (PE:EE = 20:1): $R_f = 0.28$

m.p: 282-284 °C

^{1}H-NMR ((200 MHz, CDCl$_3$):   δ (ppm) = 8.62 (d, J = 1.7 Hz, 2H, ar-H5+H11), 8.15 (dd, J = 8.2, 1.8 Hz, 2H, ar-H3+H9), 7.96 (d, J = 8.2 Hz, 2H, ar-H2+H8).

^{13}C-NMR (50 MHz, CDCl$_3$):   δ (ppm) = 181.6 (C=O), 143.4 (ar-C3+C9), 136.3 (ar-C5+C11), 133.8 (ar-C6+C12), 132.1 (ar-C1+C7), 128.7 (ar-C2+C8), 102.7 (ar-C4+C10).

1.2.3   Synthesis of novel 2PIs

1.2.3.1   Synthesis of bis(4-((4-(dibutylamino)phenyl)ethynyl)phenyl)methanone (B3BP)
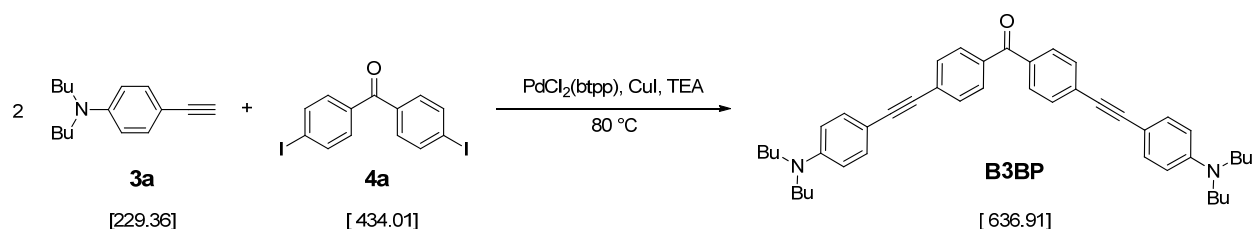
Reagents	MW [g/mol]	[g]	[mL]	[mmol]	[eq.]
iodide **4a**	434.01	0.43		1.01	1
alkyne **3a**	229.36	0.57		2.49	2.49
PdCl$_2$(btpp)	701.89	0.014		0.02	0.02
copper(I) iodide	190.45	0.0038		0.02	0.02
dry triethylamine			30		
dry THF			30		

Procedure

0.43 g (1.01 mmol) of the iodide **4a** and 14 mg of bis(triphenylphosphine) palladium (II) dichloride (PdCl$_2$(btpp)) (0.02 mmol) were dissolved in a three-neck flask in 30 mL of degassed dry THF under argon atmosphere. Then 0.57 g (2.49 mmol) of the alkyne **3a**, 30 mL of degassed dry triethylamine and 3.8 mg (0.02 mmol) of copper(I)iodide were added successively. The reaction mixture was stirred under reflux. The progress of the reaction was monitored by TLC. The red solution was poured onto 200 mL of water and extracted by ethyl acetate until the aqueous layer was colorless. The combined organic layers were washed with water (3 × 50 mL) and brine (2 × 50 mL), dried over Na$_2$SO$_4$, filtrated and concentrated. Purification by column chromatography (PE:Toluene = 1:2) yielded 0.29 g of product as yellow powder.

Yield

45 % of theory

Analysis

TLC (PE:Toluene = 1:2):	$R_f = 0.44$
m.p:	67-68 °C.
^{1}H-NMR (200 MHz, CDCl$_3$):	δ (ppm) = 7.75 (d, J = 8.2 Hz, 4H, ar-H3+H5+H8+H10), 7.56 (d, J = 8.2 Hz, 4H, ar-H2+H6+H7+H11), 7.38 (d, J = 8.7 Hz, 4H, ar-H2'+H6'+ H2''+H6''), 6.58 (d, J = 8.9 Hz, 4H, ar-H3'+H5'+ H3''+H5''), 3.28 (t, J = 7.3 Hz, 8H, 4×N-C$\underline{H}_2$), 1.63-1.49 (m, 8H, 4×CH$_2$-C$\underline{H}_2$-CH$_2$), 1.45-1.18 (m,8H, 4×CH3-C$\underline{H}_2$), 0.93 (t, J = 7.2 Hz, 12H, 4×C$\underline{H}_3$-CH$_2$).
^{13}C-NMR (50 MHz, CDCl$_3$):	δ (ppm) = 195.2 ($\underline{C}$=O), 148.3 (ar-C4'+C4''), 135.7 (ar-C1+C12), 133.1(ar-C3+C5+C8+C10), 130.8 (ar-C2'+C6'+C2''+C6''), 130.0 (ar-C2+C6+C7+C11), 128.8 (ar-C4+C9), 111.1 (ar-C1'+C1''), 107.9 (ar-C3'+C5'+C3''+C5''), 94.7 (2×N-Ar-C≡$\underline{C}$), 86.9 (2×N-Ar-$\underline{C}$≡C), 50.6 (2×N-$\underline{C}$H$_2$), 29.3 (2×CH$_2$-$\underline{C}$H$_2$-CH$_2$), 20.3 (2×CH$_3$-$\underline{C}$H$_2$), 14.0 (2×$\underline{C}$H$_3$-CH$_2$).
EA:	[calculated for C$_{45}$H$_{52}$N$_2$O]: C, 84.86; H, 8.23; N, 4.40. [found]: C, 84.60; H, 8.08; N, 4.28.

1.2.3.2 Synthesis of 2,7-bis((4-(dibutylamino)phenyl)ethynyl)-9H-fluoren-9-one (B3FL)
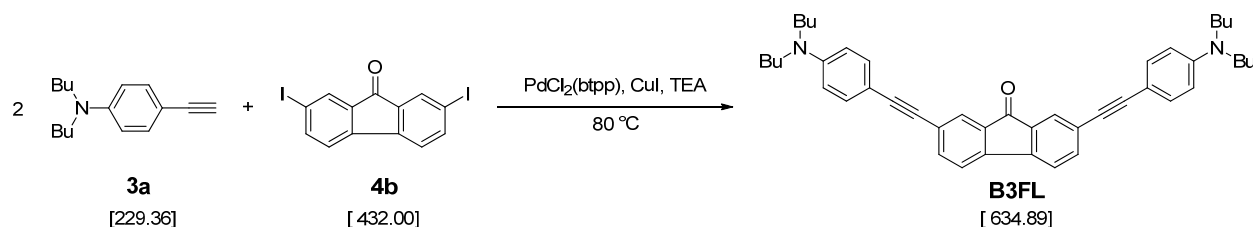
Reagents	MW [g/mol]	[g]	[mL]	[mmol]	[eq.]
iodide **4b**	432.00	0.43		1.01	1

alkyne **3a**	229.36	0.57	2.49	2.49
PdCl$_2$(btpp)	701.89	0.014	0.02	0.02
copper(I) iodide	190.45	0.0038	0.02	0.02
dry triethylamine		30		
dry THF		30		

Procedure

0.43 g (1.01 mmol) of the iodide **4b** and 14 mg of bis(triphenylphosphine) palladium (II) dichloride (PdCl$_2$(btpp)) (0.02 mmol) were dissolved in a three-neck flask in 30 mL of degassed dry THF under argon atmosphere. Then 0.57 g (2.49 mmol) of the alkyne **3a**, 30 mL of degassed dry triethylamine and 3.8 mg (0.02 mmol) of copper(I)iodide were added successively. The reaction mixture was stirred under reflux. The progress of the reaction was monitored by TLC. The red solution was poured onto 200 mL of water and extracted by ethyl acetate until the aqueous layer was colorless. The combined organic layers were washed with water (3 × 50 mL) and brine (2 × 50 mL), dried over Na$_2$SO$_4$, filtrated and concentrated. Purification by column chromatography (PE:Toluene = 1:2) yielded 0.36 g of product as red crystals.

Yield
57 % of theory

Analysis

TLC (PE:Toluene = 1:2):   R$_f$ = 0.38

m.p: 158-159 °C.

^{1}H-NMR (200 MHz, CDCl$_3$):   δ (ppm) = 7.73 (d, J = 1.4 Hz, 2H, ar-H2+H11), 7.57 (dd, J = 7.8, 1.4 Hz, 2H, ar-H4+H9), 7.42 (d, J = 7.8 Hz, 2H, ar-H5+H8), 7.34 (d, J = 8.8 Hz, 4H, ar-H2'+H6'+H2''+H6''), 6.56 (d, J = 8.9 Hz, 4H, ar-H3'+H5'+H3''+H5''), 3.31-3.23 (t, J = 7.3 Hz, 8H, 4×N-C$\underline{H}_2$), 1.71-1.46 (m, 8H, 4×CH$_2$-C$\underline{H}_2$-CH$_2$), 1.33-1.25 (m, 8H, 4×CH3-C$\underline{H}_2$), 0.95 (t, J = 7.2 Hz, 12H, 4×C$\underline{H}_3$-CH$_2$).

^{13}C-NMR (50 MHz, CDCl$_3$):   δ (ppm) = 192.8 ($\underline{C}$=O), 148.1 (ar-C4'+C4''), 142.4 (ar-C6+C7), 137.1 (ar-C1+C12), 134.4 (ar-C4+C9), 133.0 (ar-C2+C11), 126.9 (ar-C2'+C6'+C2''+C6''), 125.3 (ar-C5+C8), 120.2 (ar-C3+C10), 111.1 (ar-

C1'+C1''), 108.0 (ar-C3'+C5'+C3''+C5''), 93.1 (2×N-

Ar-C≡C̲), 86.7 (2×N-Ar-C̲≡C), 50.6 (2×N-C̲H₂), 29.3

(2×CH₂-C̲H₂-CH₂), 20.3 (2×CH₃-C̲H₂), 13.9 (2×C̲H₃-

CH₂).

EA: [calculated for C₄₅H₅₀N₂O]: C, 85.13; H, 7.94; N, 4.41.

[found]: C, 85.24; H, 7.81; N, 4.46.

1.2.3.3 Synthesis of 3,6-bis((4-(dibutylamino)phenyl)ethynyl)-9H-fluoren-9-one (3,6-B3FL)
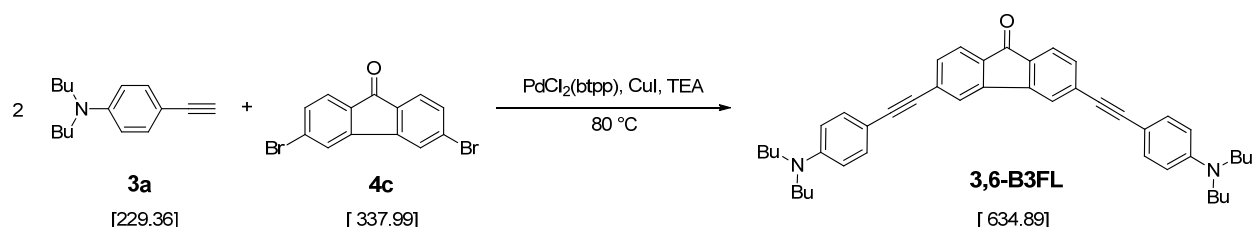
Reagents	MW [g/mol]	[g]	[mL]	[mmol]	[eq.]
bromide **4c**	337.99	0.34		1.0	1
alkyne **3a**	229.36	0.57		2.49	2.49
PdCl₂(btpp)	701.89	0.014		0.02	0.02
copper(I) iodide	190.45	0.0038		0.02	0.02
dry triethylamine			30		
dry THF			30		

Procedure

0.34 g (1.0 mmol) of the bromide **4c** and 14 mg of bis(triphenylphosphine) palladium (II) dichloride (PdCl₂(btpp)) (0.02 mmol) were dissolved in a three-neck flask in 30 mL of degassed dry THF under argon atmosphere. Then 0.57 g (2.49 mmol) of the alkyne **3a**, 30 mL of degassed dry triethylamine and 3.8 mg (0.02 mmol) of copper(I)iodide were added successively. The reaction mixture was stirred under reflux. The progress of the reaction was monitored by TLC. The red solution was poured onto 200 mL water and extracted by ethyl acetate until the aqueous layer was colorless. The combined organic layers were washed with water (3 × 50 mL) and brine (2 × 50 mL), dried over Na₂SO₄,

filtrated and concentrated. Purification by column chromatography (PE:Toluene = 1:1) yielded 0.23 g of product as red crystals.

Yield

36 % of theory

Analysis

TLC (PE:Toluene = 1:1):	R_f = 0.35
m.p:	126-127 °C.
^{1}H-NMR (200 MHz, CDCl$_3$):	δ (ppm) = 7.56 (d, J =1.5 Hz, 2H, ar-H5+H8), 7.52 (d, J =7.9 Hz, 2H, ar-H2+H11), 7.34 (dd, J = 7.8, 1.4 Hz, 2H, ar-H3+H10), 7.32 (d, J = 8.8 Hz, 4H, ar-H2'+H6'+H2''+H6''), 6.52 (d, J = 8.8 Hz, 4H, ar-H3'+H5'+H3''+H5''), 3.12 (t, J = 7.4 Hz, 8H, 4×N-C$\underline{H}_2$), 1.51-1.47 (m, 8H, 4×CH$_2$-C$\underline{H}_2$-CH$_2$), 1.29-1.26 (m, 8H, 4×CH3-C$\underline{H}_2$), 0.90 (t, J = 7.2 Hz, 12H, 4×C$\underline{H}_3$-CH$_2$).
^{13}C-NMR (50 MHz, CDCl$_3$):	δ (ppm) = 193.1 ($\underline{C}$=O), 148.4 (ar-C4'+C4''), 143.8 (ar-C6+C7), 133.2 (ar-C1+C12), 132.8 (ar-C2'+C6'+C2''+C6''), 131.8 (ar-C3+C10), 130.8 (ar-C5+C8), 124.1 (ar-C2+C11), 122.8 (ar-C4+C9), 111.1 (ar-C1'+C1''), 107.79 (ar-C3'+C5'+C3''+C5''), 95.5 (2×N-Ar-C≡$\underline{C}$), 87.5 (2×N-Ar-$\underline{C}$≡C), 50.6 (2×N-C$\underline{H}_2$), 29,3 (2×CH$_2$-C$\underline{H}_2$-CH$_2$), 20.3 (2×CH$_3$-C$\underline{H}_2$), 13.9 (2×$\underline{C}$H$_3$-CH$_2$).
EA:	[calculated for C$_{45}$H$_{50}$N$_2$O]: C, 85.13; H, 7.94; N, 4.41. [found]: C, 85.02; H, 8.06; N, 4.19.

1.2.3.4   Synthesis of 2,6-bis((4-(dibutylamino)phenyl)ethynyl)anthracene-9,10-dione (B3AN)

Reagents	MW [g/mol]	[g]	[mL]	[mmol]	[eq.]
iodide **4d**	460.01	0.46		1.0	1
alkyne **3a**	229.36	0.57		2.49	2.49
PdCl$_2$(btpp)	701.89	0.014		0.02	0.02
copper(I) iodide	190.45	0.0038		0.02	0.02
dry triethylamine			30		
dry THF			30		

Procedure

0.46 g (1.0 mmol) of the iodide **4d** and 14 mg of bis(triphenylphosphine) palladium (II) dichloride (PdCl$_2$(btpp)) (0.02 mmol) were dissolved in a three-neck flask in 30 mL of degassed dry THF under argon atmosphere. Then 0.57 g (2.49 mmol) of the alkyne **3a**, 30 mL of degassed dry triethylamine and 3.8 mg (0.02 mmol) of copper(I)iodide were added successively. The reaction mixture was stirred under reflux. The progress of the reaction was monitored by TLC. The red solution was poured onto 200 mL water and extracted by ethyl acetate until the aqueous layer was colorless. The combined organic layers were washed with water (3 × 50 mL) and brine (2 × 50 mL), dried over Na$_2$SO$_4$, filtrated and concentrated. Purification by column chromatography (PE:Toluene = 1:3) yielded 0.23 g of product as dark red powder.

Yield

35 % of theory

Analysis

TLC (PE:Toluene = 1:3):   R$_f$ = 0.37

m.p: 243-244 °C.

^{1}H-NMR (200 MHz, CDCl$_3$):	δ (ppm) = 8.34 (d, J = 1.6 Hz, 2H, ar-H5+H11), 8.23 (d, J = 8.1 Hz, 2H, ar-H2+H8), 7.80 (dd, J = 8.1, 1.7 Hz, 2H, ar-H3+H9), 7.38 (d, J = 8.8 Hz, 4H, ar-H2'+H6'+ H2''+H6''), 6.58 (d, J = 8.9 Hz, 4H, ar-H3'+H5'+H3''+H5''), 3.28 (t, J = 7.3 Hz, 8H, 4×N-C$\underline{H}_2$), 1.57-1.52 (m, 8H, 4×CH$_2$-C$\underline{H}_2$-CH$_2$), 1.45-1.16 (m, 8H, 4×CH3-C$\underline{H}_2$), 0.95 (t, J = 7.2 Hz, 12H, 4×C$\underline{H}_3$-CH$_2$).
^{13}C-NMR (50 MHz, CDCl$_3$):	δ (ppm) = 182.2 ($\underline{C}$=O), 148.7 (ar-C4'+C4''), 135.7 (ar-C3+C9), 133.5 (ar-C5+C11), 133.2 (ar-C6+C12), 131.3 (ar-C1+C7), 130.9 (ar-C2'+C6'+C2''+C6''), 129.5 (ar-C2+C8), 127.3 (ar-C4+C10), 111.1 (ar-C1'+C1''), 107.4 (ar-C3'+C5'+C3''+C5''), 97.1 (2×N-Ar-$\underline{C}$≡C), 86.8 (2×N-Ar-$\underline{C}$≡C), 50.7 (2×N-$\underline{C}$H$_2$), 29.3 (2×CH$_2$-$\underline{C}$H$_2$-CH$_2$), 20.3 (2×CH$_3$-$\underline{C}$H$_2$), 13.9 (2×$\underline{C}$H$_3$-CH$_2$).
EA:	[calculated for C$_{46}$H$_{50}$N$_2$O$_2$]: C, 83.34; H, 7.60; N, 4.23. [found]: C, 83.48; H, 7.45; N, 4.11.

1.2.3.5 Synthesis of 2,7-bis((4-(butyl(2-ethylhexyl)amino)phenyl)ethynyl)-9H-fluoren-9-one (BB3FL)
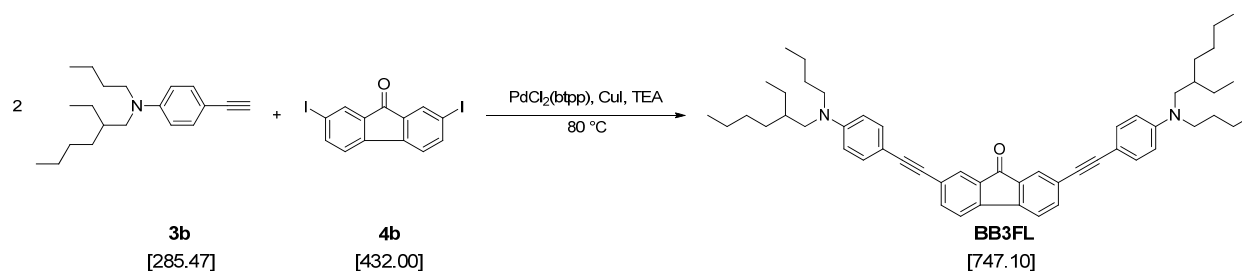
Reagents	MW [g/mol]	[g]	[mL]	[mmol]	[eq.]
iodide **4b**	432.00	0.43		1.0	1
alkyne **3b**	285.47	0.71		2.49	2.49

PdCl$_2$(btpp)	701.89	0.014		0.02	0.02
copper(I) iodide	190.45	0.0038		0.02	0.02
dry triethylamine			30		
dry THF			30		

Procedure

0.43 g (1.0 mmol) of the iodide **4b** and 14 mg of bis(triphenylphosphine) palladium (II) dichloride (PdCl$_2$(btpp)) (0.02 mmol) were dissolved in a three-neck flask in 30 mL of degassed dry THF under argon atmosphere. Then 0.71 g (2.49 mmol) of the alkyne **3b**, 30 mL of degassed dry triethylamine and 3.8 mg (0.02 mmol) of copper(I)iodide were added successively. The reaction mixture was stirred under reflux. The progress of the reaction was monitored by TLC. The red solution was poured onto 200 mL of water and extracted by ethyl acetate until the aqueous layer was colorless. The combined organic layers were washed with water (3 × 50 mL) and brine (2 × 50 mL), dried over Na$_2$SO$_4$, filtrated and concentrated. Purification by column chromatography (PE:Toluene = 1:1) yielded 0.43 g of product as red crystals.

Yield

58 % of theory

Analysis

TLC (PE:Toluene = 1:1):   R$_f$ = 0.45

m.p: 67-68 °C.

^{1}H-NMR (200 MHz, CDCl$_3$):   δ (ppm) = 7.73 (d, J = 1.4 Hz, 2H, ar-H2+H11), 7.56 (dd, J = 7.8, 1.3 Hz, 2H, ar-H4+H9), 7.42 (d, J = 7.8 Hz, 2H, ar-H5+H8), 7.34 (d, J = 8.7 Hz, 4H, ar-H2'+H6'+ H2"+H6"), 6.58 (d, J = 8.9 Hz, 4H, ar-H3'+H5'+H3"+H5"), 3.30 (t, J = 7.3 Hz, 4H, 2×N-CH$_2$-CH$_2$), 3.17 (d, J = 7.2 Hz, 4H, 2×N-CH$_2$-CH), 1.94-1.65 (m, 2H, 2×CH$_2$-CH-CH$_2$), 1.65-1.12 (m, 24H, 2×(CH$_3$-CH$_2$+CH$_3$-CH$_2$+CH$_3$-CH$_2$+CH$_2$-CH$_2$-CH$_2$+CH$_2$-CH$_2$-CH$_2$+CH-CH$_2$), 1.09-0.75 (m, 18H, 2×(CH$_3$-CH$_2$+CH$_3$-CH$_2$+CH$_3$-CH$_2$)).

^{13}C-NMR (50 MHz, CDCl$_3$):   δ (ppm) = 192.8 (C=O), 148.4 (ar-C4'+C4"), 142.4 (ar-C6+C7), 137.1 (ar-C1+C12), 134.4 (ar-C4+C9), 132.9 (ar-C2+C11), 126.9 (ar-C2'+C6'+C2"+C6"),

125.3 (ar-C5+C8), 120.2 (ar-C3+C10), 111.6 (ar-C1'+C1''), 108.1 (ar-C3'+C5'+C3''+C5''), 93.1 (2×N-Ar-C≡$\underline{C}$), 86.7 (2×N-Ar-$\underline{C}$≡C), 55.1 (2×N-$\underline{C}H_2$-CH), 51.5 (2×N-$\underline{C}H_2$-CH₂), 37.5 (2×CH₂-$\underline{C}H$-CH₂), 30.6 (2×CH-$\underline{C}H_2$-CH₂), 28.7 (2×N-CH₂-$\underline{C}H_2$), 28.5 (2×CH-CH₂-$\underline{C}H_2$), 23.9 (2×CH-$\underline{C}H_2$-CH₃), 23.1 (2×CH3-$\underline{C}H_2$-CH2-CH2-CH), 20.3 (2×CH3-$\underline{C}H_2$-CH2-CH2-N), 14.1 (2×$\underline{C}H3$-CH₂-CH2-CH2-CH), 13.9 (2×$\underline{C}H3$-CH₂-CH2-CH2-N), 10.8 (2×CH-CH₂-$\underline{C}H_3$).

EA: [calculated for $C_{53}H_{66}N_2O$]: C, 85.20; H, 8.90; N, 3.75. [found]: C, 85.17; H, 8.62; N, 3.79.

1.2.3.6   Synthesis of 2,6-bis((4-(butyl(2-ethylhexyl)amino)phenyl)ethynyl)anthracene-9,10-dione (BB3AN)

| Reagents	MW [g/mol]	[g]	[mL]	[mmol]	[eq.]
iodide **4d**	460.01	0.46		1.0	1
alkyne **3b**	285.47	0.71		2.49	2.49
PdCl₂(btpp)	701.89	0.014		0.02	0.02
copper(I) iodide	190.45	0.0038		0.02	0.02
dry triethylamine			30		
dry THF			30		

Procedure

0.46 g (1.0 mmol) of the iodide **4d** and 14 mg of bis(triphenylphosphine) palladium (II) dichloride (PdCl₂(btpp)) (0.02 mmol) were dissolved in a three-neck flask in 30 mL of

degassed dry THF under argon atmosphere. Then 0.71 g (2.49 mmol) of the alkyne **3b**, 30 mL of degassed dry triethylamine and 3.8 mg (0.02 mmol) of copper(I)iodide were added successively. The reaction mixture was stirred under reflux. The progress of the reaction was monitored by TLC. The red solution was poured onto 200 mL of water and extracted by ethyl acetate until the aqueous layer was colorless. The combined organic layers were washed with water (3 × 50 mL) and brine (2 × 50 mL), dried over Na_2SO_4, filtrated and concentrated. Purification by column chromatography (PE:Toluene = 1:2) yielded 0.43 g of product as dark red solid.

Yield

40 % of theory

Analysis

TLC (PE: Toluene = 1:2):	R_f = 0.37
m.p:	184-185 °C.
^{1}H-NMR (200 MHz, CDCl$_3$):	δ (ppm) = 8.34 (d, J = 1.5 Hz, 2H, ar-H5+H11), 8.23 (d, J = 8.1 Hz, 2H, ar-H2+H8), 7.80 (dd, J = 8.2, 1.6 Hz, 2H, ar-H3+H9), 7.38 (d, J = 8.8 Hz, 4H, ar-H2'+H6'+ H2''+H6''), 6.60 (d, J = 8.9 Hz, 4H, ar-H3'+H5'+ H3''+H5''), 3.31 (t, J = 7.3 Hz, 4H, 2×N-C$\underline{H}_2$-CH$_2$), 3.18 (d, J = 7.2 Hz, 4H, 2×N-C$\underline{H}_2$-CH), 1.87-1.66 (m, 2H, 2×CH$_2$-C$\underline{H}$-CH$_2$), 1.66-1.14 (m, 24H, 2×(CH$_3$-C$\underline{H}_2$+CH$_3$-C$\underline{H}_2$+CH$_3$-C$\underline{H}_2$+CH$_2$-C$\underline{H}_2$-CH$_2$+CH$_2$-C$\underline{H}_2$-CH$_2$+CH-C$\underline{H}_2$)), 1.08-0.76 (m, J = 10.4, 7.2 Hz, 18H, 2×(C$\underline{H}_3$-CH$_2$+C$\underline{H}_3$-CH$_2$+C$\underline{H}_3$-CH$_2$)).
^{13}C-NMR (50 MHz, CDCl$_3$):	δ (ppm) = 182.2 ($\underline{C}$=O), 148.9 (ar-C4'+C4''), 135.7 (ar-C3+C9), 133.5 (ar-C5+C11), 133.3 (ar-C6+C12), 131.3 (ar-C1+C7), 131.0 (ar-C2'+C6'+C2''+C6''), 129.5 (ar-C2+C8), 127.3 (ar-C4+C10), 111.6 (ar-C1'+C1''), 107.4 (ar-C3'+C5'+C3''+C5''), 97.1 (2×N-Ar-C≡$\underline{C}$), 86.8 (2×N-Ar-$\underline{C}$≡C), 55.1 (2×N-$\underline{C}$H$_2$-CH), 51.4 (2×N-$\underline{C}$H$_2$-CH$_2$), 37.5 (2×CH$_2$-$\underline{C}$H-CH$_2$), 30.6 (2×CH-$\underline{C}$H$_2$-CH$_2$), 28.7 (2×N-CH$_2$-$\underline{C}$H$_2$), 28.5 (2×CH-CH$_2$-$\underline{C}$H$_2$), 23.9 (2×CH-$\underline{C}$H$_2$-CH$_3$), 23.1 (2×CH3-$\underline{C}$H$_2$-CH2-CH2-CH), 20.3 (2×CH3-$\underline{C}$H$_2$-CH2-CH2-N), 14.0

(2×<u>C</u>H3-CH$_2$-CH2-CH2-CH), 13.9 (2×<u>C</u>H3-CH$_2$-CH2-CH2-N), 10.7 (2×CH-CH$_2$-<u>C</u>H$_3$).

EA: [calculated for C$_{54}$H$_{66}$N$_2$O$_2$]: C, 83.68; H, 8.58; N, 3.61. [found]: C, 83.51; H, 8.63; N, 3.49.

2 Benzylidene ketone-based 2PIs

2.2 Synthesis of cycloketone-based 2PIs

2.2.1 Synthesis of (2E,6E)-2,6-bis(4-(dimethylamino)benzylidene)-cyclohexanone (M2CHK)

[98.07]   [149.19]   [360.22]
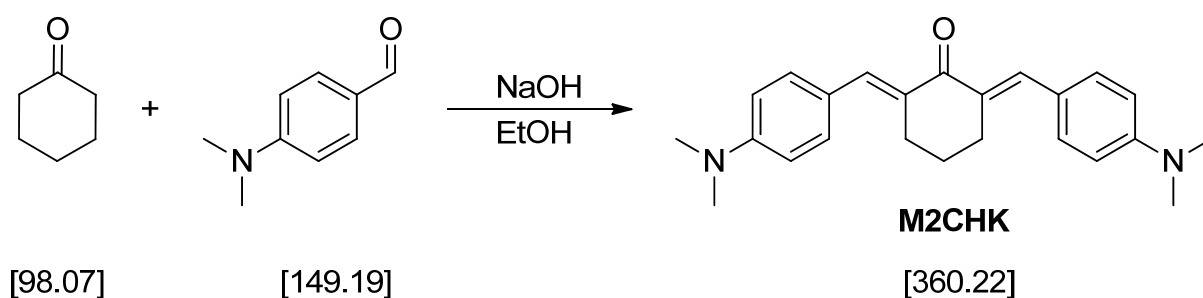
Reagents	MW [g/mol]	[g]	[mL]	[mmol]	[eq.]
cyclohexanone	98.07	0.98		10	1
4-(dimethylamino)benzaldehyde	149.19	2.98		20	2
NaOH	40	0.4		10	1
deionized water			3		
EtOH			30		

Procedure

2.98 g (20 mmol) of 4-(dimethylamino)benzaldehyde and 0.98g (10 mmol) of freshly distilled cyclohexanone were dissolved in 30 mL of EtOH. To this solution 0.4 g (10 mmol) of sodium hydroxide dissolved in 3 mL of deionized water were added dropwise. The reaction was stirred at room temperature until the benzaldehyde compound was completely consumed (TLC analysis). The solution was diluted with 200 mL of chloroform and washed with a saturated NH_4Cl solution (3 × 75 mL) until the aqueous phase was neutral. The combined organic phases were dried over Na_2SO_4, filtered and the solvents were evaporated. The crude product was purified by recrystallization from ethanol yielded 1.62 g of the product as orange powder.

Yield

45% of theory

Analysis

TLC (PE:Chloroform = 1:3):	R_f = 0.28
m.p:	245-247 °C (lit[280]: 247-248 °C)
^{1}H-NMR (200 MHz, CDCl$_3$):	(ppm) = 7.77 (s, 2 H, 2×C=C<u>H</u>), 7.46 (d, J = 8.8 Hz, 4 H, ar-H2+H6+H2'+H6'), 6.72 (d, J = 8.8 Hz, 4 H, ar-H3+H5+H3'+H5'), 3.03 (s, 12 H, 4×C<u>H</u>$_3$-N), 2.98-2.90 (m, 4 H, 2×C-C<u>H</u>$_2$), 1.87-1.81 (m, 2 H, CH$_2$-C<u>H</u>$_2$-CH$_2$).
^{13}C-NMR (50 MHz, CDCl$_3$):	δ (ppm) = 190.1 (<u>C</u>=O), 150.3 (ar-C4+C4'), 137.0 (2×<u>C</u>=CH), 132.4 (2×C=<u>C</u>H), 131.6 (ar-C2+C6+ C2'+C6'), 124.3 (ar-C1+C1'), 111.6 (ar-C3+C5+C3'+C5'), 40.2 (4×<u>C</u>H$_3$-N), 28.7 (2×C-<u>C</u>H$_2$), 23.2 (CH$_2$-<u>C</u>H$_2$-CH$_2$).

2.2.2 Synthesis of (2E,6E)-2,6-bis(4-(dimethylamino)benzylidene)-4-methylcyclohexanone (M2CMK)

[112.17]   [149.19]   [374.52]

Reagents	MW [g/mol]	[g]	[mL]	[mmol]	[eq.]
4-methylcyclohexanone	112.17	1.12		10	1
4-(dimethylamino)benzaldehyde	149.19	2.98		20	2
NaOH	40	0.4		10	1
deionized water			3		
EtOH			30		

Procedure

2.98 g (20 mmol) of 4-(dimethylamino)benzaldehyde and 1.12g (10 mmol) of freshly distilled 4-methylcyclohexanone were dissolved in 30 mL of EtOH. To this solution 0.4 g (10 mmol) of sodium hydroxide dissolved in 3 mL of deionized water were added dropwise. The reaction was stirred at room temperature until the benzaldehyde compound was completely consumed (TLC analysis). The solution was diluted with 200 mL of chloroform and washed with a saturated NH_4Cl solution (3 × 75 mL) until the aqueous phase was neutral. The combined organic phases were dried over sodium sulfate, filtered and the solvents were evaporated. The crude product was purified by recrystallization from ethanol yielded 1.49 g of products as orange powder.

Yield

40% of theory

Analysis

TLC (PE:Chloroform = 1:3): $R_f = 0.42$

m.p: 209-210 °C (lit[281]: 212-214 °C)

^{1}H-NMR (200 MHz, CDCl$_3$):   δ (ppm) = 7.77 (s, 2 H, 2×C=C$\underline{H}$), 7.46 (d, J = 8.8 Hz, 4 H, ar-H2+H6+H2'+H6'), 6.77 (d, J = 8.8 Hz, 4 H, ar-H3+H5+H3'+H5'), 3.05-3.14 (m, 2H, 2×C-C$\underline{H}_a$), 3.04 (s, 12 H, 4×C$\underline{H}_3$-N), 2.62-2.41 (m, 2 H, 2×C-C$\underline{H}_b$), 1.85-1.93 (m, 1H, CH$_2$-C$\underline{H}$-CH$_2$), 1.11 (d, J = 6.7 Hz, 3 H, C$\underline{H}_3$-CH)

^{13}C-NMR (50 MHz, CDCl$_3$):   δ (ppm) = 189.7 ($\underline{C}$=O), 149.9 (ar-C4+C4'), 137.4 (2×$\underline{C}$=CH), 132.3 (2×C=$\underline{C}$H), 131.6 (ar-C2+C6+ C2'+C6'), 124.3 (ar-C1+C1'), 111.7 (ar-C3+C5+C3'+C5'), 40.2 (4×$\underline{C}$H$_3$-N), 36.8 (CH$_2$-$\underline{C}$H-CH$_2$), 29.5 (2×C-$\underline{C}$H$_2$), 22.0 ($\underline{C}$H$_3$-CH).

3 Water-soluble 2PIs

3.2 Synthesis of water-soluble 2PIs

3.2.3 Synthetic route III^{ester} to give WS-B3FL

3.2.3.1 **Synthesis of iodo precursor 6**

3.2.3.1.1 **Synthesis of 4-iodo-N-methylaniline (5)[190]**
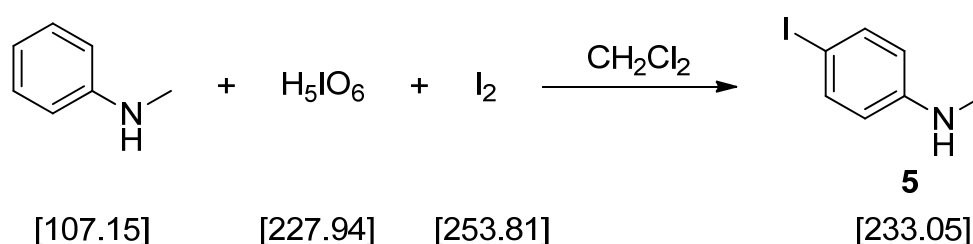
Reagents	MW [g/mol]	[g]	[mL]	[mmol]	[eq.]
N-methylaniline	107.15	2.06		19.25	7
H_5IO_6	227.94	0.63		2.75	1
powdered diiodine	253.81	1.9		7.5	2.7
CH_2Cl_2			25		

Procedure

0.63 g (2.75 mmol) of H_5IO_6 and 1.9 g (7.5 mmol) of finely powdered diiodine were suspended with stirring in CH_2Cl_2 (25 mL). Then, 2.06 g (19.25 mmol) of N-methylaniline were added and the solution was heat to reflux until N-methylaniline was completely consumed (monitored by GC-MS analysis). The cooled reaction mixtures were poured into a vigorously stirred excess of aqueous Na_2SO_3 solution to destroy any unreacted diiodine and all possible oxidized species. The organic layers were separated, dried over Na_2SO_4 and the volatile compounds were removed in vacuum. The final product **5** was obtained as yellow oil after column chromatography (PE:EE= 10:1).

Yield

60% of theory (101% of lit[190])

Analysis

TLC (PE:EE = 10:1): R_f = 0.32

^{1}H-NMR (200 MHz, CDCl$_3$):   δ (ppm) = 7.44 (d, J = 8.80 Hz, 2 H, ar-H2+H6), 6.40
                                  (d, J = 8.80 Hz, 2 H, ar-H3+H5), 3.74 (br, s, 1 H, N<u>H</u>),
                                  2.82 (s, 3H, C<u>H</u>$_3$).

^{13}C-NMR (50 MHz, CDCl$_3$): δ (ppm) = 148.8 (ar-C4), 137.7 (ar-C2+C6), 114.6 (ar-
                                  C3+C5), 77.6 (ar-C1), 30.5 (<u>C</u>H$_3$).

GS-MS analysis: (m/z) = 233.03, 105.10, 77.06.

3.2.3.1.2   Synthesis of methyl 2-((4-iodophenyl)(methyl)amino)acetate (6)[191]

	5		6
	[152.97]	[233.05]	[305.11]
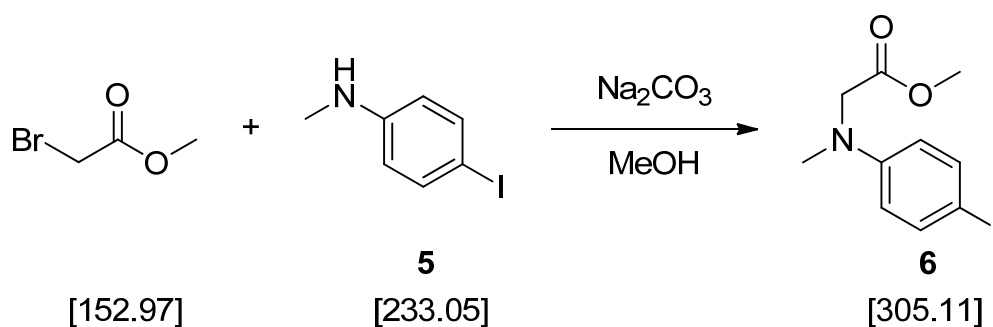
Reagents	MW [g/mol]	[g]	[mL]	[mmol]	[eq.]
4-iodo-N-methylaniline	233.05	1.49		6.43	1
methyl bromoacetate	152.97	1.08		7.07	1.1
Na$_2$CO$_3$	105.99	1.01		9.51	1.5
MeOH			20		

Procedure

1.08 g (7.07 mmol) of methyl bromoacetate and 1.01 g (9.51 mmol) of Na$_2$CO$_3$ were
added to a solution of 1.49 g (6.43 mmol) of 4-iodo-N-methylaniline in 20 mL of MeOH.
The reaction mixture was stirred at 80 °C until 4-iodo-N-methylaniline was completely
consumed (monitored by GC-MS analysis). After cooling to room temperature, the
solution was concentrated by evaporation and diluted with 30 mL of DCM. The
precipitated salts were removed by filtration. The filtrate was separated and the aqueous
layer was extracted with DCM. The combined organic layers were washed with water (3

× 30 mL) and brine (30 mL), dried over Na_2SO_4 and the volatile compounds were evaporated under vacuum. The crude product was purified by column chromatography (DCM:PE = 1:2) giving the final product **6** as yellow oil.

Yield

80% of theory

Analysis

TLC (DCM:PE = 10:1):	R_f = 0.43
^{1}H-NMR (200 MHz, CDCl$_3$):	δ (ppm) = 7.49 (d, J = 9.00 Hz, 2 H, ar-H2+H6), 6.47 (d, J = 9.00 Hz, 2 H, ar-H3+H5), 4.06 (s, 2H, N-C$\underline{H}_2$), 3.74 (s, 3 H, O-C$\underline{H}_3$), 3.05 (s, 3H, N-C$\underline{H}_3$).
^{13}C-NMR (50 MHz, CDCl$_3$):	δ (ppm) = 171.1 ($\underline{C}$=O), 148.4 (ar-C4), 137.7 (ar-C2+C6), 114.6 (ar-C3+C5), 78.6 (ar-C1), 54.1 (N-$\underline{C}$H$_2$), 52.1 (O-$\underline{C}$H$_3$), 39.5 (N-$\underline{C}$H$_3$).
GS-MS analysis:	(m/z) = 304.67, 245.77, 118.95.

3.2.3.2 Synthesis of alkyne precursor 7

3.2.3.2.1 Synthesis of 2,7-bis((trimethylsilyl)ethynyl)-9H-fluoren-9-one (8)[193]

4b
[432.00]

[98.22]

8
[372.61]
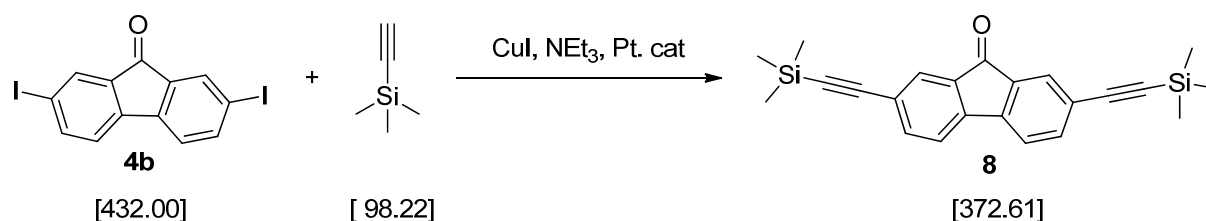
Reagents	MW [g/mol]	[g]	[mL]	[mmol]	[eq.]
2,7-diiodo-9H-fluoren-9-one	432.00	2.0		4.63	1
ethynyltrimethylsilane	98.22	1.14	1.64	11.57	2.5
PdCl$_2$(btpp)	701.89	0.32		0.46	0.1
copper(I) iodide	190.45	0.17		0.92	0.2
dry triethylamine			10		
dry THF			10		

Procedure

2.0 g (4.63 mmol) of 2,7-diiodo-9H-fluoren-9-one and 0.32 g of bis(triphenylphosphine) palladium (II) dichloride (PdCl$_2$(btpp)) (0.46 mmol) were dissolved in 10 mL of degassed dry THF under argon atmosphere. Then 1.64 mL (11.57 mmol) of ethynyltrimethylsilane, 10 mL of degassed dry triethylamine and 0.17 g (0.92 mmol) of copper(I)iodide were added successively. The reaction mixture was stirred at room temperature and the progress of the reaction was monitored by TLC. When the 2,7-diiodo-9H-fluoren-9-one was completely consumed, the solid salts were filtered off and extracted by ether (3 × 30 mL). The combined organic phases were concentrated under reduced pressure and the crude product was purified by column chromatography (PE:DCM = 3:1) giving the product **8** as yellow solid.

Yield

62% of theory (79% of lit[193])

Analysis

TLC (PE:DCM = 3:1): R_f = 0.32

m.p: 164-166 °C. (lit[193]: 164-168 °C)

^{1}H-NMR (200 MHz, CDCl$_3$):   δ (ppm) = 7.75 (s, 2 H, ar-H2+H11), 7.64 (d, J = 7.7, 2 H, ar-H5+H8), 7.46 (d, J = 7.8 Hz, 2H, ar-H4+H9), 0.27 (s, 18 H, 6×C$\underline{H}_3$-Si).

^{13}C-NMR (50 MHz, CDCl$_3$):   δ (ppm) = 192.1 ($\underline{C}$=O), 143.4 (ar-C6+C7), 138.1 (ar-C1+C12), 134.3 (ar-C4+C9), 128.4 (ar-C2+C11), 124.3 (ar-C5+C8), 120.5 (ar-C3+C10), 103.9 (2×Ar-$\underline{C}$≡C), 96.7 (2×Ar-C≡$\underline{C}$), -0.4 (6×$\underline{C}$H$_3$-Si).

3.2.3.2.2   Synthesis of 2,7-diethynyl-9H-fluoren-9-one (7)[193]

| 8 | | 7 |
| [372.61] | [138.21] | [228.24] |
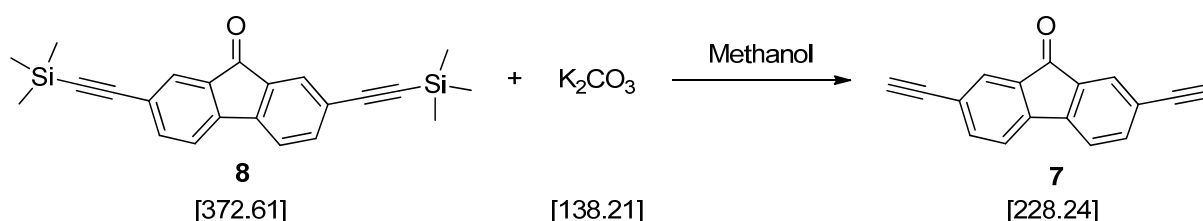
Reagents	MW [g/mol]	[g]	[mL]	[mmol]	[eq.]
2,7-bis((trimethylsilyl)ethynyl)-9H-fluoren-9-one **8**	372.61	1.59		4.29	1
K_2CO_3	138.21	2.96		21.47	5
methanol			50		

Procedure

2.96 g (21.47 mmol) of dry K_2CO_3 powder were added to a solution of 1.59 g (4.29 mmol) of the protected alkyne **8** in 50 mL of dry and degassed methanol under argon atmosphere. The suspension was stirred under room temperature until the fluorenone compound **8** was completely consumed (monitored by TLC). The solid residue was filtered off and the solvent was removed under vacuum. The yellow residual was dissolved in 30 mL of DCM and washed with water (3 × 50 mL) and brine (50 mL). The combined organic layers were dried over Na_2SO_4, filtered off and the solvent was evaporated. The crude product was purified by column chromatography (DCM) giving compound **7** as yellow solid.

Yield

60 % of theory (61% of lit[193])

Analysis

TLC (DCM): R_f = 0.33

m.p: 237-240 °C. (lit[193]: 237-239 °C)

^{1}H-NMR (200 MHz, CDCl$_3$):   δ (ppm) = 7.76-7.74 (m, 2H, ar-H2+H11), 7.61 (d, J = 7.72, 2H, ar-H5+H8), 7.48 (d, J = 7.8 Hz, 2H, ar-H4+H9), 3.17 (s, 2H, 2×C≡CH).

^{13}C-NMR (50 MHz, CDCl$_3$):   δ (ppm) = 191.9 (C=O), 143.6 (ar-C6+C7), 138.5 (ar-C1+C12), 134.3 (ar-C4+C9), 128.1 (ar-C2+C11), 123.4 (ar-C5+C8), 120.6 (ar-C3+C10), 82.5 (2×Ar-C≡CH), 79.2 (2×Ar-C≡CH).

3.2.4   Synthetic route I[after] to give benzylidene cycloketone-based 2PIs

3.2.4.1   Synthesis of 4-methylamino-benzaldehyde (9)[196]

| [135.16] | [126.93] | [163.17] | [135.16] |
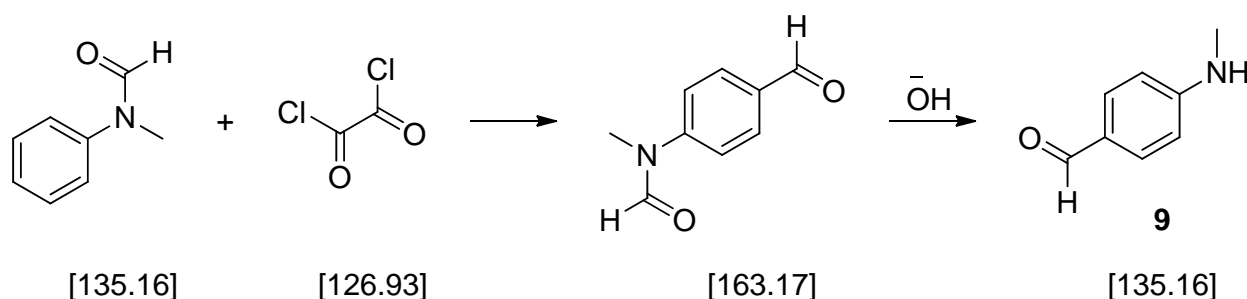
Reagents	MW [g/mol]	[g]	[mL]	[mmol]	[eq.]
oxalyl chloride	126.93	0.55		0.44	2
N-methylformanilide	135.16	0.29		0.22	1
water			150		

Procedure

0.55 g (0.44 mmol) of oxalyl chloride was slowly added to 0.29 g (0.22 mmol) of N-methylformanilide while maintaining the temperature between 40-50 °C. The solution was stirred at room temperature for 12 h. Then the solution was dissolved in 150 mL of water and alkalized with 6N sodium hydroxide solution. The by-product N-methylaniline was removed by steam distillation and the residual solution was extracted with CH_2Cl_2 (3 × 50 mL). After removing the solvent, kugelrohr distillation was performed to distill the residual red oil (185-187 °C/15mm) giving the desired product **9** as light yellow oil.

Yield

36 % of theory (90% of lit[196])

Analysis

TLC (DCM:EE = 2:1): $R_f = 0.62$

^{1}H-NMR (200 MHz, CDCl$_3$):   δ (ppm) = 9.74 (s, 1 H, C$\underline{H}$=O), 7.72 (d, J = 8.61 Hz, 2 H, ar-H3+H5), 6.62 (d, J = 8.61 Hz, 2 H, ar-H2+H6), 4.42 (bs, 1H, N$\underline{H}$), 2.94 (d, J = 4.89 Hz, 3 H, C$\underline{H}_3$-NH).

^{13}C-NMR (50 MHz, CDCl$_3$):   δ (ppm) = 190.3 ($\underline{C}$=O), 154.3 (ar-C1), 132.3 (ar-C1+C5), 126.3 (ar-C4), 111.5 (C2+C6), 30.0 ($\underline{CH}_3$-NH).

GS-MS analysis: (m/z) = 134.03, 106.01, 79.00, 77.06.

3.2.5   Synthetic route I^{before} to give benzylidene cycloketone-based 2PIs

3.2.5.1   Synthesis of benzaldehyde precursor 10

3.2.5.1.1   Synthesis of methyl 2-(methyl(phenyl)amino)acetate (12)[198]

[152.97]   [107.15]   [179.22]
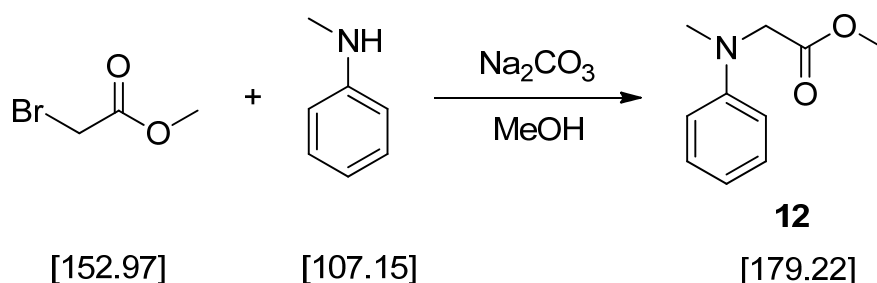
Reagents	MW [g/mol]	[g]	[mL]	[mmol]	[eq.]
N-methylaniline	107.15		10.9	100	1
bormoacetate	152.97		12.2	110	1.1
sodium carbonate	105.99	15.9		150	1.5
MeOH			150		

Procedure

To a solution of 12.2 mL (110 mmol) of ethyl bormoacetate, 10.9 mL (100 mmol) of N-methylaniline and 150 mL of methanol were added 15.9 g of sodium carbonate (150 mmol). The reaction mixture was stirred under reflux until N-methylaniline was completely consumed (GC-MS analysis). Then the solution was filtered off, the solid residue was extracted with ethyl acetate (2 × 50 mL) and the combined organic phases were distilled under vacuum to remove the solvents. The crude product was dissolved in 150 mL of ethyl acetate and washed with water (3 × 100 mL) and brine (1 × 100 mL). The organic layer was dried over Na$_2$SO$_4$, filtered and concentrated. Purification by column chromatography (PE:EE = 20:1) yielded 15.2g of products as light yellow oil.

Yield

85 % of theory

Analysis

TLC (PE:EE = 10:1): R_f = 0.52

^{1}H-NMR (200 MHz, CDCl$_3$): δ (ppm) = 7.51-7.10 (m, 2H, ar-H3+H5), 6.85-6.74 (m, 3H, ar-H2+H4+H6), 4.14 (s, 2H, N-C$\underline{H}_2$), 3.77 (s, 3H, O-C$\underline{H}_3$), 3.13 (s, 3H, N-C$\underline{H}_3$).

^{13}C-NMR (50 MHz, CDCl$_3$): δ (ppm) = 171.6 ($\underline{C}$=O), 148.8 (ar-C1), 129.2 (ar-C3+C5), 117.4 (ar-C4), 112.3 (ar-C2+C6), 54.3 N-$\underline{C}$H$_2$, 51.9 (O-$\underline{C}$H$_3$), 39.5 (N-$\underline{C}$H$_3$).

GS-MS analysis: (m/z) = 179.20, 120.16, 91.11, 77.08.

3.2.5.1.2 Synthesis of methyl 2-((4-formylphenyl)(methyl)amino)acetate (10)[198]

| | **12** | | **10** |
| [179.22] | [73.09] | [153.33] | [207.23] |
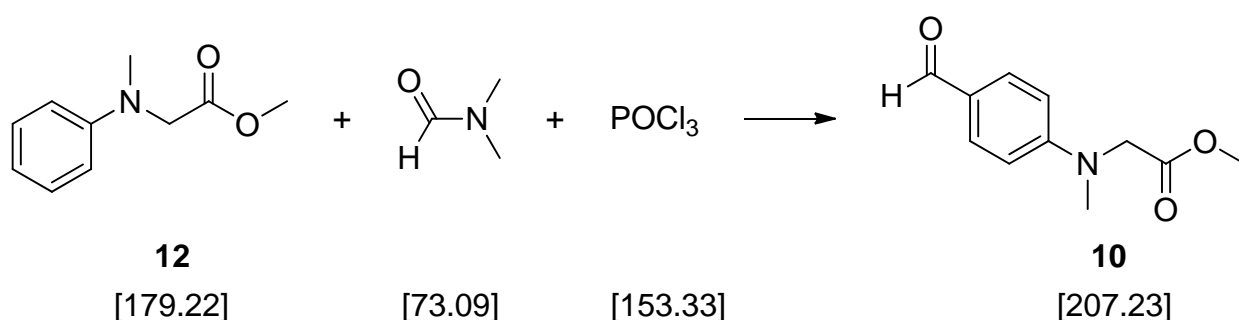
Reagents	MW [g/mol]	[g]	[mL]	[mmol]	[eq.]
acetate **12**	179.22	4.48		25	1
phosphorous oxychloride	153.33		2.3	25	1
dry DMF	73.09		20		

Procedure

2.3 mL (25 mmol) of phosphorous oxychloride were added dropwise to 20 mL of dry DMF at 0 °C. After 30 min 4.48 g (25 mmol) of methyl 2-(methyl(phenyl)amino)acetate **12** were added to the reaction mixture, which was subsequently heated to 75 °C for 4h. Then the solution was cooled and poured into ice water (250 mL) with vigorous stirring

overnight. The mixture was extracted with DCM (3 × 50 mL) and the combined organic layers were washed with water (3 × 50 mL) and brine (1 × 50 mL) and finally dried over Na_2SO_4. The solvent was evaporated and the crude product was purified by column chromatography (PE:EE = 2:1) to yield 3.1 g of the product **10** as white solid.

Yield

60 % of theory

Analysis

TLC (PE:EE =2:1): R_f = 0.52

m.p: 76-78 °C

^{1}H-NMR (200 MHz, CDCl$_3$):   δ (ppm) = 9.68 (s, 1H, C$\underline{H}$=O), 7.66 (d, J = 8.9 Hz, 2H, ar-H3+H5), 6.62 (d, J = 8.9 Hz, 2H, ar-H2+H6), 4.09 (s, 2H, N-C$\underline{H}_2$), 3.66 (s, 3H, O-C$\underline{H}_3$), 3.07 (s, 3H, N-C$\underline{H}_3$).

^{13}C-NMR (50 MHz, CDCl$_3$):   δ (ppm) = 190.3 (Ar-$\underline{C}$H=O), 170.2 (O-$\underline{C}$=O), 153.3 (ar-C1), 131.9 (ar-C3+C5), 126.3 (ar-C4), 111.3 (ar-C2+C6), 53.8 (N-$\underline{C}$H$_2$), 52.2 (O-$\underline{C}$H$_3$), 39.6 (N-$\underline{C}$H$_3$).

GS-MS analysis: (m/z) = 207.28, 148.22, 118.20, 77.10.

3.2.5.3   Synthesis of sodium 2-((4-formylphenyl)(methyl)amino)acetate (13)
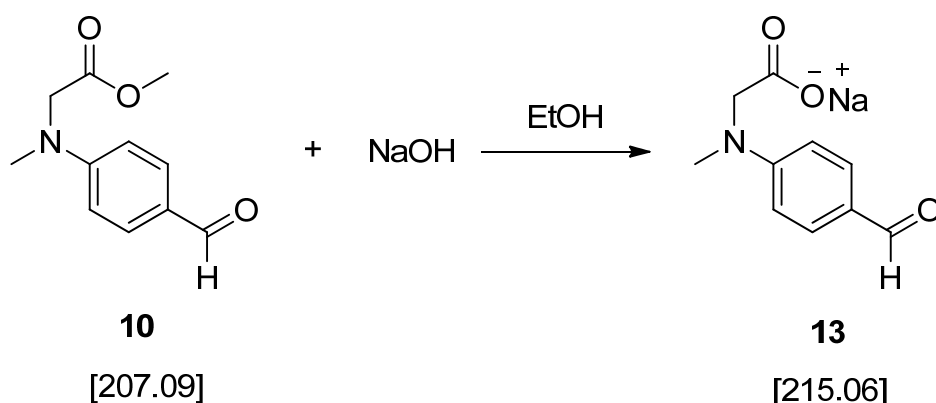
Reagents	MW [g/mol]	[g]	[mL]	[mmol]	[eq.]
acetate **10**	207.23	0.99		4.82	1

	40	0.61		15	3
NaOH					
EtOH			20		

Procedure

A mixture of 0.99 g (4.82 mmol) of the acetate **10** and 0.6 g (15 mmol) of NaOH powder in 20 mL of EtOH was stirred for 24h at room temperature. The solvent was removed in vacuum and the crude product was used directly for the next step without further purification.

Analysis

^{1}H-NMR (200 MHz, D$_2$O): δ (ppm) = 9.29 (s, 1 H, C$\underline{H}$=O), 7.56 (d, J = 8.8 Hz, 2 H, ar-H3+H5), 6.53 (d, J = 8.8 Hz, 2 H, ar-H2+H6), 3.82 (s, 2 H, N-C$\underline{H}_2$), 2.93 (s, 3 H, N-C$\underline{H}_3$).

^{13}C-NMR (50 MHz, D$_2$O): δ (ppm) = 193.4 (Ar-$\underline{C}$H=O), 177.6 (O-$\underline{C}$=O), 154.7 (ar-C1), 132.8 (ar-C3+C5), 123.5 (ar-C4), 111.0 (ar-C2+C6), 56.0 (N-$\underline{C}$H$_2$), 38.9 (N-$\underline{C}$H$_3$).

3.2.5.4 Synthesis of hydrophilic benzaldehyde 14

3.2.5.4.1 Synthesis of methyl 3-(methyl(phenyl)amino)propanoate (15)[282]

[107.15] [86.09] **15** [193.24]
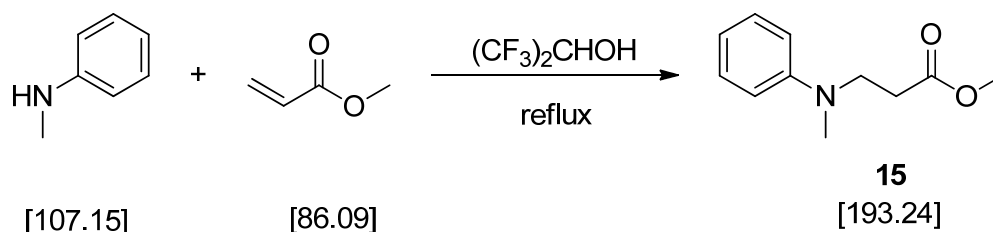
Reagents	MW [g/mol]	[g]	[mL]	[mmol]	[eq.]
N-methylaniline	107.15	1.61		15	1
methyl acrylate	86.09	3.87		45	3
hexafluoropropan-2-ol	168.04		10		

Procedure

1.61 g (15 mmol) of N-methylaniline and 3.87 g (45 mmol) of methyl acrylate were mixed in 10 mL of hexafluoropropan-2-ol. The solution was heated under reflux until N-methylaniline was completely consumed (TLC monitoring). The volatile compounds were removed in vacuum and the crude product was purified by column chromatography (PE:EE = 10:1) yielded 2.61 g of the ester as light yellow oil.

Yield

90 % of theory (93% of lit[282])

Analysis

TLC (PE:EE = 10:1): R_f = 0.52

^{1}H-NMR (200 MHz, CDCl$_3$):   δ (ppm) = 7.22-7.31 (m, 2 H, ar-H3+H5), 6.71-6.78 (m, 3 H, ar-H2+H4+H6), 3.71 (t, J = 7.2 Hz, 2 H, N-CH$_2$), 3.70 (s, 3 H, O-CH$_3$), 2.96 (s, 3 H, N-CH$_3$), 2.60 (t, J = 7.2 Hz, 2 H, CH$_2$-C=O).

^{13}C-NMR (50 MHz, CDCl$_3$):   δ (ppm) = 172.8 (C=O), 148.6 (ar-C1), 129.3 (ar-C3+C5), 116.8 (ar-C4), 112.5 (ar-C2+C6), 51.7 (N-CH$_2$), 48.6 (O-CH$_3$), 38.2 (N-CH$_3$), 31.5 (CH$_2$-C=O).

3.2.5.4.2 Synthesis of methyl 3-((4-formylphenyl)(methyl)amino)propanoate (11)
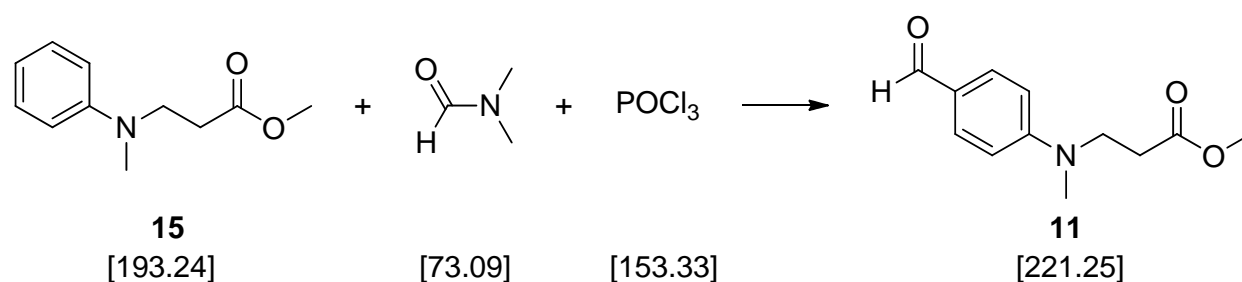
Reagents	MW [g/mol]	[g]	[mL]	[mmol]	[eq.]
acetate **15**	193.24	0.96		5	1
phosphorous oxychloride	153.33		1.3	15	3
dry DMF	73.09		10		

Procedure

1.3 mL (15 mmol) of phosphorous oxychloride was added dropwise to 10 mL of dry DMF at 0 °C. After 30 min 0.96 g (5 mmol) of the acetate **15** were added to the reaction mixture, which was subsequently heated to 90 °C for 3h. Then the solution was cooled and poured into ice water (100 mL) with vigorous stirring overnight. The mixture was extracted with DCM (3 × 50 mL) and the combined organic layers were washed with water (3 × 50 mL) and brine (1 × 50 mL) and finally dried over Na_2SO_4. The solvent was evaporated and the crude product was purified by column chromatography (PE:EE = 3:2) to yield 0.66 g of products as yellow solid.

Yield

60 % of theory

Analysis

TLC (PE:EE =3:2):	R_f = 0.42
^{1}H-NMR (200 MHz, CDCl$_3$):	δ (ppm) = 9.75 (s, 1 H, C<u>H</u>=O), 7.74 (d, J = 8.8 Hz, 2 H, ar-H3+H5), 6.72 (d, J = 8.8 Hz, 2 H, ar-H2+H6), 3.78 (t, J = 7.0 Hz, 2 H, N-C<u>H</u>$_2$), 3.69 (s, 3 H, O-C<u>H</u>$_3$), 3.07 (s, 3 H, N-C<u>H</u>$_3$), 2.63 (t, J = 7.1 Hz, 2 H, C<u>H</u>$_2$-C=O)
^{13}C-NMR (50 MHz, CDCl$_3$):	δ (ppm) = 190.3 (Ar-<u>C</u>H=O), 172.1 (O-<u>C</u>=O), 152.9 (ar-C1), 132.1 (ar-C3+C5), 125.6 (ar-C4), 111.1 (ar-C2+C6), 51.9 (N-<u>C</u>H$_2$), 48.1 (O-<u>C</u>H$_3$), 38.6 (N-<u>C</u>H$_3$), 31.7 (<u>C</u>H$_2$-C=O).

3.2.5.4.3   Synthesis of 3-[(4-formyl-phenyl)-methyl-amino]-propionic acid (14)
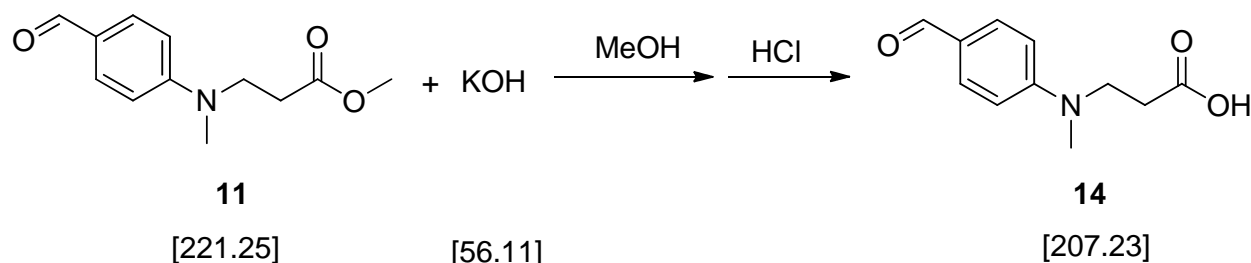
Reagents	MW	[g]	[mL]	[mmol]	[eq.]

	[g/mol]			
acetate **11**	221.25	0.61	2.71	1
KOH	56.11	0.34	6	2.2
MeOH			10	

Procedure

A mixture of 0.61 g (2.71 mmol) of the acetate **11** and 0.34 g (6 mmol) of KOH powder in 10 mL of MeOH was stirred for 24h at room temperature. The solvent was removed in vacuum and residuals were dissolved in 20 mL of water, neutralized with dilute HCl and extract with ether acetate (3 × 50 mL). The combined organic phases were washed with water (3 × 50 mL) and brine (1 × 50 mL) and finally dried over sodium sulfate. The solvent was removed in vacuum yielded 0.47 g of the product **14** as yellow solid. The sodium salt precursor was obtained by neutralizing the propionic acid with NaOH aqueous solution before starting the aldol condensation.

Yield

85 % of theory

Analysis

m.p: 124-126 °C

^{1}H-NMR (200 MHz, DMSO-d$_6$):   δ (ppm) = 9.66 (s, 1 H, C$\underline{H}$=O), 7.67 (d, J = 8.8 Hz, 2 H, ar-H3+H5), 6.80 (d, J = 8.8 Hz, 2 H, ar-H2+H6), 3.68 (t, J = 7.0 Hz, 2 H, N-C$\underline{H}_2$), 3.00 (s, 3 H, N-C$\underline{H}_3$), 2.64 - 2.19 (2 H, overlap with the peaks of DMSO).

^{13}C-NMR (50 MHz, DMSO-d$_6$):   δ (ppm) = 188.7 (Ar-$\underline{C}$H=O), 171.8 (O-$\underline{C}$=O), 151.8 (ar-C1), 130.5 (ar-C3+C5), 123.5 (ar-C4), 109.9 (ar-C2+C6), 46.3 (N-$\underline{C}$H$_2$), 36.9 (N-$\underline{C}$H$_3$), 30.2 ($\underline{C}$H$_2$-C=O).

3.2.5.4.4   Synthesis of 3-[(4-formyl-phenyl)-methyl-amino]-propionic acid (14)[199]

[188.09]   [207.23]
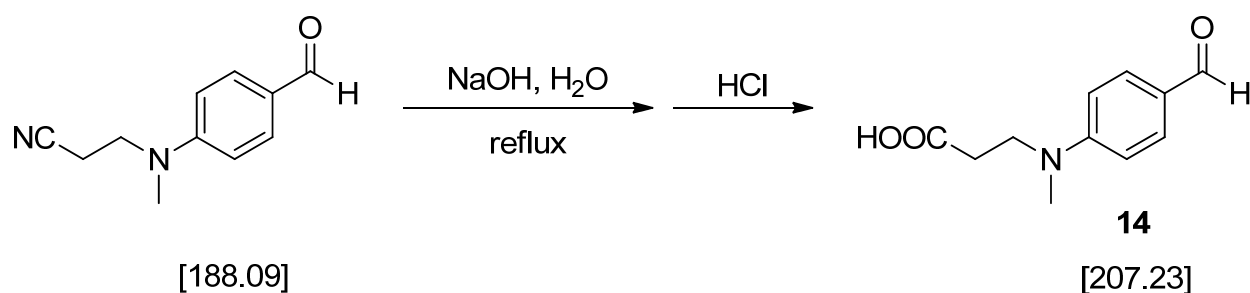
Reagents	MW [g/mol]	[g]	[mL]	[mmol]	[eq.]
propanenitrile	188.09	8.99		47.8	1
NaOH	40	5.61		140	3
Water			200		

Procedure

5.61 g (140 mmol) of sodium hydroxide and 8.99g (47.8 mmol) of 3-((4-formylphenyl)-(methyl)-amino) propanenitrile were suspended in 200 mL of water. The reaction mixture was refluxed for 5 h, then cooled and filtrated. A dilute HCl solution was added dropwise into the filtrate with stirring until no precipitate formed. Precipitates were collected, washed with water (3 × 150 mL) and dried to yield 8.91 g of the desired product **14** as yellow solid. The sodium salt precursor was obtained by neutralizing the propionic acid with NaOH aqueous solution before starting the aldol condensation.

Yield

90 % of theory (93% of lit[199])

Analysis

TLC (PE:EE = 3:2): R_f = 0.42

m.p: 124-126 °C

^{1}H-NMR (200 MHz, DMSO-d$_6$):   δ (ppm) = 9.66 (s, 1 H, C<u>H</u>=O), 7.67 (d, J = 8.8 Hz, 2 H, ar-H3+H5), 6.80 (d, J = 8.8 Hz, 2 H, ar-H2+H6), 3.68 (t, J = 7.0 Hz, 2 H, N-C<u>H$_2$</u>), 3.00 (s, 3 H, N-C<u>H$_3$</u>), 2.64 - 2.19 (2 H, overlap with the peaks of DMSO).

^{13}C-NMR (50 MHz, DMSO-d$_6$):   δ (ppm) = 188.7 (Ar-<u>C</u>H=O), 171.8 (O-<u>C</u>=O), 151.8 (ar-C1), 130.5 (ar-C3+C5), 123.5

(ar-C4), 109.9 (ar-C2+C6), 46.3 (N-$\underline{C}H_2$), 36.9
(N-$\underline{C}H_3$), 30.2 ($\underline{C}H_2$-C=O).

3.2.5.5   Synthesis of water-soluble 2PIs

3.2.5.5.1   Synthesis of sodium 3,3'-((((1E,1'E)-(2-oxocyclopentane-1,3-diylidene) bis (methanylylidene))bis(4,1-phenylene))bis(methylazanediyl)) dipropanoate (P2CK)
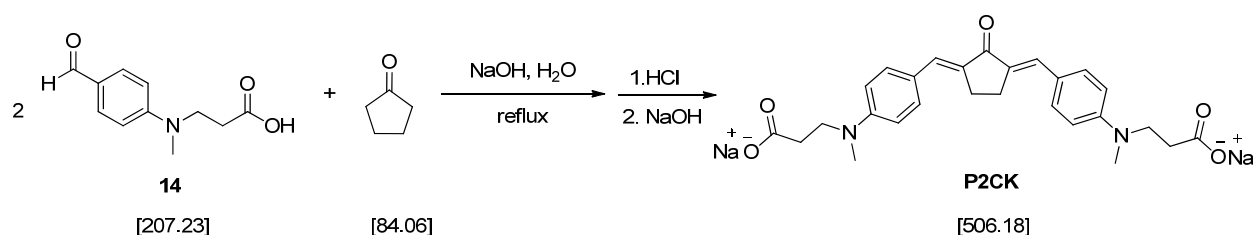
Reagents	MW [g/mol]	[g]	[mL]	[mmol]	[eq.]
benzaldehyde **14**	207.23	0.93		4.52	2
cyclopentanone	84.06	0.19		2.26	1
NaOH	40	0.18		4.52	2
EtOH			20		
Water			10		

Procedure

In an orange light room, 0.18 g of of sodium hydroxide (4.52 mmol), 0.93 g of the benzaldehyde compound **14** (4.52 mmol) and 0.19 g of freshly distilled cyclopentanone (2.26 mmol) were dissolved in 10 mL of water. The reaction was stirred at 80 °C for 4h and then cooled to room temperature. 20 mL of EtOH and 1M HCl were added consequently until no precipitate formed. The red solids were collected by centrifugation and dried in vacuum. The purification was performed by washing with 1 mL of cold methanol or by recrystallization from 2-propanol. The obtained red solids were put into 20 mL of water and 0.1M NaOH was added dropwise until pH 8.5 was reached (monitored with pH meter). The undissolved solids were filtered off and water was removed via freeze-drying to yield desired products as orange powder.

Yield

50 % of theory

Analysis

m.p	>300 °C

^{1}H-NMR (200 MHz, D$_2$O): δ (ppm) = 7.10 (d, J = 8.2 Hz, 4 H, ar-H2+H6+H2'+H6'), 6.94 (s, 2 H, 2×C=C$\underline{H}$), 6.40 (d, J = 8.2 Hz, 4 H, ar-H3+H5+H3'+H5'), 3.39 (t, J = 7.1 Hz, 4 H, 2×N-C$\underline{H}_2$), 2.68 (s, 6H, N-C$\underline{H}_3$), 2.49-2.42 (m, 4 H, 2×=C-C$\underline{H}_2$), 2.24 (t, J = 7.2 Hz, 4 H, 2×C$\underline{H}_2$-C=O).

^{13}C-NMR (50 MHz, D$_2$O): δ (ppm) = 196.9 (=C-$\underline{C}$=O), 180.7 (O-$\underline{C}$=O), 149.7 (ar-C4+C4'), 135.0 (2×$\underline{C}$=CH), 133.3 (2×C=$\underline{C}$H), 132.7 (ar-C2+C6+ C2'+C6'), 123.1 (ar-C1+C1'), 111.9 (ar-C3+C5+C3'+C5'), 49.1 (2×N-$\underline{C}$H$_2$), 37.3 (2×N-$\underline{C}$H$_3$), 34.7 (2×$\underline{C}$H$_2$-C=O), 26.4 (2×=C-$\underline{C}$H$_2$).

EA: [calculated for C$_{27}$H$_{28}$N$_2$O$_5$Na$_2$]: C, 64.03; H, 5.57; N, 5.53; [found]: C, 64.33; H, 5.38; N, 5.42.

3.2.5.5.2 Synthesis of sodium 3,3'-(((((1E,1'E)-(5-methyl-2-oxocyclohexane-1,3-diylidene)bis (methanylylidene))bis(4,1-phenylene))bis (methylazanediyl)) dipropanoate (E2CK)
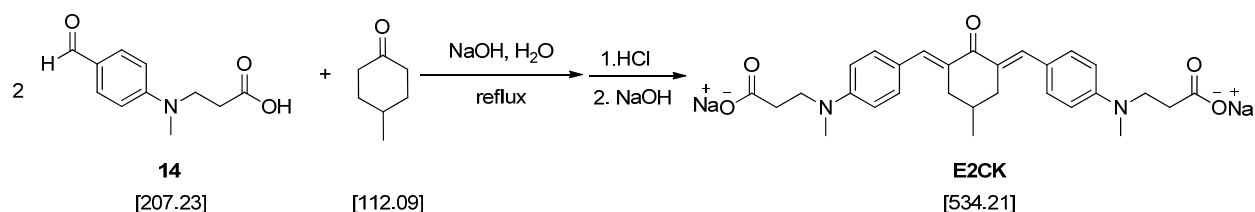
Reagents	MW [g/mol]	[g]	[mL]	[mmol]	[eq.]
benzaldehyde **14**	207.23	0.93		4.52	2
4-methylcyclohexanone	112.09	0.25		2.26	1
NaOH	40	0.18		4.52	2
EtOH			20		

Water   10

Procedure

In an orange light room, 0.18 g of of sodium hydroxide (4.52 mmol), 0.93 g of the benzaldehyde **14** (4.52 mmol) and 0.25 g of freshly distilled 4-methylcyclohexanone (2.26 mmol) were dissolved in 10 mL of water. The reaction was stirred at 80 °C for 6h and then cooled to room temperature. 20 mL of EtOH and 1M HCl were added consequently until no precipitate formed. The red solids were collected by centrifugation and dried in vacuum. The purification was performed by washing with 1 mL of cold methanol or by column chromatography using chloroform with 3% of acetic acid as eluent. The obtained red solids were put into 20 mL of water and 0.1M NaOH was added dropwise until pH 8.5 was reached (monitored with pH meter). The undissolved solids were filtered off and water was removed via freeze-drying to yield desired products as orange powder.

Yield

30 % of theory

Analysis

M.P   >300 °C

^{1}H-NMR (200 MHz, D$_2$O):   δ (ppm) = 7.40 (s, 2 H, 2×C=C$\underline{H}$), 7.27 (d, J = 8.6 Hz, 4 H, ar-H2+H6+H2'+H6'), 6.63 (d, J = 8.6 Hz, 4 H, ar-H3+H5+H3'+H5'), 3.49 (t, J = 7.1 Hz, 4 H, 2×N-C$\underline{H}_2$), 2.78 (s, 6 H, 2×N-C$\underline{H}_3$), 2.73-2.67 (m, 2 H, 2×=C-C$\underline{H}_a$), 2.28 (t, J = 7.2 Hz, 4H, 2×C$\underline{H}_2$-C=O), 2.18-1.90 (m, 3 H, C$\underline{H}$+2×=C-C$\underline{H}_b$), 0.83 (d, J = 6.3 Hz, 3 H, CH-C$\underline{H}_3$).

^{13}C-NMR (50 MHz, D$_2$O):   δ (ppm) = 192.7 (=C-$\underline{C}$=O), 181.1 (O-$\underline{C}$=O), 149.6 (ar-C4+C4'), 138.7 (2×$\underline{C}$=CH), 133.2 (2×C=$\underline{C}$H), 131.5 (ar-C2+C6+ C2'+C6'), 123.5 (ar-C1+C1'), 112.2 (ar-C3+C5+C3'+C5'), 49.3 (N-$\underline{C}$H$_2$), 37.4 (CH$_2$-$\underline{C}$H-CH$_2$+2×N-$\underline{C}$H$_3$), 34.4 (2×$\underline{C}$H$_2$-C=O), 20.7 ($\underline{C}$H$_3$-CH). =C-$\underline{C}$H$_2$ may overlap with $\underline{C}$H$_2$-C=O.

EA: [calculated for C$_{29}$H$_{32}$N$_2$O$_5$Na$_2$]: C, 65.16; H, 6.03; N, 5.24; [found]: C, 65.37; H, 5.92; N, 5.08.

3.2.5.5.3 Synthesis of sodium 2,2'-(((((1E,1'E)-(5-methyl-2-oxocyclohexane-1,3-diylidene) bis (methanylylidene)) bis(4,1-phenylene))bis (methylazanediyl))diacetate (G2CK)
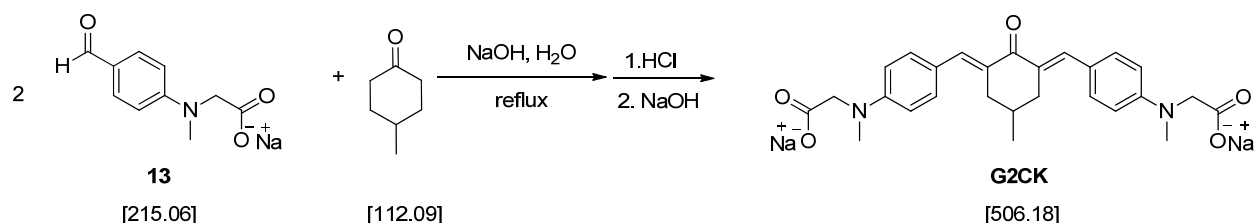
Reagents	MW [g/mol]	[g]	[mL]	[mmol]	[eq.]
benzaldehyde **13**	215.06	0.97		4.52	2
4-methylcyclohexanone	112.09	0.25		2.26	1
NaOH	40	0.09		2.26	1
EtOH			20		
Water			10		

Procedure

In an orange light room, 0.09 g of of sodium hydroxide (2.26 mmol), 0.97 g of the benzaldehyde **13** (4.52 mmol) and 0.25 g of freshly distilled 4-methylcyclohexanone (2.26 mmol) were dissolved in 10 mL of water. The reaction was stirred at 80 °C for 6h and then cooled to room temperature. 20 mL of EtOH and 1M HCl were added consequently until no precipitate formed. The red solids were collected by centrifugation and dried in vacuum. The purification was performed by washing with 1 mL of cold methanol or by column chromatography using chloroform with 2% of acetic acid as eluent. The obtained red solids were put into 20 mL of water and 0.1M NaOH was added dropwise until pH 8.5 was reached (monitored with pH meter). The undissolved solids were filtered off and water was removed via freeze-drying to yield desired products as orange powder.

Yield

33 % of theory

Analysis

M.P   >300 °C

^{1}H-NMR (200 MHz, D$_2$O):	δ (ppm) = 7.44 (s, 2 H, 2×C=C$\underline{H}$), 7.29 (d, J = 8.6 Hz, 4 H, ar-H2+H6+H2'+H6'), 6.52 (d, J = 8.6 Hz, 4 H, ar-H3+H5+H3'+H5'), 3.75 (s, 4 H, 2×C$\underline{H_2}$-C=O), 2.88 (s, 6 H, 2×N-C$\underline{H_3}$), 2.78-2.45 (m, 2 H, 2×=C-C$\underline{H_a}$), 2.23-1.94 (m, 3 H, C$\underline{H}$+2×=C-C$\underline{H_b}$), 0.83 (d, J = 6.3 Hz, 3 H, CH-C$\underline{H_3}$).
^{13}C-NMR (50 MHz, D$_2$O):	δ (ppm) = 192.6 (=C-$\underline{C}$=O), 178.4 (O-$\underline{C}$=O), 150.2 (ar-C4+C4'), 138.9 (2×$\underline{C}$=CH), 133.2 (2×C=$\underline{C}$H), 131.2 (ar-C2+C6+ C2'+C6'), 123.0 (ar-C1+C1'), 111.4 (ar-C3+C5+C3'+C5'), 56.1 (N-$\underline{C}$H2), 38.4 (CH$_2$-$\underline{C}$H-CH$_2$+2×N-$\underline{C}$H$_3$), 28.6 (2×=C-$\underline{C}$H$_2$), 20.9 ($\underline{C}$H$_3$-CH).
Anal.	[calculated for C$_{27}$H$_{28}$N$_2$O$_5$Na$_2$]: C, 64.03; H, 5.57; N, 5.53; [found:] C, 64.31; H, 5.33; N, 5.47.

4   Multiphoton grafting with commercial arylazides

4.4.3   Postmodification of the patterned matrix via CuAAC click reaction

4.4.3.1   Synthesis of 2,4-dibromo-1-(prop-2-yn-1-yloxy)benzene (15)

[251.90]   [118.96]   [289.95]
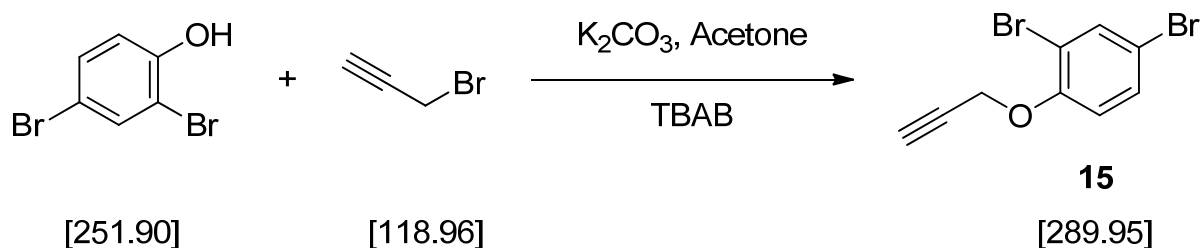
Reagents	MW [g/mol]	[g]	[mL]	[mmol]	[eq.]
2,4-dibromophenol	251.90	2.51		10	1
3-bromoprop-1-yne	118.96	1.79		15	1.5
K_2CO_3	105.99	1.06		10	1
TBAB	322.37	0.05		0.15	0.015
acetone			50		

Procedure

Anhydrous K_2CO_3 (1.06 g, 10 mmol) was added to a solution of 2,4-dibromophenol (2.51 g, 10 mmol), 3-bromoprop-1-yne (1.79 g, 15 mmol) and tetra- n-butylammonium bromide (50 mg, 0.15 mmol) in acetone (50 mL). The suspension was stirred at 60 °C under an argon atmosphere until the 2,4-dibromophenol was completely consumed (GC-MS analysis). The mixture was filtered off, the solid residue was washed with ethyl acetate and the volatile compounds were removed in vacuum. The crude product was dissolved in ethyl acetate and washed with water and brine. The organic layer was dried over sodium sulfate, filtered and concentrated. The purification by column chromatography (PE: EE = 8:1) yielded 2.67 g of product as a light yellow solid.

Yield
92 % of theory

Analysis

TLC (PE:EE = 8:1):	$R_f = 0.36$
m.p:	69-71 °C

^{1}H-NMR (200 MHz, CDCl$_3$): δ (ppm) = 7.80 (d, J = 2.2 Hz, 1 H, ar-H6), 7.56 (dd, J = 2.2, 8.9 Hz, 1 H, ar-H4), 7.14 (d, J = 9.0 Hz, 1 H, ar-H3), 4.91 (d, J = 2.2 Hz, 2 H, O-C$\underline{H}_2$), 3.64 (t, J = 2.1 Hz, 1 H, C≡C$\underline{H}$).

^{13}C NMR (50 MHz, CDCl$_3$): δ (ppm) = 153.0 (ar-C2), 134.8 (ar-C6), 131.4 (ar-C4), 115.9 (ar-C3), 113.0 (ar-C1), 112.2 (ar-C5), 79.1 ($\underline{C}$≡CH), 78.3 (C≡$\underline{C}$H), 56.7 (O-$\underline{C}$H$_2$).

GS-MS analysis: (m/z) = 291.91, 289.91, 260.96, 250.95, 222.95, 211.05, 182.01, 130.12, 102.13, 74.07, 63.11.

4.4.3.2   Model CuAAC click reaction[258]
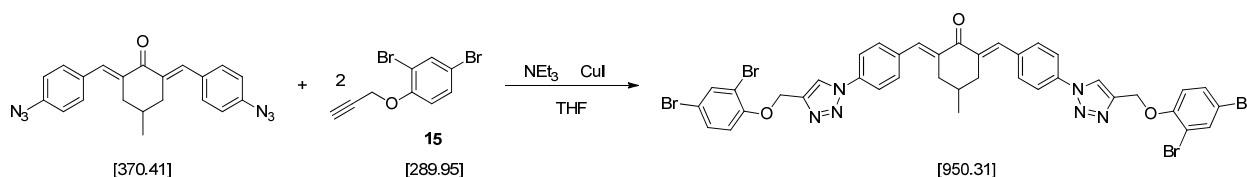
Reagents	MW [g/mol]	[mg]	[mL]	[mmol]	[eq.]
azide **BAC-M**	370.74	46.25		0.125	1
alkyne **15**	289.95	72.25		0.25	2
CuI	190.45	19		0.1	0.8
degassed Et$_3$N			0.1		
degassed THF			5		

Procedure

72.25 mg (0.25 mmol) of the alkyne **15** were dissolved in 5 mL of degassed THF in a brown glass vial. To the solution, 46.25 mg (0.125 mmol) of the azide **BAC-M**, 19 mg (0.1 mmol) of CuI and 0.1 mL degassed triethylamine were added. The reaction was stirred in dark at room temperature. After 24h, the orange precipitates were collected and washed with water, acetone and chloroform, respectively, before the ^{1}H-NMR measurement.

4.4.3.3   **Postmodification of grafted pellet via CuAAC click reaction**[258]
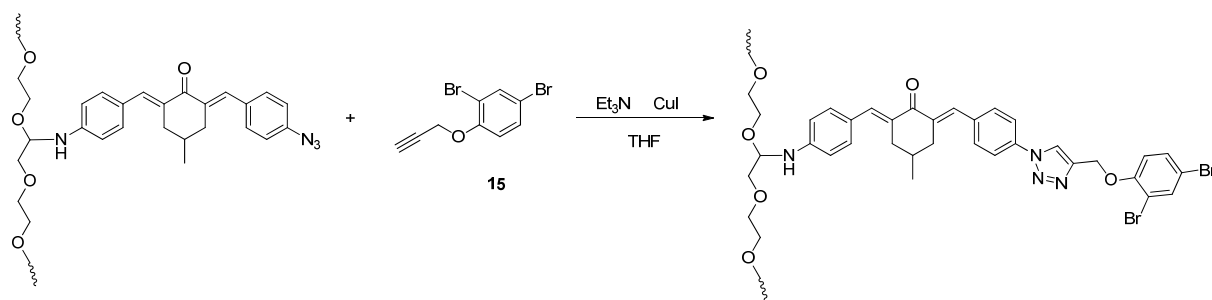
Reagents	MW [g/mol]	[mg]	[mL]	[mmol]	[eq.]
PEGDa pettlet					
alkyne **15**	289.95	20		0.068	
CuI	190.45	10		0.052	
degassed Et₃N			0.1		
degassed THF			3		

Procedure

20 mg (0.068 mmol) of the alkyne **15** were dissolved in 3 mL of degassed THF in a brown glass vial. To the solution, laser-grafted pellets, 10 mg (0.052 mmol) of CuI and 0.1 mL of degassed triethylamine were added. The vial was placed on a rotation mixer after being sealed and the reaction was carried out at room temperature under argon for 12 h. Afterwards, the pellet was removed, washed with fresh DMF several times to remove the residual alkyne **16** and dried under vacuum before the EDX measurement.

5   AFA series for photografting under 2PA

5.2   Synthesis of AFA series compounds

5.2.1   Synthesis 4-azido-2,3,5,6-tetrafluorobenzaldehyde (16)[225c]

	[196.07]		[65.01]		[219.10]	

Reagents	MW [g/mol]	[g]	[mL]	[mmol]	[eq.]
NaN₃	196.07	0.31		4.6	1.1
pentafluorobenzaldehyde	65.01	0.88		4.3	1
acetone			8		
water			3		

Procedure

0.31 g (4.6 mmol) of NaN_3 and 0.88 g (4.3 mmol) of pentafluorobenzaldehyde were dissolved in a mixture of acetone (8 mL) and water (3 mL). The solution was refluxed for 8 h, then cooled to room temperature, diluted with water (10 mL) and extracted by ether (3 × 10 mL). The extract was dried over $MgSO_4$ and evaporated. Purification by sublimation (25 °C/0.1 mm) yielded 0.78 g of product as white crystalline.

Yield

80 % of theory (96% of lit[225c])

Analysis

m.p:	43-44 °C (lit [264]: 44-45 °C).
^{1}H-NMR (200 MHz, CDCl₃):	δ (ppm) = 10.24 (s, 1H, CHO).
^{19}F NMR (376MHz, CDCl₃):	δ (ppm) = -144.9 (m, 2F), -150.9 (m, 2F)
IR (cm⁻¹):	2118 (-N₃), 1707, 1644, 1480, 1399, 1234, 1092, 982.

5.2.2   Synthesis of N,N-diallyl-benzene-1,4-diamine (18)

5.2.2.1   Synthesis of diallyl-(4-nitro-phenyl)-amine (17)[267]

| [138.12] | [120.98] | [218.25] |
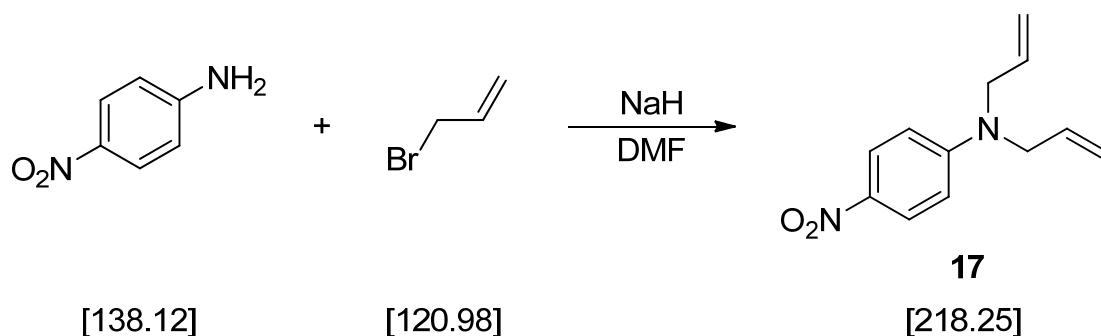
Reagents	MW [g/mol]	[g]	[mL]	[mmol]	[eq.]
4-nitro-phenylamine	138.12	1.38		10	1
sodium hydride	24	1.74		40	4
3-bromo-propene	120.98	3.62		30	3
dry DMD			25+5		
NH$_4$Cl			50		

Procedure

1.74 g (55% in mineral oil) of sodium hydride (40 mmol) was suspended into 25 mL of dry DMF under stirring at 0 °C, followed by addition of 1.38 mg of 4-nitro-phenylamine (10 mmol) dissolved in 5 mL of dry DMF. The mixture was kept stirring until no bubble formed and then 3.62 g of 3-bromo-propene (30 mmol) was added dropwise. The reaction was warmed up to room temperature and monitored by TLC. After the entire conversion of 4-nitro-phenylamine, 50 mL of the aqueous solution of NH$_4$Cl was slowly added to quench the reaction. The mixture was extracted with dichloromethane (2 × 100 mL). The combined organic layers were dried over Na$_2$SO$_4$, filtered, and concentrated. Purification by column chromatography (PE:EE = 20:1) to yield 1.74 g of products as orange oil.

Yield

80 % of theory

Analysis

TLC (PE:EE = 20:1):	$R_f = 0.43$
^{1}H NMR (200 MHz, CDCl$_3$)	δ (ppm) = 8.10 (d, J = 9.39 Hz, 2 H, ar-H2+H6), 6.63 (d, J = 9.39 Hz, 2 H, ar-H3+H5), 5.70-6.14 (m, 2 H, 2×C$\underline{H}$=CH$_2$), 4.87-5.51 (m, 4 H, 2×CH=C$\underline{H_2}$), 3.76-4.32 (m, 4 H, 2×N-C$\underline{H_2}$)
^{13}C NMR (50 MHz, CDCl$_3$):	δ (ppm) = 153.1 (ar-C4), 137.4 (ar-C1), 131.5 (2×$\underline{C}$H=CH$_2$), 124.7 (ar-C2+C6), 116.5 (2×CH=$\underline{C}$H$_2$), 110.1 (ar-C3+C5), 52.9 (2×N-$\underline{C}$H$_2$).
GC-MS:	218.19, 189.16, 157.22, 145.20, 117.21, 103.22, 77.12.

5.2.2.2   Synthesis of N,N-diallyl-benzene-1,4-diamine (18)[270]
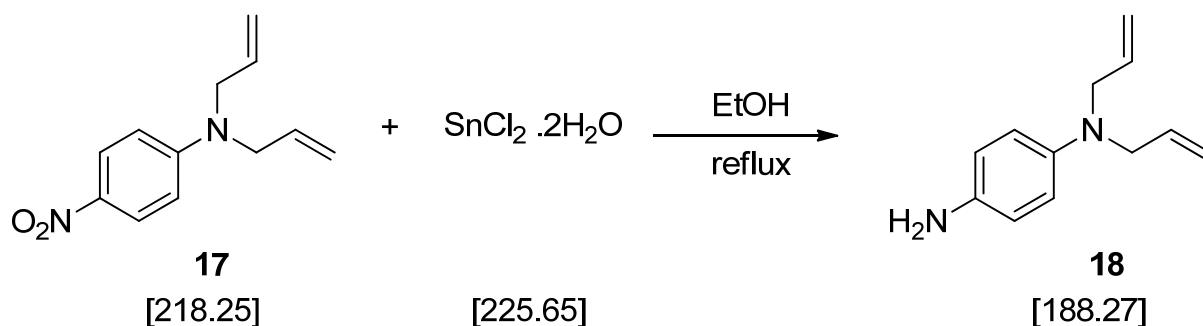
Reagents	MW [g/mol]	[g]	[mL]	[mmol]	[eq.]
nitro compound **17**	218.25	0.2		0.92	1
tin (II) chloride dihydrate	225.65	1.03		4.6	5
EtOH			30		

Procedure

0.2 g (0.92 mmol) of the nitro compound **17** and 1.03 g (4.6 mmol) of tin (II) chloride dihydrate were dissolved in 30 mL of EtOH. The mixture was stirred and heated under reflux and monitored by TLC until the entire conversion of **17**. The cooled reaction mixture was neutralized by the addition of 5 M NaOH. The precipitate was removed by centrifugation and the solution was extracted with EtOAc (2 × 30 mL). The combined organics were washed with brine (50 mL) and dried over Na$_2$SO$_4$. The obtained brown

product was purified by chromatography (PE:DCM = 2:1) to give the product **18** as orange oil.

Yield

50% of theory (84% of lit[270])

Analysis

TLC (PE:DCM = 2:1):	R_f = 0.42
^{1}H-NMR (200 MHz, CDCl$_3$):	δ (ppm) = 6.64 (br. s, 4 H, ar-H), 5.95-5.76 (m, 2 H, 2×C$\underline{H}$=CH$_2$), 5.21-5.11 (m, 4 H, 2×CH=C$\underline{H_2}$), 3.82-3.71 (m, 4 H, 2×N-C$\underline{H_2}$). N$\underline{H_2}$ was not observed due to the high amount of water in CDCl$_3$.
^{13}C NMR (50 MHz, CDCl$_3$):	δ (ppm) = 142.5 (ar-C4), 137.2 (ar-C1), 134.8 (2×$\underline{C}$H=CH$_2$), 116.5 (2×CH=$\underline{C}$H$_2$), 115.4 (ar-C3+C5), 113.6 (ar-C2+C6), 53.9 (2×N-$\underline{C}$H$_2$).

5.2.3   Synthesis of N,N-diallyl-benzene-1,4-diamine (18)

5.2.3.1   **Synthesis of N-methyl-4-nitro-N-(prop-2-yn-1-yl)aniline (19)[271]**
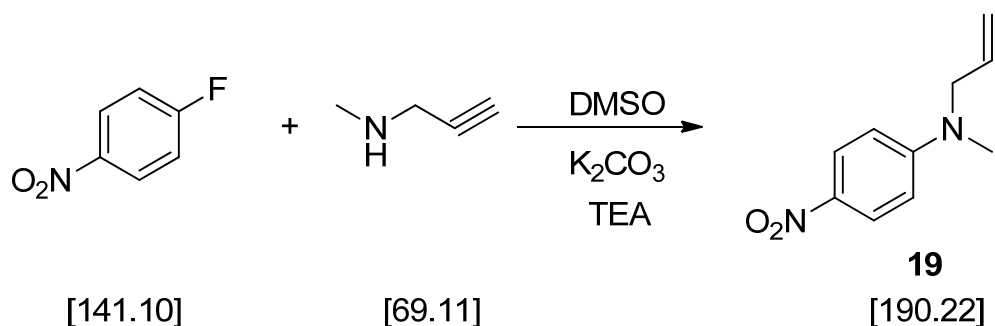
Reagents	MW [g/mol]	[g]	[mL]	[mmol]	[eq.]
4-fluoro-1-nitrobenzene	141.10	1.93		13.74	1
N-methylpropargylamine	69.11	0.95		13.74	1
potassium carbonate	138.21	2.27		16.48	1.2
triethylamine			1		
DMSO			20		

Procedure

1.93 g (13.74 mmol) of 4-fluoro-1-nitrobenzene, 0.95 g (13.74 mmol) of N-methylpropargylamine, 2.27 g (16.48 mmol) of potassium carbonate and 1 mL of triethylamine were dissolved in 20 mL of DMSO. The mixture is stirred overnight at 50 °C and then poured into 50 mL of cold water. The precipitate is collected by filtration and washed with water (3 × 50 mL) and 2-propanol (20 mL) to yield the product **19** as yellow solid.

Yield

75 % of theory (101% of lit[271])

Analysis

m.p:	93-95 °C.
^{1}H-NMR (200 MHz, CDCl$_3$):	δ (ppm) = 8.09 (d, J = 9.4 Hz, 2 H, ar-H2+H6), 6.68 (d, J = 9.4 Hz, 2 H, ar-H3+H5), 4.09 (d, J = 2.3 Hz, 2 H, N-C$\underline{H}_2$), 3.07 (s, 3 H, N-C$\underline{H}_3$), 2.20 (t, J = 2.3 Hz, 1 H, C≡C$\underline{H}$).
^{13}C NMR (50 MHz, CDCl$_3$):	δ (ppm) = 153.1 (ar-C4), 126.0 (ar-C1), 111.6 (ar-C2+C6), 110.0 (ar-C3+C5), 77.7 ($\underline{C}$≡CH), 72.8 (C≡$\underline{C}$H), 42.0 (N-$\underline{C}$H$_2$), 38.6 (N-$\underline{C}$H$_3$).

5.2.3.2   Synthesis of N^1-methyl-N^1-(prop-2-yn-1-yl)benzene-1,4-diamine (20)
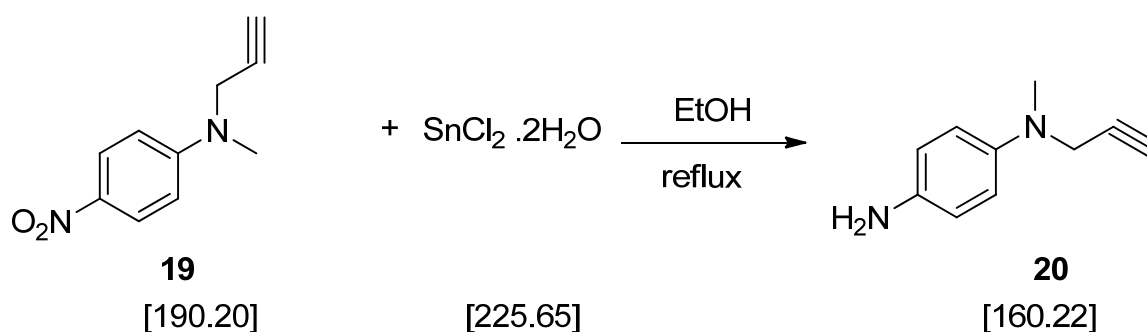
Reagents	MW [g/mol]	[g]	[mL]	[mmol]	[eq.]

nitro compound **19**	190.20	0.21		0.91	1
tin (II) chloride dihydrate	225.65	2.05		9.1	10
EtOH			30		

Procedure

0.21 g (0.91 mmol) of the nitro compound **19** and 2.05 g (9.1 mmol) of tin (II) chloride dehydrate were dissolved in 30 mL of EtOH. The mixture is stirred and heated under reflux for 21 h. The cooled reaction mixture was neutralized by the addition of 5 M NaOH. The precipitate was removed by centrifugation and the solution was extracted with EtOAc (2 × 30 mL). The combined organics were washed with brine (50 mL) and dried over Na_2SO_4. The brown product (116.4 mg, purity > 95% from NMR) was used for the next step without further purification.

Analysis

^{1}H-NMR (200 MHz, CDCl$_3$): δ = 6.81 (d, J = 9.4 Hz, 2 H, ar-H2+H6), 6.67 (d, J = 9.4 Hz, 2 H, ar-H3+H5), 3.95 (d, J = 2.2 Hz, 2 H, N-CH$_2$), 3.70-3.20 (bs, 2 H, NH$_2$), 2.87 (s, 3 H, N-CH$_3$), 2.18 (t, J = 2.2 Hz, 1 H, C≡CH).

^{13}C NMR (50 MHz, CDCl$_3$): δ = 142.5 (ar-C1), 139.4 (ar-C4), 117.5 (ar-C3+C5), 116.4 (ar-C2+C6), 79.5 (C≡CH), 72.4 (C≡CH), 44.2 (N-CH$_2$), 39.5 (N-CH$_3$).

5.2.4   Synthesis of novel fluoroaryl azides

5.2.4.1   Synthesis of N^1-(4-azido-2,3,5,6-tetrafluorobenzylidene)-N^4,N^4-dimethylbenzene-1,4-diamine (AFA)

16   **AFA**

[196.07]   [136.19]   [314.25]
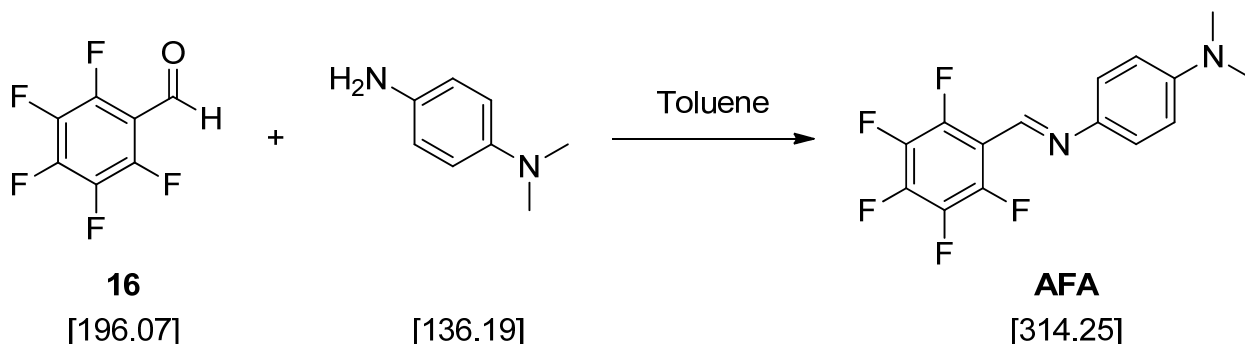
Reagents	MW [g/mol]	[mg]	[mL]	[mmol]	[eq.]
benzaldehyde **16**	196.07	196		1.0	1
N,N-dimethylbenzene-1,4-diamine	136.19	136		1.0	1
toluene			10		

Procedure

196 mg (1.0 mmol) of the benzaldehyde 16 and 136 mg (1.0 mmol) of N,N-dimethylbenzene-1,4-diamine were dissolved in 10 mL of dry toluene. The solution was stirred overnight under room temperature and then the solvent was evaporated under vacuum. The dark mixture was washed with cold dry acetone to yield 0.21 g of product as orange powder.

Yield

66 % of theory

Analysis

m.p: 141-143°C (decomposition).

^{1}H-NMR (200 MHz, CDCl$_3$):   δ (ppm) = 8.61 (s, 1 H, N=C$\underline{H}$), 7.31 (d, J = 9.0 Hz, 2 H, ar-H2+H6), 6.75 (d, J = 9.0 Hz, 2 H, ar-H3+H5), 3.02 (s, 6 H, 2×N-C$\underline{H_3}$).

^{13}C NMR (50 MHz, CDCl$_3$):   δ (ppm) = 150.4 (N=$\underline{C}$H), 146.9-141.0 (m, F-C), 139.8 (ar-C4), 122.7 (ar-C1), 112.4 (ar-C2+C6), 112.0 (ar-C3+C5), 40.5 (2×N-$\underline{C}$H$_3$). It is difficult to assign all the peaks due to the F-C coupling.

^{19}F NMR (376MHz, CDCl$_3$):   δ = -143.1 (m, 2F), -152.5 (m, 2F).

IR (cm^{-1}):   2112, 1616, 1591, 1562, 1512, 1471, 1342, 1222, 1008, 823.

Anal.   [calculated for C$_{15}$H$_{11}$F$_4$N$_5$]: C, 53.42; H, 3.29; N, 20.76; [found:] C, 53.18; H, 3.48; N, 20.53.

5.2.4.2   Synthesis of N,N-diallyl-N'-(4-azido-2,3,5,6-tetrafluoro-benzylidene)-benzene-1,4-diamine (AFA-2)

	16	**+**	**18**	Toluene →	**AFA-2**
	[219.10]		[188.27]		[389.35]
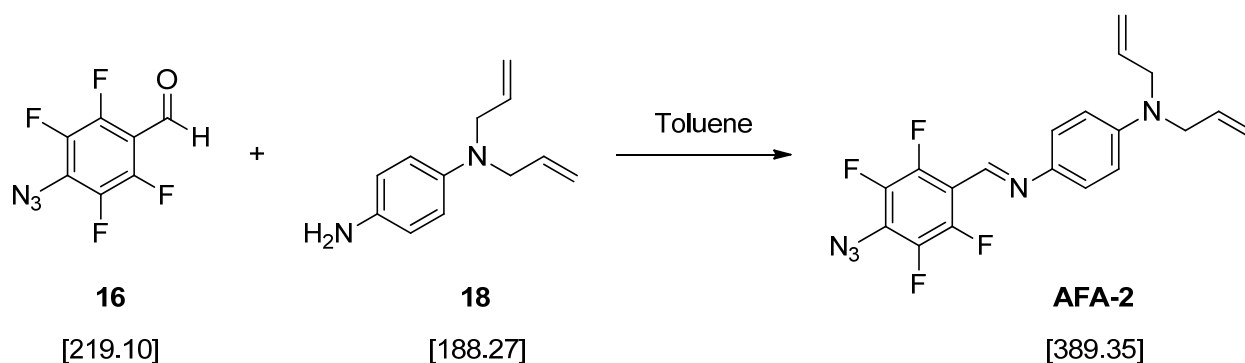
Reagents	MW [g/mol]	[mg]	[mL]	[mmol]	[eq.]
benzaldehyde **16**	219.10	109.5		0.52	1
diamine **18**	188.27	98		0.52	1
dry toluene			10		

Procedure

109.5 mg of 4-azido-2,3,5,6-tetrafluorobenzaldehyde (0.52 mmol) and 98 mg of N^1-methyl-N^1-(prop-2-yn-1-yl)benzene-1,4-diamine (0.52 mmol) were dissolved in 10 mL of dry toluene. The solution was stirred overnight under room temperature and then the solvent was evaporated under vacuum. The dark mixture was washed with cold dry ether to yield 107 mg of product as yellow powder.

Yield

53 % of theory

Analysis

m.p:	103-105 °C (decomposed)
^{1}H-NMR (200 MHz, CDCl$_3$):	δ (ppm) = 8.59 (s, 1 H, N=C$\underline{H}$), 7.27 (d, J = 9.00 Hz, 2 H, ar-H2+H6), 6.72 (d, J = 9.00 Hz, 2 H, ar-H3+H5), 5.97-5.79 (m, 2 H, 2×C$\underline{H}$=CH$_2$), 5.23-5.14 (m, 4 H, 2×CH=C$\underline{H_2}$), 4.00 - 3.97 (m, 4 H, 2×N-C$\underline{H_2}$).
^{13}C NMR (50 MHz, CDCl$_3$):	δ (ppm) = 148.7 (N=$\underline{C}$H), 143.7-142.6 (m, F-C), 139.8 (ar-C4), 133.4 (2×$\underline{C}$H≡CH$_2$), 122.7 (ar-C1), 116.2 (2×CH≡$\underline{C}$H$_2$), 112.4 (ar-C2+C6+C3+C5), 52.8 (2×N-

<u>CH</u>$_2$). It is difficult to assign all the peaks due to the F-C coupling.

^{19}F NMR (376MHz, CDCl$_3$):	δ = -143.1 (m, 2F), -152.5 (m, 2F).
IR (cm^{-1}):	3084, 2896, 2117, 1643, 1559, 1478, 1401, 1165, 985, 855.
Anal.	[calculated for C$_{57}$H$_{47}$F$_{12}$N$_{15}$O]: C, 58.61; H, 3.88; N, 17.99; [found:] C, ; H, ; N, .

5.2.4.3 Synthesis of (E)-N^1-(4-azido-2,3,5,6-tetrafluorobenzylidene)-N^4-methyl-N^4-(prop-2-yn-1-yl)benzene-1,4-diamine (AFA-3)

	16	**20**	**AFA-3**
	[219.10]	[160.22]	[361.30]
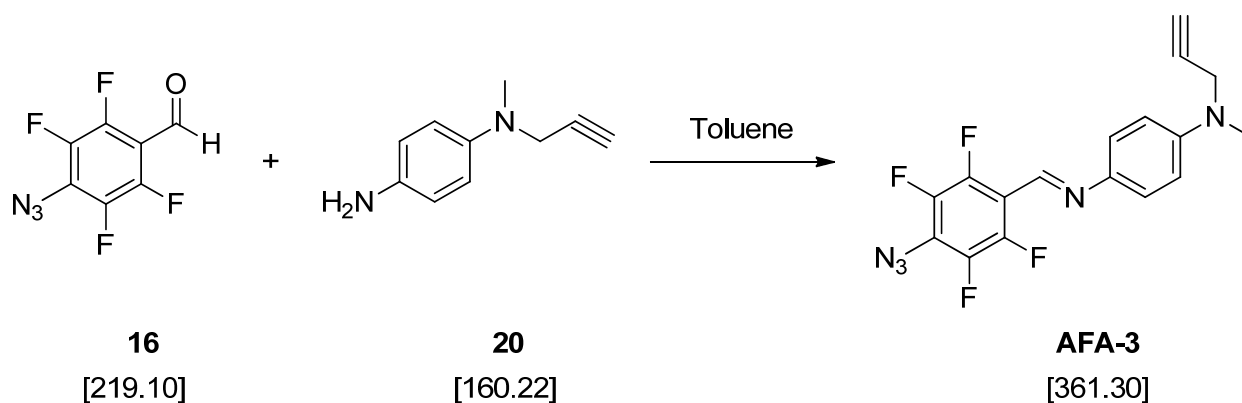
Reagents	MW [g/mol]	[mg]	[mL]	[mmol]	[eq.]
benzaldehyde **16**	219.10	109		0.52	1
diamine **20**	160.22	83		0.52	1
dry toluene			10		

Procedure

109 mg (0.52 mmol) of the benzaldehyde **16** and 83 mg (0.52 mmol) of the diamine **20** were dissolved in 10 mL of dry toluene. The solution was stirred overnight under room temperature and then the solvent was evaporated under vacuum. The dark mixture was washed with dry ether to yield 93 mg of product as yellow powder.

Yield

50 % of theory

Analysis

m.p:	127-129 °C (decomposition).
^{1}H-NMR (200 MHz, CDCl$_3$):	δ = 8.54 (s, 1 H, N=C$\underline{H}$), 7.28 (d, J = 9.0 Hz, 2 H, ar-H2+H6), 6.86 (d, J = 9.0 Hz, 2 H, ar-H3+H5), 4.04 (d, J = 2.2 Hz, 2 H, N-C$\underline{H}_2$), 2.98 (s, 3 H, N-C$\underline{H}_3$), 2.15 (t, J = 2.2 Hz, 1 H, C≡C$\underline{H}$).
^{13}C NMR (50 MHz, CDCl$_3$):	δ = 148.8 (N=$\underline{C}$H), 144.2-144.1 (m, F-C), 143.4-143.0 (m, F-C), 141.5 (ar-C4), 138.4-137.9 (m, F-C), 122.6 (ar-C1), 114.2 (ar-C2+C6), 112.3-111.8 (m, F-C), 78.9 ($\underline{C}$≡CH), 72.2 (C≡$\underline{C}$H), 42.4 (N-$\underline{C}$H$_2$), 38.7 (N-$\underline{C}$H$_3$).It is difficult to assign all the peaks due to the F-C coupling.
^{19}F NMR (376MHz, CDCl$_3$):	δ = -142.9 (m, 2F), -152.4 (m, 2F).
IR (cm^{-1}):	3254, 2182, 2110, 1618, 1594, 1568, 1514, 1496, 1482, 1412, 1360, 1242, 1000, 821.
Anal.	[calculated for C$_{17}$H$_{11}$F$_4$N$_5$]: C, 56.51; H, 3.07; N, 19.38; [found:] C, 56.33; H, 2.97; N, 19.55.

5.6 Post modification of AFA-3
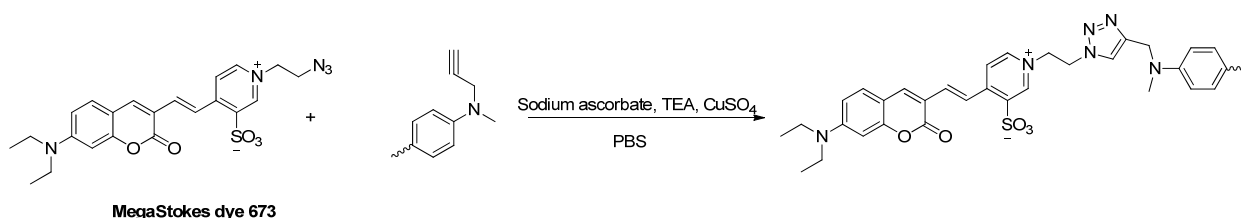
MegaStokes dye 673

Reagents	MW [g/mol]	[mg]	[mL]	[μmol]	[eq.]
PEGDa pettlet					
Mega Stokes dye	483.54	1		2.13	1
Sodium ascorbate	198.1	2.47		12.46	5.8
CuSO$_4$	159.62	0.99		6.20	2.9
Et$_3$N			1 drop		
PBS			2		

Procedure

1 mg (2.13 µmol) of MegaStokes dye 673 was dissolved in 2 mL of PBS solution in a brown glass vial. To the solution, laser-grafted pellets, 0.99 mg (6.20 µmol) of $CuSO_4$, 2.47 mg of sodium ascorbate (12.46 µmol) and 1drop of triethylamine were added. The vial was placed on a rotation mixer after being sealed and the reaction was carried out at room temperature in dark for 12 h. Afterwards, the pellet was removed, washed several times with fresh PBS and DMF to remove residual MegaStokes dye 673 and immersed into DMF solution for LSM observation.

Conclusion

Two-photon excitation provides the possibility of the activation of chemical or physical processes with high spatial resolution in 3D. To develop two-photon absorption (2PA) active organic materials is essential to realize the desired functions. In the present work, a series of novel 2PA active organic compounds have been designed and synthesized for specific applications. The first part of the thesis focuses on the novel 2PA photoinitiators (2PIs) used for two-photon induced photopolymerization (2PP), a versatile technique for precise 3D microfabrications. High initiation efficiency is always the most important character for an efficient 2PI. Based on a potent lead structure 1,5-bis(4-(*N,N*-dibutylamino) phenyl)penta-1,4-diyn-3-one, several aromatic ketone-based 2PIs containing triple bonds and dialkylamino groups were synthesized via Sonogashira coupling reactions.
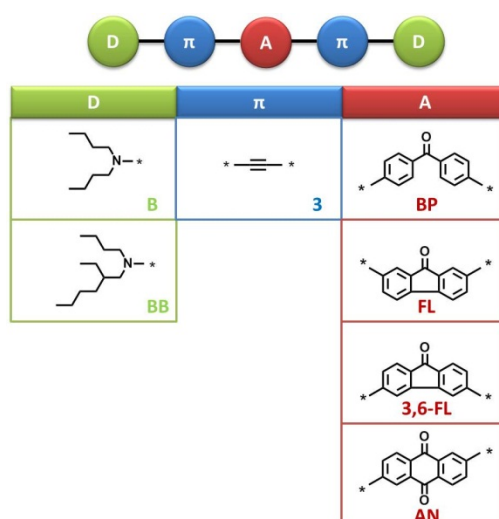
Due to the long conjugation length and good coplanarity, the evaluated initiators show large two-photon cross section (σ^{2PA}) values, with strongly solvent dependent fluorescence lifetimes and quantum yields. With suitably strong absorption at the desired wavelength, the 2-,7-substituted fluorenone-based 2PI **B3FL** has the highest σ^{2PA} value (440 GM at 800 nm) among the studied 2PIs. In terms of the two-photon polymerization structuring test (2PP), 2PIs based on fluorenone as electron withdrawing functional group with good coplanarity show broader processing windows than those possessing benzophenone or anthraquinone moieties. Significantly better results were obtained compared to commercially available initiators and also a slight improvement in relative to well-known highly active initiators **R1** from the literature. The introduction of

branched-alkyl chains significantly improve the solubility of the fluorenone-based PIs, but also slightly decrease the processing windows due to the lower migration ability of the 2PI with the increase of its molecular size. **B3FL** turns out to be the best performing initiator among the presented initiators, having the broadest ideal structuring process windows in 2PP tests and good solubility in the resin.
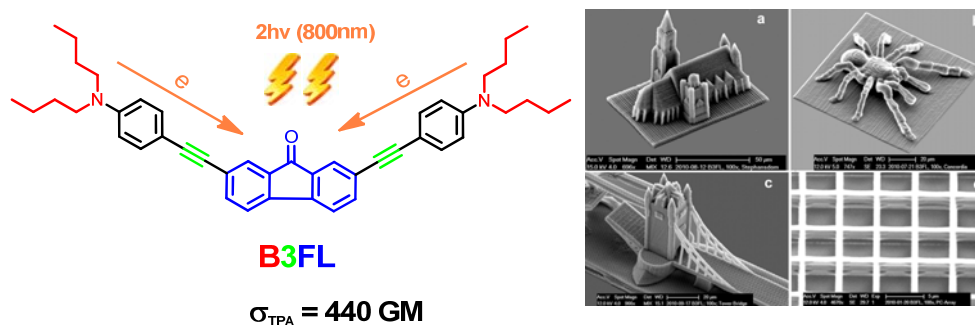
Two novel evaluation methods based on FTIR microscopy and nanoindentation were developed to study the double bond conversion (DBC) and the Young's modulus of the microstructures, respectively. Although **B3FL** has a better performance than **R1** in 2PP structuring tests, the DBC of formulation with **R1** increases faster than that of formulation with **B3FL** from the FTIR-measurements. Moreover, the microstructures fabricated with **R1** as initiator have higher Young's modulus and thus better mechanical property than the ones fabricated with **B3FL** from the nanoindentation measurements.

Beside initiation efficiency of 2PIs, the ease and cost of preparation are also critical factors from practical aspect. To overcome the problem of the reported 2PIs derived from the complicated syntheses and expensive catalysts, a series of linear and cyclic benzylidene ketone-based 2PIs containing double bonds and dialkylamino groups were synthesized in one step via classical aldol condensation reactions. The systematic evaluation of structure-property relationships via quantum chemical calculations combined with experimental tests confirms the significant central ring effects on the photophysical and photochemical properties. The cyclohexanone-based initiators show much weaker fluorescence emission and shorter fluorescence lifetime than their acetone and cyclopentanone counterparts. With good coplanarity and a suitably strong absorption at the desired wavelength, cyclopentanone-based 2PI **M2CPK** possesses the largest σ^{2PA} of 466 GM at 800 nm in the z-scan measurement, while cyclohexanone-based 2PIs exhibited reduced σ^{2PA} due to the non-planarity of the six-membered rings, which leads to a decreasing degree of conjugation. Surprisingly, the 4-methylcyclohexanone-based 2PI

M2CMK with the smallest σ^{2PA} among the investigated initiators, displays much broader ideal processing windows than other benzylidene ketone PIs and the reference in 2PP tests. The activity of **M2CMK** in 2PP tests is as high as that of **B3FL**, but the preparation of **M2CMK** is much simpler and more economical. A writing speed as high as 80 mm/s was obtained for microfabrication of complex 3D structures with acrylate-based formulations containing **M2CMK** as photoinitiator. The straightforward synthetic route combined with high 2PA initiation efficiency of these 2PIs shows great potential for commercialization.
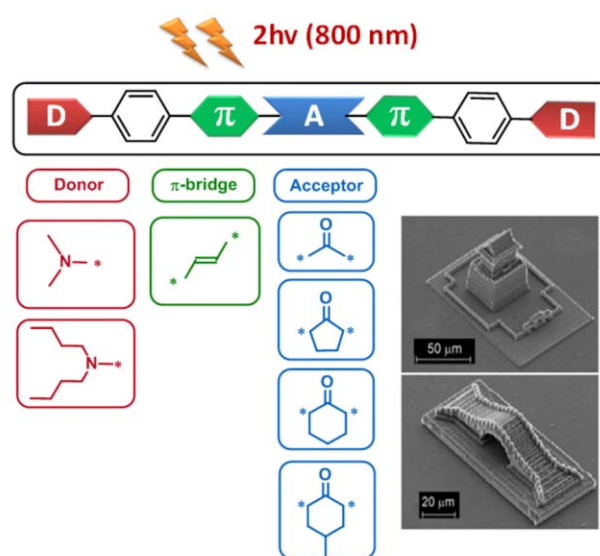
Based on the efficient core structures of cyclic benzylidene ketone, carboxylic acid sodium salts as water-borne functionalities were incorporated in order to expand the application range of 2PP to biofabrication. Due to the long conjugation length and the presence of strong electron donors and acceptors, the investigated water-soluble 2PIs exhibit moderate σ^{2PA} ranging from 163 GM to 201 GM at 800 nm in water. The σ^{2PA} values obtained under aqueous condition are reduced compared to those of their hydrophobic analogues measured in organic solvents. In 2PP tests, all novel initiators exhibited large ideal processing windows for hydrophilic photopolymers with up to 50 wt% of water. The ideal processing windows of the cyclohexanone initiators are broader than those of cyclopentanone initiators. Impressively, a writing speed as high as 100 mm/s was obtained for precise microfabrication of hydrogels.

Significantly improved initiation efficiency can be obtained for **T2CK** with tetrabutylammonium cations as counter-ion rather than sodium cations as in other investigated hydrophilic 2PIs. Enhanced performance of **T2CK** may derive from 2PA induced decarboxylation, which can effectively prevent back electron transfer and ensure the formation of active radicals in high quantum yields and thus efficient polymerization.

The dark cytotoxicity of 4-methylcyclohexanone-based initiators significantly increases with increasing incubation time, especially for outgrowth endothelial cells (OECs). The cyclopentanone-based initiator yields the highest cytocompatibility comparable to Irgacure 2959 for both OECs and MG63 cell lines.

The second part of the thesis concerned on the novel arylazide used for multi-photon induced photografting (MPG), a powerful tool for 3D site-specific functionalization. As a proof-of-concept, commercial aromatic azide **BAC-M** with long conjugation length was selected and successfully grafted within the 3D PEGDa-based matrix under three-photon excitation. Since 3PA induced photografting occurs only within the tiny laser focal spot, site-specific functionalization with high spatial resolution down to 4 μm in 3D was obtained. The presented grafting method with arylazides is universal and is applicable to a wide variety of matrices containing C–H or N–H bonds. The density of immobilization can be spatially controlled by simply altering the irradiation exposure time or laser intensity during the photopatterning process. The post modification was carried out via copper catalyzed azide-alkyne click reaction (CuAAC) between the residual azide groups on the matrices and Br-containing alkyne. The successful immobilization to the patterned areas was verified by Energy-dispersive X-ray spectroscopy (EDX) screening of the Br content on the grafted areas. Such developed 3D site-specific functionalization method is simple and versatile, which reveals great potential applications in microarray-based proteome analysis, biosensors, cell patterning, and drug screening.
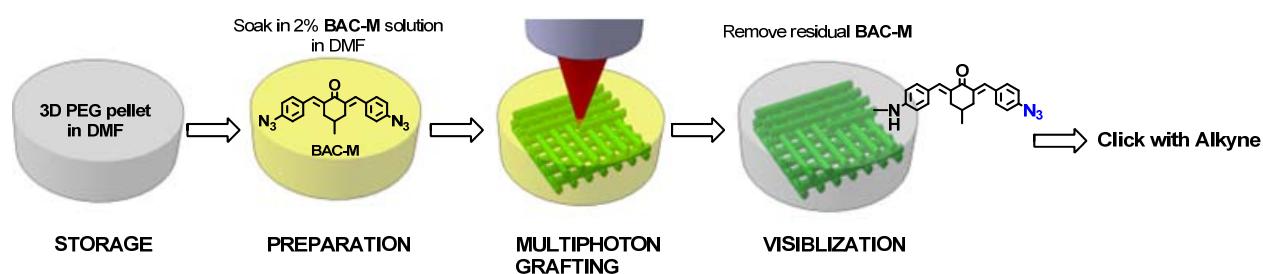
Due to the lack of efficient electron donor groups, the activation of **BAC-M** needs to be realized under 3PA, which means more laser energies are needed compared to the excitation under 2PA. In order to enhance the grafting efficiency and reduce the required energies, we designed a series of novel 2PA active fluoroaryl azides containing ''push-pull'' structures and developed a straightforward strategy for the preparation. The simple synthesis provides the possibility to incorporate not only azides group into the 2PA chromophore, but also other functionalities, such as alkyne and alkene groups, for the postmodification after photografting.

2PA grafting agent **AFA**, containing a C=N bond as a π bridge, N,N-dimethylaniline as a donor and fluorinated aromatic azide as an acceptor, exhibits a large σ^{2PA} of 178 GM at 800 nm. The introduction of terminal functional groups as in **AFA-2** and **AFA-3** does not significantly alter the electronic structure of the whole molecules and the σ^{2PA} values nearly remain unchanged. Comparison between the **AFA** and **BAC-M** demonstrated that the intensity required to induce the grafting reactions in **AFA** is a few times lower than for **BAC-M**. As a consequence the **AFA** exhibits larger processing window and supports higher writing speed in photografting process. However, the patterning resolution of **BAC-M** is higher than that of **AFA** due to the more confined excited area derived from 3PA interaction nature. When using **AFA-3** with a terminal alkyne moiety as 2PA photografting agent, 3D ''clickable'' micropatterns with a lateral resolution down to 3.6 μm within a PEGDa-matrix was obtained. The generated grafting patterns well meet the requirement of stability for various bioapplications. The successful modification via 3D

CuAAC click reaction was confirmed by the localized conjugation of the azide-fluorophores onto the ''clickable'' covalently attached alkyne moieties.
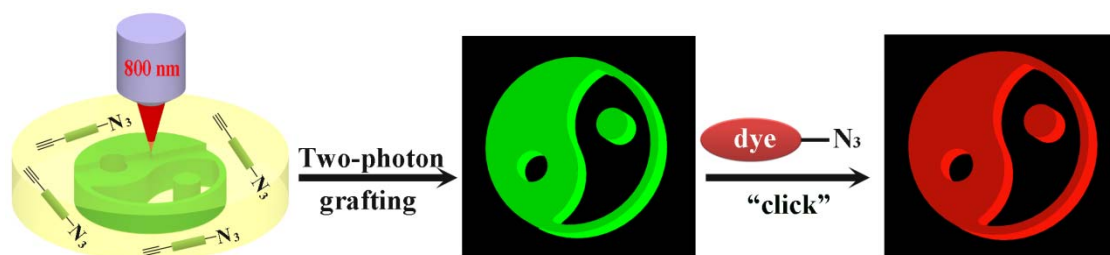
Technical Equipment & Characterization Methods

Chemicals

All reagents were purchased from Sigma-Aldrich, Fluka, TCI or ABCR and were used without further purification. The solvents were dried and purified by standard laboratory methods or were dried over Al_2O_3 cartridges. Trimethylolpropane triacrylate (**TTA**, Genomer 1330) and ethoxylated-(20/3)-trimethylolpropane triacrylate (**ETA**, Sartomer 415) were received as a gift from Rahn and Sartomer, respectively. Petroleum ether (PE) refers to the fraction boiling in the range 40-60 °C. (Flash) column chromatography was performed with conventional techniques on VWR silica gel 60 (0.040–0.063 mm particle size). Aluminum backed silica gel plates were used for TLC analyses.

Mode of practice for photosensitive compounds

The preparation and analysis of the photosensitive compounds and formulations was conducted in a yellow light lab. This laboratory was placed in a window-less room to avoid admittance of day light. Adhesive foils of the company IFOHA (article nr. 11356, melon yellow) were used to cover fluorescent lamps.

Thin layer chromatography (TLC) analysis

Thin layer chromatography analysis was performed on silica gel 60 F_{254} aluminium sheets from Merck.

Melting points (m.p.) analysis

Melting points were determined either with a "Zeiss Axioskop" microscope equipped with a heating device from Leitz. Melting points are not corrected or by thermal differential scanning calorimetry experiments on a Shimadzu DSC50 with a heating rate of 5°C/min under air.

Nuclear magnetic resonance (NMR) spectroscopy

^{1}H-NMR (200 MHz) and ^{13}C-NMR (50 MHz) spectra were measured with a BRUKER AC-E 200 FT-NMR-spectrometer. The chemical shift (s = singlet, bs = broad singlet, d = doublet, t = triplet, m = multiplet) is displayed in ppm using the non deuterated solvent as internal standard. Solvents with a grade of deuteration of at least 99.5 % were used. The spectra were calibrated using the chemicals shifts of the deuterated solvents according to H. Gottlieb *et al.*[248]

Gas-chromatography mass-spectroscopy (GC-MS) measurements

GC-MS runs were performed on a Thermo Scientific DSQ II using a BGB 5 column (l = 30 m, d = 0.32 mm, 1.0 µm film; achiral) with the following standard temperature method (injection volume: 1 µL): 3 min at 80°C, 20°C/min until 280°C, 2 min at 280°C. MS spectra were recorded using EI ionization (70 eV) and a quadrupole analyzer. For compounds with a very low or high boiling point the method was adjusted to obtain appropriate results.

Fourier transformed-infrared (FTIR) spectroscopy

FTIR measurements were carried out on a Biorad FTS 135 spectrophotometer with a Golden Gate MkII diamond ATR equipment (L.O.T.).

Elemental analysis (EA)

EA tests were performed at the microanalytic lab of the Department of Physical Chemistry of the University of Vienna under the supervision of Mag. J. Theiner.

UV-vis spectroscopy

Absorption spectra were recorded on a Cary 50 absorption spectrometer. Emission spectra and excitation anisotropy spectra were obtained on a Cary Eclipse at a controlled temperature of 20°C. Absorption and emission spectra were baseline corrected using the pure solvent. Absorption spectra were obtained on samples with a maximal absorbance of approximately 1, while the maximal absorbance for the emission spectra did not exceed 0.15. The emission spectra were corrected for the wavelength sensitivity of the apparatus using a set of fluorescence standards.[283] Emission quantum yields were obtained using Coumarin 314 in ethanol as a secondary emission standard (Φ_{em} = 0.86)[284] and using the following equation[285]

$$\Phi_s = \frac{\int I_s(\lambda)\, d\lambda}{\int I_r(\lambda)\, d\lambda} \frac{1 - 10^{-A_r}}{1 - 10^{-A_s}} \frac{n_s^2}{n_r^2} \Phi_r$$

where Φ_x is the fluorescence quantum yield of the sample (s) and reference (r), $I_x(\lambda)$ denotes the corresponding fluorescence spectra. A_x is the absorbance at the excitation wavelength and n_x denotes the refractive index of the sample (s) and reference (r) solution.

Fluorescence lifetimes were measured on a home-built time-correlated single photon counting device using either a 400 or 470 nm laser diode (PicoQuant) as excitation source. The time-resolution, as judged from the full width at half maximum of the instrument response function, was approximately 200 ps.s.

Open aperture z-scan devices & tests[150]

A Ti:sapphire laser (Femtopower Compact Pro) was used for the open aperture z-scan measurement to determine MPA. The Laser beam diameter is 15 mm and the shortest pulse width is 25. The central wavelength of the laser beam is 798 nm with the bandwidth of 44 nm and the beam quality factor of 2.2. Some key components for z-scan measurement are shown in **Fig 86.**

1: Refrence Diode   4: Translation Stage
2: Beam Spliter   5: Collecting Lens
3: Focusing Lens   6: Detecting Diode

Fig 86 Scheme of the open aperture z-scan analysis[150]

A large 5 cm diameter beam splitter (**2**) splits the output laser beam into two parts with fraction of 1/3 and 2/3. The less intense part is directed towards the reference diode (1 cm² Si) (**1**) and the more intense part propagates straightly through the focusing lens (**3**) (plano-convex lens - Thorlabs, BK7 B-coated, f = 175 mm, d = 25.4 mm) and then through the sample. It should be noticed that the Rayleigh range, which is proportional to the focal length square of the focusing lens, must be larger than the thickness of the sample. For liquid samples like dyes or photoinitiator solutions, a 0.2 mm thick one-time flow cell (170.700 QS from HELLMA Company) connected to a syringe pump (NE-300 from SYRINGPUMP) providing a wide range of flow rates was used. The cell was mounted on a translation stage (**4**) with a stepper motor (DC-Motor model MFA-CC from Newport Company), which allows the movement of the sample

up to 25 mm along the beam propagation direction through the beam focus in minimum steps of 50 nm. The motor can be controlled by computer exploiting a Lab VIEW program. A collecting lens (**5**) with a large diameter and short focal length (50 mm diameter and 60 mm focal length) was used to ensure the entire energy transmitted through the sample was collected and directed toward the detecting diode (**6**) to be measured. The signals at the diodes were recorded with a two-channel PC Oscilloscope (model: Picoscope3204 from Picotech). A self-programmed computer software analysed the intensity of individual laser pulses (including averaging over several laser shots) and also handled the movement of the translation stage as well as the entire data acquisition process (LabView).

Rhodamine B in MeOH was used as reference to verify the reliability of the experimental setup. All investigated compounds were prepared as 1.0×10^{-2} M solutions in spectroscopic grade water. The solutions were measured in a 0.2 mm thick flow cell in a non-recycling volumetric flow of 4 mL/h. The excited volume is therefore refreshed approximately every 100 pulses, which approximately corresponds to 10 times for each z-position, which was found to be sufficient. The measurements were carried out at different pulse energies. At higher energies a signal of the pure solvent appears and the solvent will contribute to the effective nonlinear absorption and even thermal effects are more likely to influence the measurement. Care had to be taken to collect the whole transmitted laser energy using a big diameter and short focal length lens. Additionally, a proper Gaussian beam profile in time and space is essential for the analysis.

2PP and MPG structuring devices

Two structuring devices were used for the 2PP and multiphoton grafting tests. Micro Processing system M3DL was used in chapter 1 and 2 for the 2PP tests of organo-soluble 2PIs. Processing system Mipro was applied for the fast writing with the benzylidene ketone-based 2PIs in chapter 2 and for the hydrogel fabrication with water-soluble 2PIs in chapter 3, as well as for the multiphoton grafting with arylazides in chapter 4 and 5.

2PP Micro Processing system M3DL[85]

The micro 3-dimensional structuring device (M3DL) (Laser Zentrum Hannover (LZH)) contains a Ti:sapphire laser (High Q laer) with 100 fs pulsed and 810 nm wavelength at a repetition rate of 73 MHz combined with 400 mW power output. The laser beams passing

through an AOM were diffracted, leaving the first order waves for the polymerization. The intensity can be adjusted by a λ/2 waveplate together with a polarization dependent beam-splitter. The laser was focused into the resins by microscope objectives with different magnifications (100x NA = 1.35, 63x NA = 0.75, 20x NA = 0.4, all manufactured by Carl Zeiss). The laser intensity for the structuring test can be measured with a power meter after the objective. The precise movement of the beam-focusing objective along X- and Y-dimension was realized by two high precision air-bearing axes (Aerotech). A similar air-bearing Z-axis carried the samples. The mirror system ensured that the X- and Y-movement was only parallel to the direction of the laser beam, so that the guidance of the beam was stable throughout the whole structuring process. For the online process observation, a camera viewed along the laser beam and got focused on the polymerization spot through the same objective used for focusing the laser. Mounting the axes on a hard stone frame ensured appropriate damping of noises and vibrations. The whole setup's base was an optical table with an air friction damping, again to suppress vibrations. For controlling the machine, the axes and the laser intensity power meter were plugged to an electronic device, which processed the commands given by the control computer. A red LED lamp illuminated the sample preventing premature polymerization (**Fig 87**).
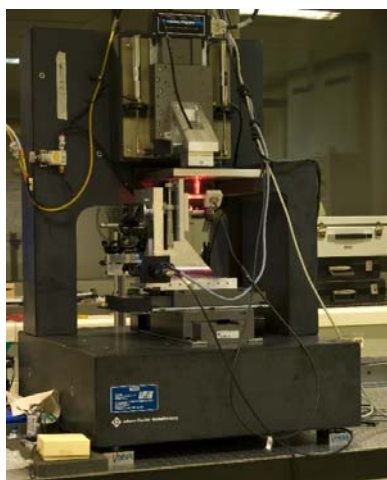
Fig 87 Structuring devices M3DL[85]

2PP Micro Processing system Mipro[23]

A novel 2PP system based on an old setup from LZH was designed to increase the processing speed (**Fig 88**).
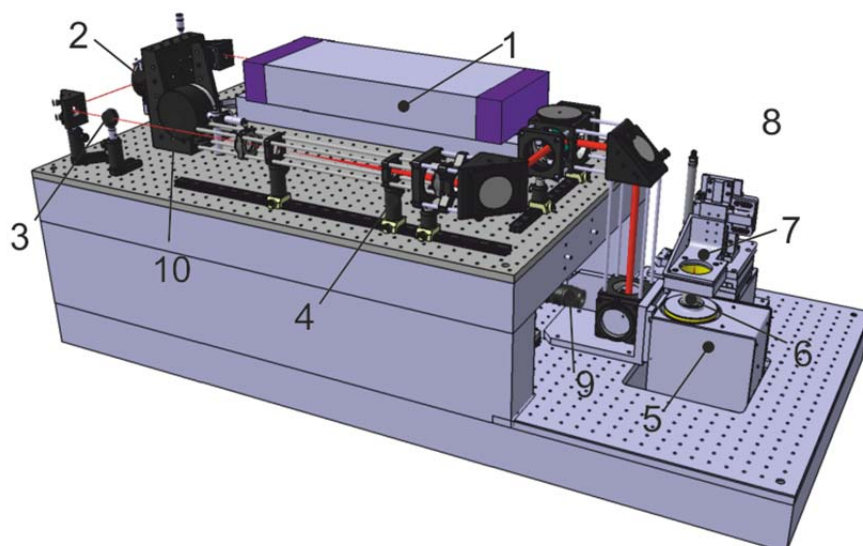
Fig 88 CAD drawing of 2PP Mipro setup; (1) Laser, (2) AOM, (3) Pinhole, (4) Beamexpander, (5) Galvanoscanner, (6) Microscope objective, (7) Specimen clamp, (8) XYZ translation axes, (9) CCD camera, (10) Laser power meter.[23]

In the new setup, the laser beam passed through the AOM leaving the first order of diffraction for the structuring. The beam could be switched and controlled in its intensity by applying waves of different amplitudes inside the crystal. A pinhole (**2**) blocked the other beam orders from further propagation in the setup. Leaving the pinhole, the beam was expanded six times of its initial 1.8 mm diameter (**3**). The galvanoscanner deflected the beam before focusing it with a microscope objective (**6**). To create 3D polymeric structures, the rotating mirrors of the galcanoscanner (**5**) traced the focal point inside the formulation. A clamp carried the formulation container and was mounted to a linear XYZ axes system (**7**). The axes from the old setup (**8**) were adapted and used to position the specimen clamp for creating the third order of dimension (Z-axis) and to increase the limited field of view of the objective. For online process observation, a CCD camera (**9**) monitored the polymerisation process. The whole setup was mounted on the old setup's hard stone frame to damp vibrations. The laser power was measured behind the AOM (**10**).

In contrast to the M3DL setup, minimizing the amount of mirrors and lenses reduced distortions of the pulse width and ensured high beam quality when focused into the photo sensitive materials. More detailed information can be found in Dr. Jan Torgersen's PhD thesis.[23]

2PP tests[23]

The samples for 2PP tests were prepared by casting a liquid formulation on a microscope slide as depicted in **Fig 89**.
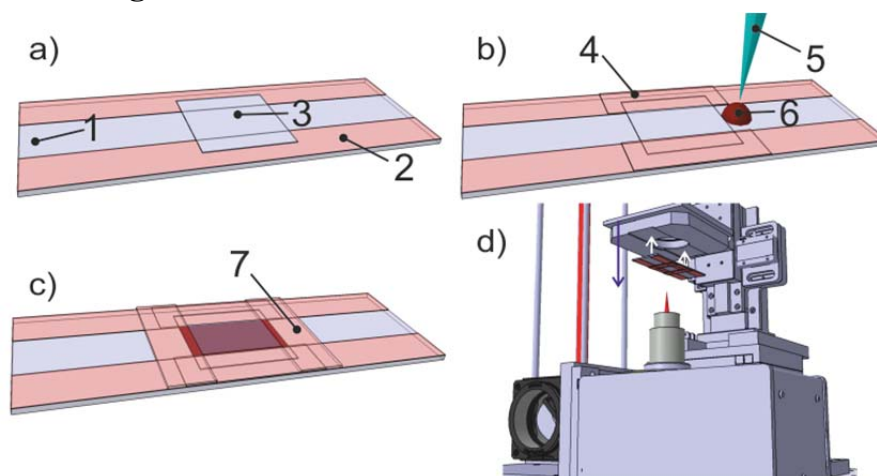
Fig 89 Sample preparation and loading; a) strip spacers and coverglass on coverslip, b) fixation of coverglass and pipetting formulation drop next to building volume, c) sealing of building volume, d) loading of specimen onto the clamp.[23]

Firstly, an $18 \times 18 \times 0.17$ mm^3 coverslip was placed on a glass slide (1) containing two pieces of parallel adhesive strip (2) with specified distance of about 120 μm. For 2PP tests with water-soluble 2PIs, the glass substrate was functionalized with methacrylate functional groups according to literature.[286] Secondly, the coverslip was attached underneath the layer of another two pieces of adhesive strip (4). The building area is roughly $18 \times 10 \times 0.12$ mm^3 and the totally required amount of formulation was approximately 22 mm^3 of unit volume. Thirdly, 30 µl of liquid formulation was applied to the microscope slide by a syringe (5) and the drop (6) was soaked into the space between slide and coverslip. After the full building volume was completely filled up, the excess formulation not soaked into the building volume was removed. Fourthly, two additional pieces of strip were attached on either side of the coverslip (7), where the building volume was exposed to the surrounding. This was especially important for water-based resins as this prevented the water from evaporation and hence the formulation from drying out and from getting unusable. Finally, the prepared sample was loaded into the designated clamp on the XYZ axes system.

Subsequently, the samples were exposed to the laser beam, and the focus was scanned across the photosensitive material, which leads to an embedded 3D structure inside the material volume. After laser writing, the unexposed material was removed by

development of the structures in suitable solvents (using ethanol for hydrophobic 2PIs and DI water for hydrophilic 2PIs). The resulting structures, particularly their structural dimensions, integrity and surface quality, were studied by means of SEM (JEOL JSM-5600 or FEI Philips XL 30). For water-soluble 2PIs, the fabricated structures could be visualized via laser scanning microscopy (LSM700 ZEN software, Carl-Zeiss).

MPG tests

The formulation to prepare PEGDa-based matrix involved poly(ethylene glycol) diacrylate (PEGda, average M_n 700, Sigma Aldrich) and DMF mixture (ratio 50:50) with an addition of 1 wt% of the photoinitiator Irgacure819 (Ciba Specialty Chemicals Inc.). The resulting formulation was photopolymerized with UV light for 5 min (Intelliray 600) in silicone molds (diameter 6 mm; thickness 1 mm). The photopolymerized material pellets were soaked in DMF solution for at least 1 week, with the solvent being exchanged on a regular basis, in order to remove residual monomer and photoinitiator. For laser photografting, the samples were immersed into the 14 mmol/L solution of the investigated azides in DMF. A Ti:sapphire femtosecond laser (High Q, Femtotrain), emitting pulses with duration of 80 fs at a 73 MHz repetition rate around 793 nm was used for laser grafting. The laser beam was focused with a 20× microscope objective (Zeiss, NA = 0.8) into the sample. An acousto-optical modulator was used for fast switching of the laser beam and for adjusting its intensity. The laser power was measured before the objective. The patterns were obtained by scanning the focused laser beam within the sample by the galvo-scanner (HurryScan, ScanLab). The grafted patterns were produced by a set of adjacent line scans with various distances. After the grafting procedure, the samples were placed in DMF in order to remove the residual azides. Rapid decoloration of the pellet indicated the successful removal of possible residuals from the sample. The fluorescence of the patterned samples was analyzed by laser scanning microscopy (LSM700 ZEN software, Carl-Zeiss) at different excitation wavelength.

Cell culture and MTT assay

Outgrowth endothelial cells (OECs) were isolated from two different donors as described elsewhere.[287] All donors gave written formal consent to the use of the biological material, with formal approval by the local ethical committee. OECs were cultured in full EGM-2 medium (Lonza) containing 5% FBS on plastic dishes coated with 2 µg mL^{-1} fibronectin (Sigma). The cells were used between passages 5 and 9 for cytotoxicity experiments. The osteosarcoma cell line MG63 was cultured in DMEM containing 10% FBS. To determine the cytotoxicity of different photoinitiators, 10^4 cells were seeded in selected wells on a

96-well plate (Corning) and incubated over night at 37°C. Photoinitiators were dissolved in 1× PBS without Ca^{2+} and Mg^{2+} to a final concentration of 1.82 mM. Before exposing the cells to the PI solution, the supernatants were aspirated and the cells were washed once with PBS. The sterile-filtered PI solution was added to the cells and the plate was incubated for 10 or 30 minutes at 37 °C. The PI solution was removed and cells were washed twice with PBS. Fresh growth medium was then added to the cells. All steps were performed without direct exposure to light. Following additional 24 hours of incubation, the supernatants were removed and cells were washed three times with PBS. MTT reagent (Sigma) was dissolved in 1× PBS (5 g/L). Before adding to the cells, this stock solution was diluted with the respective growth medium to 3.25 g/L and the plate was incubated for 1 hour at 37°C. The supernatant was removed and formazan crystals were dissolved using DMSO (Sigma). The plate was incubated on a shaker in the dark at room temperature for 20 minutes and absorbance was measured at 540 nm with 650 nm as reference.

Raw data were collected from two different experiments done in triplicate and analysed using Prism 5 (Graphpad). Significance was determined using nonparametric, unpaired, two-tailed Mann-Whitney test (each PI group vs. control group).

Abbreviations

1PA	one-photon absorption	HWE	Horner-Wadsworth-Emmons
2D	two dimensional	ISC	intersystem crossing
2PA	two-photon absorption	kHz	kilohertz
2PIs	two-photon photoinitiators	LED	light-emitting diode
2PL	two-photon lithography	LM	Lippert-Mataga
3D	three dimensional	LSM	laser scanning microscopy
3PA	three-photon absorption	LTEL	lower threshold energy level
A	electron acceptor	M	mol L^{-1}
AOM	acousto-optical modulator	MDEA	N-methyldiethanolamine
BA	butyl acetate	MeOH	methanol
BE	butyl ether	m.p	melting point
CAD	computer aided design	MPA	multiple-photon absorption
CCD	charge-coupled device	MPG	multi-photon induced photografting
CuAAC	copper(I)-catalyzed azide-alkyne cycloaddition	MW	molecular weight
		mW	milliwatt
CW	continuous wave	n	refractive index
CX	cyclohexane	N$_A$	Avogadro's number
D	electron donor	NA	numerical aperture
DCM	dichloromethane	NIR	near infrared
DBC	double bond conversion	nm	nanometer
DI	deionized	NMR	nuclear magnetic resonance
DK	dielectric constant	NPG	N-phenylglycine
DMEM	dulbecco's modified eagle medium	OECs	outgrowth endothelial cells
DMF	dimethylformamide	PA	propyl acetate
DMSO	dimethylsulfoxide	PAGs	photo acid generators
EA	elementar analysis	PBS	phosphate buffered saline
EDX	Energy-dispersive X-ray spectroscopy	PdCl$_2$(btpp)	bis[triphenylphosphine]palladium(II) dichloride
EE	ethyl acetate	P$_{dam}$	damage threshold
ESA	excited-state absorption	PDT	Photodynamic therapy
ET	electron transfer	PE	petroleum ether
ETA	ethoxylated (20/3)-trimethylolpropane triacrylate	PEG	poly(ethylene glycol)
		PEGDa	polyetheleneglycol diacrylate
EtOH	ethanole	PET	photo-induced electron transfer
FBS	fetal bovine serum	PI	photoinitiator
FTIR	fourier transformed infrared	ppm	parts per million
Fs	femtosecond	P$_{th}$	polymerisation/fabrication threshold
GC-MS	gas chromatography mass spectroscopy	RAPID	resolution augmentation through photo-induced deactivation
GM	Göppert-Mayer (SI unit) 1 GM°= 10^{-50} cm^4 s photon^{-1} molecule	R$_f$	retention factor (TLC)
		SEM	scanning electron microscope
HPLC	high performance liquid chromatography	STED	stimulated-emission-depletion
		TEA	triethyl amine

THF	tetrahydrofurane	ε	molar extinction coefficient
Ti:S	titanium sapphire laser	ε_{max}	maximum molar extinction coefficient
TLC	thin layer chromatography	Φ_{em}	fluorescence emission quantum yield
TMS	trimethylsilane	λ	wavelength
TTA	trimethylolpropane triacrylate	λ_{max}	absorption maximum
TBAB	tetrabutylammonium bromide	σ^{2PA}	TPA cross section
UV-vis	ultraviolet/visible	ν_a	energies of the maximum of the reduced
voxel	volumetric pixel		fluorescence spectrum
β	non-linear absorption coefficient	ν_f	energies of the maximum of the reduced
δ	chemical shift (NMR)		fluorescence spectrum

Initiators

B3K	1,5-bis[4-(*N,N*-dibutylamino)phenyl]penta-1,4-diyn-3-one
R1	4,4'-((2,5-dimethoxy-1,4-phenylene)di-(1*E*)-2,1-ethenediyl)bis[*N,N*-dibutylbenzenamine]
IRG 369	(2-benzyl-2-(dimethylamino)-1-(4-morpholinophenyl)butan-1-one)
Omnicat 820	4,4'-dimethyl-diphenyliodinium hexafluorophosphate
Irgacure 184	1-hydroxycyclohexyl phenyl ketone
Irgacure 2959	(2-hydroxyethoxy)-2-methylpropiophenone
Lucirin TPO-L	ethyl (2,4,6-trimethylbenzoyl) phenylphosphinate
Irgacure 819	phenylbis(2,4,6-trimethylbenzoyl)phosphine oxide
B3BP	bis(4-((4-(dibutylamino)phenyl)ethynyl)phenyl)methanone
ITX	2-Isopropylthioxanthone
B3FL	2,7-bis((4-(dibutylamino)phenyl)ethynyl)-9H-fluoren-9-one
3,6-B3FL	3,6-bis((4-(dibutylamino)phenyl)ethynyl)-9H-fluoren-9-one
B3AN	2,6-bis((4-(dibutylamino)phenyl)ethynyl)anthracene-9,10-dione
BB3FL	2,7-bis((4-(butyl(2-ethylhexyl)amino)phenyl)ethynyl)-9H-fluoren-9-one
BB3AN	2,6-bis((4-(butyl(2-ethylhexyl)amino)phenyl)ethynyl)anthracene-9,10-dione
Michler's ketone	4,4-tetramethyl-diaminobenzophenone
M2K	(1E,4E)-1,5-bis(4-(dimethylamino)phenyl)penta-1,4-dien-3-one
M2CPK	(2E,5E)-2,5-bis(4-(dimethylamino)benzylidene)cyclopentanone
B2CPK	(2E,5E)-2,5-bis(4-(dibutylamino)benzylidene)cyclopentanone
M2CHK	(2E,6E)-2,6-bis(4-(dimethylamino)benzylidene)-cyclohexanone
M2CMK	(2E,6E)-2,6-bis(4-(dimethylamino)benzylidene)-4-methylcyclohexanone
P2CK	sodium 3,3'-(((((1E,1'E)-(2-oxocyclopentane-1,3-diylidene) bis (methanylylidene))bis(4,1-phenylene))bis(methylazanediyl)) dipropanoate
E2CK	sodium 3,3'-(((((1E,1'E)-(5-methyl-2-oxocyclohexane-1,3-diylidene) bis (methanylylidene))bis(4,1-phenylene))bis (methylazanediyl)) dipropanoate
G2CK	sodium 2,2'-(((((1E,1'E)-(5-methyl-2-oxocyclohexane-1,3-diylidene) bis (methanylylidene)) bis(4,1-phenylene))bis (methylazanediyl))diacetate
T2CK	tetrabutylammonium 2,2'-(((((1E,1'E)-(5-methyl-2-oxocyclohexane-1,3-diylidene)bis(methanylylidene))bis(4,1-phenylene))bis(methylazanediyl))diacetate

| **WSPI** | 1,4-bis(4'-(*N,N*-bis(6''-(*N,N,N*-trimethylammonium)hexyl)amino)-styryl)-2,5-dimethoxybenzene tetraiodide |

Azides

BAC-M	(2E,6E)-2,6-bis(4-azidobenzylidene)-4-methylcyclohexanone
DSAD	sodium 6,6'-(ethene-1,2-diyl)bis(3-azidobenzenesulfonate) tetrahydrate
EBM	3-amino-8-azido-5-ethyl-6-phenylphenanthridin-5-ium bromide
AFA	N^1-(4-azido-2,3,5,6-tetrafluorobenzylidene)-N^4,N^4-dimethylbenzene-1,4-diamine
AFA-2	N,N-diallyl-N'-(4-azido-2,3,5,6-tetrafluoro-benzylidene)-benzene-1,4-diamine
AFA-3	(E)-N^1-(4-azido-2,3,5,6-tetrafluorobenzylidene)-N^4-methyl-N^4-(prop-2-yn-1-yl)benzene-1,4-diamine

References

1.   Goppert-Mayer, M., Elementary processes with two quantum jumps. *Ann. Phys. (Berlin, Ger.)* **1931,** *9*, 273-94.

2.   Kaiser, W.; Garrett, C. G. B., Two-photon excitation in CaF2:Eu++. *Phys. Rev. Lett.* **1961,** *7*, 229-31.

3.   Lin, T.-C.; Chung, S.-J.; Kim, K.-S.; Wang, X.; He, G. S.; Swiatkiewicz, J.; Pudavar, H. E.; Prasad, P. N., Organics and polymers with high two-photon activities and their applications. *Adv. Polym. Sci.* **2003,** *161* (Polymers for Photonics Applications II), 157-193.

4.   He, G. S.; Tan, L.-S.; Zheng, Q.; Prasad, P. N., Multiphoton absorbing materials: molecular designs, characterizations, and applications. *Chemical reviews* **2008,** *108* (4), 1245-1330.

5.   Lee, K.-S.; Kim, R. H.; Yang, D.-Y.; Park, S. H., Advances in 3D nano/microfabrication using two-photon initiated polymerization. *Progress in Polymer Science* **2008,** *33* (6), 631-681.

6.   Rumi, M.; Perry, J. W., Two-photon absorption: an overview of measurements and principles. *Advances in Optics and Photonics* **2010,** *2* (4), 451-518.

7.   Rumi, M.; Barlow, S.; Wang, J.; Perry, J. W.; Marder, S. R., Two-photon absorbing materials and two-photon-induced chemistry. In *Advances in Polymer Science, Photoresponsive Polymers I* Springer: 2008; Vol. 213, pp 1-95.

8.   Reinhardt, B. A., Two-photon technology. New materials and evolving applications. *Photonics Sci. News* **1999,** *4* (2), 21-34.

9.   Pawlicki, M.; Collins, H. A.; Denning, R. G.; Anderson, H. L., Two-Photon Absorption and the Design of Two-Photon Dyes. *Angewandte Chemie International Edition* **2009,** *48* (18), 3244-3266.

10.   Ajami, A.; Husinsky, W.; Liska, R.; Pucher, N., Two-photon absorption cross section measurements of various two-photon initiators for ultrashort laser radiation applying the Z-scan technique. *JOSA B* **2010,** *27* (11), 2290-2297.

11.   Makarov, N. S.; Drobizhev, M.; Rebane, A., Two-photon absorption standards in the 550-1600 nm excitation wavelength range. *Optics Express* **2008,** *16* (6), 4029-4047.

12.   Andrade, C. D.; Yanez, C. O.; Rodriguez, L.; Belfield, K. D., A series of fluorene-based two-photon absorbing molecules: synthesis, linear and nonlinear characterization, and bioimaging. *The Journal of organic chemistry* **2010,** *75* (12), 3975-3982.

13.   Glezer, E. N.; Mazur, E., Ultrafast-laser driven micro-explosions in transparent materials. *Applied Physics Letters* **1997,** *71* (7), 882-884.

14.   Sun, H.-B.; Kawata, S., Two-photon photopolymerization and 3D lithographic microfabrication. In *NMR• 3D Analysis• Photopolymerization*, Springer: 2004; pp 169-273.

15.   Denk, W.; Strickler, J. H.; Webb, W. W., Two-photon laser scanning fluorescence microscopy. *Science* **1990,** *248* (4951), 73-76.

16.   Zipfel, W. R.; Williams, R. M.; Webb, W. W., Nonlinear magic: multiphoton microscopy in the biosciences. *Nature biotechnology* **2003,** *21* (11), 1369-1377.

17.   Ehrlich, J.; Wu, X.; Lee, I.; Hu, Z.-Y.; Röckel, H.; Marder, S.; Perry, J., Two-photon absorption and broadband optical limiting with bis-donor stilbenes. *Optics Letters* **1997,** *22* (24), 1843-1845.

18.   Fisher, W.; Partridge, W.; Dees, C.; Wachter, E., Simultaneous Two-Photon Activation of Type-I Photodynamic Therapy Agents. *Photochemistry and photobiology* **1997,** *66* (2), 141-155.

19.   Lenz, P., In vivo excitation of photosensitizers by infrared light. *Photochemistry and photobiology* **1995,** *62* (2), 333-338.

20.   Shen, X.; Li, L.; Chan, M.; Chow, A.; Gao, N.; Yao, S. Q.; Xu, Q. H., Water-Soluble Conjugated Polymers for Simultaneous Two-Photon Cell Imaging and Two-Photon Photodynamic Therapy. *Advanced Optical Materials* **2013,** *1* (1), 92-99.

21.   Bort, G.; Gallavardin, T.; Ogden, D.; Dalko, P. I., From One-Photon to Two-Photon Probes:"Caged" Compounds, Actuators, and Photoswitches. *Angewandte Chemie International Edition* **2013,** *52*, 4526-4537.

22.   Furuta, T.; Wang, S. S.-H.; Dantzker, J. L.; Dore, T. M.; Bybee, W. J.; Callaway, E. M.; Denk, W.; Tsien, R. Y., Brominated 7-hydroxycoumarin-4-ylmethyls: photolabile protecting groups with biologically useful cross-sections for two photon photolysis. *Proceedings of the National Academy of Sciences* **1999,** *96* (4), 1193-1200.

23.   Torgersen, J., Novel biocompatible materials for in situ two-photon polymerisation. *PhD Thesis* **2013**.

24.   Maruo, S.; Nakamura, O.; Kawata, S., Three-dimensional microfabrication with two-photon-absorbed photopolymerization. *Optics letters* **1997,** *22* (2), 132-134.

25.   Serbin, J.; Gu, M., Experimental Evidence for Superprism Effects in Three-Dimensional Polymer Photonic Crystals. *Advanced materials* **2006,** *18* (2), 221-224.

26.   Xu, B.-B.; Zhang, Y.-L.; Xia, H.; Dong, W.-F.; Ding, H.; Sun, H.-B., Fabrication and multifunction integration of microfluidic chips by femtosecond laser direct writing. *Lab Chip* **2013,** *13* (9), 1677-1690.

27.   Krivec, S.; Matsko, N.; Satzinger, V.; Pucher, N.; Galler, N.; Koch, T.; Schmidt, V.; Grogger, W.; Liska, R.; Lichtenegger, H. C., Silica-Based, Organically Modified Host Material for Waveguide Structuring by Two-Photon-Induced Photopolymerization. *Advanced Functional Materials* **2010,** *20* (5), 811-819.

28.   Jhaveri, S. J.; McMullen, J. D.; Sijbesma, R.; Tan, L.-S.; Zipfel, W.; Ober, C. K., Direct three-dimensional microfabrication of hydrogels via two-photon lithography in aqueous solution. *Chemistry of Materials* **2009,** *21* (10), 2003-2006.

29.   Park, S. H.; Yang, D. Y.; Lee, K. S., Two-photon stereolithography for realizing ultraprecise three-dimensional nano/microdevices. *Laser & Photonics Reviews* **2009,** *3* (1-2), 1-11.

30.   Sun, H.-B.; Tanaka, T.; Kawata, S., Three-dimensional focal spots related to two-photon excitation. *Applied physics letters* **2002,** *80* (20), 3673-3675.

31.   LaFratta, C. N.; Fourkas, J. T.; Baldacchini, T.; Farrer, R. A., Multiphoton fabrication. *Angewandte Chemie International Edition* **2007,** *46* (33), 6238-6258.

32.   Wu, S.; Serbin, J.; Gu, M., Two-photon polymerisation for three-dimensional micro-fabrication. *Journal of Photochemistry and Photobiology A: Chemistry* **2006,** *181* (1), 1-11.

33.   Takada, K.; Sun, H.-B.; Kawata, S., Improved spatial resolution and surface roughness in photopolymerization-based laser nanowriting. *Applied Physics Letters* **2005,** *86* (7), 071122-071122-3.

34.   Park, S. H.; Lim, T. W.; Yang, D.-Y.; Cho, N. C.; Lee, K.-S., Fabrication of a bunch of sub-30-nm nanofibers inside microchannels using photopolymerization via a long exposure technique. *Applied physics letters* **2006,** *89*, 173133.

35.   Maruo, S.; Fourkas, J. T., Recent progress in multiphoton microfabrication. *Laser & Photonics Reviews* **2008,** *2* (1-2), 100-111.

36.   Formanek, F.; Takeyasu, N.; Tanaka, T.; Chiyoda, K.; Ishikawa, A.; Kawata, S., Selective electroless plating to fabricate complex three-dimensional metallic micro/nanostructures. *Applied physics letters* **2006,** *88* (8), 083110-083110-3.

37.   Sun, H.-B.; Kawata, S., Two-photon laser precision microfabrication and its applications to micro-nano devices and systems. *Journal of lightwave technology* **2003,** *21* (3), 624.

38.   Juodkazis, S.; Mizeikis, V.; Seet, K. K.; Miwa, M.; Misawa, H., Two-photon lithography of nanorods in SU-8 photoresist. *Nanotechnology* **2005,** *16* (6), 846.

39.   Rumi, M.; Barlow, S.; Wang, J.; Perry, J. W.; Marder, S. R., Two-photon absorbing materials and two-photon-induced chemistry. In *Photoresponsive Polymers I*, Springer: 2008; pp 1-95.

40.   Serbin, J.; Egbert, A.; Ostendorf, A.; Chichkov, B.; Houbertz, R.; Domann, G.; Schulz, J.; Cronauer, C.; Fröhlich, L.; Popall, M., Femtosecond laser-induced two-photon polymerization of inorganic organic hybrid materials for applications in photonics. *Optics letters* **2003,** *28* (5), 301-303.

41.   Haas, K.-H.; Rose, K., Hybrid inorganic/organic polymers with nanoscale building blocks: precursors, processing, properties and applications. *Reviews on Advanced Materials Science* **2003,** *5* (1), 47-52.

42.   Gubler, U.; Bosshard, C., Molecular design for third-order nonlinear optics. In *Polymers for Photonics Applications I*, Springer: 2002; pp 123-191.

43.   Peticolas, W. L.; Goldsborough, J. P.; Rieckhoff, K., Double photon excitation in organic crystals. *Physical Review Letters* **1963,** *10* (2), 43.

44.   Norman, P.; Luo, Y.; Ågren, H., Large two-photon absorption cross sections in two-dimensional, charge-transfer, cumulene-containing aromatic molecules. *The Journal of chemical physics* **1999,** *111*, 7758.

45.   Barzoukas, M.; Blanchard-Desce, M., Molecular engineering of push–pull dipolar and quadrupolar molecules for two-photon absorption: A multivalence-bond states approach. *The Journal of Chemical Physics* **2000,** *113*, 3951.

46.   Albota, M.; Beljonne, D.; Brédas, J.-L.; Ehrlich, J. E.; Fu, J.-Y.; Heikal, A. A.; Hess, S. E.; Kogej, T.; Levin, M. D.; Marder, S. R., Design of organic molecules with large two-photon absorption cross sections. *Science* **1998,** *281* (5383), 1653-1656.

47.   Gu, J.; Yulan, W.; Chen, W.-Q.; Dong, X.-Z.; Duan, X.-M.; Kawata, S., Carbazole-based 1D and 2D hemicyanines: synthesis, two-photon absorption properties and application for two-photon photopolymerization 3D lithography. *New Journal of Chemistry* **2007,** *31* (1), 63-68.

48.   Zheng, S.; Leclercq, A.; Fu, J.; Beverina, L.; Padilha, L. A.; Zojer, E.; Schmidt, K.; Barlow, S.; Luo, J.; Jiang, S.-H., Two-photon absorption in quadrupolar bis (acceptor)-terminated chromophores with electron-rich bis (heterocycle) vinylene bridges. *Chemistry of materials* **2007,** *19* (3), 432-442.

49.   Pond, S. J.; Rumi, M.; Levin, M. D.; Parker, T. C.; Beljonne, D.; Day, M. W.; Brédas, J.-L.; Marder, S. R.; Perry, J. W., One-and two-photon spectroscopy of donor-acceptor-donor distyrylbenzene derivatives: effect of cyano substitution and distortion from planarity. *The Journal of Physical Chemistry A* **2002,** *106* (47), 11470-11480.

50.   Belfield, K. D.; Hagan, D. J.; Van Stryland, E. W.; Schafer, K. J.; Negres, R. A., New two-photon absorbing fluorene derivatives: Synthesis and nonlinear optical characterization. *Organic Letters* **1999,** *1* (10), 1575-1578.

51.   Lin, T.-C.; He, G. S.; Prasad, P. N.; Tan, L.-S., Degenerate nonlinear absorption and optical power limiting properties of asymmetrically substituted stilbenoid chromophores. *Journal of Materials Chemistry* **2004,** *14* (6), 982-991.

52.   Porrès, L.; Mongin, O.; Katan, C.; Charlot, M.; Pons, T.; Mertz, J.; Blanchard-Desce, M., Enhanced two-photon absorption with novel octupolar propeller-shaped fluorophores derived from triphenylamine. *Organic letters* **2004,** *6* (1), 47-50.

53.   Shao, P.; Huang, B.; Chen, L.; Liu, Z.; Qin, J.; Gong, H.; Ding, S.; Wang, Q., Synthesis and two-photon absorption properties of novel heterocycle-based organic molecules. *Journal of Materials Chemistry* **2005,** *15* (42), 4502-4506.

54.   Kannan, R.; He, G. S.; Yuan, L.; Xu, F.; Prasad, P. N.; Dombroskie, A. G.; Reinhardt, B. A.; Baur, J. W.; Vaia, R. A.; Tan, L.-S., Diphenylaminofluorene-based two-photon-absorbing chromophores with various π-electron acceptors. *Chemistry of materials* **2001,** *13* (5), 1896-1904.

55.   Kawamata, J.; Akiba, M.; Tani, T.; Harada, A.; Inagaki, Y., Two-photon absorption cross-sections of fluorene derivatives with cationic substituents. *Chemistry Letters* **2004,** *33* (4), 448-449.

56.   Rumi, M.; Ehrlich, J. E.; Heikal, A. A.; Perry, J. W.; Barlow, S.; Hu, Z.; McCord-Maughon, D.; Parker, T. C.; Röckel, H.; Thayumanavan, S., Structure-property relationships for two-photon absorbing chromophores: bis-donor diphenylpolyene and bis (styryl) benzene derivatives. *Journal of the American Chemical Society* **2000,** *122* (39), 9500-9510.

57.   Morley, J. O., Nonlinear optical properties of organic molecules. XII. Calculations of the hyperpolarizabilities of donor–acceptor polyynes. *International journal of quantum chemistry* **1993,** *46* (1), 19-26.

58.   Mongin, O.; Porrès, L.; Charlot, M.; Katan, C.; Blanchard-Desce, M., Synthesis, Fluorescence, and Two-Photon Absorption of a Series of Elongated Rodlike and Banana-Shaped Quadrupolar Fluorophores: A Comprehensive Study of Structure–Property Relationships. *Chemistry-a European Journal* **2007,** *13* (5), 1481-1498.

59.   Drobizhev, M.; Meng, F.; Rebane, A.; Stepanenko, Y.; Nickel, E.; Spangler, C. W., Strong two-photon absorption in new asymmetrically substituted porphyrins: interference between charge-transfer and intermediate-resonance pathways. *The Journal of Physical Chemistry B* **2006,** *110* (20), 9802-9814.

60.   Malval, J.-P.; Morlet-Savary, F.; Chaumeil, H. l. n.; Balan, L.; Versace, D.-L.; Jin, M.; Defoin, A., Photophysical properties and two-photon polymerization ability of a nitroalkoxystilbene derivative. *The Journal of Physical Chemistry C* **2009,** *113* (49), 20812-20821.

61.   Lee, S. K.; Yang, W. J.; Choi, J. J.; Kim, C. H.; Jeon, S.-J.; Cho, B. R., 2, 6-Bis [4-(p-dihexylaminostyryl) styryl] anthracene derivatives with large two-photon cross sections. *Organic letters* **2005,** *7* (2), 323-326.

62.   Kim, H. M.; Cho, B. R., Two-photon materials with large two-photon cross sections. Structure–property relationship. *Chemical Communications* **2009,** (2), 153-164.

63.   Wu, J.; Zhao, Y.; Li, X.; Shi, M.; Wu, F.; Fang, X., Multibranched benzylidene cyclopentanone dyes with large two-photon absorption cross-sections. *New J. Chem.* **2006,** *30* (7), 1098-1103.

64.   Chung, S.-J.; Kim, K.-S.; Lin, T.-C.; He, G. S.; Swiatkiewicz, J.; Prasad, P. N., Cooperative enhancement of two-photon absorption in multi-branched structures. *The Journal of Physical Chemistry B* **1999,** *103* (49), 10741-10745.

65.   Liu, L.; Zhou, Z.; Shi, J.; Liu, Z.; Lu, C.; He, W.; Ma, J.; Cui, Y.; Lu, G.-Y., Photophysical and two-photon absorption properties of protonation-induced tribranched chromophore having 1, 3, 5-triazine core and pyrrole end-groups. *Synthetic Metals* **2011,** *161* (9), 783-788.

66.   Cho, B. R.; Son, K. H.; Lee, S. H.; Song, Y.-S.; Lee, Y.-K.; Jeon, S.-J.; Choi, J. H.; Lee, H.; Cho, M., Two photon absorption properties of 1, 3, 5-tricyano-2, 4, 6-tris (styryl) benzene derivatives. *Journal of the American Chemical Society* **2001,** *123* (41), 10039-10045.

67.   Bartholomew, G. P.; Rumi, M.; Pond, S. J.; Perry, J. W.; Tretiak, S.; Bazan, G. C., Two-photon absorption in three-dimensional chromophores based on [2.2]-paracyclophane. *Journal of the American Chemical Society* **2004,** *126* (37), 11529-11542.

68.   Ogawa, K.; Ohashi, A.; Kobuke, Y.; Kamada, K.; Ohta, K., Strong two-photon absorption of self-assembled butadiyne-linked bisporphyrin. *Journal of the American Chemical Society* **2003,** *125* (44), 13356-13357.

69.   Wan, X.; Zhao, Y.; Xue, J.; Wu, F.; Fang, X., Water-soluble benzylidene cyclopentanone dye for two-photon photopolymerization. *Journal of Photochemistry and Photobiology A: Chemistry* **2009,** *202* (1), 74-79.

70.   Cepraga, C.; Gallavardin, T.; Marotte, S.; Lanoe, P.-H.; Mulatier, J.-C.; Lerouge, F.; Parola, S.; Lindgren, M.; Baldeck, P. L.; Marvel, J.; Maury, O.; Monnereau, C.; Favier, A.; Andraud, C.; Leverrier, Y.; Charreyre, M.-T., Biocompatible well-defined chromophore-polymer conjugates for photodynamic therapy and two-photon imaging. *Polymer Chemistry* **2013,** *4* (1), 61-67.

71.   Belfield, K. D.; Schafer, K. J.; Liu, Y.; Liu, J.; Ren, X.; Stryland, E. W. V., Multiphoton-absorbing organic materials for microfabrication, emerging optical applications and non-destructive three-dimensional imaging. *Journal of Physical Organic Chemistry* **2000,** *13* (12), 837-849.

72.   Cumpston, B. H.; Ananthavel, S. P.; Barlow, S.; Dyer, D. L.; Ehrlich, J. E.; Erskine, L. L.; Heikal, A. A.; Kuebler, S. M.; Lee, I.-Y. S.; McCord-Maughon, D., Two-photon polymerization initiators for three-dimensional optical data storage and microfabrication. *Nature* **1999,** *398* (6722), 51-54.

73.   Ovsianikov, A.; Schlie, S.; Ngezahayo, A.; Haverich, A.; Chichkov, B. N., Two-photon polymerization technique for microfabrication of CAD-designed 3D scaffolds from commercially available photosensitive materials. *Journal of Tissue Engineering and Regenerative Medicine* **2007,** *1* (6), 443-449.

74.   Mendonca, C. R.; Correa, D. S.; Baldacchini, T.; Tayalia, P.; Mazur, E., Two-photon absorption spectrum of the photoinitiator Lucirin TPO-L. *Applied Physics a-Materials Science & Processing* **2008,** *90* (4), 633-636.

75.   Schafer, K. J.; Hales, J. M.; Balu, M.; Belfield, K. D.; Van Stryland, E. W.; Hagan, D. J., Two-photon absorption cross-sections of common photoinitiators. *Journal of Photochemistry and Photobiology a-Chemistry* **2004,** *162* (2-3), 497-502.

76.   Segurola, J.; Allen, N. S.; Edge, M.; McMahon, A.; Wilson, S., Photoyellowing and discolouration of UV cured acrylated clear coatings systems: influence of photoinitiator type. *Polymer degradation and stability* **1999,** *64* (1), 39-48.

77.   Schafer, K. J.; Hales, J. M.; Balu, M.; Belfield, K. D.; Van Stryland, E. W.; Hagan, D. J., Two-photon absorption cross-sections of common photoinitiators. *Journal of Photochemistry and Photobiology A: Chemistry* **2004,** *162* (2), 497-502.

78.   Belfield, K. D.; Ren, X.; Van Stryland, E. W.; Hagan, D. J.; Dubikovsky, V.; Miesak, E. J., Near-IR two-photon photoinitiated polymerization using a fluorone/amine initiating system. *Journal of the American Chemical Society* **2000,** *122* (6), 1217-1218.

79.   Belfield, K. D.; Schafer, K. J.; Liu, Y. U.; Liu, J.; Ren, X. B.; Van Stryland, E. W., Multiphoton-absorbing organic materials for microfabrication, emerging optical applications and non-destructive three-dimensional imaging. *Journal of Physical Organic Chemistry* **2000,** *13* (12), 837-849.

80.   Malval, J.-P.; Jin, M.; Morlet-Savary, F.; Chaumeil, H. l. n.; Defoin, A.; Soppera, O.; Scheul, T.; Bouriau, M.; Baldeck, P. L., Enhancement of the Two-Photon Initiating Efficiency of a Thioxanthone Derivative through a Chevron-Shaped Architecture. *Chemistry of Materials* **2011,** *23* (15), 3411-3420.

81.   Malval, J. P.; Morlet-Savary, F.; Chaumeil, H.; Balan, L.; Versace, D. L.; Jin, M.; Defoin, A., Photophysical Properties and Two-Photon Polymerization Ability of a Nitroalkoxystilbene Derivative. *Journal of Physical Chemistry C* **2009,** *113* (49), 20812-20821.

82.   Jin, M.; Malval, J. P.; Versace, D. L.; Morlet-Savary, F.; Chaumeil, H.; Defoin, A.; Allonas, X.; Fouassier, J. P., Two-photon absorption and polymerization ability of intramolecular energy transfer based photoinitiating systems. *Chemical Communications* **2008,** (48), 6540-6542.

83.   Xing, J.-F.; Chen, W.-Q.; Gu, J.; Dong, X.-Z.; Takeyasu, N.; Tanaka, T.; Duan, X.-M.; Kawata, S., Design of high efficiency for two-photon polymerization initiator: combination of radical stabilization and large two-photon cross-section achieved by N-benzyl 3, 6-bis (phenylethynyl) carbazole derivatives. *Journal of Materials Chemistry* **2007,** *17* (14), 1433-1438.

84.   Lemercier, G.; Martineau, C.; Mulatier, J.-C.; Wang, I.; Stéphan, O.; Baldeck, P.; Andraud, C., Analogs of Michler's ketone for two-photon absorption initiation of polymerization in the near infrared: synthesis and photophysical properties. *New journal of chemistry* **2006,** *30* (11), 1606-1613.

85.   Pucher, N., Synthesis and Evaluation of Novel Initiators for the Two-Photon Induced Photopolymerization Process – A Precise Tool for Real 3D Sub-Micrometer Laser Structuring. *PhD Thesis* **2010**.

86.   Lin, T.-C.; Chung, S.-J.; Kim, K.-S.; Wang, X.; He, G. S.; Swiatkiewicz, J.; Pudavar, H. E.; Prasad, P. N., Organics and polymers with high two-photon activities and their applications. In *Advances in Polymer Science, Polymers for Photonics Applications II*, Springer: 2003; Vol. 161, pp 157-193.

87.   Tian, Y.; Zhang, M.; Yu, X.; Xu, G.; Ren, Y.; Yang, J.; Wu, J.; Zhang, X.; Tao, X.; Zhang, S., Two novel two-photon polymerization initiators with extensive application prospects. *Chemical physics letters* **2004,** *388* (4), 325-329.

88.   Porshnev, Y. N.; Churkina, V.; Titov, V., Synthesis of styryl-substituted 2-phenyl-and 1, 2-diphenylcyclopenta [b]-chromenes. *Chemistry of Heterocyclic Compounds* **1978,** *14* (10), 1070-1074.

89.   Lin, T.-C.; Hsu, C.-S.; Hu, C.-L.; Chen, Y.-F.; Huang, W.-J., Synthesis and two-photon properties of a multipolar chromophore containing indenofluorenyl units. *Tetrahedron Letters* **2009,** *50* (2), 182-185.

90.   Beletskaya, I. P.; Cheprakov, A. V., The Heck reaction as a sharpening stone of palladium catalysis. *Chemical Reviews* **2000,** *100* (8), 3009-3066.

91.   Chinchilla, R.; Nájera, C., The Sonogashira reaction: a booming methodology in synthetic organic chemistry. *Chemical reviews* **2007,** *107* (3), 874-922.

92. (a) Wang, T.; Zhao, Y. X.; Shi, M. Q.; Wu, F. P., The synthesis of novel coumarin dyes and the study of their photoreaction properties. *Dyes and Pigments* **2007,** *75* (1), 104-110; (b) Wu, J.; Zhao, Y. X.; Li, X.; Shi, M. Q.; Wu, F. P.; Fang, X. Y., Multibranched benzylidene cyclopentanone dyes with large two-photon absorption cross-sections. *New Journal of Chemistry* **2006,** *30* (7), 1098-1103; (c) Xue, J. Q.; Zhao, Y. X.; Wu, F. P.; Fang, D. C., Effect of Bridging Position on the Two-Photon Polymerization Initiating Efficiencies of Novel Coumarin/Benzylidene Cyclopentanone Dyes. *Journal of Physical Chemistry A* **2010,** *114* (15), 5171-5179; (d) Xue, J. Q.; Zhao, Y. X.; Wu, H.; Wu, F. P., Novel benzylidene cyclopentanone dyes for two-photon photopolymerization. *Journal of Photochemistry and Photobiology a-Chemistry* **2008,** *195* (2-3), 261-266.

93. Lu, Y.; Hasegawa, F.; Goto, T.; Ohkuma, S.; Fukuhara, S.; Kawazu, Y.; Totani, K.; Yamashita, T.; Watanabe, T., Highly sensitive measurement in two-photon absorption cross section and investigation of the mechanism of two-photon-induced polymerization. *Journal of luminescence* **2004,** *110* (1), 1-10.

94. Lu, Y.; Hasegawa, F.; Kawazu, Y.; Totani, K.; Yamashita, T.; Toshiyuki, W., Investigation of mechanism of photo induced polymerization excited by two-photon absorption. *Sen'i Gakkaishi* **2004,** *60* (6), 165-172.

95. Lalevee, J.; Graff, B.; Allonas, X.; Fouassier, J.-P., Aminoalkyl radicals: Direct observation and reactivity toward oxygen, 2, 2, 6, 6-tetramethylpiperidine-N-oxyl, and methyl acrylate. *The Journal of Physical Chemistry A* **2007,** *111* (30), 6991-6998.

96. Nazir, R.; Danilevicius, P.; Gray, D.; Farsari, M.; Gryko, D. T., Push–Pull Acylo-Phosphine Oxides for Two-Photon-Induced Polymerization. *Macromolecules* **2013**.

97. Kabouraki, E.; Giakoumaki, A. N.; Danilevicius, P.; Gray, D.; Vamvakaki, M.; Farsari, M., Redox Multiphoton Polymerization for 3D Nanofabrication. *Nano letters* **2013,** *13* (8), 3831-3835.

98. Spangenberg, A.; Malval, J.-P.; Akdas-Kilig, H.; Fillaut, J.-L.; Stehlin, F.; Hobeika, N.; Morlet-Savary, F.; Soppera, O., Enhancement of Two-Photon Initiating Efficiency of a 4, 4′-Diaminostyryl-2, 2′-bipyridine Derivative Promoted by Complexation with Silver Ions. *Macromolecules* **2012,** *45* (3), 1262-1269.

99. Ovsianikov, A.; Deiwick, A.; Van Vlierberghe, S.; Pflaum, M.; Wilhelmi, M.; Dubruel, P.; Chichkov, B., Laser Fabrication of 3D Gelatin Scaffolds for the Generation of Bioartificial Tissues. *Materials* **2011,** *4* (1), 288-299.

100. Vogel, A.; Venugopalan, V., Mechanisms of pulsed laser ablation of biological tissues. *Chemical Reviews* **2003,** *103* (2), 577-644.

101. (a) Campagnola, P. J.; Delguidice, D. M.; Epling, G. A.; Hoffacker, K. D.; Howell, A. R.; Pitts, J. D.; Goodman, S. L., 3-dimensional submicron polymerization of acrylamide by multiphoton excitation of xanthene dyes. *Macromolecules* **2000,** *33* (5), 1511-1513; (b) Farsari, M.; Filippidis, G.; Sambani, K.; Drakakis, T. S.; Fotakis, C., Two-photon polymerization of an Eosin Y-sensitized acrylate composite. *Journal of Photochemistry and Photobiology A: Chemistry* **2006,** *181* (1), 132-135.

102. (a) Basu, S.; Rodionov, V.; Terasaki, M.; Campagnola, P. J., Multiphoton-excited microfabrication in live cells via Rose Bengal cross-linking of cytoplasmic proteins. *Optics letters* **2005,** *30* (2), 159-161; (b) Pitts, J. D.; Campagnola, P. J.; Epling, G. A.; Goodman, S. L., Submicron multiphoton free-form fabrication of proteins and polymers: studies of reaction efficiencies and applications in sustained release. *Macromolecules* **2000,** *33* (5), 1514-1523.

103. Ullrich, G.; Burtscher, P.; Salz, U.; Moszner, N.; Liska, R., Phenylglycine derivatives as coinitiators for the radical photopolymerization of acidic aqueous formulations. *Journal of Polymer Science Part A: Polymer Chemistry* **2006,** *44* (1), 115-125.

104.   Huang, S.; Heikal, A. A.; Webb, W. W., Two-photon fluorescence spectroscopy and microscopy of NAD (P) H and flavoprotein. *Biophysical journal* **2002,** *82* (5), 2811-2825.

105.   Spivey, E. C.; Ritschdorff, E. T.; Connell, J. L.; McLennon, C. A.; Schmidt, C. E.; Shear, J. B., Multiphoton Lithography of Unconstrained Three-Dimensional Protein Microstructures. *Advanced Functional Materials* **2013,** *23* (3), 333-339.

106.   Torgersen, J.; Ovsianikov, A.; Mironov, V.; Pucher, N.; Qin, X.; Li, Z.; Cicha, K.; Machacek, T.; Liska, R.; Jantsch, V.; Stampfl, J., Photo-sensitive hydrogels for three-dimensional laser microfabrication in the presence of whole organisms. *Journal of Biomedical Optics* **2012,** *17* (10), 105008.

107.   Seidlits, S. K.; Schmidt, C. E.; Shear, J. B., High-Resolution Patterning of Hydrogels in Three Dimensions using Direct-Write Photofabrication for Cell Guidance. *Advanced Functional Materials* **2009,** *19* (22), 3543-3551.

108.   Pitts, J. D.; Howell, A. R.; Taboada, R.; Banerjee, I.; Wang, J.; Goodman, S. L.; Campagnola, P. J., New Photoactivators for Multiphoton Excited Three-dimensional Submicron Cross-linking of Proteins: Bovine Serum Albumin and Type 1 Collagen¶†. *Photochemistry and photobiology* **2002,** *76* (2), 135-144.

109.   Woo, H. Y.; Liu, B.; Kohler, B.; Korystov, D.; Mikhailovsky, A.; Bazan, G. C., Solvent effects on the two-photon absorption of distyrylbenzene chromophores. *Journal of the American Chemical Society* **2005,** *127* (42), 14721-14729.

110.   Zhao, Y.; Wang, W.; Wu, F.; Zhou, Y.; Huang, N.; Gu, Y.; Zou, Q.; Yang, W., Polyethylene glycol-functionalized benzylidene cyclopentanone dyes for two-photon excited photodynamic therapy. *Organic & biomolecular chemistry* **2011,** *9* (11), 4168-4175.

111.   Xing, J. F.; Dong, X. Z.; Chen, W. Q.; Duan, X. M.; Takeyasu, N.; Tanaka, T.; Kawata, S., Improving spatial resolution of two-photon microfabrication by using photoinitiator with high initiating efficiency. *Applied Physics Letters* **2007,** *90* (13).

112.   Park, S. H.; Lim, T. W.; Yang, D. Y.; Kim, R. H.; Lee, K. S., Improvement of spatial resolution in nano-stereolithography using radical quencher. *Macromolecular Research* **2006,** *14* (5), 559-564.

113.   Takada, K.; Sun, H. B.; Kawata, S., Improved spatial resolution and surface roughness in photopolymerization-based laser nanowriting. *Applied Physics Letters* **2005,** *86* (7).

114.   Lu, W. E.; Dong, X. Z.; Chen, W. Q.; Zhao, Z. S.; Duan, X. M., Novel photoinitiator with a radical quenching moiety for confining radical diffusion in two-photon induced photopolymerization. *Journal of Materials Chemistry* **2011,** *21* (15), 5650-5659.

115.   Sakellari, I.; Kabouraki, E.; Gray, D.; Purlys, V.; Fotakis, C.; Pikulin, A.; Bityurin, N.; Vamvakaki, M.; Farsari, M., Diffusion-assisted high-resolution direct femtosecond laser writing. *ACS nano* **2012,** *6* (3), 2302-2311.

116.   (a) Li, L.; Gattass, R. R.; Gershgoren, E.; Hwang, H.; Fourkas, J. T., Achieving λ/20 resolution by one-color initiation and deactivation of polymerization. *Science* **2009,** *324* (5929), 910-913; (b) Fischer, J.; von Freymann, G.; Wegener, M., The Materials Challenge in Diffraction-Unlimited Direct-Laser-Writing Optical Lithography. *Advanced Materials* **2010,** *22* (32), 3578-3582.

117.   Wolf, T. J.; Fischer, J.; Wegener, M.; Unterreiner, A.-N., Pump–probe spectroscopy on photoinitiators for stimulated-emission-depletion optical lithography. *Optics letters* **2011,** *36* (16), 3188-3190.

118.   Stocker, M. P.; Li, L.; Gattass, R. R.; Fourkas, J. T., Multiphoton photoresists giving nanoscale resolution that is inversely dependent on exposure time. *Nature Chemistry* **2011,** *3* (3), 223-227.

119.   Fischer, J.; Wegener, M., Three-dimensional optical laser lithography beyond the diffraction limit. *Laser & Photonics Reviews* **2013,** *7* (1), 22-44.

120.   Zhou, W.; Kuebler, S. M.; Braun, K. L.; Yu, T.; Cammack, J. K.; Ober, C. K.; Perry, J. W.; Marder, S. R., An efficient two-photon-generated photoacid applied to positive-tone 3D microfabrication. *Science* **2002,** *296* (5570), 1106-1109.

121.   Murakami, Y.; Coenjarts, C. A.; Ober, C. K., Preparation and two-photon lithography of a sulfur containing resin with high refractive index. *Journal of Photopolymer Science and Technology* **2004,** *17* (1), 115-118.

122.   Yuan, H.; Zhao, Y.; Wu, F., Two-Photon Acid Generation Systems Based on Dibenzylidene Ketone Dyes Intermolecular Sensitization. *Chemistry of Materials* **2012,** *24* (7), 1371-1377.

123.   Yanez, C. O.; Andrade, C. D.; Belfield, K. D., Characterization of novel sulfonium photoacid generators and their microwave-assisted synthesis. *Chemical Communications* **2009,** (7), 827-829.

124.   Xia, R.; Malval, J.-P.; Jin, M.; Spangenberg, A.; Wan, D.; Pu, H.; Vergote, T.; Morlet-Savary, F.; Chaumeil, H. l. n.; Baldeck, P., Enhancement of Acid Photogeneration Through a Para-to-Meta Substitution Strategy in a Sulfonium-Based Alkoxystilbene Designed for Two-Photon Polymerization. *Chemistry of Materials* **2012,** *24* (2), 237-244.

125.   Steidl, L.; Jhaveri, S. J.; Ayothi, R.; Sha, J.; McMullen, J. D.; Ng, S. Y. C.; Zipfel, W. R.; Zentel, R.; Ober, C. K., Non-ionic photo-acid generators for applications in two-photon lithography. *Journal of Materials Chemistry* **2009,** *19* (4), 505-513.

126.   Lin, Y.; Stansbury, J. W., Near-infrared spectroscopy investigation of water effects on the cationic photopolymerization of vinyl ether systems. *Journal of Polymer Science Part A: Polymer Chemistry* **2004,** *42* (8), 1985-1998.

127.   Liu, J.; Gao, F.; Yang, L.; Wang, C.; Li, H.; Zhang, S., Two-photon absorption properties of novel conjugated dyes containing a benzophenone unit. *Chem. Lett.* **2010,** *39* (4), 324-325.

128.   (a) Belfield, K. D.; Bondar, M. V.; Przhonska, O. V.; Schafer, K. J., One- and two-photon photostability of 9,9-didecyl-2,7-bis(N,N-diphenylamino)fluorene. *Photochem. Photobiol. Sci.* **2004,** *3* (1), 138-141; (b) Belfield, K. D.; Bondar, M. V.; Yanez, C. O.; Hernandez, F. E.; Przhonska, O. V., Two-photon absorption and lasing properties of new fluorene derivatives. *Journal of Materials Chemistry* **2009,** *19* (40), 7498-7502; (c) Corredor, C. C.; Belfield, K. D.; Bondar, M. V.; Przhonska, O. V.; Yao, S., One- and two-photon photochemical stability of linear and branched fluorene derivatives. *Journal of Photochemistry and Photobiology A: Chemistry* **2006,** *184* (1-2), 105-112.

129.   Estrada, L. A.; Neckers, D. C., Synthesis and Photophysics of Ambipolar Fluoren-9-ylidene Malononitrile Derivatives†. *The Journal of Organic Chemistry* **2009,** *74* (21), 8484-8487.

130.   (a) Takalo, H.; Kankare, J.; Hanninen, E., Synthesis of some substituted dimethyl and diethyl 4-(phenylethynyl)-2,6-pyridinedicarboxylates. *Acta Chem. Scand., Ser. B* **1988,** *B42* (7), 448-54; (b) Suh, S. C.; Suh, M. C.; Shim, S. C., Photoconductivity of 3,5-dinitrobenzoate of poly[1-phenyl-1-penten-3-yn-5-ol] (DN-PPPYO) blended with poly[4-(p-N,N-diphenylaminophenyl)-1-phenyl-1-buten-3-yne] (PPAPBEY) as a hole transporting polymer. *Macromolecular Chemistry and Physics* **1999,** *200* (9), 1991-1997.

131.   Michel, P.; Gennet, D.; Rassat, A., A one-pot procedure for the synthesis of alkynes and bromoalkynes from aldehydes. *Tetrahedron Letters* **1999,** *40* (49), 8575-8578.

132.   Pucher, N.; Rosspeintner, A.; Satzinger, V.; Schmidt, V.; Gescheidt, G.; Stampfl, J. r.; Liska, R., Structure−Activity Relationship in D-π-A-π-D-Based Photoinitiators for the Two-Photon-Induced Photopolymerization Process. *Macromolecules* **2009,** *42* (17), 6519-6528.

133.   Rondeau-Gagné, S.; Curutchet, C.; Grenier, F.; Scholes, G. D.; Morin, J.-F., Synthesis, characterization and DFT calculations of new ethynyl-bridged C60 derivatives. *Tetrahedron* **2010,** *66* (23), 4230-4242.

134.   Yamamoto, M.; Zheng, S. Silole chromophores for photorefractive nonlinear optical material compositions and process of preparation thereof. WO2008109701A1, 2008.

135.   Aiken, S.; Gabbut, C. D.; Heron, B. M.; Kershaw, C. S.; Smith, N. J.; Cano, J.-P. Photochromic dichroic naphthopyrans and optical articles containing them. WO2009109546A1, 2009.

136.   Pucher, N.; Rosspeintner, A.; Satzinger, V.; Schmidt, V.; Gescheidt, G.; Stampfl, J. r.; Liska, R., Structure− Activity Relationship in D-π-A-π-D-Based Photoinitiators for the Two-Photon-Induced Photopolymerization Process. *Macromolecules* **2009,** *42* (17), 6519-6528.

137.   Novikov, A. N.; Slyusarchuk, V. T.; Chaikovskaya, L. G. 4,4'-Diiodobenzophenone. SU642288A1, 1979.

138.   Takalo, H.; Hänninen, E.; Kankare, J., Preparation of complexing compounds containing two 2, 6-bis [N, N-bis (carboxymethyl) aminomethyl]-4-ethynylpyridine subunits. *Acta Chemica Scandinavica* **1988,** *42*, 662-665.

139.   Albrecht, K.; Yamamoto, K., Dendritic structure having a potential gradient: new synthesis and properties of carbazole dendrimers. *Journal of the American Chemical Society* **2009,** *131* (6), 2244-2251.

140.   Fleischer, J. C.; Rule, M. Process for the production of aromatic diiodoketones. WO9405618A1, 1994.

141.   Thirion, D.; Poriel, C.; Métivier, R.; Rault-Berthelot, J.; Barrière, F.; Jeannin, O.,

Violet-to-Blue Tunable Emission of Aryl-Substituted Dispirofluorene–Indenofluorene

Isomers by Conformationally-Controllable Intramolecular Excimer Formation. *Chemistry-A European Journal* **2011,** *17* (37), 10272-10287.

142.   Sharmoukh, W.; Ko, K. C.; Noh, C.; Lee, J. Y.; Son, S. U., Designed Synthesis of Multi-Electrochromic Systems Bearing Diaryl Ketone and Isophthalates. *The Journal of Organic Chemistry* **2010,** *75* (19), 6708-6711.

143.   (a) Chaikovski, V. K.; Filimonov, V. D.; Yagovkin, A. Y.; Kharlova, T. S., 2, 4, 6, 8-Tetraiodoglycoluril in sulfuric acid as a new powerful reagent for iodination of deactivated arenes. *Tetrahedron Letters* **2000,** *41* (47), 9101-9104; (b) Chaikovskii, V.; Funk, A.; Filimonov, V.; Petrenko, T.; Kets, T., Facile iodination of aromatic compounds having electron-withdrawing substituents. Generation of triiodine cation in the system tetra-N-iodoglycoluril-iodine-sulfuric acid. *Russian Journal of Organic Chemistry* **2008,** *44* (6), 935-936.

144.   Hauser, A.; Thurner, J. U.; Hinzmann, B., The transmission of substituent effects in fluorenes and fluorenones. *Journal fuer Praktische Chemie (Leipzig)* **1988,** *330* (3), 367-78.

145.   Ahmed, S. A. M.; Al-Raqa, S. Y., Photochromism of dihydroindolizines: part XIV.

Synthesis and photophysical behavior of photochromic dihydroindolizine-tripodal linkers toward anchoring sensitizers to semiconductor nanoparticles. *Journal of Physical Organic Chemistry* **2011,** *24* (3), 173-184.

146.   Abashev, G.; Lebedev, K. Y.; Osorgina, I.; Shklyaeva, E., New 2, 7-diiodo-9, 9-disubstituted fluorene containing tetrathiafulvalene fragments. *Russian journal of organic chemistry* **2006,** *42* (12), 1873-1876.

147.   Kryska, A.; Skulski, L., Improved, acid-catalyzed iodinating procedures for activated aromatics with (diacetoxyiodo) benzene as the oxidant. *Journal of Chemical Research, Synopses* **1999,** (10), 590-591.

148.   Stone, M. T.; Anderson, H. L., A cyclodextrin-insulated anthracene rotaxane with enhanced fluorescence and photostability. *Chem. Commun.* **2007,** (23), 2387-2389.

149.   Fujiwara, T.; Lee, J.-K.; Zgierski, M. Z.; Lim, E. C., Photophysical and spectroscopic manifestations of the low-lying πσ* state of 4-(dimethylamino) benzethyne: solvent-polarity dependence of fluorescence and excited-state absorptions. *Physical Chemistry Chemical Physics* **2009,** *11* (14), 2475-2479.

150.   Ajami, A., Two-photon Modification of materials with ultrashort laser radiation: Z-scan measurements and 3D-modification of selected materials. *PhD Thesis* **2012**.

151.   Sheik-bahae, M.; Said, A. A.; Wei, T. H.; Wu, Y. Y.; Hagan, D. J.; Soileau, M. J.; Van Stryland, E. W., Z-scan: a simple and sensitive technique for nonlinear refraction measurements. *Proc. SPIE-Int. Soc. Opt. Eng.* **1990,** *1148* (Nonlinear Opt. Prop. Mater.), 41-51.

152.   Rumi, M.; Ehrlich, J. E.; Heikal, A. A.; Perry, J. W.; Barlow, S.; Hu, Z.; McCord-Maughon, D.; Parker, T. C.; Röckel, H.; Thayumanavan, S.; Marder, S. R.; Beljonne, D.; Brédas, J.-L., Structure−Property Relationships for Two-Photon Absorbing Chromophores: Bis-Donor Diphenylpolyene and Bis(styryl)benzene Derivatives. *Journal of the American Chemical Society* **2000,** *122* (39), 9500-9510.

153.   Xing, J.-F.; Dong, X.-Z.; Chen, W.-Q.; Duan, X.-M.; Takeyasu, N.; Tanaka, T.; Kawata, S., Improving spatial resolution of two-photon microfabrication by using photoinitiator with high initiating efficiency. *Applied physics letters* **2007,** *90* (13), 131106-131106-3.

154.   Xing, J.-F.; Chen, W.-Q.; Dong, X.-Z.; Tanaka, T.; Fang, X.-Y.; Duan, X.-M.; Kawata, S., Synthesis, optical and initiating properties of new two-photon polymerization initiators: 2,7-Bis(styryl)anthraquinone derivatives. *Journal of Photochemistry and Photobiology A: Chemistry* **2007,** *189* (2â€"3), 398-404.

155.   Heller, C.; Pucher, N.; Seidl, B.; Kalinyaprak-Icten, K.; Ullrich, G.; Kuna, L.; Satzinger, V.; Schmidt, V.; Lichtenegger, H. C.; Stampfl, J.; Liska, R., One- and two-photon activity of cross-conjugated photoinitiators with bathochromic shift. *Journal of Polymer Science Part A: Polymer Chemistry* **2007,** *45* (15), 3280-3291.

156.   Schafer, K. J.; Hales, J. M.; Balu, M.; Belfield, K. D.; Van Stryland, E. W.; Hagan, D. J., Two-photon absorption cross-sections of common photoinitiators. *Journal of Photochemistry and Photobiology A: Chemistry* **2004,** *162* (2-3), 497-502.

157.   Li, Z.; Siklos, M.; Pucher, N.; Cicha, K.; Ajami, A.; Husinsky, W.; Rosspeintner, A.; Vauthey, E.; Gescheidt, G.; Stampfl, J., Synthesis and structure-activity relationship of several aromatic ketone-based two-photon initiators. *Journal of Polymer Science Part A: Polymer Chemistry* **2011,** *49* (17), 3688-3699.

158.   Scott, T. F.; Cook, W. D.; Forsythe, J. S., Photo-DSC cure kinetics of vinyl ester resins. I. Influence of temperature. *Polymer* **2002,** *43* (22), 5839-5845.

159.   Schmidt, L. E.; Leterrier, Y.; Vesin, J. M.; Wilhelm, M.; Månson, J. A. E., Photorheology of Fast UV-Curing Multifunctional Acrylates. *Macromolecular materials and engineering* **2005,** *290* (11), 1115-1124.

160.   Cicha, K.; Li, Z.; Stadlmann, K.; Ovsianikov, A.; Markut-Kohl, R.; Liska, R.; Stampfl, J., Evaluation of 3D structures fabricated with two-photon-photopolymerization by using FTIR spectroscopy. *Journal of Applied Physics* **2011,** *110* (6), 064911-064911-5.

161.   Cicha, K.; Koch, T.; Torgersen, J.; Li, Z.; Liska, R.; Stampfl, J., Young's modulus measurement of two-photon polymerized micro-cantilevers by using nanoindentation equipment. *Journal of Applied Physics* **2012,** *112*, 094906.

162.   (a) Wu, J.; Zhao, Y.; Li, X.; Shi, M.; Wu, F.; Fang, X., Multibranched benzylidene cyclopentanone dyes with large two-photon absorption cross-sections. *New J. Chem. 30* (7), 1098-1103; (b) Xue, J.; Zhao, Y.; Wu, J.; Wu, F., Novel benzylidene cyclopentanone dyes for two-photon photopolymerization. *Journal of Photochemistry and Photobiology A: Chemistry* **2008,** *195* (2), 261-266.

163.   Xue, J.; Zhao, Y.; Wu, F.; Fang, D.-C., Effect of Bridging Position on the Two-Photon Polymerization Initiating Efficiencies of Novel Coumarin/Benzylidene Cyclopentanone Dyes. *J. Phys. Chem. A 114* (15), 5171-5179.

164.   Sarkisov, S. S.; Peterson, B. H.; Curley, M. J.; Nesterov, V. N.; Timofeeva, T.; Antipin, M.; Radovanova, E. I.; Leyderman, A.; Fleitz, P. A., Two-photon absorption and fluorescence of new derivatives of cyclohexanone and piperidone. *Journal of Nonlinear Optical Physics & Materials* **2005,** *14* (1), 21-40.

165.   Wang, P.; Du, W.; Wu, S., Study on the spectra and photophysical behavior of bis[p-N,N-dimethylaminobenzylidene] ketone compounds. *Huaxue Xuebao* **1992,** *50* (11), 1140-4.

166.   Yamashita, K.; Imahashi, S.; Ito, S., Synthesis of benzylideneketone dyes and their photochemical properties as a sensitizer for alkali-developable photopolymerization systems. *Dyes and Pigments* **2008,** *76* (3), 748-753.

167.   An, L.-T.; Zou, J.-P.; Zhang, L.-L., Polymer-supported sulphonic acid catalyzed cross-aldol condensation: An expeditious synthesis of α, α′-bis (substituted benzylidene) cycloalkanones. *Catalysis Communications* **2008,** *9* (3), 349-354.

168.   Watanabe, K.-i.; Imazawa, A., Aldol Condensations Catalyzed by Co (II) Complexes of Pyridine-containing Copolymers. *Bulletin of the Chemical Society of Japan* **1982,** *55* (10), 3208-3211.

169.   Azagarsamy, M. A.; Anseth, K. S., Bioorthogonal Click Chemistry: An Indispensable Tool to Create Multifaceted Cell Culture Scaffolds. *Acs Macro Letters* **2013,** *2* (1), 5-9.

170.   Vatsadze, S. Z.; Golikov, A. G. e.; Kriven'ko, A. P.; Zyk, N. V. e., Chemistry of cross-conjugated dienones. *Russian Chemical Reviews* **2008,** *77* (8), 661-681.

171.   Li, Z.; Pucher, N.; Cicha, K.; Torgersen, J.; Ligon, S. C.; Ajami, A.; Husinsky, W.; Rosspeintner, A.; Vauthey, E.; Naumov, S., A Straightforward Synthesis and Structure–Activity Relationship of Highly Efficient Initiators for Two-Photon Polymerization. *Macromolecules* **2013,** *46* (2), 352-361.

172.   Li, Z.-Q.; Siklos, M.; Pucher, N.; Cicha, K.; Ajami, A.; Husinsky, W.; Rosspeintner, A.; Vauthey, E.; Gescheidt, G.; Stampfl, J.; Liska, R., Synthesis and structure-activity relationship of several aromatic ketone-based two-photon initiators. *Journal of Polymer Science, Part A: Polymer Chemistry* **2011,** *49* (17), 3688-3699.

173.   Marcus, Y., *The properties of solvents*. Wiley Chichester: 1998; Vol. 4.

174.   Ovsianikov, A.; Gruene, M.; Pflaum, M.; Koch, L.; Maiorana, F.; Wilhelmi, M.; Haverich, A.; Chichkov, B., Laser printing of cells into 3D scaffolds. *Biofabrication* **2010,** *2* (1), 014104.

175.   Mendonca, C.; Correa, D.; Baldacchini, T.; Tayalia, P.; Mazur, E., Two-photon absorption spectrum of the photoinitiator Lucirin TPO-L. *Applied Physics A* **2008,** *90* (4), 633-636.

176. Justin, G.; Finley, S.; Rahman, A. R. A.; Guiseppi-Elie, A., Biomimetic hydrogels for biosensor implant biocompatibility: electrochemical characterization using micro-disc electrode arrays (MDEAs). *Biomedical microdevices* **2009,** *11* (1), 103-115.

177. Ovsianikov, A.; Mironov, V.; Stampfl, J.; Liska, R., Engineering 3D cell-culture matrices: multiphoton processing technologies for biological and tissue engineering applications. *Expert Review of Medical Devices* **2012,** *9* (6), 613-633.

178. Zou, Q.; Zhao, Y.; Makarov, N. S.; Campo, J.; Yuan, H.; Fang, D.-C.; Perry, J. W.; Wu, F., Effect of alicyclic ring size on the photophysical and photochemical properties of bis (arylidene) cycloalkanone compounds. *Physical Chemistry Chemical Physics* **2012,** *14* (33), 11743-11752.

179. Ikeda, S.; Murata, S.; Ishii, K.; Hamaguchi, H.-o., Mechanistic studies of the pyrene-sensitized photodecomposition of N-phenylglycine: Acceleration of the photodecomposition by the addition of an electron acceptor. *Bulletin of the Chemical Society of Japan* **2000,** *73* (12), 2783-2792.

180. Balta, D. K.; Temel, G.; Aydin, M.; Arsu, N., Thioxanthone based water-soluble photoinitiators for acrylamide photopolymerization. *European Polymer Journal* **2010,** *46* (6), 1374-1379.

181. Han, W.; Ofial, A. R., Iron catalyzed oxidative cyanation of tertiary amines. *Chemical Communications* **2009,** (33), 5024-5026.

182. Castañon, S. L.; Beristain, M. F.; Ortega, A.; Gómez-Sosa, G.; Muñoz, E.; Perez-Martínez, A. L.; Ogawa, T.; Halim, M. F.; Smith, F.; Walser, A., The synthesis, characterization and third-order nonlinear optical character of poly (2, 5-dipropargyloxybenzoate) containing a polar aromatic diacetylene. *Dyes and Pigments* **2011,** *88* (2), 129-134.

183. Monnereau, C.; Marotte, S.; Lanoë, P.-H.; Maury, O.; Baldeck, P. L.; Kreher, D.; Favier, A.; Charreyre, M.-T.; Marvel, J.; Leverrier, Y., Water-soluble chromophores with star-shaped oligomeric arms: synthesis, spectroscopic studies and first results in bio-imaging and cell death induction. *New Journal of Chemistry* **2012,** *36* (11), 2328-2333.

184. Thiemann, T.; Umeno, K.; Wang, J.; Tabuchi, Y.; Arima, K.; Watanabe, M.; Tanaka, Y.; Gorohmaru, H.; Mataka, S., Elongated phosphoranes by C-C coupling of haloaroylmethylidenetriphenylphosphoranes: synthesis and applications. *Journal of the Chemical Society, Perkin Transactions 1* **2002,** (18), 2090-2110.

185. Shaikh, T. M.; Hong, F. E., Iron-Catalyzed Oxidative Cleavage of Olefins and Alkynes to Carboxylic Acids with Aqueous tert-Butyl Hydroperoxide. *Advanced Synthesis & Catalysis* **2011,** *353* (9), 1491-1496.

186. Sniady, A.; Morreale, M. S.; Dembinski, R., Electrophilic cyclization with N-iodosuccinimide: preparation of 5-(4-Bromophenyl)-3-iodo-2-(4-methylphenyl)furan. *Organic Syntheses* **2007,** *84*, 199-208.

187. Chui, C.-H.; Wang, Q.; Chow, W.-C.; Yuen, M.-W.; Wong, K.-L.; Kwok, W.-M.; Cheng, G.-M.; Wong, R.-M.; Tong, S.-W.; Chan, K.-W., 5-(Dimethylamino)-N-(4-ethynylphenyl)-1-naphthalenesulfonamide as a novel bifunctional antitumor agent and two-photon induced bio-imaging probe. *Chemical Communications* **2010,** *46* (20), 3538-3540.

188. Shen, H.; Vollhardt, K. P. C., Remarkable Switch in the Regiochemistry of the Iodination of Anilines by N-Iodosuccinimide: Synthesis of 1, 2-Dichloro-3, 4-diiodobenzene. *Synlett* **2012,** *2012* (02), 208-214.

189. Firouzabadi, H.; Iranpoor, N.; Kazemi, S., Direct halogenation of organic compounds with halides using oxone in water-A green protocol. *Canadian Journal of Chemistry* **2009,** *87* (12), 1675-1681.

190.   Sosnowski, M.; Skulski, L.; Wolowik, K., Microwave-Accelerated or Conventionally Heated Iodination Reactions of Some Aromatic Amines, Using ortho-Periodic Acid as the Oxidant†. *Molecules* **2004,** *9* (7), 617-621.

191.   Parisel, S. L.; Adrio, L. A.; Pereira, A. A.; Pérez, M. M.; Vila, J. M.; Hii, K. K. M., Reversal of aryl bromide reactivity in Pd-catalysed aryl amination reactions promoted by a hemilabile aminophosphine ligand. *Tetrahedron* **2005,** *61* (41), 9822-9826.

192.   (a) Yuan, W. Z.; Hu, R.; Lam, J. W.; Xie, N.; Jim, C. K.; Tang, B. Z., Conjugated Hyperbranched Poly (aryleneethynylene) s: Synthesis, Photophysical Properties, Superquenching by Explosive, Photopatternability, and Tunable High Refractive Indices. *Chemistry-A European Journal* **2012,** *18* (10), 2847-2856; (b) Lewis, J.; Raithby, P. R.; Wong, W.-Y., Synthesis of new bis (acetylide)-substituted fluorene derivatives and their bimetallic and polymeric complexes. *Journal of organometallic chemistry* **1998,** *556* (1), 219-228.

193.   Rodriguez, J. G.; Tejedor, J. L.; La, P. T.; Diaz, C., Synthesis of conjugated 2,7-bis(trimethylsilylethynyl)-(phenylethynyl)nfluoren-9-one and 9-(p-methoxyphenyl)-9-methyl derivatives: optical properties. *Tetrahedron* **2006,** *62* (14), 3355-3361.

194.   Goswami, A.; Goswami, B. N.; Borthakur, N.; Rastogi, R. C., A convenient synthesis of amines from phenols. *Journal of Chemical Research, Synopses* **1996,** (9), 424-425.

195.   Jiao, J.; Zhang, X.-R.; Chang, N.-H.; Wang, J.; Wei, J.-F.; Shi, X.-Y.; Chen, Z.-G., A facile and practical copper powder-catalyzed, organic solvent-and ligand-free ullmann amination of aryl halides. *The Journal of Organic Chemistry* **2011,** *76* (4), 1180-1183.

196.   Blaser, D.; Calmes, M.; Daunis, J.; Natt, F.; Tardy-Delassus, A.; Jacquier, R., Improvement of the Vilsmeier-Haack reaction. *Organic preparations and procedures international* **1993,** *25* (3), 338-341.

197.   Zhou, J.; Qiao, J.; Gan, C.; Wang, C.; Ge, J.; Nan, D. Preparation of cyclic ketone derivatives as imaging agents and aggregation inhibitors of amyloid precipitate and neurofibrillary tangle. CN102557969A, 2012.

198.   Zheng, Q.; He, G. S.; Lin, T.-C.; Prasad, P. N., Synthesis and properties of substituted (p-aminostyryl)-1-(3-sulfooxypropyl) pyridinium inner salts as a new class of two-photon pumped lasing dyes. *Journal of Materials Chemistry* **2003,** *13* (10), 2499-2504.

199.   Yang, W.; Zou, Q.; Zhou, Y.; Zhao, Y.; Huang, N.; Gu, Y.; Wu, F., Carboxylate modified benzylidene cyclopentanone dyes for one-and two-photon excited photodynamic therapy. *Journal of Photochemistry and Photobiology A: Chemistry* **2011,** *222* (1), 228-235.

200.   Li, Z.; Pucher, N.; Cicha, K.; Torgersen, J.; Ligon, S. C.; Ajami, A.; Husinsky, W.; Rosspeintner, A.; Vauthey, E.; Naumov, S.; Scherzer, T.; Stampfl, J. r.; Liska, R., A Straightforward Synthesis and Structure-Activity Relationship of Highly Efficient Initiators for Two-Photon Polymerization. *Macromolecules* **2013,** *46* (2), 352-361.

201.   Nag, A.; Goswami, D., Solvent effect on two-photon absorption and fluorescence of rhodamine dyes. *Journal of Photochemistry and Photobiology, A: Chemistry* **2009,** *206* (2-3), 188-197.

202.   Woo, H. Y.; Liu, B.; Kohler, B., Solvent effects on the two-photon absorption of distyrylbenzene chromophores. *Journal of The American Chemical Society* **2005,** *127* (10), 14721-14729.

203.   Yamashita, K.; Imahashi, S.; Ito, S., Synthesis of benzylideneketone dyes and their photochemical properties as a sensitizer for alkali-developable photopolymerization systems. *Dyes and Pigments* **2007,** *76* (3), 748-753.

204.   Bartoszewicz, J.; Hug, G. L.; Pietrzak, M.; Kozubek, H.; Paczkowski, J.; Marciniak, B., Benzophenone-phenylthioacetic acid tetraalkylammonium salts as effective initiators of

free-radical photopolymerization of vinyl monomers, mechanistic studies. *Macromolecules* **2007,** *40* (24), 8642-8648.

205.   Lu, Y.; Watanabe, T., Determination of electron transfer mechanism of two-photon-induced polymerization via an efficient way: one-photon process. *Proc. SPIE-Int. Soc. Opt. Eng.* **2005,** *5935* (Linear and Nonlinear Optics of Organic Materials V), 593517/1-593517/10.

206.   Yilmaz, G.; Aydogan, B.; Temel, G.; Arsu, N.; Moszner, N.; Yagci, Y., Thioxanthone− Fluorenes as Visible Light Photoinitiators for Free Radical Polymerization. *Macromolecules* **2010,** *43* (10), 4520-4526.

207.   Li, Z.; Torgersen, J.; Ajami, A.; Mühleder, S.; Qin, X.; Husinsky, W.; Holnthoner, W.; Ovsianikov, A.; Stampfl, J.; Liska, R., Initiation Efficiency and Cytotoxicity of Novel Water-soluble Two-photon Photoinitiators for Direct 3D Microfabrication of Hydrogels. *RSC Adv.* **2013**.

208.   Deng, J.; Wang, L.; Liu, L.; Yang, W., Developments and new applications of UV-induced surface graft polymerizations. *Progress in Polymer Science* **2009,** *34* (2), 156-193.

209.   Deng, J. P.; Yang, W. T.; Rånby, B., Surface photografting polymerization of vinyl acetate (VAc), maleic anhydride, and their charge transfer complex. I. VAc (1). *Journal of Applied Polymer Science* **2000,** *77* (7), 1513-1521.

210.   Busson, M.; Berisha, A.; Combellas, C.; Kanoufi, F.; Pinson, J., Photochemical grafting of diazonium salts on metals. *Chemical Communications* **2011,** *47* (47), 12631-12633.

211.   Herbert, C. B.; McLernon, T. L.; Hypolite, C. L.; Adams, D. N.; Pikus, L.; Huang, C. C.; Fields, G. B.; Letourneau, P. C.; Distefano, M. D.; Hu, W.-S., Micropatterning gradients and controlling surface densities of photoactivatable biomolecules on self-assembled monolayers of oligo(ethylene glycol) alkanethiolates. *Chemistry & Biology* **1997,** *4* (10), 731-737.

212.   Wang, H.; Brown, H. R., Ultraviolet grafting of methacrylic acid and acrylic acid on high-density polyethylene in different solvents and the wettability of grafted high-density polyethylene. I. Grafting. *Journal of Polymer Science Part A: Polymer Chemistry* **2004,** *42* (2), 253-262.

213.   El Kholdi, O.; Lecamp, L.; Lebaudy, P.; Bunel, C.; Alexandre, S., Modification of adhesive properties of a polyethylene film by photografting. *Journal of applied polymer science* **2004,** *92* (5), 2803-2811.

214.   Richey, T.; Iwata, H.; Oowaki, H.; Uchida, E.; Matsuda, S.; Ikada, Y., Surface modification of polyethylene balloon catheters for local drug delivery. *Biomaterials* **2000,** *21* (10), 1057-1065.

215.   Chambers, L. D.; Stokes, K. R.; Walsh, F. C.; Wood, R. J., Modern approaches to marine antifouling coatings. *Surface and Coatings Technology* **2006,** *201* (6), 3642-3652.

216.   Kloxin, A. M.; Tibbitt, M. W.; Anseth, K. S., Synthesis of photodegradable hydrogels as dynamically tunable cell culture platforms. *nature protocols* **2010,** *5* (12), 1867-1887.

217.   Hahn, M. S.; Miller, J. S.; West, J. L., Three-dimensional biochemical and biomechanical patterning of hydrogels for guiding cell behavior. *Advanced Materials* **2006,** *18* (20), 2679-2684.

218.   Hahn, M. S.; Miller, J. S.; West, J. L., Three-dimensional biochemical and biomechanical patterning of hydrogels for guiding cell behavior. *Advanced Materials* **2006,** *18* (20), 2679-2684.

219.   Quick, A. S.; Fischer, J.; Richter, B.; Pauloehrl, T.; Trouillet, V.; Wegener, M.; Barner-Kowollik, C., Preparation of Reactive Three-Dimensional Microstructures via Direct

Laser Writing and Thiol-ene Chemistry. *Macromolecular rapid communications* **2013,** *34* (4), 335-340.

220.   Farrer, R. A.; LaFratta, C. N.; Li, L.; Praino, J.; Naughton, M. J.; Saleh, B. E.; Teich, M. C.; Fourkas, J. T., Selective functionalization of 3-D polymer microstructures. *Journal of the American Chemical Society* **2006,** *128* (6), 1796-1797.

221.   (a) Wosnick, J. H.; Shoichet, M. S., Three-dimensional chemical patterning of transparent hydrogels. *Chemistry of Materials* **2007,** *20* (1), 55-60; (b) Wylie, R. G.; Shoichet, M. S., Two-photon micropatterning of amines within an agarose hydrogel. *Journal of Materials Chemistry* **2008,** *18* (23), 2716-2721.

222.   Wylie, R. G.; Ahsan, S.; Aizawa, Y.; Maxwell, K. L.; Morshead, C. M.; Shoichet, M. S., Spatially controlled simultaneous patterning of multiple growth factors in three-dimensional hydrogels. *Nature materials* **2011,** *10* (10), 799-806.

223.   Holden, M. A.; Cremer, P. S., Light activated patterning of dye-labeled molecules on surfaces. *Journal of the American Chemical Society* **2003,** *125* (27), 8074-8075.

224.   Kotzyba-Hibert, F.; Kapfer, I.; Goeldner, M., Recent trends in photoaffinity labeling. *Angewandte Chemie International Edition in English* **1995,** *34* (12), 1296-1312.

225.   (a) Platz, M. S., Comparison of phenylcarbene and phenylnitrene. *Accounts of chemical research* **1995,** *28* (12), 487-492; (b) Banks, R.; Sparkes, G., Studies in azide chemistry. Part V. Synthesis of 4-azido-2, 3, 5, 6-tetrafluoro-, 4-azido-3-chloro-2, 5, 6-trifluoro-, and 4-azido-3, 5-dichloro-2, 6-difluoro-pyridine, and some thermal reactions of the tetrafluoro-compound. *Journal of the Chemical Society, Perkin Transactions 1* **1972**, 2964-2970; (c) Keana, J. F.; Cai, S. X., New reagents for photoaffinity labeling: synthesis and photolysis of functionalized perfluorophenyl azides. *The Journal of Organic Chemistry* **1990,** *55* (11), 3640-3647.

226.   Bräse, S.; Gil, C.; Knepper, K.; Zimmermann, V., Organic azides: an exploding diversity of a unique class of compounds. *Angewandte Chemie International Edition* **2005,** *44* (33), 5188-5240.

227.   Patel, P.; Garson, J. A.; Tettmar, K. I.; Ancliff, S.; McDonald, C.; Pitt, T.; Coelho, J.; Tedder, R. S., Development of an ethidium monoazide–enhanced internally controlled universal 16S rDNA real-time polymerase chain reaction assay for detection of bacterial contamination in platelet concentrates. *Transfusion* **2012,** *52* (7), 1423-1432.

228.   Gadzikwa, T.; Lu, G.; Stern, C. L.; Wilson, S. R.; Hupp, J. T.; Nguyen, S. T., Covalent surface modification of a metal–organic framework: selective surface engineering via CuI-catalyzed Huisgen cycloaddition. *Chemical Communications* **2008,** (43), 5493-5495.

229.   Brase, S.; Gil, C.; Knepper, K.; Zimmermann, V., Organic azides: An exploding diversity of a unique class of compounds. *Angewandte Chemie-International Edition* **2005,** *44* (33), 5188-5240.

230.   Pinard, R.; Heckman, J. E.; Burke, J. M., Alignment of the two domains of the hairpin ribozyme-substrate complex defined by interdomain photoaffinity crosslinking. *Journal of Molecular Biology* **1999,** *287* (2), 239-251.

231.   Eisenhart, J. M.; Ellis, A. B., Perturbation of the excited-state properties of trans, trans-1, 5-bis [4-(dimethylamino) phenyl]-1, 4-pentadien-3-one through adduct formation and silica gel adsorption. *The Journal of Organic Chemistry* **1985,** *50* (21), 4108-4113.

232.   Kolb, H. C.; Finn, M.; Sharpless, K. B., Click chemistry: diverse chemical function from a few good reactions. *Angewandte Chemie International Edition* **2001,** *40* (11), 2004-2021.

233.   Maynard, H. D.; Broyer, R. M.; Kolodziej, C. M., Protein and Peptide Conjugation to Polymers and Surfaces Using Oxime Chemistry. *Click Chemistry for Biotechnology and Materials Science* **2009**, 53-68.

234.   Broyer, R. M.; Schopf, E.; Kolodziej, C. M.; Chen, Y.; Maynard, H. D., Dual Click reactions to micropattern proteins. *Soft Matter* **2011,** *7* (21), 9972-9977.

235.   Enomoto, K.; Haino, K. Electrophotographic charge-generating azo pigment. JP62232658A, 1987.

236.   Zhang, G.; Wen, X.; Wang, Y.; Mo, W.; Ding, C., Sodium nitrite catalyzed aerobic oxidative deoximation under mild conditions. *The Journal of Organic Chemistry* **2011,** *76* (11), 4665-4668.

237.   Dimmock, J.; Sidhu, K.; Quail, J.; Jia, Z.; Duffy, M.; Reid, R.; Kirkpatrick, D.; Zhu, L.; Fletcher, S., Synthesis and cytotoxic evaluation of some 6-arylidene-2-(α-hydroxyamino-α-arylmethyl) cyclohexanone oximes and related compounds. *Journal of pharmaceutical sciences* **1992,** *81* (11), 1059-1064.

238.   Amarasekara, A. S., Nitrosation of β′-hydroxylamino-α, β-unsaturated oximes: synthesis of 1, 7-dioxa-2, 6-diaza-spiro [4, 4] nona-2, 8-diene ring system. *Tetrahedron letters* **2005,** *46* (15), 2635-2638.

239.   Lowe, A. B., Thiol-ene "click" reactions and recent applications in polymer and materials synthesis. *Polymer Chemistry* **2010,** *1* (1), 17-36.

240.   Nimmo, C. M.; Shoichet, M. S., Regenerative biomaterials that "click": Simple, aqueous-based protocols for hydrogel synthesis, surface immobilization, and 3D patterning. *Bioconjugate chemistry* **2011,** *22* (11), 2199-2209.

241.   Hoyle, C. E.; Bowman, C. N., Thiol–ene click chemistry. *Angewandte Chemie International Edition* **2010,** *49* (9), 1540-1573.

242.   Girgis, A.; Ibrahim, Y.; Mishriky, N.; Lisgarten, J.; Potter, B.; Palmer, R., Regioselective synthetic approaches towards 1, 2, 8, 9-tetraazadispiro [4.1. 4.3] tetradeca-2, 9-dien-6-ones. *Tetrahedron* **2001,** *57* (10), 2015-2019.

243.   Fang, Q.; Yamamoto, T., New soluble unsaturated polyketone derived from diarylidenecycloalketone: synthesis and optical and electrochemical properties of π-conjugated poly (diarylidenecyclohexanone) with long side chains. *Polymer* **2003,** *44* (10), 2947-2956.

244.   Yousif, N.; Gad, F.; Fahmy, A.; Amine, M.; Sayed, H., REACTIONS WITH α, β-SPIROEPOXY-ALKANONES. PART I. SYNTHESIS AND REACTIONS OF OXASPIRO (2, 5) OCTA-4-ONES. *Phosphorus, Sulfur, and Silicon and the Related Elements* **1996,** *117* (1), 11-19.

245.   Killops, K. L.; Campos, L. M.; Hawker, C. J., Robust, efficient, and orthogonal synthesis of dendrimers via thiol-ene "click" chemistry. *Journal of the American Chemical Society* **2008,** *130* (15), 5062-5064.

246.   Natarajan, L. V.; Shepherd, C. K.; Brandelik, D. M.; Sutherland, R. L.; Chandra, S.; Tondiglia, V. P.; Tomlin, D.; Bunning, T. J., Switchable holographic polymer-dispersed liquid crystal reflection gratings based on thiol-ene photopolymerization. *Chemistry of materials* **2003,** *15* (12), 2477-2484.

247.   Hoyle, C. E.; Lee, T. Y.; Roper, T., Thiol–enes: Chemistry of the past with promise for the future. *Journal of Polymer Science Part A: Polymer Chemistry* **2004,** *42* (21), 5301-5338.

248.   (a) Ferreri, C.; Samadi, A.; Sassatelli, F.; Landi, L.; Chatgilialoglu, C., Regioselective cis-trans isomerization of arachidonic double bonds by thiyl radicals: the influence of phospholipid supramolecular organization. *Journal of the American Chemical Society* **2004,**

126 (4), 1063-1072; (b) Chatgilialoglu, C.; Altieri, A.; Fischer, H., The kinetics of thiyl radical-induced reactions of monounsaturated fatty acid esters. *Journal of the American Chemical Society* **2002,** *124* (43), 12816-12823.

249. Köhn, M.; Breinbauer, R., The Staudinger ligation—a gift to chemical biology. *Angewandte Chemie International Edition* **2004,** *43* (24), 3106-3116.

250. Jewett, J. C.; Bertozzi, C. R., Cu-free click cycloaddition reactions in chemical biology. *Chemical Society Reviews* **2010,** *39* (4), 1272-1279.

251. Ciampi, S.; Böcking, T.; Kilian, K. A.; James, M.; Harper, J. B.; Gooding, J. J., Functionalization of acetylene-terminated monolayers on Si (100) surfaces: A click chemistry approach. *Langmuir* **2007,** *23* (18), 9320-9329.

252. (a) Owen, S. C.; Shoichet, M. S., Design of three-dimensional biomimetic scaffolds. *Journal of Biomedical Materials Research Part A* **2010,** *94* (4), 1321-1331; (b) Quick, A. S.; Fischer, J.; Richter, B.; Pauloehrl, T.; Trouillet, V.; Wegener, M.; Barner-Kowollik, C., Preparation of Reactive Three-Dimensional Microstructures via Direct Laser Writing and Thiol-ene Chemistry. *Macromolecular Rapid Communications* **2013,** *34* (4), 335-340.

253. Adzima, B. J.; Tao, Y.; Kloxin, C. J.; DeForest, C. A.; Anseth, K. S.; Bowman, C. N., Spatial and temporal control of the alkyne–azide cycloaddition by photoinitiated Cu(II) reduction. *Nature chemistry* **2011,** *3* (3), 256-259.

254. Orski, S. V.; Poloukhtine, A. A.; Arumugam, S.; Mao, L.; Popik, V. V.; Locklin, J., High density orthogonal surface immobilization via photoactivated copper-free click chemistry. *Journal of the American Chemical Society* **2010,** *132* (32), 11024-11026.

255. Thomas, J. R.; Liu, X.; Hergenrother, P. J., Size-specific ligands for RNA hairpin loops. *Journal of the American Chemical Society* **2005,** *127* (36), 12434-12435.

256. Goldstein, J.; Newbury, D. E.; Joy, D. C.; Lyman, C. E.; Echlin, P.; Lifshin, E.; Sawyer, L.; Michael, J. R., *Scanning electron microscopy and X-ray microanalysis*. Springer: 2003.

257. Lasek, W.; Makosza, M., Phase-transfer catalyzed nucleophilic addition of arylalkanenitrile carbanions to substituted propenylarenes. *Synthesis* **1993,** *1993* (08), 780-782.

258. Gallardo, H.; Bortoluzzi, A. J.; De Oliveira Santos, D. M. P., Synthesis, crystalline structure and mesomorphic properties of new liquid crystalline 1, 2, 3-triazole derivatives. *Liquid Crystals* **2008,** *35* (6), 719-725.

259. Tomioka, H.; Sawai, S., Photolysis of regioisomeric diazides of 1, 2-diphenylacetylenes studied by matrix-isolation spectroscopy and DFT calculations. *Organic & biomolecular chemistry* **2003,** *1* (24), 4441-4450.

260. Nielsen, C. B.; Arnbjerg, J.; Johnsen, M.; Jo rgensen, M.; Ogilby, P. R., Molecular tuning of phenylene-vinylene derivatives for two-photon photosensitized singlet oxygen production. *The Journal of Organic Chemistry* **2009,** *74* (23), 9094-9104.

261. Strehmel, B.; Sarker, A. M.; Detert, H., The Influence of σ and π Acceptors on Two-Photon Absorption and Solvatochromism of Dipolar and Quadrupolar Unsaturated Organic Compounds. *ChemPhysChem* **2003,** *4* (3), 249-259.

262. Antonov, L.; Kamada, K.; Ohta, K.; Kamounah, F. S., A systematic femtosecond study on the two-photon absorbing D-π-A molecules–π-bridge nitrogen insertion and strength of the donor and acceptor groups. *Physical Chemistry Chemical Physics* **2003,** *5* (6), 1193-1197.

263. Keana, J. F. W.; Cai, S. X., New reagents for photoaffinity labeling: synthesis and photolysis of functionalized perfluorophenyl azides. *Journal of Organic Chemistry* **1990,** *55* (11), 3640-7.

264. Keana, J. F. W.; Cai, S. X., New reagents for photoaffinity labeling: synthesis and photolysis of functionalized perfluorophenyl azides. *The Journal of Organic Chemistry* **1990,** *55* (11), 3640-3647.

265. Lord, S. J.; Lee, H.-l. D.; Samuel, R.; Weber, R.; Liu, N.; Conley, N. R.; Thompson, M. A.; Twieg, R. J.; Moerner, W. E., Azido Push−Pull Fluorogens Photoactivate to Produce Bright Fluorescent Labels†. *The Journal of Physical Chemistry B* **2009,** *114* (45), 14157-14167.

266. Trump, R. P.; Blanc, J.-B. E.; Stewart, E. L.; Brown, P. J.; Caivano, M.; Gray, D. W.; Hoekstra, W. J.; Willson, T. M.; Han, B.; Turnbull, P., Design and synthesis of an array of selective androgen receptor modulators. *Journal of Combinatorial Chemistry* **2007,** *9* (1), 107-114.

267. Ramachary, D. B.; Narayana, V. V., Sequential Combination of Ruthenium-, Base-, and Gold-Catalysis–A New Approach to the Synthesis of Medicinally Important Heterocycles. *European Journal of Organic Chemistry* **2011,** *2011* (19), 3514-3522.

268. Mandal, P. K.; McMurray, J. S., Pd-C-induced catalytic transfer hydrogenation with triethylsilane. *The Journal of Organic Chemistry* **2007,** *72* (17), 6599-6601.

269. Gamble, A. B.; Garner, J.; Gordon, C. P.; O'Conner, S. M.; Keller, P. A., Aryl nitro reduction with iron powder or stannous chloride under ultrasonic irradiation. *Synthetic Communications* **2007,** *37* (16), 2777-2786.

270. Larch, C. P.; Storey, J. M. D.; Williamson, C.; Marshall, C.; Kemp, S. J. Process for preparation of diaminophenothiazinium derivatives. WO2010130977A1, 2010.

271. Wolfe, D. B.; Oldenburg, S. J.; Westcott, S. L.; Jackson, J. B.; Paley, M. S.; Halas, N. J., Photodeposition of molecular layers on nanoparticle substrates. *Langmuir* **1999,** *15* (8), 2745-2748.

272. Weiss, R.; Pühlhofer, F. G., Electrostatics and color: Massive electrostatic perturbation of chromophores by ion cluster ligands. *Journal of the American Chemical Society* **2007,** *129* (3), 547-553.

273. Lu, C.; Cui, Y.; Gu, B.; Wang, F., STUDY ON THE REFRACTIVE NON-LINEARITY OF THREE-PHOTON ABSORBING MEDIA WITH THE Z-SCAN TECHNIQUE. *Journal of Nonlinear Optical Physics & Materials* **2010,** *19* (02), 327-338.

274. Rezende, R. A.; Pereira, F. D. A. S.; Kasyanov, V.; Ovsianikov, A.; Torgensen, J.; Gruber, P.; Stampfl, J.; Brakke, K.; Nogueira, J. A.; Mironov, V.; da Silva, J. V. L., Design, physical prototyping and initial characterisation of 'lockyballs'. *Virtual and Physical Prototyping* **2012,** *7* (4), 287-301.

275. Eisenhart, J. M.; Ellis, A. B., Perturbation of the excited-state properties of trans,trans-1,5-bis(4-(dimethylamino)phenyl)-1,4-pentadien-3-one through adduct formation and silica gel adsorption. *Journal of Organic Chemistry* **1985,** *50* (21), 4108-4113.

276. Nagy, K.; Orban, E.; Bosze, S.; Kele, P., Clickable Long-Wave "Mega-Stokes" Fluorophores for Orthogonal Chemoselective Labeling of Cells. *Chemistry-an Asian Journal* **2010,** *5* (4), 773-777.

277. Bhatt, M. V., Quinone studies. I. Evidence for a new type of substitution reaction of phenanthrenequinone derivatives. *Tetrahedron* **1964,** *20* (4), 803-21.

278. Ipaktschi, J.; Hosseinzadeh, R.; Schlaf, P.; Dreiseidler, E.; Goddard, R., Self-organization of molecules by covalent bonds. Selective tetramerization of a para-quinodimethane. *Helvetica Chimica Acta* **1998,** *81* (10), 1821-1834.

279. Brunner, K.; van Dijken, A.; Börner, H.; Bastiaansen, J. J.; Kiggen, N. M.; Langeveld, B. M., Carbazole compounds as host materials for triplet emitters in organic light-emitting

diodes: tuning the HOMO level without influencing the triplet energy in small molecules. *Journal of the American Chemical Society* **2004,** *126* (19), 6035-6042.

280.   Rao, C. B.; Raju, P. V. N., Syntheses and pyrolysis of some α,α'-bis[spiro(4-aryl-1-pyrazoline)]cycloalkanones. *Indian Journal of Chemistry, Section B: Organic Chemistry Including Medicinal Chemistry* **1984,** *23B* (4), 321-7.

281.   Wallach, *Chem. Zentralbl.* **1908,** *79*, 639.

282.   De, K.; Legros, J.; Crousse, B.; Bonnet-Delpon, D., Solvent-Promoted and -Controlled Aza-Michael Reaction with Aromatic Amines. *Journal of Organic Chemistry* **2009,** *74* (16), 6260-6265.

283.   Gardecki, J.; Maroncelli, M., Set of secondary emission standards for calibration of the spectral responsivity in emission spectroscopy. *Applied Spectroscopy* **1998,** *52* (9), 1179-1189.

284.   Van Gompel, J. A.; Schuster, G. B., Photophysical behavior of ester-substituted aminocoumarins: a new twist. *The Journal of Physical Chemistry* **1989,** *93* (4), 1292-1295.

285.   Valeur, B., *Molecular fluorescence: principles and applications*. John Wiley & Sons: 2013.

286.   Goss, C. A.; Charych, D. H.; Majda, M., Application of (3-mercaptopropyl) trimethoxysilane as a molecular adhesive in the fabrication of vapor-deposited gold electrodes on glass substrates. *Analytical chemistry* **1991,** *63* (1), 85-88.

287.   (a) Fuchs, S.; Hermanns, M. I.; Kirkpatrick, C. J., Retention of a differentiated endothelial phenotype by outgrowth endothelial cells isolated from human peripheral blood and expanded in long-term cultures. *Cell and tissue research* **2006,** *326* (1), 79-92; (b)

Holnthoner, W.; Hohenegger, K.; Husa, A. M.; Muehleder, S.; Meinl, A.; Peterbauer-Scherb,

A.; Redl, H., Adipose-derived stem cells induce vascular tube formation of outgrowth

endothelial cells in a fibrin matrix. *Journal of Tissue Engineering and Regenerative Medicine* **2012**.